THE UNIVERSITY OF CHICAGO

DENSITY-DEPENDENT INTERACTIONS IN SPATIALLY STRUCTURED COMMUNITIES

A DISSERTATION SUBMITTED TO
THE FACULTY OF THE DIVISION OF THE BIOLOGICAL SCIENCES
AND THE PRITZKER SCHOOL OF MEDICINE
IN CANDIDACY FOR THE DEGREE OF
DOCTOR OF PHILOSOPHY

COMMITTEE ON EVOLUTIONARY BIOLOGY

BY
DANIEL J. B. SMITH

CHICAGO, ILLINOIS
DECEMBER 2022

Table of Contents

List of Figures

List of Tables

Acknowledgments

Although this dissertation reports a single author, it is more accurate to describe it as a group project. I owe a great debt to many individuals who have helped me, either directly or indirectly, throughout this difficult journey.

First and foremost, I am forever indebted to my advisor Tim Wootton who has been of singular importance in my development as a scientist. There are many experiences I could highlight throughout my years with Tim – from the enjoyable lab culture to our stimulating conversations about natural history. However, I will simply stress one factor that can be summarized in a word: balance. I mean this in several respects. Firstly, I mean this in terms of Tim's approach to science. Few ecologists balance empirical and theoretical perspectives as well as Tim. Indeed, it is this trait that drew me to Tim's lab in the first place. Although I cannot claim to be balanced in the same way myself (at least, not yet), I strongly believe I have been pushed in the correct direction. While my thesis work is primarily theoretical, I have moved toward more empirically-oriented modeling efforts. Tim's style of advising is similarly balanced. I am reminded of a quote (though I have forgotten the origin). It goes something like this – "give people enough to do something, but not enough to do nothing". I think this applies to intellectual creativity that advisors allow their students. Obviously, the work performed by any PhD student could never fairly described as nothing (except perhaps by the PhD students themselves when facing the profound difficulties of research). However, to balance providing a student with a sufficiently strong guiding hand while allowing them room to develop creatively as a researcher is remarkably difficult. I am forever thankful that

I found this balance in Tim's lab.

I am similarly grateful to Cathy Pfister and the overall Wootton-Pfister lab community. In particular, I am grateful for the flexibility I was allowed with my approach to science. While the Wootton-Pfister lab most regularly performs intense long-term field experiments, I was welcomed into their midst despite my deeply theoretical inclinations. Through this, I have been exposed to many study systems examined by members of the lab and the fascinating empirical studies conducted therein. I will remember the natural history I have learned during my time in the lab throughout my life (both professional and otherwise). I am similarly indebted to the members (both past and present) of the Pfister-Wootton lab with whom I overlapped. This includes Mark Bitter, Max Bogan, Natasha Ershova, Theresa Fonseca, Leo Gaskin, Khashiff Miranda, John Park, Casey Richards, Katherine Silliman, Brooke Weigel, and Hengxing Zou.

My dissertation committee – Mercedes Pascual, Cathy Pfister, and Trevor Price – have acted as mentors throughout my PhD and pushed me to constantly improve as a scientist. I am also grateful for having the opportunity to be part of the broader scientific community at the University of Chicago, particularly the Darwinian cluster which houses the Committee on Evolutionary Biology, the department of Ecology and Evolution, and the department of Organismal Biology and Anatomy. I have been lucky to be part of a community that, despite seemingly disparate interests (from mollusk fossils to eigenvalues), the community at the University of Chicago is always filled with rich discussions holding the interest of all. Of staff and faculty, I would particularly like to thank Stefano Allesina, Audrey Aronowsky, Michael I. Coates, Mike Guerra, Shannon Hackett, Marcy J. Hochberg, David Jablonski, Caroline Johnson, and Stephen Pruett-Jones for discussions and support over the years. The student community within the Darwinian cluster also deserves to be highlighted for their excellence – both in terms of their academic acumen and (perhaps more importantly) their excellent character. In particular, I would like to thank Maryn Carlson, Katie Dixon,

Zach Miller, and Rahul Subramanian for discussions over the years.

As I have learned, it is impossible to complete a PhD without strong support. I have made many friends throughout this journey. Firstly, I would like to thank my CEB cohort: Nadya Ali, Abby Caron, Jordan Greer, Anna Petrosky, and Mariah Wild Scott. You dramatically eased the entire PhD process for me, especially during those difficult and uncertain times that comprise the first years of a PhD. In addition to my cohort, I would also like to especially thank Keven Dooley, Marie Greaney, Abhimanyu Lele, Daniel Schwartz, Aileen Tartanian, and Yuqing Zhu. I will forever treasure your friendship and kindness.

Finally, I would like to thank my family: my parents Sandy Berger and Fred Smith (listed in alphabetic order), my brother Aaron Smith, and my partner Inés Moldavsky for love, support, and deeply bettering me as a person. There are too many things to say and too many adventures to speak of, so I shall simply say this: you have acted as anchors during the turbulent (and pandemic) days of my PhD. Words cannot express my gratitude.

Abstract

Nearly all natural communities exhibit spatial structure, particularly those composed of sessile organisms like forests. To this effect, spatial heterogeneity is thought to play an important role in the maintenance of species coexistence. Recent work indicates that local feedbacks – processes in which the presence or density of an individual organism modifies the local environment – are a particularly important source of spatial heterogeneity. Here, I study mathematical models that depict how local density-dependent interactions in spatially structured communities affect plant competition, community dynamics, and species richness. First, I examine how Janzen-Connell effects (distance-dependent specialized predation pressure) affects tree species richness. Recent theory indicates that Janzen-Connell effects may be unable to maintain diversity when realistic levels of fitness variation are considered. I demonstrate that the ability of Janzen-Connell effects to maintain species richness largely depends on how density-dependent interactions occur in space. Second, I extend the above framework to examine the interaction between local biotically-generated negative density-dependent feedbacks (e.g. Janzen-Connell effects) and abiotically generated spatial heterogeneity (e.g. soil topography). I demonstrate that biotically and abiotically generated spatial heterogeneity can strongly interact to shape species richness, particularly when the latter exhibits positive autocorrelation. Third, I examine how juvenile plant demography impacts the strength of negative density dependence. I analyze a stage-structured model and show that density-independent demographic rates strongly influence the strength and measurement of density-dependence. These results provide insight into empirical mea-

surements of negative density-dependence, particularly recent results indicating that the strength of negative density dependence varies on environmental gradients. Fourth, I extend this lens of analysis to examine how temporal variation in seed availability impacts generalist predators, localized specialist predators, and tree coexistence. Many perennial trees exhibit masting, irregular periodic intra-specific synchronous production of seeds. Masting is thought to an evolutionary adaption to satiate predators. However, previous theory does not examine how masting affects the ability of localized predators to maintain species richness. I show that masting can be stabilizing (increases species richness) or destabilizing (decreases species richness) depending on the relatively non-linearity of specialist and generalist functional responses. Fifth, and in conclusion, I review these results in the context of similar models, highlight existing theoretical gaps, synthesize theoretical results from the literature, and point toward ways to better integrate empirical and theoretical work related to density-dependent feedbacks in spatially structured communities.

Chapter 1

Introduction

Ecological literature is rich with explanations for the diversity maintained in natural communities: there is a diversity of diversity hypothesis. Many of these efforts in theoretical community ecology can conceptually trace their origin to the so-called "Paradox of Plankton" first outlined by Hutchinson in 1961 (Hutchinson, 1961). In this classic work, Hutchinson asks how numerous species of plankton can coexist on few limiting resources; these observations seemingly contradict predictions derived from the competitive exclusion principle (Gause, 1932; Hardin, 1960; Levin, 1970). The fixation with the paradox of plankton has not persisted because the majority of theoretical ecologists are particularly invested in plankton *per se*. Rather, this work embodies a broader theoretical problem in ecology yet to be fully solved: how are the high levels of diversity in many ecological communities maintained in a world in which the number of resources are so often limited?

This question is especially puzzling in communities like tropical forests in which hundreds of woody plant species coexist on relatively few limiting abiotic factors (i.e. nutrients, space, and light availability). Classical approaches to theoretical community ecology that consider how processes such as resource partitioning affect species coexistence (e.g. MacArthur, 1970; Tilman, 1982) are ill-equipped for this problem. As a result, ecologists in the last half-century have proposed dozens of coexistence mechanisms. To name a few: species can coexist if they have distinctive responses to temporally varying environmental factors (the temporal storage

effect; Chesson and Warner, 1981) or space (the spatial storage effect; Chesson, 2000a), by resource fluctuations in time or space that interact with relative non-linearity in consumer species' functional responses (Armstrong and McGehee, 1980; Huisman and Weissing, 1999), through predation (Chase et al., 2002; Chesson and Kuang, 2008, which shall be discussed in greater detail shortly), and complicated competitive structures composed of higher order interactions and intransitive competition (e.g. Grilli et al., 2017; Mack et al., 2019). Indeed, ecology is flush with proposed coexistence mechanisms and no single document can claim to comprehensively explore the broad topic of "the maintenance of species diversity".

In this thesis, I perform theoretical explorations of a particular class of spatial coexistence mechanisms based on how density-dependent interactions in space structure ecological communities. Various studies emphasize how uses of space affect species coexistence (particularly for sessile organisms; see Chesson, 2000a; Amarasekare, 2003; Amarasekare et al., 2004; Leibold et al., 2004; Leibold and Chase, 2017). Within spatial coexistence mechanisms, many recent developments focus on "local feedbacks". While there are many possible definitions, I broadly define local feedbacks as processes in which the presence or local density of a species modifies the local environment in a way that impacts the fitness of conspecifics or other species. Feedbacks come in two potential flavors. Negative feedbacks decrease local fitness and positive feedbacks increase local fitness. In forest communities, for example, the Janzen-Connell Hypothesis (JCH) is a widely observed negative local feedback mechanism that posits specialized natural enemies (e.g. pathogens, insect herbivores) accumulate near trees or areas of high density and locally inhibit the survival of their offspring (i.e. seeds and seedlings; Connell, 1971; Janzen, 1970; Kulmatiski et al., 2008; Petermann et al., 2008; Comita et al., 2014; Bever et al., 2015; Song et al., 2021a). The phenomenon of decreased juvenile survival near conspecific adult trees and/or in areas of high conspecifc density is frequently referred to as either Janzen-Connell Effects (JCEs) or Conspecific Negative Density Dependence (CNDD). I will use the terms JCEs and CNDD somewhat interchangeably

throughout this thesis (though there are subtle differences in their use throughout the literature). JCEs function similarly to a spatially structured means of intra-specific apparent competition (Holt, 1977; Comita and Stump, 2020): as a species' density increases in space, the attraction of natural enemies locally increases predation pressure for all nearby conspecifics. More broadly, resource use can also generate negative feedbacks: a predator may locally deplete its preferred prey or a plant may locally deplete its limiting nutrient, decreasing conspecific competitive ability. The key feature of negative local feedbacks is that they result in intra-specific limitation, thereby promoting coexistence. Spatial structure itself likely plays a key role in facilitating this intra-specific limitation (for example, high local densities of seedlings may dramatically increase the probability of a specialist pathogen outbreak).

Positive feedbacks can emerge through mutualistic relationships between plants and organisms such as symbiotic mycorrhizal fungi via their accumulation in the soil at local sites. (Klironomos, 2002; Reynolds et al., 2003; McGuire, 2014; Bennett et al., 2017; Teste et al., 2017). While both positive and negative feedbacks are important processes to examine, most of this thesis will focus on negative feedbacks in forest communities, largely because recent work indicates they are common in the forest communities world-wide (e.g. Comita et al., 2014; Song et al., 2021a). However, the study of positive feedbacks remains an exciting area of potential future research (Zahra et al., 2021).

Although first proposed over 50 years ago, the JCH has received renewed interest. Theoretical work has laid the baseline foundation to understand how JCEs and CNDD might affect the maintenance of species diversity in natural communities (Adler and Muller-Landau, 2005; Muller-Landau and Adler, 2007; Sedio and Ostling, 2013; Stump and Chesson, 2015; Stump and Comita, 2018; Levi et al., 2019). At the same time, an explosion of empirical research speaks to the commonness of JCEs and CNDD in natural communities (Comita et al., 2014), evidence that it varies between species (e.g. Comita et al., 2010; Mangan et al.,

2010), evidence that it varies along environmental gradients (e.g. LaManna et al., 2016; Fibich et al., 2021; Magee et al., 2021), and evidence of its simultaneous operation with other coexistence mechanisms (e.g. Bagchi et al., 2011; Yao et al., 2020; Huang et al., 2022). The implications of many of these newer developments for species coexistence remain theoretically under-developed and, simultaneously, little theory has been presented that seeks to explain these many intriguing newfound empirical patterns. Therefore, in a somewhat rare instance in modern ecology, empirical work seems to have outpaced theory. My doctoral work focuses on filling these theoretical gaps in the literature.

In Chapter 2, I revisit the basic ability of JCEs to maintain species richness. Recent analyses suggest that JCEs are unlikely to maintain high species richness in communities with realistic levels of inter-specific fitnes variation (e.g. Chisholm and Fung, 2020). I examine this issue while noting that JCEs are integrated into theoretical models through somewhat varied and inconsistent means. For this reason, drawing general conclusions on both the efficacy of JCEs in maintaining species richness and what empirical parameters are necessary to measure to evaluate said efficacy are unclear. Interestingly, the variation in modeling assumptions within the theoretical literature mirrors recent debate in statistical methods of measuring the strength of conspecific density dependence (see Detto et al., 2019). In an effort to help bridge disparate modeling efforts, I present a simple framework evaluating the community-level impacts that result from assumptions made by previous JCE-oriented models and discuss their relevance for interpreting empirical patterns.

In Chapter 3, I examine the interaction between JCEs and Habitat Partitioning (HP). Sessile organisms (e.g. trees) are often thought to coexist through persisting in different locations in spatially heterogeneous environments (i.e. via the spatial storage effect; Chesson, 2000a). Superficially, HP and JCEs seem to operate through opposing forces – while JCEs function through reducing the probability individuals colonize locations nearby conspecifics, HP functions by aggregating conspecifics into specific areas that are often in close proximity.

This implies that their simultaneous operation might reduce their efficacy in maintaining species richness. Contrary to this intuition, however, I show the opposite is true – JCEs and HP most strongly maintain diversity when species tend to induce negative feedbacks on patches most favorable to them.

Chapter 4 serves to develop a theoretical framework for understanding how demographic processes generate variation in CNDD measurements. As noted above, empirical work finds that CNDD strength varies between species (often associated with life history strategies such as growth rate) and varies strongly with environmental conditions (e.g. precipitation, soil moisture, temperature, and light availability). While verbal explanations have been put forward to explain these measurements, no quantitative framework has been put forward to elucidate the factors underlying these observations. In this Chapter, I develop a simple demographic model to understand how density-dependent feedbacks between life history stages interact with environmental factors that modify density-independent demographic traits and life history trade-offs between demographic traits.

In Chapter 5, I examine how temporal variation in seed production interacts with specialized and generalized predation to shape species coexistence. Many perennial tree species exhibit masting, intra-specifically synchronized production of a large number of seeds over irregular periods of two or greater years (Kelly and Sork, 2002). This is thought to be an evolutionary adaptation to satiate the functional responses of seed predators, therefore increasing the proportion of seeds that escape predation. On first blush, this phenomenon appears to countervail JCEs – JCEs rely on local negative density dependence while predator satiation creates positive density dependence. In this Chapter, I evaluate how the interactions of generalist predation, localized specialized predation, masting, and predator satiation affect the ability of specialized predators to maintain species diversity.

In a sixth and final Chapter, I provide a synopsis and review of the work presented in this thesis in the context of previous theoretical work. First, I address several gaps left

by the previous chapters. Then, I provide a brief review of previous models that examine how local feedbacks in spatially structured communities affect species coexistence and the modeling assumptions therein. I conclude by discussing future directions for better integrating theoretical and empirical approaches to evaluating the impact CNDD has on species diversity.

Chapter 2

The functional form of specialized predation affects whether Janzen-Connell effects can prevent competitive exclusion[1]

2.1 Abstract

Janzen-Connell Effects (JCEs), specialized predation of seeds and seedlings near conspecific trees, are hypothesized to maintain species richness. While previous studies show JCEs can maintain high richness relative to neutral communities, recent theoretical work indicates JCEs may weakly inhibit competitive exclusion when species exhibit inter-specific fitness variation. However, recent models make somewhat restrictive assumptions about the functional form of specialized predation – that JCEs occur at a fixed rate when offspring are within a fixed distance of a conspecific tree. Using a theoretical model, I show that the functional form of JCEs largely impacts their ability to maintain coexistence. If predation pressure increases additively with adult tree density and decays exponentially with distance, JCEs maintain considerably higher species richness than predicted by recent models. Loosely

. [1]Originally published as: Smith, Daniel. "The functional form of specialised predation affects whether Janzen-Connell effects can prevent competitive exclusion." *Ecology Letters* (2022).

parameterizing the model with data from a Panamanian tree community, I elucidate the conditions under which JCEs are capable of maintaining high species richness.

2.2 Introduction

The Janzen-Connell hypothesis is a species coexistence mechanism frequently invoked to explain the high diversity of tropical forests (Janzen, 1970; Connell, 1971; Wright, 2002; Terborgh, 2012). It is based on the observation that specialized natural enemies (e.g. insects, fungi, and pathogens) reduce the survivorship of seeds and seedlings when they are near conspecific adult trees. These phenomena are frequently referred to as Janzen-Connell Effects (JCEs). JCEs are thought to promote coexistence by generating negative frequency dependence: the more common a species is, the greater the proportion of the environment its offspring experience JCEs. However, the efficacy of this mechanism remains contested on theoretical grounds.

Empirical evidence supports the presence of JCEs in a variety of systems (e.g. Hyatt et al., 2003; Petermann et al., 2008; Mangan et al., 2010; Swamy and Terborgh, 2010; Johnson et al., 2012; Comita et al., 2014; Bever et al., 2015; Hazelwood et al., 2021). Theoretical work demonstrates JCEs can effectively delay extinction from ecological drift and maintain high species richness relative to neutral communities (Armstrong, 1989; Adler and Muller-Landau, 2005; Sedio and Ostling, 2013; Levi et al., 2019). However, for a stabilizing mechanism to maintain coexistence, it must be sufficiently strong to offset inter-specific fitness differences (Chesson, 2000b). Recent studies that integrate inter-specific variation into JCE models call into question their ability to promote deterministic coexistence (Stump and Comita, 2018; Hülsmann et al., 2021; Cannon et al., 2021) causing some to label JCEs "a weak impediment to competitive exclusion" (Chisholm and Fung, 2020).

A notable assumption of several recent JCE-type models (e.g. Levi et al., 2019; Chisholm and Fung, 2020) is the functional form of specialized predation pressure. These studies as-

sume that JCEs impact offspring within a fixed distance of a conspecific adult tree. Where JCEs induce offspring mortality, they reduce survivorship by a fixed proportion that is independent of conspecific adult density. I refer to this as the "Non-additive−Fixed-distance" (NF) model (Fig. 2.2A). The NF model is likely used because it decreases model complexity and requires relatively low computational power. However, empirical evidence indicates that offspring mortality increases additively with conspecific adult density and declines monotonically with conspecific distance (e.g. Hubbell et al., 2001; Comita et al., 2010, 2014; Johnson et al., 2014; Liu et al., 2015). I refer to this as the "Additive−Distance-decay" (AD) model (Fig. 2.2D). Several previous studies use this functional form (e.g. Adler and Muller-Landau, 2005; Muller-Landau and Adler, 2007; Sedio and Ostling, 2013; Stump and Comita, 2020). If offspring mortality increases with the local abundance of natural enemies that disperse from nearby conspecific trees, this model captures more biological realism.

There are two axes on which the aforementioned functional forms vary. In terms of adult density, predation pressure acts either additively or non-additively. In terms of distance, predation occurs over a fixed distance or decays monotonically. To tease out the effect each functional form assumption has on species coexistence, I develop an Ordinary Differential Equation (ODE) approximation of each of the four possible spatially explicit JCE models that incorporate these functional form assumptions (Fig. 2.1). I use the ODEs to compare the relative ability of each JCE functional form to promote deterministic coexistence in a community exhibiting inter-specific fitness variation. Overall, I show that the functional form of specialized predation strongly affects the ability of JCEs to maintain species richness. This study highlights the need to more precisely determine the functional form of specialized predation, quantify the parameters that affect its strength, and better integrate these empirical results into theoretical models.

2.3 Model and methods

I consider a tree community of N species that contains M patches in which the center of every patch contains a single adult tree. Below, I describe the discrete-time spatially explicit model.

2.3.1 Offspring (within-patch) dynamics

Each tree produces a set number of seeds each time-step. All trees uniformly disperse a portion of their seeds (D) among patches and retain the remaining portion of their seeds ($1 - D$) on the local patch. The number of offspring species i disperses to each patch is proportional to Y_i, henceforth intrinsic fitness (a composite parameter of fecundity and offspring survival). On each patch, JCEs kill offspring. Let $J_{i,k}(x)$ define the probability an offspring of species i survives JCEs on a patch occupied by species k at location x. Then, letting $S_{i,k}(x)$ represent the number of offspring of species i on a patch occupied by species k at a location x:

$$\begin{aligned} S_{i,i}(x) &= Y_i\big[(1-D) + p_i D\big] J_{i,i}(x) \\ S_{i,k}(x) &= Y_i p_i D J_{i,k}(x) \\ S_{all,i}(x) &= \sum_{n=1}^{N} S_{n,i}(x) \end{aligned} \tag{2.1}$$

where p_i is the proportion of species i in the population, $i = 1, 2, ..., N$. $i \neq k$. If the adult on the patch at location x dies during the time-step, a lottery determines which species replaces the adult (see "Tree dynamics"). If the adult survives, all offspring on the patch die. Appendix A5 provides a more detailed description.

2.3.2 Janzen-Connell effect functional forms

Non-additive−Fixed-distance (NF) model

JCEs kill a fixed proportion of a species' offspring when they are within r meters of a conspecific adult (Fig. 2.1A):

$$
\begin{aligned}
J_{i,i}(x) &= \exp\big[-a\big] \\
J_{i,k}(x) &= \begin{cases} 1, & \text{if } \min(x_i) > r \\ \exp\big[-a\big], & \text{if } \min(x_i) \leq r \end{cases}
\end{aligned}
\tag{2.2}
$$

where $\min(x_i)$ is the minimum distance between of an adult of species i and a patch at location x. a represents baseline predation pressure (a composite trait of predation rate and the time over which predation occurs; see Appendix A5). I assume a does not vary between species.

Additive−Fixed-distance (AF) model

JCEs occur over a fixed radius, r, in which predation pressure increases linearly with the number of conspecific adults (Fig. 2.1B):

$$
\begin{aligned}
J_{i,i}(x) &= \exp\left[-a\left(1 + \sum_{m \in r} \mathbb{1}_m(i)\right)\right] \\
J_{i,k}(x) &= \exp\left[-a \sum_{m \in r} \mathbb{1}_m(i)\right]
\end{aligned}
\tag{2.3}
$$

where $m \in r$ depicts the trees falling within the JCE radius. $\mathbb{1}_m(i)$ is an indicator function for which $\mathbb{1}_m(i) = 1$ if $m = i$ and $\mathbb{1}_m(i) = 0$ if $m \neq i$.

Non-additive−Distance-decay model (ND) model

Predation pressure is non-additive and decreases exponentially with distance (Fig. 2.1C):

$$\begin{aligned} J_{i,i}(x) &= \exp\big[-a\big] \\ J_{i,k}(x) &= \exp\Big[-ae^{-\min(x_i)/v}\Big] \end{aligned} \tag{2.4}$$

where v defines rate at which predation declines with distance and $\min(x_i)$ is the same as defined in the NF model.

Additive−distance-decay (AD) model

Predation pressure increases linearly as a function of local conspecific density and decreases exponentially with distance (Fig. 2.1D):

$$\begin{aligned} J_{i,i}(x) &= \exp\Big[-a\Big(1+\sum_{m=1}^{Mp_i} e^{-x_{i,m}/v}\Big)\Big] \\ J_{i,k}(x) &= \exp\Big[-a\sum_{m=1}^{Mp_i} e^{-x_{i,m}/v}\Big] \end{aligned} \tag{2.5}$$

where $x_{i,m}$ is the m_{th} smallest distance between the focal patch (x) and an adult of species i. Mp_i represents all trees of species i in the community. See Appendices A1-A5 for more details on each functional form and the modeling assumptions therein.

2.3.3 Tree dynamics

Each time-step, adult trees die with probability δ. When a tree dies, it is immediately replaced by a randomly selected offspring on the patch (a lottery model; Chesson and Warner (1981)). Let $P_{A,B}(x)$ be the probability an offspring of species A colonizes a patch previously occupied by species B at location x. Then, $P_{i,i}(x) = S_{i,i}(x)/S_{all,i}(x)$

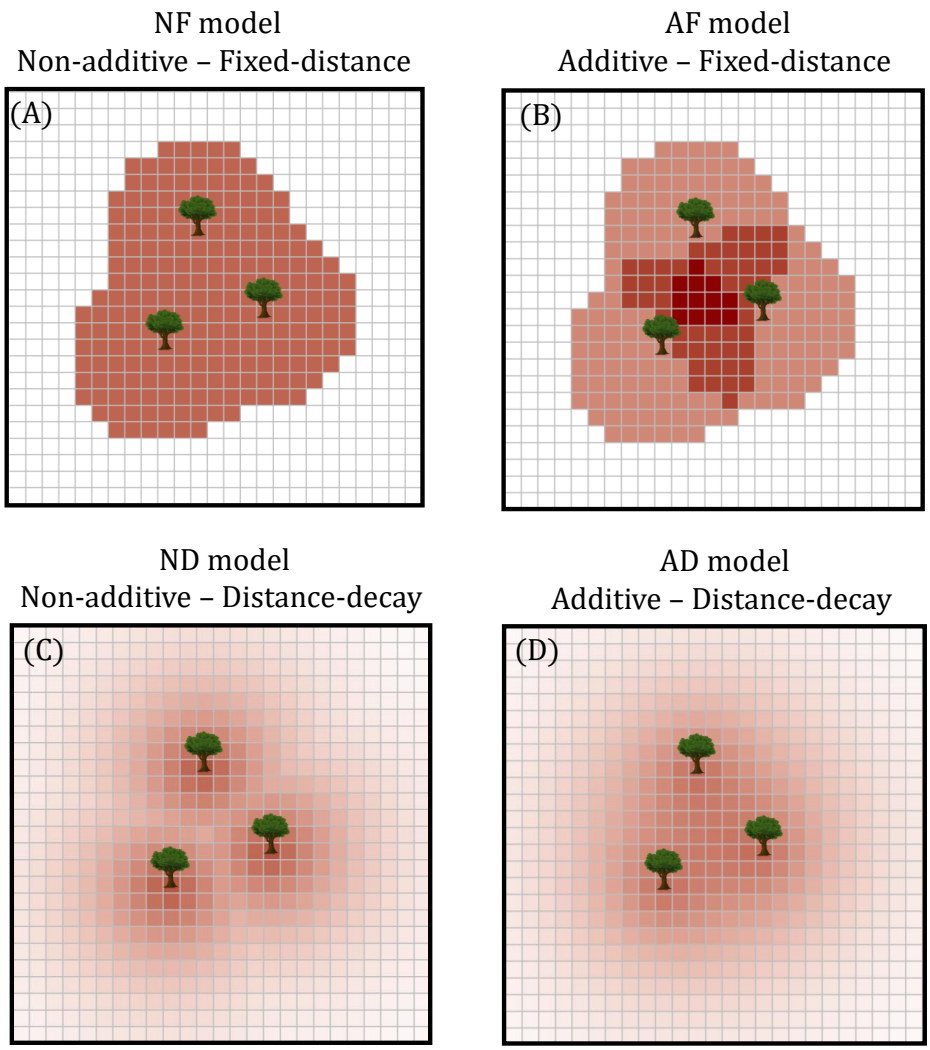

Figure 2.1: Visualization of how each JCE functional form induces offspring mortality in 2D space. Each grid cell represents a patch on which an adult persists. For simplicity, only three adults of a single species are depicted. Shading depicts the relative probability of offspring mortality in space. Redder shading corresponds to higher offspring mortality; white corresponds 100% offspring survival. The plots highlight the distinct features of each modeling assumption. The fixed-distance models (NF and AF models; panels A and B) induce concentrated predation pressure over a relatively small area while the distance-decay models (ND and AD; panels C and D) distribute less concentrated predation pressure over a larger area. The non-additive models (NF and ND; panels A and C) induce relatively strong predation pressure near adults that does not increase with adult density whereas the additive models (AF and AD; panels B and D) exhibit the highest mortality where multiple conspecific adults are close in proximity. The images depict when $v = 10$, $r = 10\sqrt{2}$, $g = 0.172$, $N = 250$, $a_{\mathrm{A}} = 0.5$, and $a_{\mathrm{N}} = a_{\mathrm{A}} + a_{\mathrm{A}}E/N$ where $E = E_F = E_D = 2\pi v^2 g$ (as per the additive−non-additive normalization; see "Model normalizations" and Appendix A5).

and $P_{i,k}(x) = S_{i,k}(x)/S_{all,k}(x)$. In the spatially explicit model, patches are discretized in space on a gridded torus of $M = 275 \times 275$ patches. For the distance-decay models (AD, ND), the distance between two patches is defined by the euclidean distance between their center points. For the fixed-distance models (AF, NF), I incorporate JCEs using Moore neighborhoods.

I developed a deterministic ODE approximation for each spatially explicit model by taking the expected offspring abundance on each patch type. The dynamics for the proportion of species i (p_i) in the community are

$$\frac{dp_i}{dt} = \delta\left[\frac{\mathbb{E}[S_{i,i}(x)]}{\mathbb{E}[S_{all,i}(x)]}p_i + \sum_{k\neq i}\frac{\mathbb{E}[S_{i,k}(x)]}{\mathbb{E}[S_{all,k}(x)]}p_k - p_i\right] \tag{2.6}$$

for which $i = 1, 2, ..., N$. The first term in the parentheses is the rate at which species i recolonizes patches previously occupied by conspecifics, the second term is the rate at which species i colonizes patches previously occupied by species k ($k \neq i$), and the third term is the rate at which adults of species i die.

For the NF model, offspring abundances are:

$$\begin{aligned}\mathbb{E}[S_{i,i}(x)] &= Y_i\big[(1-D) + p_iD\big]e^{-a}\\ \mathbb{E}[S_{i,k}(x)] &= Y_ip_iD\big[e^{-p_iE_F} + e^{-a}(1-e^{-p_iE_F})\big]\end{aligned} \tag{2.7}$$

where $E_F = \pi g r^2$ where g is density (adults per square meter). E_F is the expected number of trees that fall within the effect radius, r. For the AF model, the offspring abundances are:

$$\begin{aligned}\mathbb{E}[S_{i,i}(x)] &= Y_i\big[(1-D) + p_iD\big]e^{-a}e^{-(1-e^{-a})p_iE_F}\\ \mathbb{E}[S_{i,k}(x)] &= Y_ip_iDe^{-(1-e^{-a})p_iE_F}\end{aligned} \tag{2.8}$$

where E_F is the same as in the NF model. For the ND model, the offspring abundances are:

$$\begin{aligned}
\mathbb{E}[S_{i,i}(x)] &= Y_i\big[(1-D)+p_iD\big]e^{-a} \\
\mathbb{E}[S_{i,k}(x)] &= Y_i p_i D e^{-ae^{-\sqrt{\frac{\pi}{2E_D p_i}}}}\left(1+ae^{-\sqrt{\frac{\pi}{2E_D p_i}}}\left(ae^{-\sqrt{\frac{\pi}{2E_D p_i}}}-1\right)\left(1-\frac{\pi}{4}\right)\frac{1}{p_iE_D}\right)
\end{aligned} \tag{2.9}$$

where $E_D = 2\pi g v^2$. E_D relates to the predation pressure each tree induces. For the AD model, the seedling equations are:

$$\begin{aligned}
\mathbb{E}[S_{i,i}(x)] &= Y_i\big[(1-D)+p_id\big]e^{-a}e^{-ap_iE_DH(a)} \\
\mathbb{E}[S_{i,k}(x)] &= Y_i p_i D e^{-ap_iE_DH(a)}
\end{aligned} \tag{2.10}$$

where $H(a) = {}_3F_3(1,1,1;2,2,2;-a)$, a Generalized Hypergeometric Function. See Appendix A1-A4 for details.

Model parameterizations

I roughly parameterized several key quantities using data from the Barro Colordo Island (BCI) forest plot in Panama. g (adult density) can be estimated by dividing the total number of individuals in the community by its area in square meters. The plot at BCI is 50-ha and contains approximately $86,069$ individuals of reproductive diameter based on the 1995 BCI census (Condit et al., 2019; Chisholm and Fung, 2020). This yields $g \approx 0.172$ adults per square meter.

Comita et al. (2010) estimated a distance decay parameter at BCI (β) similar to v, finding best and second best fit values equivalent to $v = 5$ and $v = 10$, respectively. β differs from v in that it describes the distance decay of consepcific adult basal area on seedling survivorship based on a GLM using a logit link function, but they are conceptually similar. To examine a range of scenarios loosely based on this measurement, I examined v between 2.5 and 15.

Chisholm and Fung (2020) found inter-specific fitness variation (Y) at BCI to be log-normally distributed with inter-specific variation approximately equivalent to $Y \sim$ lognormal $[\mu = 0, \sigma_Y = 1.0]$. I examined when σ_Y between 0.1 and 1.0. Note that the nature of the lottery model (in which one species always wins the lottery) means that only relative, rather than absolute, values of intrinsic fitness matter.

I examined several values of a (baseline predation pressure). In every model, $1 - e^{-a}$ corresponds to the probability an offspring dies due to JCEs when it is on a patch occupied by a conspecific. I henceforth frame a in terms of $1 - e^{-a}$ because it is easy to interpret. I examined when $1 - e^{-a} = 0.4$, 0.7, and 0.99, which encompasses when JCEs range from moderately strong to very strong.

2.3.4 Model normalizations

To compare models, I perform two inter-model normalizations that equalize predation pressure across distance-dependent and density-dependent modeling assumptions. See Appendix A5 for full details.

To normalize distance-decay and fixed-distance functional forms, I equalize the predation pressure each individual tree induces over space. Let $G(x)$ represent the relative predation pressure induced x meters away from a single adult tree ($G(x) \leq 1$). The total predation pressure induced by a single tree in 2-dimensional space is $2\pi g \int_0^\infty xG(x)\mathrm{d}x$. For the distance-decay models (predation declines exponentially with distance) $G(x) = e^{-x/v}$, giving $2\pi g \int_0^\infty xe^{-x/v}\mathrm{d}x = 2g\pi v^2$. For the fixed-distance models (predation occurs within a fixed area, r) $G(x) = 1$ for $x \leq r$ and $G(x) = 0$ if $x > r$, giving $2\pi g \int_0^r x\mathrm{d}x = g\pi r^2$. Setting these values equal yields $r = v\sqrt{2}$ (which also implies $E_F = E_D$). This normalization is similar to methods used in previous models (Adler and Muller-Landau, 2005; Sedio and Ostling, 2013) and can be interpreted as equalizing the total number of predators that disperse from trees (Appendix A5).

Secondly, I normalize additive and non-additive models. To do so, I modify the baseline predation pressure of the non-additive models such that additive and non-additive models exhibit the same mean predation. Let E represent either E_D or E_F (which are equal under the first normalization). On a random patch in a community of N species, it can be shown that additive predation increases mean predation pressure by aE/N relative to when predation is non-additive. This is derived by taking the expected predation pressure a species' offspring experiences on a random patch in the community (see Appendix A5). Then, letting a_{n} and a_{A} be the baseline predation pressure of the non-additive and additive models, respectively, mean predation pressure is equal between models if $a_{\mathrm{n}} = a_{\mathrm{A}} + a_{\mathrm{A}}E/N$. I henceforth use the notation a_{A} when referring to baseline predation pressure.

2.3.5 Presentation of results

Ordinary Differential Equation (ODE) analysis

Using the ODE model (Equation (2.6)), I ran simulations with the above-mentioned parameterizations and normalizations under different levels of dispersal limitation (D) to compare how each functional form maintains species richness. The initial number of species for each simulations was set to 300. 300 was selected on the basis that the forest plot at BCI contains approximately 300 woody plant species (Condit et al., 2019). Simulations were run for 10,000 generations, more than sufficient for the system to reach equilibrium (Appendix A7, Fig. 2.39). I considered species i to be extinct if $\log p_i < -11$ (recalling p_i the proportion of species i). This approximately corresponds to less than one individual at the BCI forest plot ($\log 1/86,006 \approx -11$). The additive−non-additive normalization was implemented by running a simulation with additive models and using the number of species maintained to normalize baseline predation. For example, if the AD model maintained N species, then the NF and ND models were normalized by setting $a_{\mathrm{n}} = a_{\mathrm{A}} + a_{\mathrm{A}}E_D/N$. Simulations were performed in R (R Core Team, 2021) using the package deSolve (Soetaert et al., 2010).

I performed additional analyses to explain the simulation outputs. First, I examined how each functional form induces negative frequency dependence by analyzing equations (2.7-2.10). Then, I analyzed approximate invasion criteria for each model. The invasion criteria quantify the minimum fitness that permits the invasion of a rare species in a community of N residents under the assumption of global dispersal ($D = 1$; Table 2.1; Appendices A.1-A.4).

ODE validation

I ran spatially explicit and ODE model simulations using identical parameterizations and compared species richness outputs. Spatially explicit simulations were run on the 275×275 patch community until the transient dynamics had approximately concluded (after species richness approximately stabilized; Appendices A1-A4). I ran simulations with $\sigma_Y \sim \{0.1, 0.45, 0.8\}$ and $a \sim \{0.5, 1.0, 2.75, 4.5\}$. For each of the 12 parameter combinations, I ran simulations with model $v \sim \{5, 7.5, 10\}$ for the distance-decay functional forms with $g = 0.2$. For the fixed-distance model, I ran simulations with Moore neighborhoods ranging in size from 3×3 (small) to 11×11 (large) which corresponds to r values between $4.0 - 14$ for $g = 0.2$.

2.4 Results

2.4.1 Species richness maintained by each model

For all models, species richness increased with baseline predation pressure (a_{A}) and the spatial scale of predation (v and r; Figs. 2.2 and 2.3) and decreased with inter-specific fitness variation (σ_Y; Fig. 2.3). The AD model promoted the highest species richness in all cases. Which model promoted the second highest species richness depended on a_{A}. For low to moderate a_{A}, the AF model maintained the second greatest species richness (Figs. 2.2 and 2.3, columns 1-2). In these cases, the species richness maintained by the non-additive models

(ND and NF) declined rapidly with increasing σ_Y (Fig. 2.3, columns 1-2). While species richness also decreased with σ_Y for the additive models (AD and AF), the decline was much less pronounced (particularly for large v and r). For large a_{A}, the ND model maintained the second highest diversity (Figs. 2.2 and 2.3, column 3). While all models were capable of maintaining somewhat high species richness for large a_{A}, the distance-decay models (AD and ND) were more robust to inter-specific fitness variation than the fixed-distance models (Fig. 2.3, column 3).

The initial pool of 300 species limited species richness when JCEs were strong (e.g. Fig. 2.2 column 3; Fig. 2.3I). With a larger initial species pool ($1,000$ species, similar to the number of trees in central Panama; Condit et al., 2013) differences in species richness maintained by each model were considerably more pronounced in these cases (Appendix A7, Figs. 2.40-2.41). Therefore, Figs. 2.2 and 2.3 may understate model differences.

Dispersal limitation trivially affected the additive models, but decreased species richness for the non-additive models (Fig. 2.2; Appendix A7, Fig. 2.40). This can be understood as follows. In the absence of dispersal limitation ($D = 1$), a rare species suffers no offspring mortality due to JCEs; when $D < 1$, a rare species' locally dispersed offspring suffer JCE-induced mortality. When predation is non-additive, a rare species' locally dispersed offspring experience the same mortality as those of resident species. When predation is additive, resident species' locally dispersed offspring always experience greater mortality than those of rare species due to additive effects. Thus, dispersal limitation decreases rare species advantage when predation is non-additive but not when it is additive. Dispersal limitation most strongly affected species richness for intermediate a_{A}. It can be shown that the dispersal limited and non-dispersal limited cases converge when a_{A} is very large or small (Appendix A6).

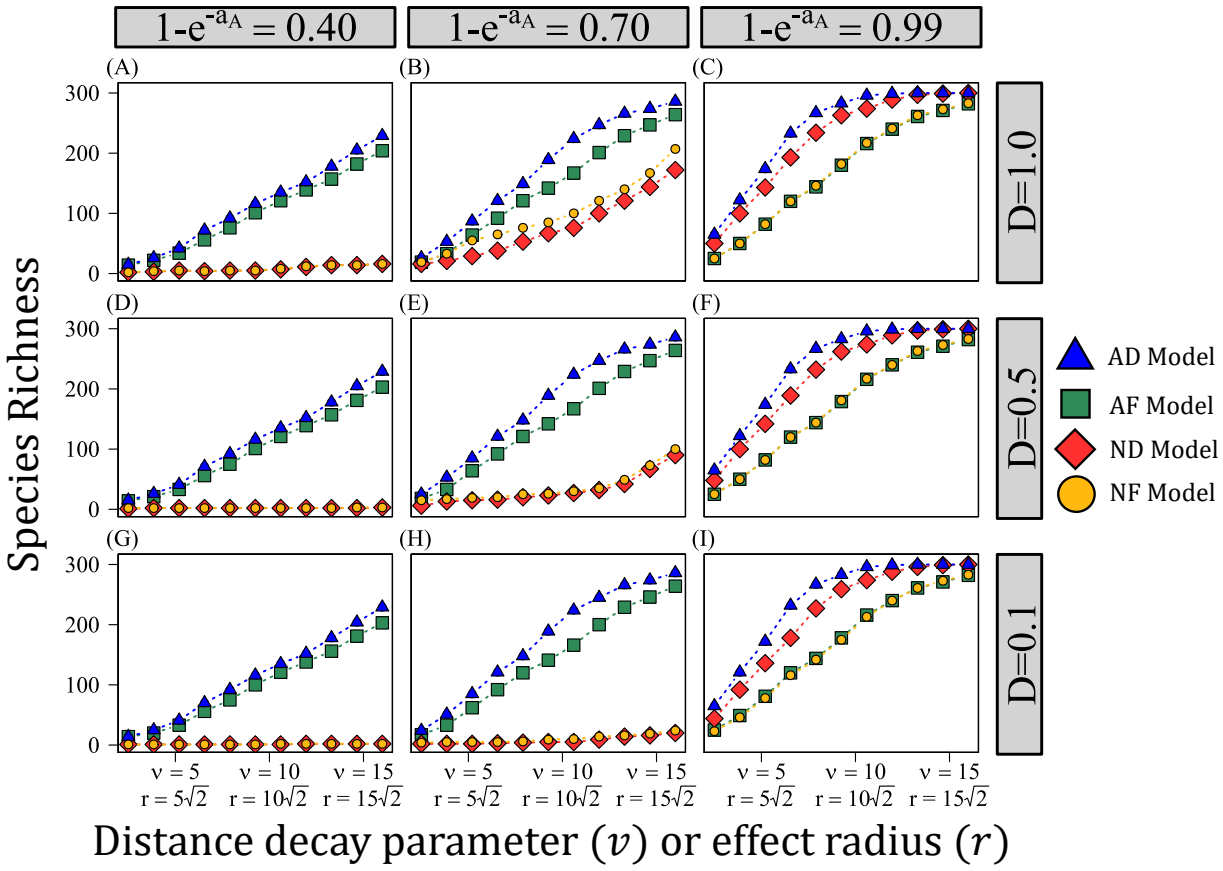

Figure 2.2: Species richness maintained by each JCE functional form under different values of baseline predation pressure (a_{A}), dispersal limitation (D), and the spatial scale of predation (v and r). For each plot, the x-axis depicts either v or r (depending on the JCE functional form) and the y-axis is species richness (the number of species maintained in the community at equilibrium). Models are differentiated by point shape and color. Each column depicts a different value of a_{A} (the baseline predation pressure for the additive models) and each row shows a different value of D ($D = 1$, $D = 0.5$, and $D = 0.1$, respectively). The non-additive models are normalized such that $a_{\mathrm{N}} = a_{\mathrm{A}} + a_{\mathrm{A}} E/N_{\mathrm{A}}$ where a_{N} is the normalized predation pressure for the non-additive models, N_{A} is the diversity maintained by the additive model to which the non-additive model is being compared, and E is either E_F or E_D (which are equivalent). a_{N} was calculated based on the diversity maintained by the AD model for the additive – non-additive normalizations of both NF and ND models. Using AF model outputs to quantify a_{N} yielded trivially similar results. All simulations were conducted with 300 species initially in the population. Parameters not noted on the figure are as follows: $g = 0.172$ and $\sigma_Y = 0.55$ ($Y \sim \mathrm{lognormal}[\mu = 0, \sigma_Y]$).

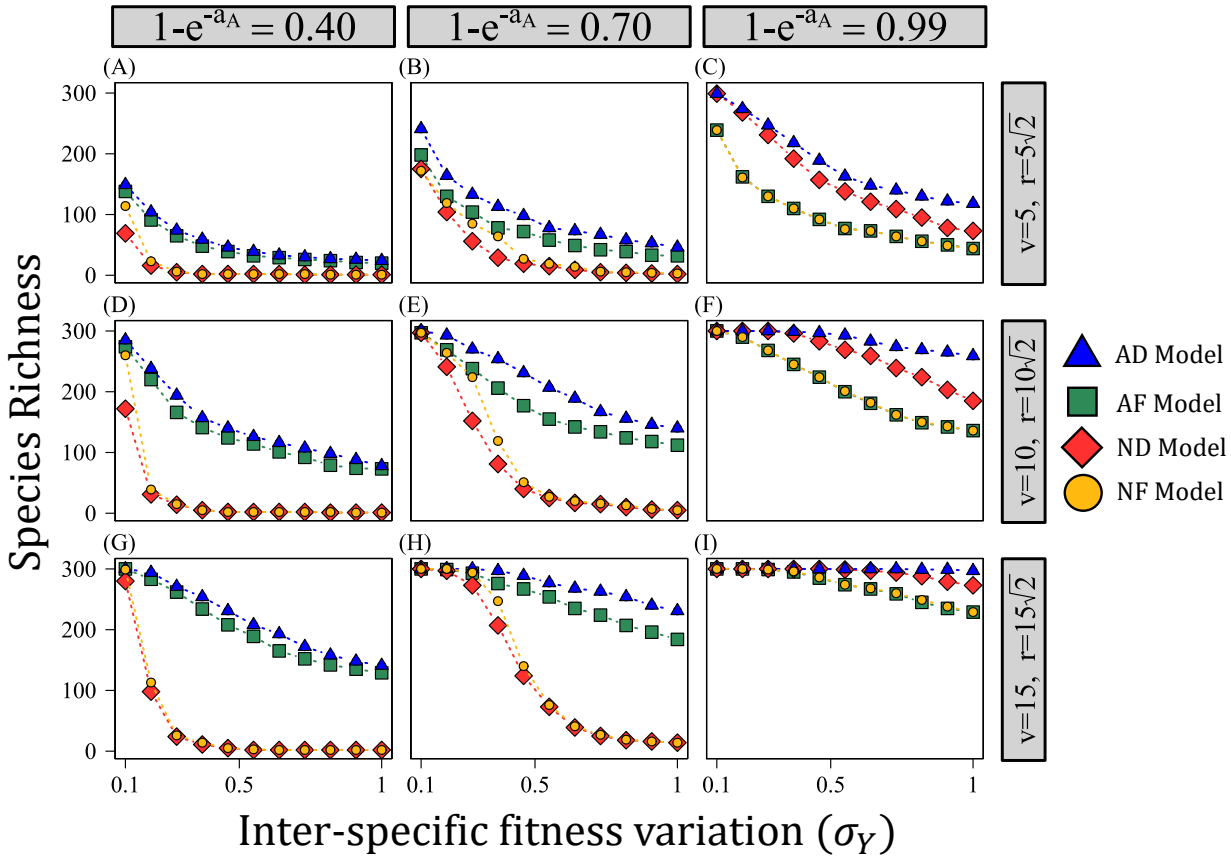

Figure 2.3: How the level of inter-specific fitness variation (σ_Y) affects species richness for each JCE functional form ($Y \sim \text{lognormal}[\mu = 0, \sigma_Y]$). For each plot, the x-axis is σ_Y and the y-axis is species richness (the number of species maintained in the community at equilibrium). Each column depicts a different value of a_{A} (the baseline predation pressure for the additive models) and each row shows a different value of v or r (the spatial scale of predation). Additive – non-additive normalizations were calculated using the same method noted in Fig. 2.2. For lower a_{A} (columns 1 and 2) the additive models (AD and AF) are much more robust to fitness differences (σ_Y), particularly over larger spatial scales (row 2 and 3). For large a_{A} (column 3), distance-decay models (AD and ND) are more robust to inter-specific fitness differences than the fixed-distance models. All simulations were conducted with 300 species initially in the population. Parameters not noted on the figure are as follows: $g = 0.172$ and $D = 0.5$.

2.4.2 Mechanisms of diversity maintenance

The AD model always promotes the highest species richness, the AF model promotes the second highest species richness for lower baseline predation pressure (a_{A}), and the ND model promotes the second highest species richness for large a_{A} (Figs. 2.2 and 2.3; Appendix A7, Figs. 2.40-2.41). Below, I explain these results.

Examining equations (2.7-2.10), the proportion of surviving offspring of species i on a random patch declines with increasing conspecific adult proportion in the community (p_i) for each model (Fig. 2.4). The nature of this decline, which reflects the strength of negative frequency dependence, depends on whether predation is additive or non-additive. When predation is additive (AD and AF models), offspring survival declines monotonically with p_i; when predation is non-additive (ND and NF models), offspring survival decreases as a saturating function of p_i (saturating to the fixed value set non-additive predation pressure, a_{n}; Fig. 2.4). This difference between additive and non-additive functional forms is pronounced when a_{A} is relatively small (Figs. 2.4A, 2.4C). For large a_{A}, all models strongly reduce offspring survivorship when a species is common (fig. 2.4B, 1.4C), though still more so for the additive models (Appendix A7, Fig. 2.42). However, under large a_{A}, when species proportion is near the population mean ($p_i \approx 1/N$), the distance-decay (AD and ND) models induce lower offspring survivorship than the fixed-distance (AF and NF) models (Figs. 2.4B, 2.4D; dotted lines). Thus, additive predation induces relatively strong negative frequency dependence for small a_{A} while the distance-decay functional form produces lower mean offspring survival for large a_{A}.

The invasion criteria quantify how these differences affect the growth rate of a rare species. The right hand side of each invasion criterion (henceforth the "minimum invader fitness"; Table 2.1) quantifies the minimum fitness required for a rare species to invade a community of N residents. The minimum invader fitness is broken into two parts. **(1)** The mean-JCE-fitness term, which consists of the product of the mean fitness of the resident

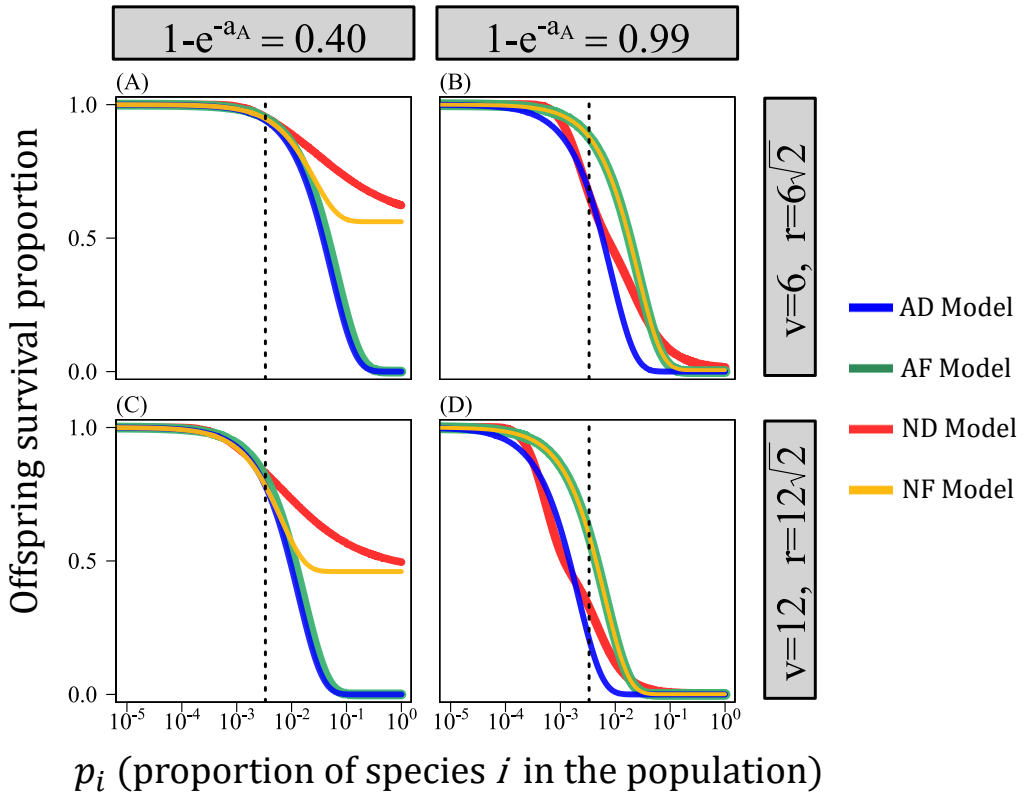

Figure 2.4: How offspring survivorship scales with conspecific adult proportion for each functional form. For each plot, the x-axis is the proportion of adults of a focal species in the population (p_i) and the y-axis is the expected proportion of surviving offspring on random patch occupied by a heterospecific. These values are taken from equations (2.7-2.10). For the AD model, for example (equation (2.10)): $\mathbb{E}[S_{i,k}(x)] = Y_i p_i D e^{-a_i p_i E_D H(a_i)}$. The y-axis of this figure is $e^{-a_i p_i E_D H(a_i)}$, which is equivalent to $\mathbb{E}[J_{i,k}(x)]$ (see Appendices A1-A4). The other curves show the analogous terms from equations (2.7-2.9). Models are indexed by color. Each model assumes $N = 300$; the dotted lines depict $1/N$, the mean proportion of the population. Columns show different values of $1-e^{-a_A}$ (baseline predation pressure; 0.4 and 0.99, respectively). Rows show different values of v (5 and 10, respectively). First consider low $1-e^{-a_A}$ (column 1; A and C). When p_i is low (on the order of $1/N$) all models produce similar offspring survival. When p_i is large, the additive models (AD and AF; blue and green curves) produce lower offspring survival than the non-additive models (ND, NF). Now, consider high $1-e^{-a_A}$ (column 2; B and D). All models produce low offspring survival when species i is common (large p_i). When p_i is small (on the order of $1/N$, the mean proportion) the distance-decay models (AD an ND; blue and red curves) induce much lower survival than the fixed-distance models. Note that the fixed-distance (AF and NF) models converge for large a_A (the orange and green curves are essentially identical). This is because nearly all offspring die if a conspecific adult is found with the effect area, in which case additive predation does not meaningfully increase offspring mortality. Parameters are as follows: $g = 0.172$, $D = 1.0$, $N = 300$, and $a_N = a_A(1+E/N)$ where $E = E_F = E_D = 2\pi v^2 g$.

Model	Abbreviation	Approximate Invasion Criteria
Non-additive–Fixed-distance	NF	$Y_i > \underbrace{\overline{Y}\left(1-\left(1-e^{-a}\right)\left(1-e^{\frac{-E_F}{N}}\right)\right)}_{\text{mean JCE-fitness term}} + \underbrace{N\text{Cov}(p,Y)\left(e^{-\frac{E_F}{N}}\left(1-e^{-a}\right)\left(1-\frac{E_F}{N}\right)+e^{-a}\right)}_{\text{covariance-JCE term}}$
Additive–Fixed-distance	AF	$Y_i > \underbrace{\overline{Y}e^{-\left(1-e^{-a}\right)\frac{E_F}{N}}}_{\text{mean JCE-fitness term}} + \underbrace{N\text{Cov}(p,Y)\left(1-\left(1-e^{-a}\right)\frac{E_F}{N}\right)e^{-\left(1-e^{-a}\right)\frac{E_F}{N}}}_{\text{covariance-JCE term}}$
Non-additive–Distance-decay	ND	$Y_i > \underbrace{\overline{Y}e^{-ae^{-\sqrt{\frac{\pi N}{2E_D}}}}\left(1+ae^{-\sqrt{\frac{\pi N}{2E_D}}}\left(ae^{-\sqrt{\frac{\pi N}{2E_D}}}-1\right)\left(1-\frac{\pi}{4}\right)\frac{N}{E_D}\right)}_{\text{mean JCE-fitness term}} + \underbrace{N\text{Cov}(p,Y)\Gamma^*}_{\text{covariance-JCE term}}$
Additive–Distance-decay	AD	$Y_i > \underbrace{\overline{Y}e^{-aH(a)\frac{E_D}{N}}}_{\text{mean JCE-fitness term}} + \underbrace{N\text{Cov}(p,Y)\left(1-aH(a)\frac{E_D}{N}\right)e^{-aH(a)\frac{E_D}{N}}}_{\text{covariance-JCE term}}$

Table 2.1: Model types, their abbreviations, and their approximate invasion criterion. The right hand side of each approximate invasion criterion quantifies the minimum fitness of a rare species, Y_i, required for invasion (deterministic increase in abundance). I refer to this as the "minimum invader fitness". $\overline{Y} = \frac{1}{N}\sum_{k=1}^{N} Y_k$. Γ^* is a large and complicated expression. See Appendix A3 for the full expression and Appendices A1-A4 for derivations.

community ($\overline{Y}$) and the average proportion of offspring that survive JCEs in the resident community (the latter component being equivalent to the dotted lines in Fig. 2.4). This term quantifies the mean JCE-scaled fitness of the resident species that an invader competes against. **(2)** The covariance-JCE term, which consists of two components: the covariance between species proportion and intrinsic fitness ($\text{Cov}(p, Y)$) and several coefficients. Because species differ only in intrinsic fitness, $\text{Cov}(p, Y)$ is positive (fitter species are more common). The coefficients, in part, quantify how JCEs reduce the offspring survivorship of relatively common species. The covariance-JCE term therefore quantifies the amount of competition the invader faces from relatively fit and common species; lower values correspond to stronger negative frequency dependence.

Examining the invasion criteria through numerical simulations, the AD model exhibited the lowest minimum invader fitness in all cases (fig. 2.5). For relatively weak predation pressure (low a_{A}), the AF model exhibited the second lowest minimum invader fitness whereas the non-additive models (ND and NF) produced relatively high invader minimum fitness, especially for larger v and r (Figs. 2.5A, 2.5D). The covariance-JCE terms of the non-additive

(ND, NF) models were much greater those of their additive counterparts while mean-JCE terms were similar, indicating the strength of negative frequency dependence underlies model differences for low a_A (Figs. 2.5C, 2.5F). When a_A was large, the ND model produced the lowest minimum invader fitness (Figs. 2.5A, 2.5D). In this case, the mean-JCE-fitness terms of the distance-decay (AD and ND) models were considerably lower than those of the fixed-distance (AF and NF) models whereas the covariance-JCE terms were similar. This indicates that mean offspring survival underlies model differences for large a_A (Fig. 2.5B and 2.5E; 2.5C and 2.5F). These results are consistent with the above analysis (Fig. 2.4) and species richness outputs (Figs. 2.2 and 2.3).

2.4.3 ODE validation

The ODE model yielded species richness outputs highly similar to the spatially explicit models. Across simulations, the mean difference in species richness between the spatially explicit models and ODEs for each functional form was less than 3.5 species. The r^2 (coefficient of determination) for species richness between spatially explicit and ODE models was greater that 0.98 for all functional forms. (Appendices A1-A4; see Appendix A7 Fig. 2.37 for a summary figure). Results for Shannon diversity were similar (Appendix A7, Fig. 2.38).

2.5 Discussion

2.5.1 How the functional form of specialized predation affects species richness

In this paper, I demonstrate that the functional form of specialized predation strongly affects the ability of Janzen-Connell Effects (JCEs) to inhibit competitive exclusion. This is important in the context of recent modeling studies which indicate JCEs are unable to maintain diversity if species exhibit inter-specific fitness variation (e.g. Stump and Comita, 2018; Chisholm and Fung, 2020). These and similar studies (Levi et al., 2019) assume that

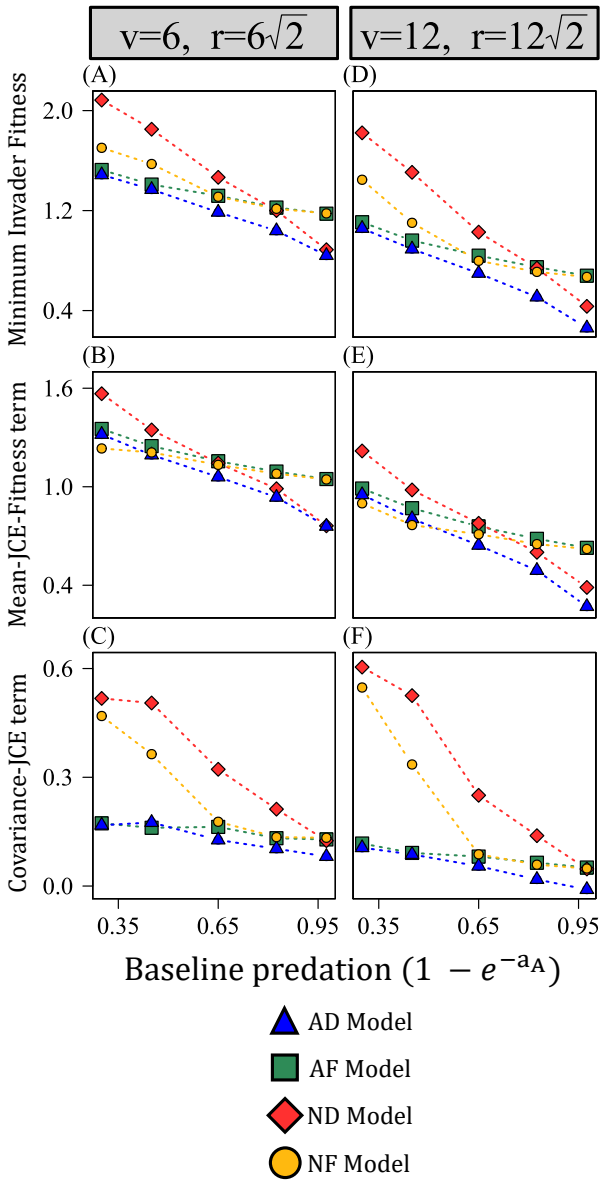

Figure 2.5: How the different functional forms promote invasion as defined by their invasion criteria quantified from simulated communities. All simulations began with 300 species. First, additive model simulations were run and normalizations were performed as described in the main text, fig. 2.2, and Appendix A5. Simulations were run until each model to reached equilibrium. Using the equilibrium values, the invasion criteria components were calculated for each model. Each row shows a different component of the invasion criteria. (A-C) show $v = 6$ ($r = 6\sqrt{2}$) and (D-F) show $v = 12$ ($r = 12\sqrt{2}$). The x-axis of each plot shows the baseline predation pressure for the additive models ($1 - e^{-a_A}$). (A, D) show the minimum invader fitness for each invasion criteria (i.e. the right hand side of the invasion criteria), (B, E) show the mean-JCE-fitness term, and (C, F) show the covariance-JCE term. Values for each model in (A) are the sum of values (B) and (C); values for each model in (D) are the sum of values in (E) and (F). The key results are as follows: when a_A is small, the additive (AD and AF) models yield a much lower covariance-JCE terms than the non-additive (ND and NF) models. Hence, the additive models produce lower minimum invader fitness than the non-additive models. When a_A is large, the distance-decay (AD and ND) models induce lower mean-JCE fitness terms than the fixed-distance (AF and NF) models. Hence, the distance-decay produce lower minimum invader fitness than the fixed-distance models. Parameters are as follows: $D = 1$, $g = 0.172$, and $\sigma_Y = 0.375$. Appendix A7, Fig. 2.43 shows how the exact invasion criteria values (the minimum invader fitness values) compare to the approximations (A, D). Outputs are qualitatively similar.

specialized predation pressure affects offspring at a fixed rate within a discrete distance of a conspecific tree (the NF model; Fig. 2.1A). Such functional forms leave out biological details as an approximation; previous work indicates that JCEs increase additively with adult density decay monotonically with distance (the AD model; Hubbell et al., 2001; Comita et al., 2010). To investigate how the functional form of specialized predation affects competitive outcomes, I developed four models that utilize these combinations of assumptions (the AD, ND, AF, and NF models). Overall, I find the AD model (the model with the greatest biological complexity) promotes the highest species richness.

The importance of each functional form assumption depended on the parameter space. When baseline predation pressure was relatively weak (low a_{A}), additive predation produced communities much more robust to high inter-specific fitness variation than non-additive predation (Figs. 2.2-2.3; Appendix A7, Figs. 2.40-2.41). This result reflects how additive predation produces relatively strong negative frequency dependence (Fig. 2.4) and limits how much competition invaders experience from highly fit species (fig. 2.5C, 2.5F). Notably, offspring recruitment near conspecific adults is likely not uncommon for low a_{A}. Therefore, contrary to previous arguments (Chisholm and Fung, 2020), the close proximity of conspecific adults is not incompatible with the operation of strongly stabilizing JCEs if predation is additive.

For large a_{A}, the distance-decay (AD and ND) models maintained higher diversity than the fixed-distance (AF and NF) models. The fixed-distance models induce concentrated predation pressure within a highly localized area while the distance-decay models spread less concentrated predation over a wider space (fig. 2.1) which can generate lower mean offspring survival (Figs. 2.4B, 2.4D, 2.5B, 2.5E). Therefore, contrary to how JCEs are often conceptualized (Terborgh, 2012), JCEs maintain higher species richness when predation pressure is less (rather than more) localized (conceptually similar to Stump and Chesson, 2015).

Results also suggest that dispersal limitation decreases species richness when predation is non-additive but not when additive (Fig. 2.2). This asymmetry helps to explain seemingly inconsistent results of previous JCE-type models. Models that consider non-additive predation find dispersal limitation decreases species richness (Stump and Chesson, 2015; Chisholm and Fung, 2020) whereas several studies using additive functional forms indicate dispersal limitation can increase species richness (Adler and Muller-Landau, 2005; Detto and Muller-Landau, 2016; Wiegand et al., 2021). Although Stump and Chesson (2015) argue that the combination dispersal limitation and localized predation decreases the stabilizing effects of JCEs, results suggest this is the case only when predation is non-additive (see Appendix A6).

2.5.2 Empirical measurements in relation to the model

The parameter a_{A} encapsulates the sum of all JCE-related mortality that occurs throughout juvenile development. Careful long-term measurements of inter-life history stage interactions are necessary to quantify the probability of conspecific recruitment. Meta-analyses such as Comita et al. (2014) indicate adult effects on conspecific seedlings are fairly strong. Song et al. (2021a), examining 52 tree species across latitudes, found that seedlings near conspecific adult trees experienced an average reduction in survivorship near 63% (Song et al. (2021a), Fig. 6). Alvarez-Loayza and Terborgh (2011) found that seeds and seedlings near adult trees experience nearly 100% mortality in an Amazonian forest. Overall, while estimates of a_{A} are inconclusive, it seems likely that JCEs are often strong enough to stabilize large fitness differences if they occur on a sufficiently large spatial scale and predation is additive.

Determining the spatial scale of specialized predation requires accurately quantifying v (or r) and g (tree density). Hubbell et al. (2001) found that negative density-dependent effect lost significance ~ 15 meters away from adult trees at BCI (although negative effects were measured up to 30 meters away) and Comita et al. (2010) measured a parameter similar to v,

for which the best and second best fits were equal to 5 and 10, respectively (as noted earlier). While more measurements are warranted, these results point toward an intermediate value of v, for which the AD model can maintain moderately high species richness, at least in tropical communities such as BCI (Figs 2.2-2.3, Appendix A7, 2.40-2.41).

The effective spatial scale over which JCEs operate is determined by the interaction of v and density (g). If individuals are tightly packed in space (high g), predation extending a modest distance affects many patches. Consistent with this, lower species richness is maintained when models are parameterized with lower g (Appendix A7, Fig. 2.44). This suggests JCEs are more stabilizing in highly dense communities, consistent with the hypothesis that JCEs are particularly important in dense, species-rich tropical forests.

2.5.3 Limitations and future directions

Results are based on Ordinary Differential Equation (ODE) approximations of spatially explicit models. The ODEs examine deterministic coexistence, ignoring ecological drift. Although JCEs can stabilize against drift in otherwise neutral communities (Levi et al., 2019), inter-specific variation in fitness induces variance in species' equilibrium abundances, making weaker competitors more susceptible to stochastic extinction over long time periods (Nisbet and Gurney, 1982; Miranda et al., 2015). Similarly, this paper does not consider species immigration, which May et al. (2020) suggest can drown out the signal of JCEs.

The JCE functional form comparisons of this study depend on normalizations which have built-in assumptions. While these normalizations are biologically meaningful (Appendix A5), they are not the only feasible method by which they could be performed. A better understanding of the biological processes comprising JCEs would allow for more informed comparisons.

A major simplification of this study is that species are modeled identically except for intrinsic fitness (Y). However, life history traits such as shade tolerance and mycorrhizal

association affect which natural enemies attack specific host species (Jia et al., 2020) which likely determines species-specific natural enemy dispersal (v) and baseline predation strength (Zhu et al., 2018). Inter-specific variation in these traits can reduce species richness (Stump and Comita, 2018). v also likely depends on host organism size: the roots, leaf litter, and natural enemies of relatively large tree species are more likely to affect larger areas. Future models should better integrate JCEs into life history theory, building on the work of Stump and Comita (2020).

Similarly, adult density (g) was calculated by dividing the number of reproductive adults at the BCI forest plot ($\sim 86,000$) by its area (50 ha). This comprises disparate lifeforms, from shrubs to canopy trees. There are fewer canopy trees than smaller plants, yet canopy trees make up a considerable proportion of community DBH (diameter at 1.3 meters above ground; Comita et al., 2007). Therefore, g may be inflated for larger organisms. Conversely, while the calculation of g included only adults, density-dependent interactions occur at multiple life history stages. The BCI plot contains approximately $210,000$ stems with DBH$\geq$ 1cm and many more smaller seedlings (Condit et al., 2019) which also contribute to conspecific negative density effects (Comita et al., 2010; Zhu et al., 2015). These complications make g difficult to confidently parameterize when modeling only adult-offspring interactions. Future models should incorporate organism size structure and interactions between multiple plant life history stages.

Assessing the importance of JCEs also requires a better characterization of distance and density-dependent predation. A key factor to determine is the extent to which predation is additive. This paper examines when predation pressure is either non-additive or linearly additive, which represent two non-exhaustive baseline cases. Detto et al. (2019) found adult density effects on seedling survival to be additive, but sub-linearly so. Empirical research should emphasize measuring the precise functional form and theoretical studies should quantify the impact of sub-linear density effects on species richness.

2.5.4 Conclusion

Unraveling the importance of JCEs in species-rich communities remains a difficult empirical and theoretical challenge. It is my hope that this paper will motivate more precise empirical measurements of the functional form of specialized predation and motivate theoreticians to more critically examine how modeling assumptions affect distance and density dependent processes.

2.6 Acknowledgments

I acknowledge support from National Science Foundation grants NSF DGE 1735359 and the NSF OCE 1851489. I thank J. Timothy Wootton, Catherine A Pfister, Mercedes Pascual, Trevor Price, the Wootton-Pfister lab, and Inés Moldavsky for insightful discussion, helpful comments, and feedback on the manuscript. I also thank Helene Muller-Landau and three anonymous reviewers whose comments greatly improved the manuscript.

Appendix A

Appendix A.1: Non-additive−Fixed-distance model SEM and ODE approximation

Introduction

In this Appendix, I derive and analyze the non-additive−Fixed-distance (NF) model from the main text. This Appendix is composed of three sections: **(1)** I introduce a spatially explicit model (SEM) for the NF model. Then, I demonstrate that taking the expected offspring abundances on each patch yields the Ordinary Differential Equation (ODE) model discussed in the main text. **(2)** To asses the accuracy of the ODE approximation, I provide outputs of the ODE model and the SEM model under identical parameterizations. I show the outputs are highly similar, hence demonstrating that the ODE is a sufficiently accurate approximation of the SEM. **(3)** I provide the derivation of the approximate invasion criteria of the NF model.

SEM and derivation of ODE approximation

In this section, I assume the reader is generally familiar with the model discussed in the main text. First, I discuss the SEM, briefly reviewing within-patch dynamics. Then, I show the derivation of the ODE approximation.

Spatially Explicit Model (SEM)

Using the methods similar to recent JCH-type models (Levi et al., 2019; Chisholm and Fung, 2020) I developed a spatially explicit model. The model depicts a community with M total patches modeled as an $L \times L$ grid ($L \times L = L^2 = M$). A torus was used to avoid edge effects. A single tree is present on every patch of the torus. At each time-step, each tree dies with probability δ. Tree replacements occur via a lottery model determined by the relative abundances of offspring of each species on each patch. As noted in the main text, offspring abundances are defined by

$$\begin{aligned} S_{i,i}(x) &= Y_i\big[(1-D) + p_i D\big] J_{i,i}(x) \\ S_{i,k}(x) &= Y_i p_i D J_{i,k}(x) \\ S_{all,i}(x) &= \sum_{n=1}^{N} S_{n,i}(x) \end{aligned} \tag{2.11}$$

where $S_{A,B}(x)$ is the offspring abundance of species A on a patch occupied by species B at location x, $J_{i,i}(x)$ and $J_{i,k}(x)$ are how JCEs affect offspring surivorship, p_i is the proportion of species i in the population, Y_i is the intrinsic fitness of species i, and D is the dispersal proportion. For the NF model, I consider when JCEs kill a fixed proportion of a species' offspring on the nearest E_F patches as defined by the Moore neighborhood surrounding the patch. $E_F = 9$ indicates a 3×3 Moore neighborhood, $E_F = 25$ indicates a 5×5 Moore neighborhood, and $E_F = 49$ indicates a 7×7 Moore neighborhood, etc. Then,

$$\begin{aligned} J_{i,i}(x) &= e^{-a_i} \\ J_{i,k}(x) &= \begin{cases} 1, & \text{if } i \notin E_F \\ e^{-a_i}, & \text{if } i \in E_F \end{cases} \end{aligned} \tag{2.12}$$

This yields the following offspring abundances:

$$
\begin{aligned}
S_{i,i}(x) &= Y_i\big[(1-D)+p_iD\big]e^{-a} \\
S_{i,k}(x) &= \begin{cases} Y_iDp_i, & \text{if } i \notin E_F \\ Y_iDp_ie^{-a}, & \text{if } i \in E_F \end{cases} \\
S_{all,i}(x) &= Y_i\big[(1-D)+p_iD\big]e^{-a} + D\sum_{k\in E_F} Y_kp_ke^{-a} + D\sum_{j\notin E_F} Y_jp_j
\end{aligned}
\tag{2.13}
$$

$i \in E_F$ is the condition that an adult of species i is within the Moore neighborhood around a patch occupied by species k and $i \notin E_F$ is the condition an adult is not within the Moore neighborhood around a patch occupied by species k ($k \neq i$). Noting that I use the notation $\in E_F$ rather than $\in r$, as I do in the main text. This is simply to emphasize that the SEM uses a discrete lattice to model the area of effect, but these two notations can be used interchangeably. $E_F = \pi r^2 g$ where g is tree density in individuals per square meters. To examine parameterizations of the SEM in terms of r, values of r must be selected such that they correspond to viable Moore neighborhood values (such that $E_F = \pi r^2 g = 9$, 25, 49, etc.).

Tree replacement is determined by a lottery model. Let $P_{A,B}(x)$ be the probability species A colonizes a patch previously occupied by species B on patch x. Then, $P_{i,i}(x) = S_{i,i}(x)/S_{all,i})x)$ and $P_{i,k}(x) = S_{i,k}(x)/S_{all,k}(x)$.

Ordinary Differential Equation (ODE) Model

To derive the ODE model, I take approximations of the expected values of $P_{i,i}(x)$ and $P_{i,k}(x)$. To do so, I take the expected abundance of $S_{i,i}(x)$, $S_{i,k}(x)$, and $S_{all,i}(x)$ and then take their quotients. Expectations are taken with respect to space. Using this, I derive the the ODE

approximation

$$\frac{dp_i}{dt} = \delta\left[\frac{\mathbb{E}[S_{i,i}(x)]}{\mathbb{E}[S_{all,i}(x)]}p_i + \sum_{k\neq i}\frac{\mathbb{E}[S_{i,k}]}{\mathbb{E}[S_{all,k}(x)]}p_k - p_i\right] \tag{2.14}$$

that captures the behavior of the SEM. See "Note" at the end of this Appendix for additional information about the assumptions of this approximation.

The SEM incorporates JCEs based on the nearest E_F neighbors of each patch that, computationally, are stored in a matrix. In contrast, the deterministic ODE model is spatially implicit. Therefore, it is necessary to use an approximation of the terms that does not require spatial information. With this in mind, the quantity $S_{i,k}(x)$ must be approximated as a spatially implicit term. I accomplish this by taking the expected offspring abundance on each patch. Note that by the linearity of expectation,

$$\begin{aligned}\mathbb{E}[S_{all,i}(x)] &= \mathbb{E}\left[\sum_{n=1}^{N} S_{n,i}(x)\right] \\ &= \mathbb{E}\left[S_{i,i}(x) + \sum_{n\neq i}^{N} S_{n,i,x}\right] \\ &= \mathbb{E}[S_{i,i}(x)] + \sum_{n\neq i}\mathbb{E}\left[S_{n,i}(x)\right]\end{aligned} \tag{2.15}$$

Additionally, $\mathbb{E}[S_{i,i}(x)]$ does not contain spatial information, as $\mathbb{E}[S_{i,i}(x)] = \mathbb{E}[Y_i\big[(1-D) + p_iD\big]e^{-a}] = Y_i\big[(1-D)+p_iD\big]e^{-a}$. Therefore, it suffices to calculate the expectation of $S_{i,k}(x)$, from which the other terms of interest (i.e. $\mathbb{E}[S_{all,k}(x)]$) can be calculated.

The expected offspring abundance of species i on a given patch is equal to the number of offspring it would have given it is not affected by JCEs multiplied the probability it does not experience JCEs added to the number of offspring it would have given it experiences JCEs multiplied the probability it does experience JCEs:

$$\mathbb{E}[S_{i,k}(x)] = \mathrm{P}[i \notin E_F] \times S_{i,k}^{i\notin E_F}(x) + \mathrm{P}[i \in E_F] \times S_{i,k}^{i\in E_F}(x) \tag{2.16}$$

Here, I again define E_F. As noted in the main text, if the neighborhood is of radius r meters and trees are of density g individuals per square meter, there will be on average $g\pi r^2$ individuals within the neighborhood defined by r. Therefore, $E_F = g\pi r^2$.

The calculation of $\mathbb{E}[S_{i,k}(x)]$ is as follows. Consider a single patch occupied by species k. It is necessary to calculate the probability an adult of species i is within E_F. Recall p_i be the proportion of species i in the population. Assuming species are approximately randomly distributed, the probability that a conspecific is within the radius r of a random patch can be captured with a 2D Poisson process (i.e. a spatial Poisson process) with a rate parameter of $\lambda = p_i g$. The waiting time of first event of a 2D Poisson process is exponentially distributed such that

$$\mathrm{P}[i \notin E_F] = e^{-\lambda \mathrm{A}} \tag{2.17}$$

where A is the area of the circle of radius r stemming from the focal patch. Therefore $\mathrm{A} = \pi r^2$ and $\lambda A = p_i g \pi r^2$ such that

$$\begin{aligned} \mathrm{P}[i \notin E_F] &= e^{-p_i g \pi r^2} \\ \mathrm{P}[i \in E_F] &= 1 - e^{-p_i g \pi r^2} \end{aligned} \tag{2.18}$$

Additionally, as defined by equation (A.3), $S_{i,k}^{i \notin E_F}(x) = Y_i p_i D$ and $S_{i,k}^{i \in E_F}(x) = Y_i p_i D e^{-a}$. Letting $g\pi r^2 = E_F$ and using the above probabilities, the expected offspring value of $S_{i,k}(x)$ is:

$$\begin{aligned} \mathbb{E}[S_{i,k}(x)] &= \mathrm{P}[i \notin E_F] \times S_{i,k}^{i \notin E_F}(x) + \mathrm{P}[i \in E_F] \times S_{i,k}^{i \in E_F}(x) \\ &= Y_i p_i D\big[e^{-p_i E_F} + e^{-a}(1 - e^{-p_i E_F})\big] \end{aligned} \tag{2.19}$$

Plugging this value into the offspring abundance terms yields

$$\begin{aligned}\mathbb{E}[S_{i,i}(x)] &= Y_i\big[(1-D)+p_iD\big]e^{-a}\\ \mathbb{E}[S_{i,k}(x)] &= Y_ip_iD\big[e^{-p_iE_F}+e^{-a}(1-e^{-p_iE_F})\big]\end{aligned} \tag{2.20}$$

noting that $S_{all,i}(x) = \sum_{n=1}^{N} S_{n,i}(x)$. These equations are identical to the offspring abundance equations for the NF model in the main text.

Comparison between ODE model and SEM

In this section, I describe simulations that compare the ODE model to the SEM. Results show that the SEM and ODE models yield highly similar outputs of species abundance and species richness.

ODE and SEM parameterization

Each SEM simulation began with 300 species at equal abundance, with individuals randomly distributed throughout the community. Simulations were conducted on a 275×275 torus (thus containing 275^2 individual trees). I use the following parameters: $Y \sim \text{lognormal}[\mu = 0, \sigma_Y]$ with $\sigma_Y \sim \{0.1, 0.45, 0.8\}$ and $a \sim \{0.5, 1.0, 2.75, 4.5\}$. In all simulations, $D = 1$. I tested each of the 12 parameter combinations of σ_Y and a with $E_F = 9$, 25, 49, 81, and 121. This corresponds to examining a range of r approximately between 4 and 14 (assuming $g = 0.2$). This generated 60 outputs. Simulations were run for about 75 generations, sufficient time for the community to approximately reach equilibrium without drift dominating the dynamics of the lower abundance species. However, it was noticed that the cases in which $\sigma_Y = 0.1$ had longer transient dynamics. These were run for 150 generation instead. See Figs. 2.11-2.13 for examples of the transient dynamics.

I then ran a set of ODE simulations using the same parameterizations as the SEM. I compared the outputs of the SEM and ODE model in terms of species diversity, species

abundance, and Shannon diversity. I considered a species to be extinct if it had less than 1 individual at any point of the simulation. This was implemented directly in the SEM; for the ODE model, I assumed a species, i, to be extinct if $p_i^* < 1/275^2$ where p_i^* is the equilibrium proportion of species i. Note that these simulations do not attempt to demonstrate the long-term resistance against extinction due to drift. Rather, they demonstrate that the ODE model and SEM yield similar outputs of expected species abundance and richness given the same parameterization.

Results of comparison

The ODE model and SEM yielded very similar results in species richness and Shannon diversity (Figs. 2.6, 2.7). The ODE model and SEM also produced very similar species proportions (Figs. 2.8-2.10). To quantify the quality of the approximation, I calculated the mean difference in species richness between the ODE model and SEM, ΔR:

$$\Delta R = \frac{1}{S}\sum_{k=1}^{S}(R_{\text{SEM}}^k - R_{\text{ODE}}^k) \tag{2.21}$$

where S is the number of simulations, and R_{SEM}^k and R_{ODE}^k are the species diversity of the k_{th} simulation of the SEM and ODE model, respectively. I also examined the r^2 (coefficient of determination) between SEM and ODE diversity. For the comparisons, $\Delta R = 1.6$ and $r^2 = 0.987$. Overall, the ODE provides a highly similar, albeit non-exact, estimation of species diversity. Cases in which the ODE model predicted lower species richness are likely due to incomplete transient dynamics of the SEM.

Derivation of invasion criteria

In this section, I derive the approximate invasion criteria of the fixed neighborhood effect model when species experience inter-specific variation in intrinsic (Y) and $D = 1$. The

invasion criteria of an invader can be expressed as when the per capita growth rate as $p_i \to 0$. Letting

$$\mathbb{E}[J_{k,i}(x)] = e^{-p_k E_F} + e^{-a}(1 - e^{-p_k E_F}) \tag{2.22}$$

The per capita growth rate of species i, substituting in the offspring abundance values, is

$$\begin{aligned}\frac{1}{p_i}\frac{dp_i}{dt} = r_i = \delta\Bigg[&\frac{Y_i\big[(1-D)+p_iD\big]e^{-a}}{Y_i\big[(1-D)+p_iD\big]e^{-a} + \sum_{k\neq i} Y_k p_k D\,\mathbb{E}[J_{k,i}(x)]} \\ &+ Y_i D \sum_{m\neq i} \frac{1}{Y_m e^{-a}\big[(1-D)+p_mD\big] + \sum_{k\neq m} Y_k p_k D\,\mathbb{E}[J_{k,m}(x)]} p_m - 1\Bigg]\end{aligned} \tag{2.23}$$

Species i can invade is this quantity if positive when it is rare ($p_i \to 0$). When $D = 1$ (the case of interest), the above reduces to

$$Y_i \sum_{m\neq i} \frac{p_m}{Y_m e^{-a} p_m + \sum_{k\neq m} Y_k p_k\,\mathbb{E}[J_{k,m}(x)]} > 1 \tag{2.24}$$

To simplify the above equation, I ignore the term $Y_m e^{-a} p_m$ in the denominator and incorporate an additional term the summation, yielding:

$$Y_i \sum_{m\neq i} \frac{p_m}{\sum_{k\neq i} Y_k p_k\,\mathbb{E}[J_{k,i}(x)]} > 1 \tag{2.25}$$

This simplification is equivalent to making the species identity of the tree previously occupying a patch (the tree that dies) irrelevant (i.e., JCEs only result from trees nearby the patch rather than the previous occupant of the patch). As long as neighborhood effects are somewhat strong – that is, so long as E_F is not very small – this assumption should not meaningfully affect the invasion criteria.

Importantly, the denominator of Equation (2.25) is no longer directly dependent on m.

That is, Equation (2.25) can be rewritten as

$$Y_i\Big(\sum_{m\neq i} p_m\Big)\Big(\frac{1}{\sum_{k\neq i} Y_k p_k\,\mathbb{E}[J_{k,i}(x)]}\Big) > 1 \tag{2.26}$$

Because, by definition, $\sum_{m\neq i} p_m = 1$, the above equation can be rewritten as

$$Y_i > \sum_{k\neq i} Y_k p_k\,\mathbb{E}[J_{k,i}(x)] \tag{2.27}$$

Substituting the appropriate value for $\mathbb{E}[J_{k,i}(x)]$, the invasion criteria becomes

$$Y_i > \sum_{k\neq i} Y_k p_k\big(1-(1-e^{-a})(1-e^{-p_k E_F})\big) \tag{2.28}$$

noting that the above equation has been slightly rearranged, but is the same as equation (2.22). I then take the linearization of $p_k\Big(1-(1-e^{-a})(1-e^{-p_k E_F})\Big)$ around the point $1/N$ where N is the number of species in the resident community yields a close approximation of the expression so long as variation in p_k does not span values much greater than $1/N$ (mean community abundance). Then,

$$\begin{aligned} p_k\Big(1-(1-e^{-a})(1-e^{-p_k E_F})\Big) \approx & \frac{1}{N}\Big(1-(1-e^{-a})\big(1-e^{-\frac{E_F}{N}}\big)\Big)+ \\ & \Big(e^{-\frac{E_F}{N}}\left(1-e^{-a}\right)\left(1-\frac{E_F}{N}\right)+e^{-a}\Big)\Big(p_k-\frac{1}{N}\Big) \end{aligned} \tag{2.29}$$

Substituting this into the equation, the summation (the right hand side of the invasion

criteria) can be rearranged and broken into two into three summations:

$$\frac{1}{N}\left(1-(1-e^{-a})(1-e^{-\frac{E_F}{N}})\right)\sum_{k\neq i}Y_k+\left(e^{-\frac{E_F}{N}}\left(1-e^{-a}\right)\left(1-\frac{E_F}{N}\right)+e^{-a}\right)\sum_{k\neq i}Y_k p_k- \left(e^{-\frac{E_F}{N}}\left(1-e^{-a}\right)\left(1-\frac{E_F}{N}\right)+e^{-a}\right)\frac{1}{N}\sum_{k\neq i}Y_k \tag{2.30}$$

The first and third summations are trivial to evaluate:

$$\frac{1}{N}\left(1-(1-e^{-a})(1-e^{-\frac{E_F}{N}})\right)\sum_{k\neq i}Y_k=\left(1-(1-e^{-a})(1-e^{-\frac{E_F}{N}})\right)\overline{Y} \tag{2.31}$$

and

$$\left(e^{-\frac{E_F}{N}}\left(1-e^{-a}\right)\left(1-\frac{E_F}{N}\right)+e^{-a}\right)\frac{1}{N}\sum_{k\neq i}Y_k=\left(e^{-\frac{E_F}{N}}\left(1-e^{-a}\right)\left(1-\frac{E_F}{N}\right)+e^{-a}\right)\overline{Y} \tag{2.32}$$

where $\overline{Y}$ is the mean fitness of the resident community.

The second summation can be evaluated by using the property

$$\frac{1}{N}\sum_{m=1}^{N}A_m B_m=\overline{A}\times\overline{B}+\mathrm{Cov}(A,B) \tag{2.33}$$

I apply this property with respect to p and Y, noting that $\overline{p}=\frac{1}{N}$. Using this property and substituting A and B with p and Y. Doing this yields:

$$\left(e^{-\frac{E_F}{N}}\left(1-e^{-a}\right)\left(1-\frac{E_F}{N}\right)+e^{-a}\right)\sum_{k\neq i}Y_k p_k = \left(e^{-\frac{E_F}{N}}\left(1-e^{-a}\right)\left(1-\frac{E_F}{N}\right)+e^{-a}\right)\left[\overline{Y}+N\ \mathrm{Cov}(p,Y)\right] \tag{2.34}$$

noting that $\overline{p}=1/N$.

Adding all three sums together, equation (2.32) and the $\overline{Y}$ term from equation (2.34) will cancel. Then, after some rearranging, the invasion criteria becomes

$$Y_i > \underbrace{\overline{Y}\left(1-\left(1-e^{-a}\right)\left(1-e^{\frac{-E_F}{N}}\right)\right)}_{\substack{\text{mean} \\ \text{JCE-fitness term}}} + \underbrace{N\text{Cov}(p,Y)\left(e^{-\frac{E_F}{N}}\left(1-e^{-a}\right)\left(1-\frac{E_F}{N}\right)+e^{-a}\right)}_{\text{covariance-JCE term}} \tag{2.35}$$

which is the same as the corresponding equation in Table 2.1 of the main text.

Note on ODE approximation

To derive the ODE model, I took approximations of the expected values of $P_{i,i}(x)$ and $P_{i,k}(x)$. To do so, I took the expected abundance of $S_{i,i}(x)$, $S_{i,k}(x)$, and $S_{all,i}(x)$ with respect to space and then examined their quotients. Note that this assumes $\mathbb{E}[S_{i,k}(x)/S_{all,i}(x)] \approx \mathbb{E}[S_{i,k}(x)]/\,\mathbb{E}[S_{all,k}(x)]$ (I take the expectation of the numerator and denominator and then take the quotient). Using a Taylor Expansion about the mean,

$$\mathbb{E}\left[\frac{S_{i,k}(x)}{S_{all,i}(x)}\right] \approx \frac{\mathbb{E}[S_{i,k}(x)]}{\mathbb{E}[S_{all,k}(x)]} - \frac{\text{Cov}\big(S_{i,k}(x),S_{all,k}(x)\big)}{\mathbb{E}[S_{all,k}(x)]^2} + \text{Var}\big(S_{all,k}(x)\big)\frac{\mathbb{E}[S_{i,k}(x)]}{\mathbb{E}[S_{all,i}(x)]^3}$$

Because there are many species in the community, $S_{all,i}(x) >> S_{i,k}(x)$. This implies that the covariance term and the term containing $\mathbb{E}[S_{all,i}(x)]^3$ are close to zero. Additionally, $\text{Var}\big(S_{all,i}(x)\big)$ is likely small because it is assumed that dispersal is uniform across the community. Therefore, $\mathbb{E}[S_{i,k}(x)/S_{all,i}(x)] \approx \mathbb{E}[S_{i,k}(x)]/\,\mathbb{E}[S_{all,k}(x)]$ is likely a good approximation. I rely on the quantitative similarity of the SEM and ODE model to validate this assumption.

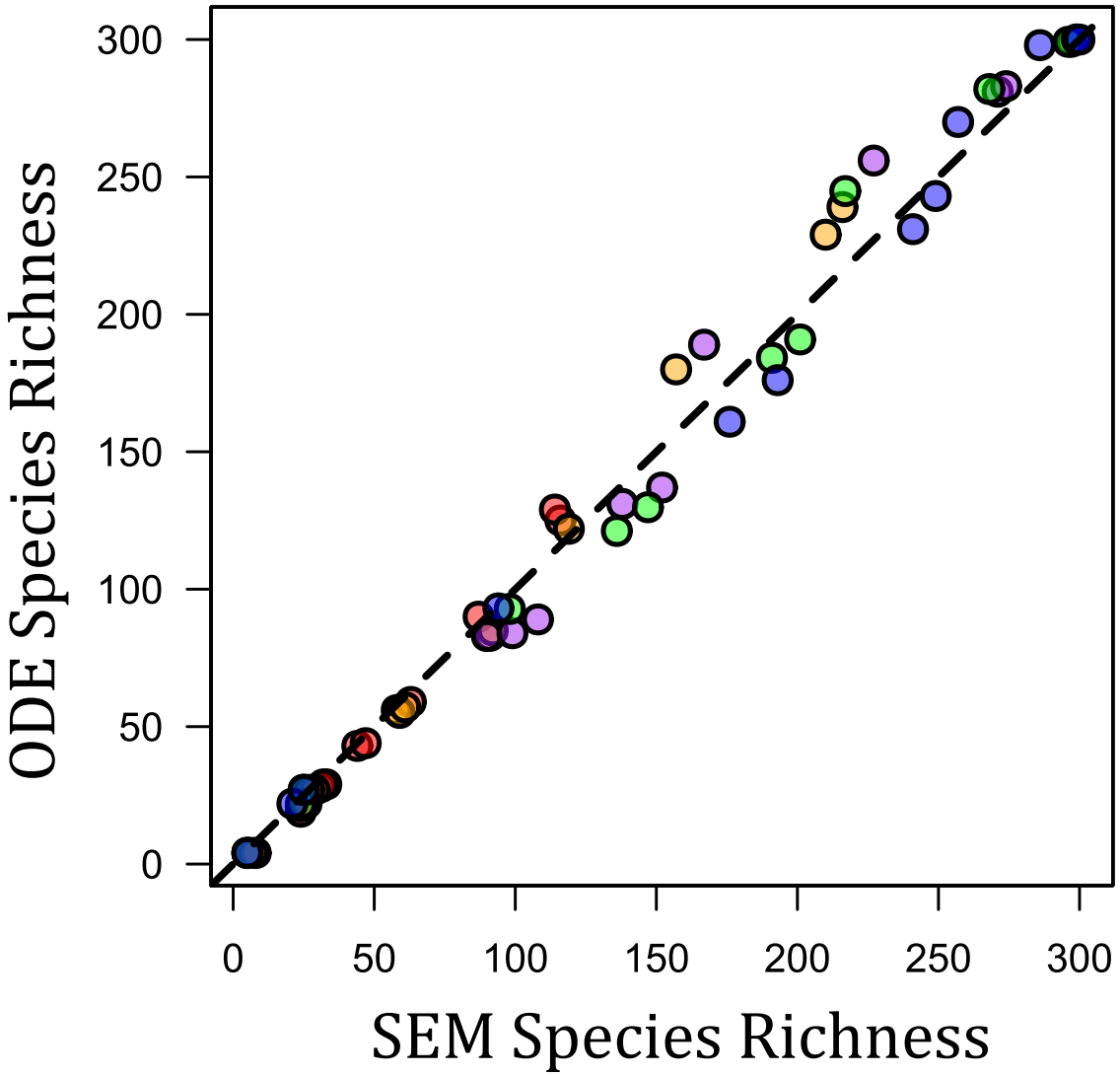

Figure 2.6: ODE model validation. The figures compare species richness between SEM and ODE model simulations under identical parameterizations. The dashed line is the one-to-one line (points on the line represent when the SEM and ODE yield the exact same diversity output). Red points are when $E_F = 9$, orange/yellow points are when $E_F = 25$, purple points are when $E_F = 49$, green points are when $E_F = 81$, and blue points are when $E_F = 121$. To a first approximation, the ODE model yields the same output as the SEM. These parameter values span the most of the parameter space explored in Figs. 2.2 and 2.3 of the main text.

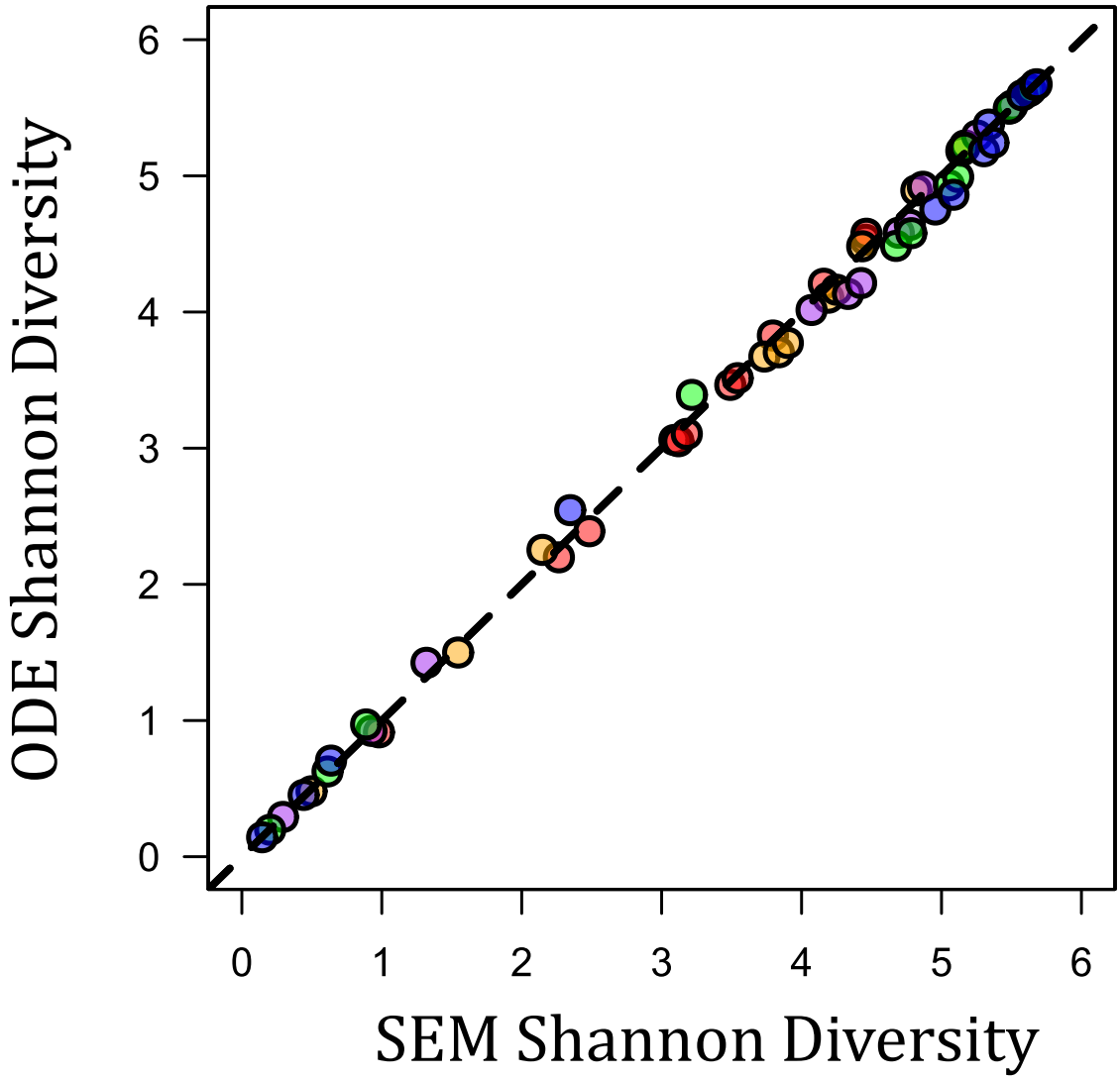

Figure 2.7: The same as the fig. 2.6, but showing Shannon Diversity instead of species richness. As in the above case, the SEM and ODE model yield very similar outputs.

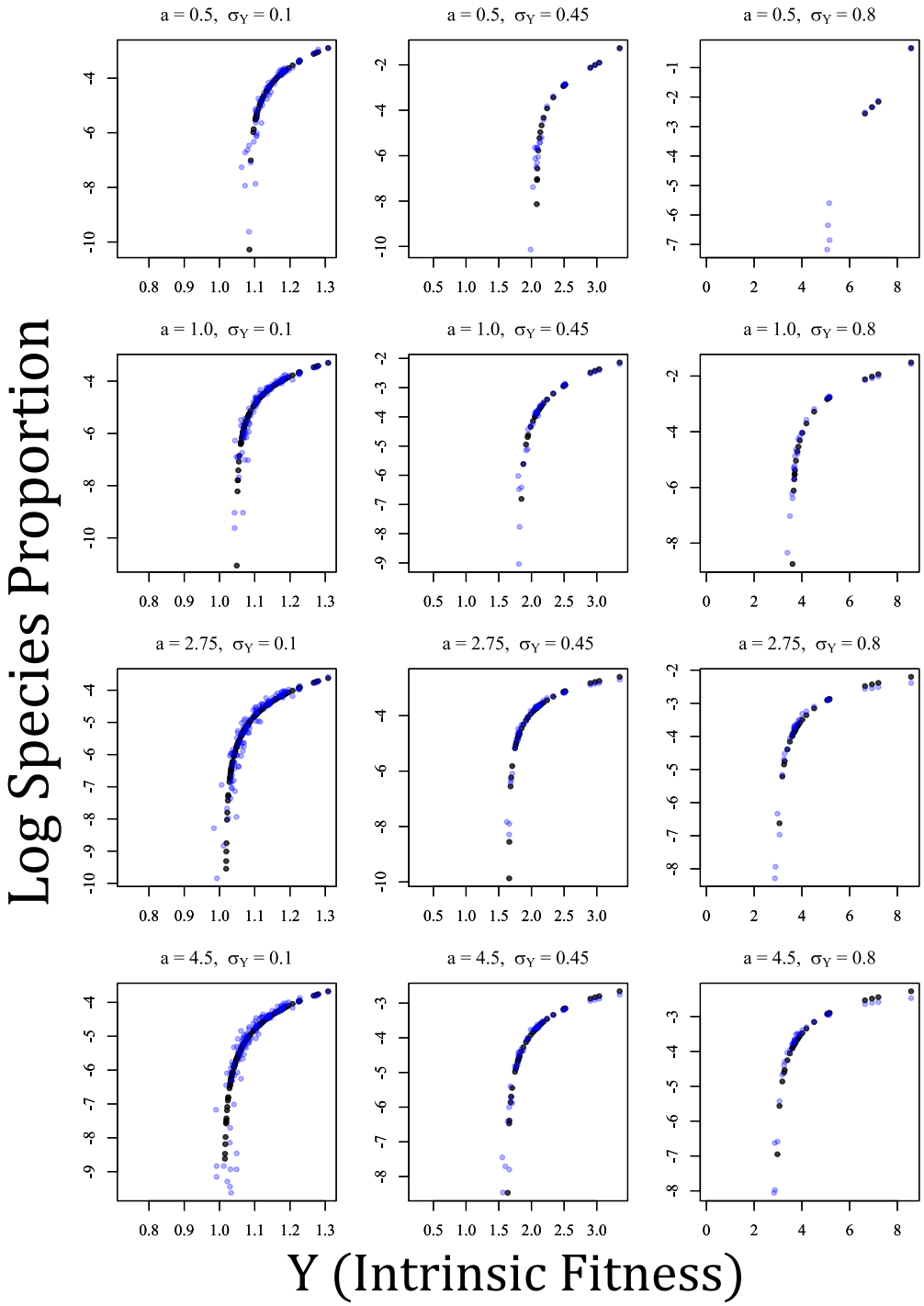

Figure 2.8: Comparisons between identical parameterizations of the ODE approximation (black) and SEM (blue) outputs under twelve parameter values when species vary in intrinsic fitness (Y). The y-axis depicts the log-proportion of each species and the x-axis depicts Y of each species. In all plots, $E_F = 9$, and $D = 1.0$. Other relevant parameters are listed on each plot.

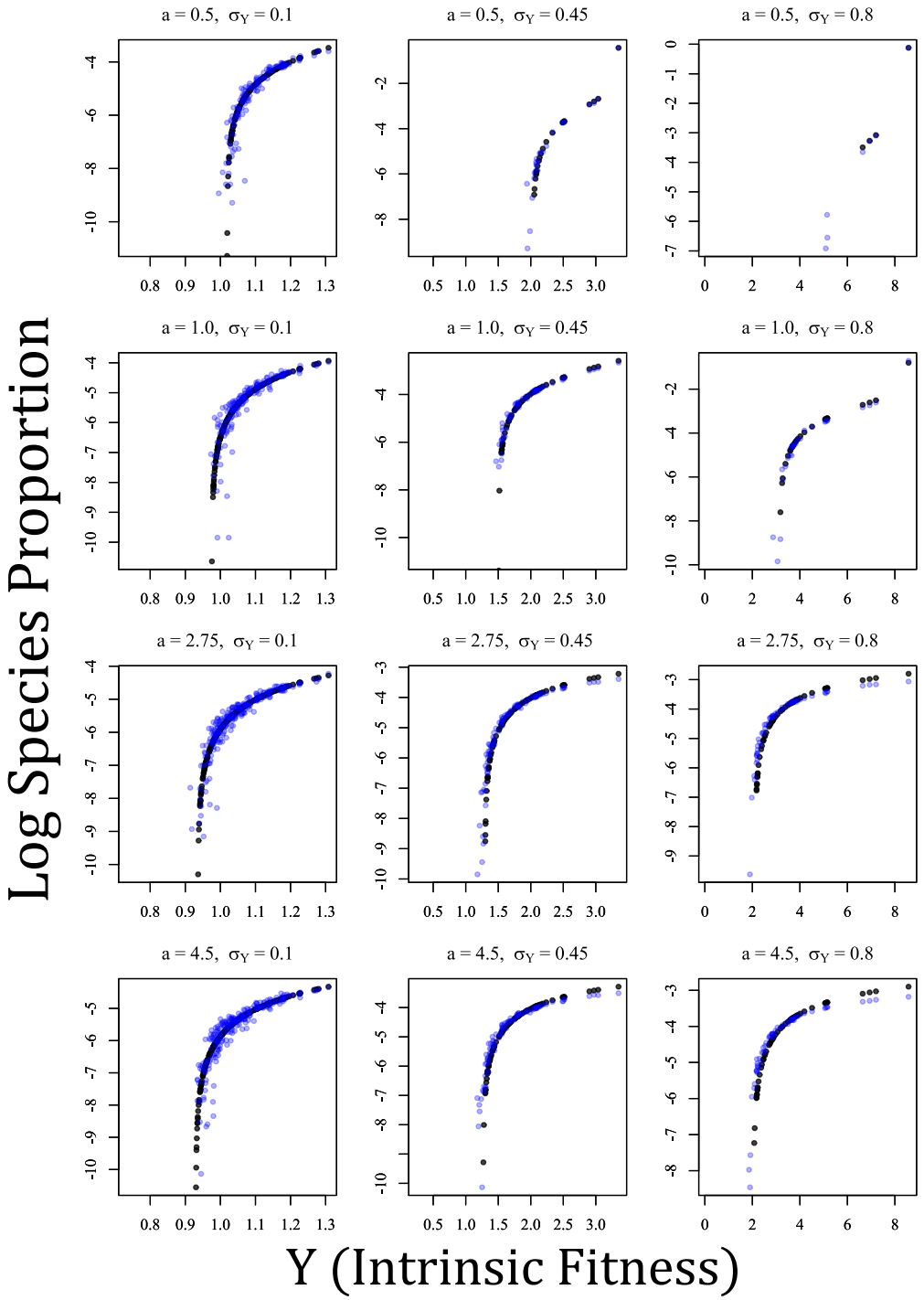

Figure 2.9: The same format as fig. 2.8, but with $E_F = 25$.

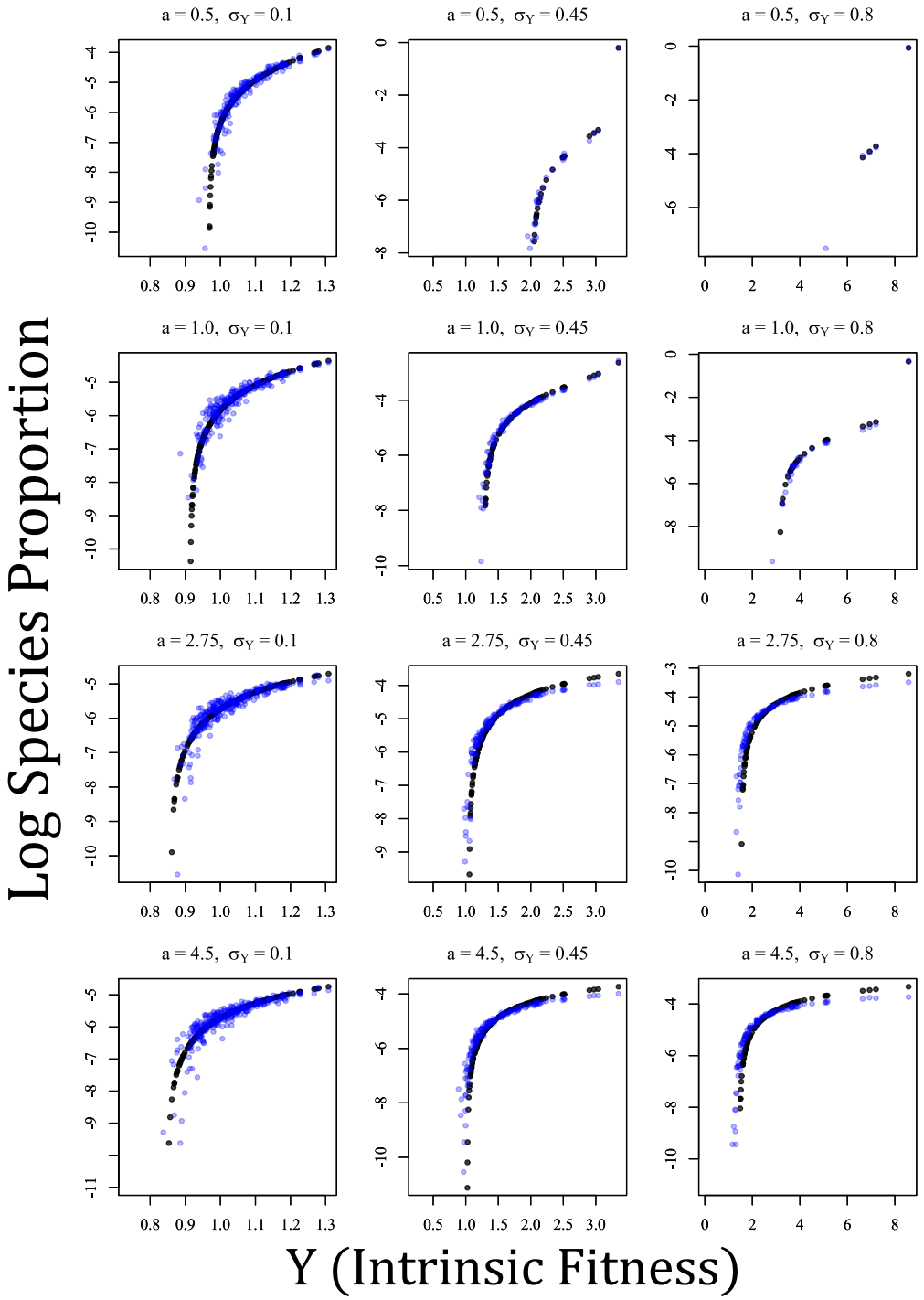

Figure 2.10: The same format as fig. 2.8, but with $E_F = 49$.

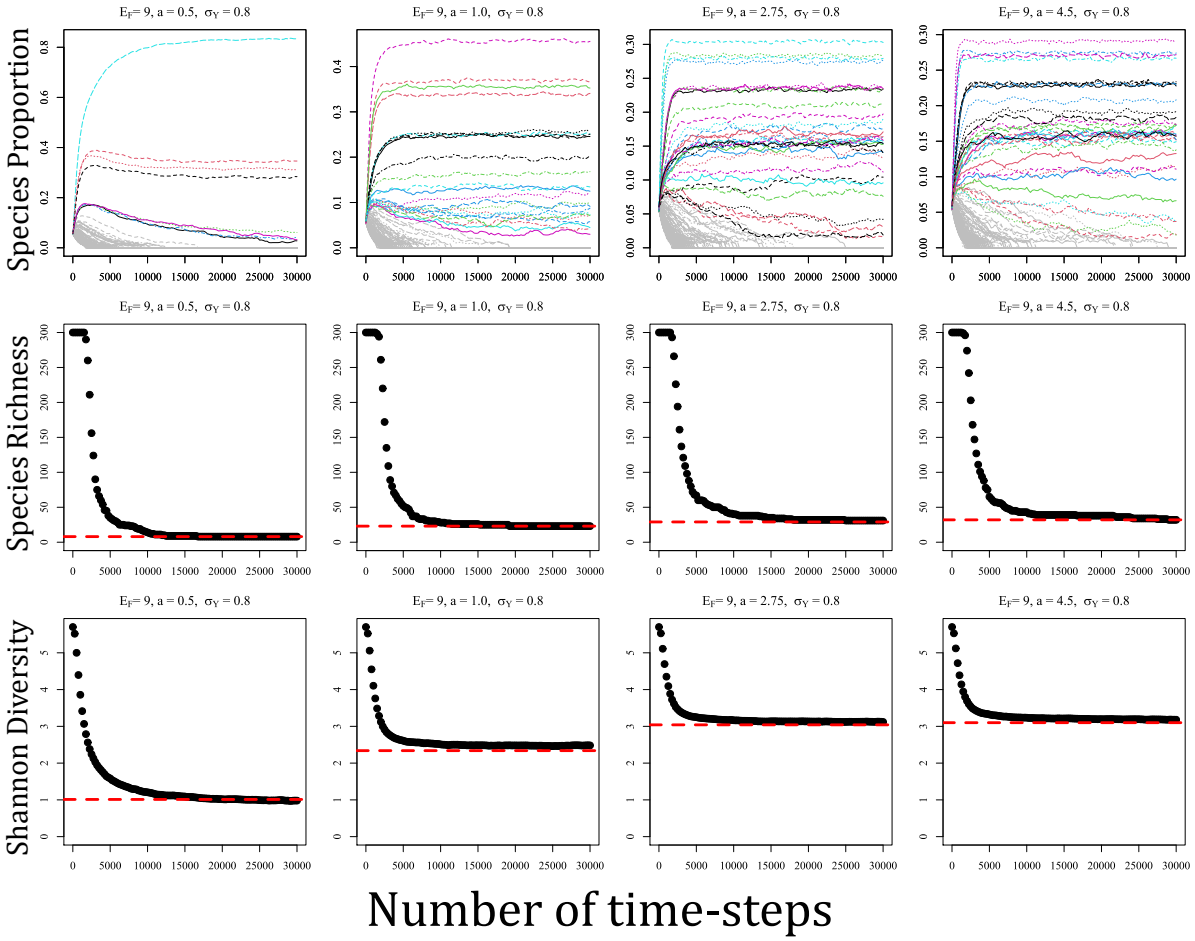

Figure 2.11: Examples of the SEM simulation time series outputs, species richness over time in the simulations, and Shannon diversity over time in the simulations. The top row shows examples of the time series outputs of the SEMs. The x-axis is time and the y-axis is each species' proportion. Proportions have been square-root transformed to aid visualization. Colored trajectories indicate species that persisted throughout the simulation; grey trajectories indicate species that went extinct. Parameters are listed on each plot. Dynamics as shown are typical examples from the SEMs. Most species settle into a relatively stable pseudo-equilibrium, while lower abundance species fluctuate due to drift. The second row shows the number of persisting species in the community as a function of time. Each panel corresponds to the plot above it. Most species that go extinct do so in the early stages of the dynamics. Therefore, the vast majority of persisting species likely persist deterministically. The dashed red line is the diversity maintained by the ODE under the same parameterization. All SEMs saturate, approximately, to the dashed line. The third row is the same as the second row, except it shows Shannon diversity instead of species richness.

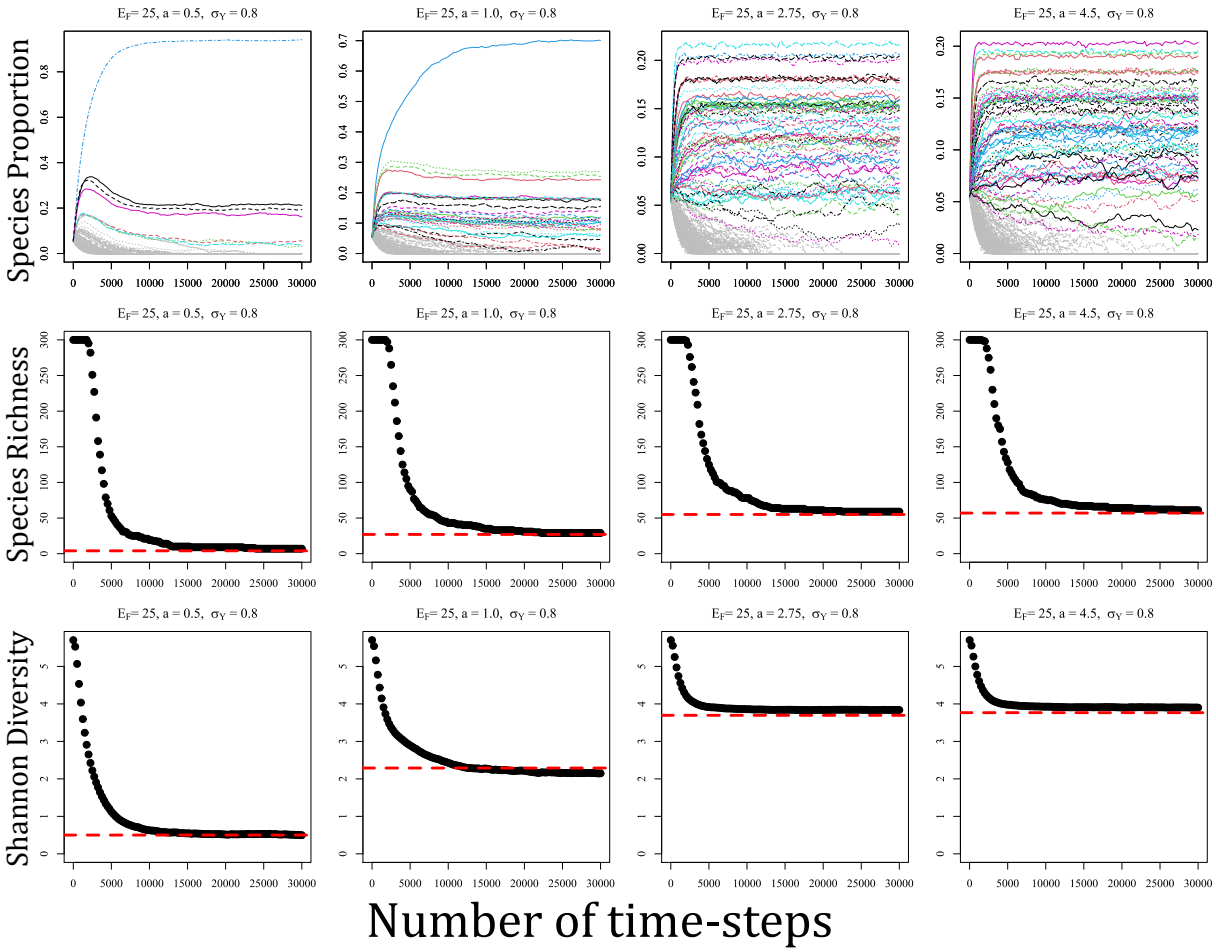

Figure 2.12: The same format as fig. 2.11, but with $E_F = 25$.

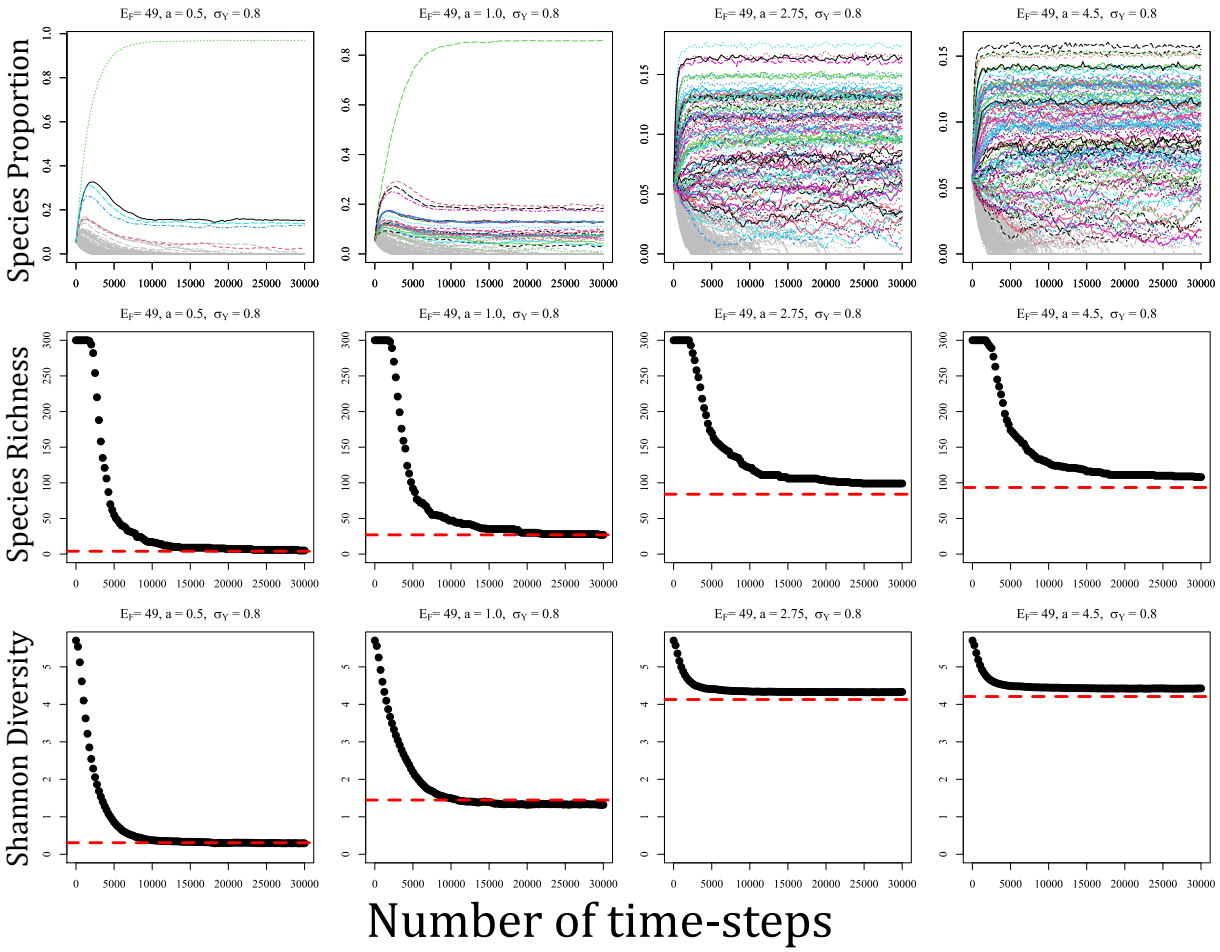

Figure 2.13: The same format as fig. 2.11, but with $E_F = 49$.

Appendix A.2: Additive−Fixed-distance model SEM and ODE approximation

Introduction

In this Appendix, I analyze the Additive−Fixed-distance (AF) model presented in the main text. This Appendix is composed of three main subsections: **(1)** I introduce a spatially explicit model (SEM) of the AF model. I then demonstrate that taking the expected offspring abundances on each patch yields the ODE model discussed in the main text. **(2)** I provide outputs of the ODE model and the SEM model under the same parameterizations. I show the outputs are very similar, hence demonstrating that the ODE is a sufficiently accurate approximation of the SEM. **(3)** I provide the derivation of the invasion criteria approximation of the AF model.

SEM and derivation of ODE approximation

In this subsection, I discuss the SEM, briefly reviewing within-patch dynamics from the main text. Then, I show the derivation of the ODE approximation. I assume the reader is generally familiar with the model discussed in the main text.

SEM

I developed a spatially explicit model (SEM) that integrates the AF model. The model consists of a community on a grid of $L \times L$ patches (M total patches, $M = L^2$) modeled as a torus to avoid edge effects. A single tree is present on every space on the grid. At each time step, each tree dies with probability δ and tree replacements occur via a lottery model based on the relative abundance of offspring of each species on each patch. For the AF model, predation pressure increases linearly as a function of local conspecific density and occurs within a fixed area surrounding each tree (as decried in the main text). As noted in

the main text, offspring abundances are defined by

$$\begin{aligned} S_{i,i}(x) &= Y_i\big[(1-D)+p_i d\big]J_{i,i}(x) \\ S_{i,k}(x) &= Y_i p_i D J_{i,k}(x) \\ S_{all,i}(x) &= \sum_{n=1}^{N} S_{n,i}(x) \end{aligned} \tag{2.36}$$

where $S_{A,B}(x)$ is the offspring abundance of species A on a patch occupied by species B at location x, $J_{i,i}(x)$ and $J_{i,k}(x)$ are how JCEs affect offspring surivorship, p_i is the proportion of species i in the population, Y_i is the intrinsic fitness of species i, and D is the dispersal proportion. For AF model,

$$\begin{aligned} J_{i,i}(x) &= \exp\bigg[-a\Big(1+\sum_{m\in r}\mathbb{1}_m(i)\Big)\bigg] \\ J_{i,k}(x) &= \exp\bigg[-a\sum_{m\in r}\mathbb{1}_m(i)\bigg] \end{aligned} \tag{2.37}$$

where $\mathbb{1}_k(i)$ is an indicator function for which

$$\mathbb{1}_m(i) = \begin{cases} 1, & \text{if } m = i \\ 0, & \text{if } m \neq i \end{cases} \tag{2.38}$$

in which case, the predation pressure is equal to the sum of individuals found within the effect area defined by r.

Offspring abundances are then determined by the following equations:

$$
\begin{aligned}
S_{i,i}(x) &= Y_i\big[(1-D)+p_iD\big]\exp\bigg[-a\bigg(1+\sum_{m\in r}\mathbb{1}_m(i)\bigg)\bigg] \\
S_{i,k}(x) &= Y_ip_iD\,\exp\bigg[-a\sum_{m\in r}\mathbb{1}_m(i)\bigg] \\
S_{all,i}(x) &= Y_i\big[(1-D)+Dp_i\big]\exp\bigg[-a\bigg(1+\sum_{m\in r}\mathbb{1}_m(i)\bigg)\bigg]+\sum_{k\neq i}Y_kp_kD\,\exp\bigg[-a\sum_{m\in r}\mathbb{1}_m(k)\bigg]
\end{aligned}
\tag{2.39}
$$

For the discrete grid cells, it makes more sense to think about the number of grid-cells that fall within r rather than r itself. Therefore, let E_F represent the number of patches that wall within an $n \times n$ Moore neighborhood around a focal tree (as would be contained within r). Thus, $E_F = \pi r^2 g$, where g is tree density in individuals per meters squared. Notably, for the SEM, values of r must be selected such that they correspond to viable Moore neighborhood values (such that $E_F = 9$, 25, 49, etc.). Technically, this is not exactly the same as the model described above (Moore neighborhoods are square rather than circular) but is essentially mathematically identical.

The lottery is determined by the relative seedling abundances. Let $P_{A,B}(x)$ be the probability species A colonizes a patch previously occupied by species B at location x. Then, $P_{i,i}(x) = S_{i,i}(x)/S_{all,i}(x)$ and $P_{i,k} = S_{i,k}(x)/S_{all,k}(x)$.

ODE Model

To derive the ODE model, I take approximations of the expected values of $P_{i,i}(x)$ and $P_{i,k}(x)$. To do so, I take the expected abundance of $S_{i,i}(x)$, $S_{i,k}(x)$, and $S_{all,i}(x)$ and then take their quotients. Expectations are taken with respect to space. Using this, I derive the the ODE approximation

$$
\frac{dp_i}{dt} = \delta\bigg[\frac{\mathbb{E}[S_{i,i}(x)]}{\mathbb{E}[S_{all,i}(x)]}p_i + \sum_{k\neq i}\frac{\mathbb{E}[S_{i,k}]}{\mathbb{E}[S_{all,k}(x)]}p_k - p_i\bigg] \tag{2.40}
$$

that captures the behavior of the SEM. See "Note" at the end of this Appendix for additional information about the assumptions of this approximation.

The additive predation function in the SEM is implemented spatially explicitly – the location of trees are, computationally, is stored in a matrix. The deterministic ODE model is implicit. Therefore, it is necessary to use an approximation of the terms that does not require spatial information. In particular, the quantity $S_{i,k}(x)/S_{all,k,x}$, which contains the term

$$\mathbb{E}[S_{i,k}(x)] = \exp\Big[- a \sum_{m \in r} \mathbb{1}_m(i) \Big] \tag{2.41}$$

This quantity must be approximated as a spatially implicit term.

Consider a single patch occupied by species k. It is necessary to calculate the expected predation experienced by species i given that the JCE effect radius is r. Recall that g is the density of trees in square meters, r is the distance in meters from the local patch that defines the effect area, and p_i is the proportion of species i in the population. Assuming trees are approximately randomly distributed, the number of trees of species i within r meters of the focal patch can be described by with a Poisson distribution with a rate parameter of $\lambda = \pi g r^2 p_i$. Then, letting X_i be the number of individuals of species i within r, the probability that there are m individuals of species i within radius r is

$$\mathrm{P}[X_i = m] = \frac{(\pi g r^2 p_i)^m}{m!} e^{-\pi g r^2 p_i}$$

Now, recalling that $E_F = \pi r^2 g$ and that offspring survival decreases exponentially with the number of conspecific adults falling within r, the expectation can be calculated as follows:

$$
\begin{aligned}
\mathbb{E}[S_{i,k}(x)] &= \mathbb{E}\left[\exp\left[-a\sum_{m=1}^{Mp_i}\mathbb{1}_m(i)\right]\right] \\
&= \sum_{m=0}^{\infty}\mathrm{P}(X_i=m)\times[\text{probability of survival given } X_i=m] \\
&= \sum_{m=0}^{\infty}\frac{(E_F p_i)^m}{m!}e^{-E_F p_i}e^{-a\,m} \\
&= e^{-E_F p_i}\sum_{m=0}^{\infty}\frac{(E_F p_i e^{-a})^m}{m!} \\
&= e^{-(1-e^{-a})p_i E_F}
\end{aligned}
\tag{2.42}
$$

Similarly,

$$
\begin{aligned}
\mathbb{E}[S_{i,i}(x)] &= \mathbb{E}\left[\exp\left[-a\left(1+\sum_{m=1}^{Mp_i}\mathbb{1}_{x_m^i}(r)\right)\right]\right] \\
&= e^{-a}\sum_{m=0}^{\infty}\mathrm{P}(X_i=m)\times[\text{probability of survival given } X_i=m] \\
&= e^{-a}\sum_{m=0}^{\infty}\mathrm{P}(X_i=m)e^{-am} \\
&= e^{-a}e^{-E_F p_i}\sum_{m=0}^{\infty}\frac{(E_F p_i e^{-a\,m})^m}{m!} \\
&= e^{-a}e^{-(1-e^{-a})p_i E_F}
\end{aligned}
\tag{2.43}
$$

Plugging these values value into the appropriated post-JCE offspring abundance terms yields

$$
\begin{aligned}
\mathbb{E}[S_{i,i}(x)] &= Y_i\big[(1-d)+dp_i\big]e^{-a}e^{-(1-e^{-a})p_i E_F} \\
\mathbb{E}[S_{i,k}(x)] &= Y_i d p_i e^{-(1-e^{-a})p_i E_F}
\end{aligned}
\tag{2.44}
$$

also noting that $S_{all,i}(x) = \sum_{n=1}^{N} S_{n,i}(x)$. This is identical to the relevant expression for the AF model in the main text.

Comparison between ODE model and SEM

In this subsection, I describe simulations that compare the ODE model to the SEM. I demonstrate that the SEM and ODE model highly similar species abundance and species richness outputs.

ODE and SEM parameterization

Each SEM simulation began with 300 species at equal abundance, with individuals randomly distributed throughout the community. Simulations were conducted on a 275×275 torus (thus containing 275^2 individual trees). I use the following parameters: $Y \sim \text{lognormal}[\mu = 0, \sigma_Y]$ with $\sigma_Y \sim \{0.1, 0.45, 0.8\}$ and $a \sim \{0.5, 1.0, 2.75, 4.5\}$. In all simulations, $D = 1$. I tested each of the 12 parameter combinations with $E_F = 9$, 25, 49, 81, and 121. This corresponds to examining a range of r between 3.8 and 14 (assuming $g = 0.2$). This generated 60 outputs. Simulations were run for about 75 generations, sufficient time for the community to approximately reach equilibrium without drift dominating the dynamics of the lower abundance species. However, it was noticed that the cases in which $\sigma_Y = 0.1$ had longer transient times. These were run for 150 generation instead. See Figs. 2.19-2.21 for examples of the transient dynamics.

I then ran a set of ODE simulations using the same parameterizations as the SEM. I compared the outputs of the SEM and ODE model in terms of species diversity, species abundance, and Shannon diversity. I considered a species to be extinct if it had less than 1 individual at any point of the simulation. This was implemented directly in the SEM; for the ODE model, I assumed a species, i, to be extinct if $p_i^* < 1/275^2$ where p_i^* is the equilibrium proportion of species i. Note that these simulations do not attempt to demonstrate the long-term resistance against extinction due to drift. Rather, they demonstrate that the ODE model and SEM yield similar outputs of expected species abundance and species richness given the same parameterization.

Results of comparison

ODE model and SEM produced very similar species richness and Shannon diversity (Figs. 2.17, 2.18). The ODE model and SEM also produced very similar species proportions (Figs. 2.16-2.18). To quantify the quality of the approximation, I calculated the mean difference in species richness between the ODE model and SEM, ΔR:

$$\Delta R = \frac{1}{S}\sum_{k=1}^{S}(R^k_{\text{SEM}} - R^k_{\text{ODE}}) \tag{2.45}$$

where S is the number of simulations, and R^k_{SEM} and R^k_{ODE} are the species richness of the k_{th} simulation of the SEM and ODE model, respectively. I also examined the r^2 (coefficient of determination) between SEM and ODE richness. For the comparisons, $\Delta R = 2.1$ and $r^2 = 0.985$. Overall, the ODE provides a highly similar, albeit non-exact, estimation of species diversity. Error in which the ODE model predicted greater diversity than the SEM is most likely due to stochastic extinction due to drift. This is particularly likely when diversity is high, where the expected abundance of each species is correspondingly smaller. Cases in which the ODE model predicted lower species richness are likely due to incomplete transient dynamics of the SEM.

Derivation of invasion criteria

In this subsection, I derive the approximate invasion criteria of the additive−fixed-distance model when species experience inter-specific variation in intrinsic (Y) and $D = 1$. The invasion criteria of an invader can be expressed as when the per capita growth rate as $p_i \to 0$. Recalling that

$$\mathbb{E}[J_{k,i}(x)] = e^{-(1-e^{-a})p_i E_F} \tag{2.46}$$

and

$$\mathbb{E}[J_{i,i}(x)] = e^{-a}e^{-(1-e^{-a})p_i E_F} \tag{2.47}$$

and using variables previous defined in this appendix, the per capita growth rate of species i (substituting in the seedling abundance values) is

$$\frac{1}{p_i}\frac{dp_i}{dt} = r_i = \delta\Bigg[\frac{Y_i\big[(1-D)+p_iD\big]}{Y_i\big[(1-D)+p_iD\big]\,\mathbb{E}[J_{i,i}(x)] + \sum_{k\neq i} Y_k p_k D\,\mathbb{E}[J_{k,i}(x)]} + Y_i D \sum_{m\neq i} \frac{1}{Y_m\big[(1-D)+p_mD\big]\,\mathbb{E}[J_{m,m}(x)] + \sum_{k\neq m} Y_k p_k D\,\mathbb{E}[J_{k,m}(x)]} p_m - 1\Bigg] \tag{2.48}$$

Species i can invade is this quantity if positive when it is rare ($p_i \to 0$). When $D = 1$ (the case of interest), the above reduces to

$$Y_i \sum_{m\neq i} \frac{p_m}{Y_m\,\mathbb{E}[J_{m,m}(x)]p_m + \sum_{k\neq m} Y_k p_k\,\mathbb{E}[J_{k,m}(x)]} > 1 \tag{2.49}$$

To simplify the above equation, I ignore the term $Y_m\,\mathbb{E}[J_{m,m}(x)]p_m$ in the denominator and incorporate an additional term representing species m into the summation, yielding:

$$Y_i \sum_{m\neq i} \frac{p_m}{\sum_{k\neq i} Y_k p_k\,\mathbb{E}[J_{k,i}(x)]} > 1 \tag{2.50}$$

This simplification is equivalent to making the species identity of the tree previously occupying a patch (the tree that dies) irrelevant (i.e., JCEs only result from trees nearby the patch rather than the previous occupant of the patch). As long as neighborhood effects are somewhat strong – that is, so long as E_F is not very small – this assumption does not meaningfully affect the invasion criteria.

With this simplification, the denominator of equation (2.50) is no longer directly depen-

dent on m. That is, equation (2.50) can be rewritten as

$$Y_i\Big(\sum_{m\neq i} p_m\Big)\Big(\frac{1}{\sum_{k\neq i} Y_k p_k\,\mathbb{E}[J_{k,i}(x)]}\Big) > 1 \tag{2.51}$$

Because, by definition, $\sum_{m\neq i} p_m = 1$, the above equation can be rewritten as

$$Y_i > \sum_{k\neq i} Y_k p_k\,\mathbb{E}[J_{k,i}(x)] \tag{2.52}$$

Substituting the appropriate value for $\mathbb{E}[J_{k,i}(x)]$, the invasion criteria becomes

$$Y_i > \sum_{k\neq i} Y_k p_k e^{-(1-e^{-a})p_k E_F} \tag{2.53}$$

recalling that $E_F = \pi r^2 g$. I take the linearization of $p_k e^{-(1-e^{-a})p_k E_F}$ about the point $1/N$ where N is the number of species in the resident community (and thus, $1/N$ is the average abundance). This yields a close approximation of the expression so long as no species exhibits an abundance much greater than the mean abundance. For simplicity, let

$$J = (1-e^{-a})E_F \tag{2.54}$$

Taking the linearization yields

$$p_k e^{-Jp_k} \approx \frac{e^{-\frac{J}{N}}}{N} + \frac{e^{-\frac{J}{N}}\left(p_k - \frac{1}{N}\right)}{N}\left(1-\frac{J}{N}\right) \tag{2.55}$$

Substituting this into the original expression, the summation can be rearranged and broken up into three parts:

$$e^{-\frac{J}{N}}\frac{1}{N}\sum_{k\neq i} Y_k + e^{-\frac{J}{N}}\left(1-\frac{J}{N}\right)\sum_{k\neq i} Y_k p_k - e^{-\frac{J}{N}}\left(1-\frac{J}{N}\right)\frac{1}{N}\sum_{k\neq i} Y_k \tag{2.56}$$

The first summation is straightforward to calculate:

$$e^{-\frac{J}{N}}\frac{1}{N}\sum_{k\neq i}Y_k = e^{-\frac{J}{N}}\overline{Y} \tag{2.57}$$

where $\overline{Y}$ is the mean intrinsic fitness of the community.

The second term can be expressed by using the property

$$\frac{1}{N}\sum_{m=1}^{N}A_mB_m = \overline{A}\times\overline{B} + \mathrm{Cov}(A,B) \tag{2.58}$$

I apply this property with respect to p and Y, noting that $\overline{p} = \frac{1}{N}$. Using this property and substituting A and B with p and Y for the first and second summations yields

$$\begin{aligned} e^{-\frac{J}{N}}\left(1-\frac{J}{N}\right)\sum_{k\neq i}p_kY_k &= e^{-\frac{J}{N}}\left(1-\frac{J}{N}\right)N\frac{1}{N}\sum_{k\neq i}p_kY_k \\ &= e^{-\frac{J}{N}}\left(1-\frac{J}{N}\right)N\left[\overline{Y}\frac{1}{N}+\mathrm{Cov}(p,Y)\right] \\ &= e^{-\frac{J}{N}}\left(1-\frac{J}{N}\right)\left[\overline{Y}+N\ \mathrm{Cov}(p,Y)\right] \end{aligned} \tag{2.59}$$

The third summation is easy to calculate:

$$-e^{-\frac{J}{N}}\left(1-\frac{J}{N}\right)\frac{1}{N}\sum_{k\neq i}Y_k = -e^{-\frac{J}{N}}\left(1-\frac{J}{N}\right)\overline{Y} \tag{2.60}$$

Adding all three summations together, the third summation term will cancel with the $\overline{Y}$ term of the second summation. Then, after some rearranging, I substitute $J = (1-e^{-a})E_F$ back into the equation. This yields:

$$Y_i > \underbrace{\overline{Y}e^{-\left(1-e^{-a}\right)\frac{E_F}{N}}}_{\substack{\text{mean}\\ \text{JCE-fitness term}}} + \underbrace{N\mathrm{Cov}(p,Y)\left(1-\left(1-e^{-a}\right)\frac{E_F}{N}\right)e^{-\left(1-e^{-a}\right)\frac{E_F}{N}}}_{\text{covariance-JCE term}} \tag{2.61}$$

which is the same as the expression given for the AF model in Table 2.1 of the main text.

Note on ODE approximation

To derive the ODE model, I took approximations of the expected values of $P_{i,i}(x)$ and $P_{i,k}(x)$. To do so, I took the expected abundance of $S_{i,i}(x)$, $S_{i,k}(x)$, and $S_{all,i}(x)$ with respect to space and then examined their quotients. Note that this assumes $\mathbb{E}[S_{i,k}(x)/S_{all,i}(x)] \approx \mathbb{E}[S_{i,k}(x)]/\,\mathbb{E}[S_{all,k}(x)]$ (I take the expectation of the numerator and denominator and then take the quotient). Using a Taylor Expansion about the mean,

$$\mathbb{E}\left[\frac{S_{i,k}(x)}{S_{all,i}(x)}\right] \approx \frac{\mathbb{E}[S_{i,k}(x)]}{\mathbb{E}[S_{all,k}(x)]} - \frac{\mathrm{Cov}\big(S_{i,k}(x), S_{all,k}(x)\big)}{\mathbb{E}[S_{all,k}(x)]^2} + \mathrm{Var}\big(S_{all,k}(x)\big)\frac{\mathbb{E}[S_{i,k}(x)]}{\mathbb{E}[S_{all,i}(x)]^3}$$

Because there are many species in the community, $S_{all,i}(x) >> S_{i,k}(x)$. This implies that the covariance term and the term containing $\mathbb{E}[S_{all,i}(x)]^3$ are close to zero. Additionally, $\mathrm{Var}\big(S_{all,i}(x)\big)$ is likely small because it is assumed that dispersal is uniform across the community. Therefore, $\mathbb{E}[S_{i,k}(x)/S_{all,i}(x)] \approx \mathbb{E}[S_{i,k}(x)]/\,\mathbb{E}[S_{all,k}(x)]$ is likely a good approximation. I rely on the quantitative similarity of the SEM and ODE model to validate this assumption.

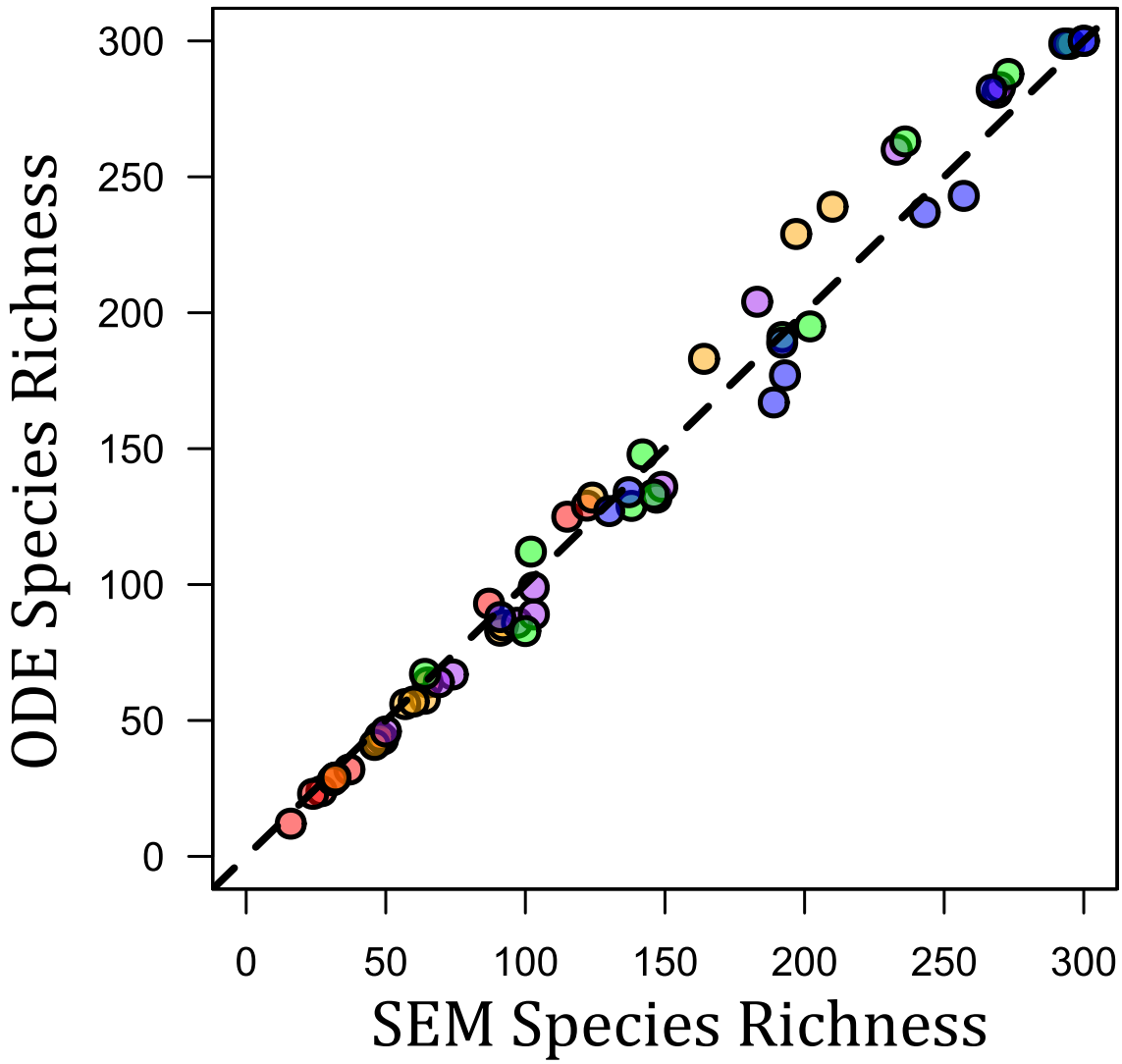

Figure 2.14: ODE model validation. The figures compare species richness between SEM and ODE model simulations under identical parameterizations. The dashed line is the one-to-one line (points on the line represent when the SEM and ODE yield the exact same diversity output). Red points are when $E_F = 9$, orange/yellow points are when $E_F = 25$, purple points are when $E_F = 49$, green points are when $E_F = 81$, and blue points are when $E_F = 121$. To a first approximation, the ODE model yields the same output as the SEM.

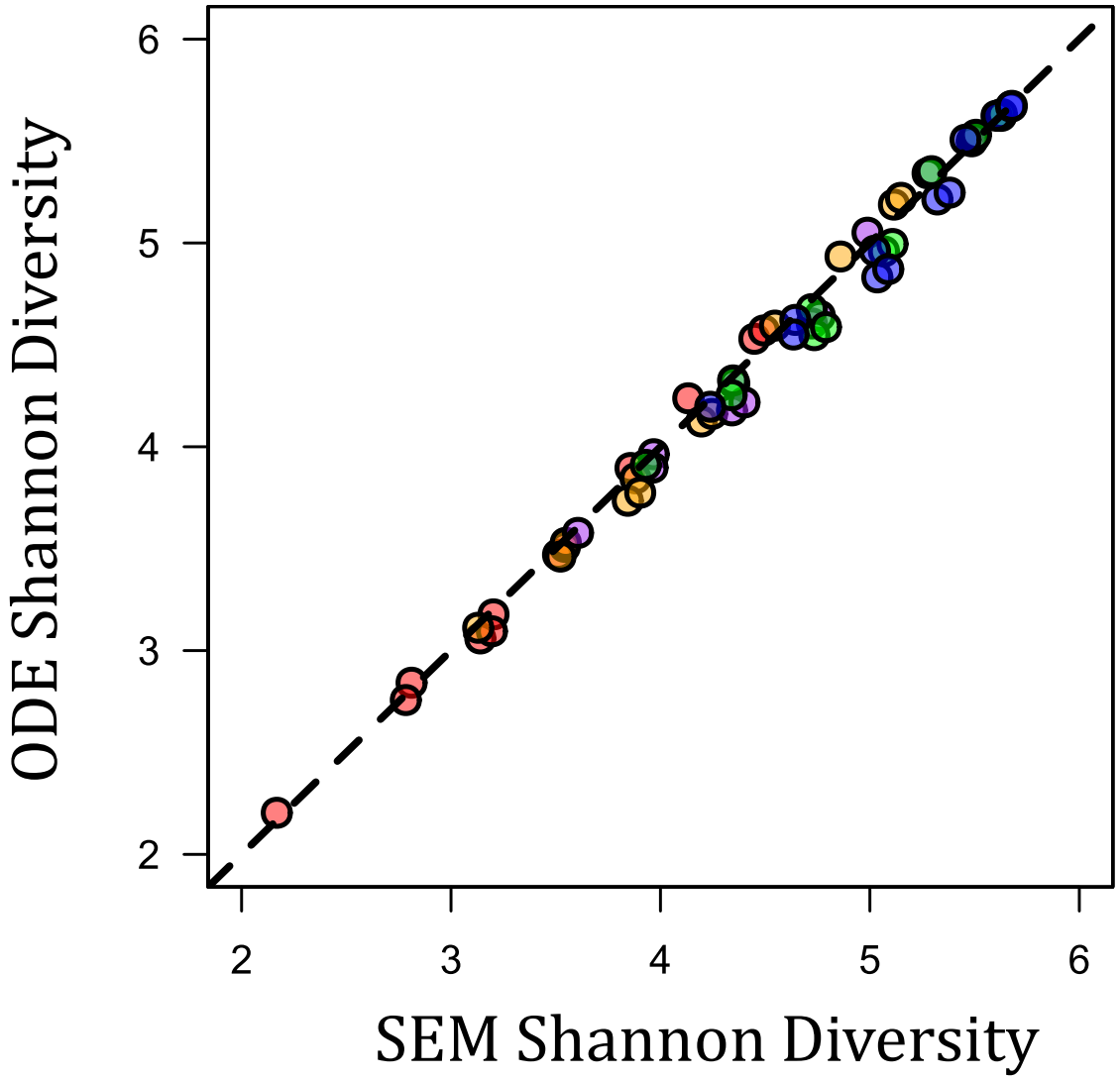

Figure 2.15: The same as the fig. 2.14, but showing Shannon Diversity instead of species richness. As in the above case, the SEM and ODE model yield very similar outputs.

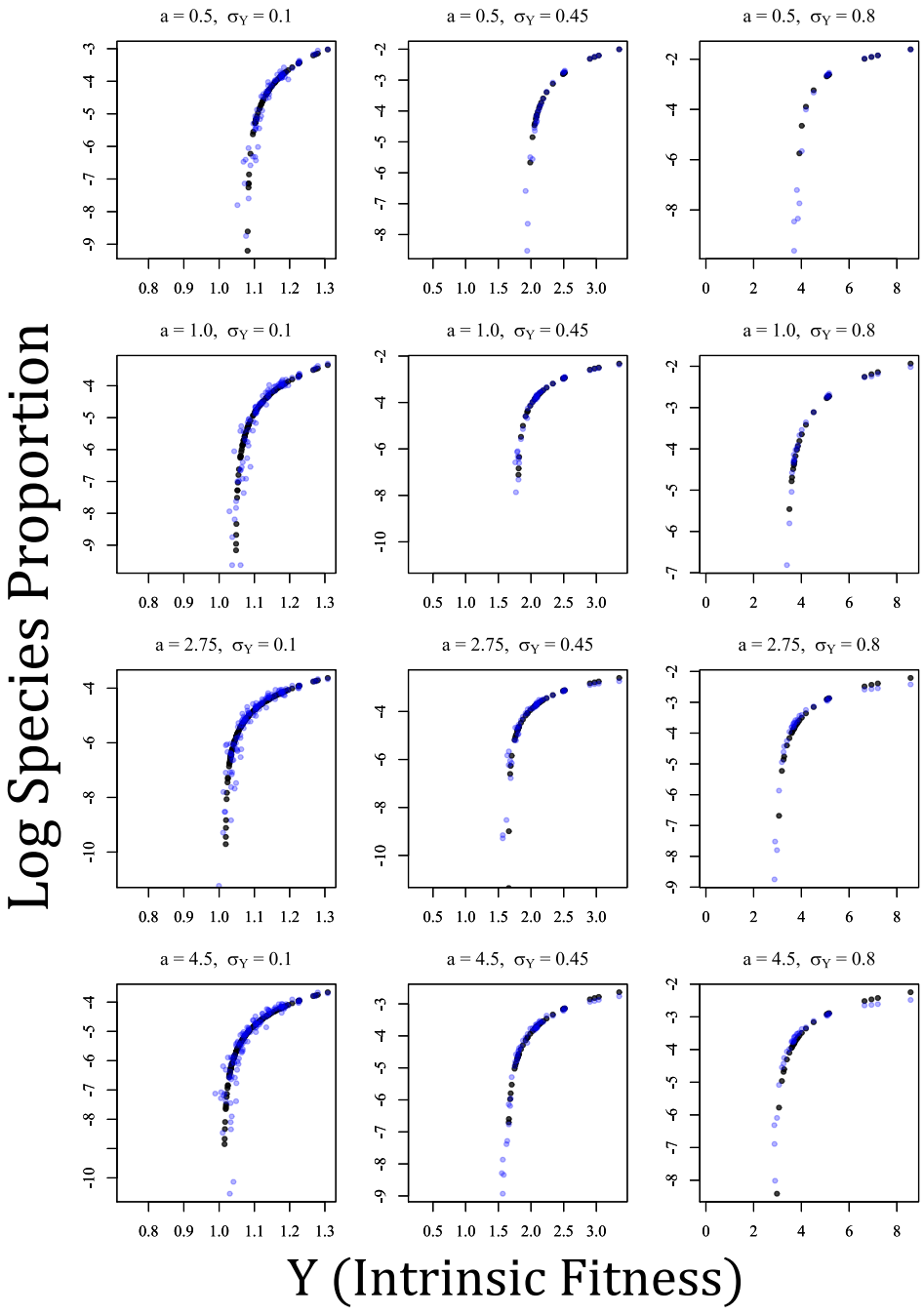

Figure 2.16: Comparisons between identical parameterizations of the ODE approximation (black) and SEM (blue) outputs under nine parameter values when species vary in intrinsic fitness (Y). The$y$-axis depicts the log-proportion of each species and the x-axis depicts Y of each species. These parameter values span the most of the parameter space explored in Fig. 4 of the main text. In all plots, $E_F = 9$, $g = 0.2$, and $D = 1.0$. Other relevant parameters are listed on each plot.

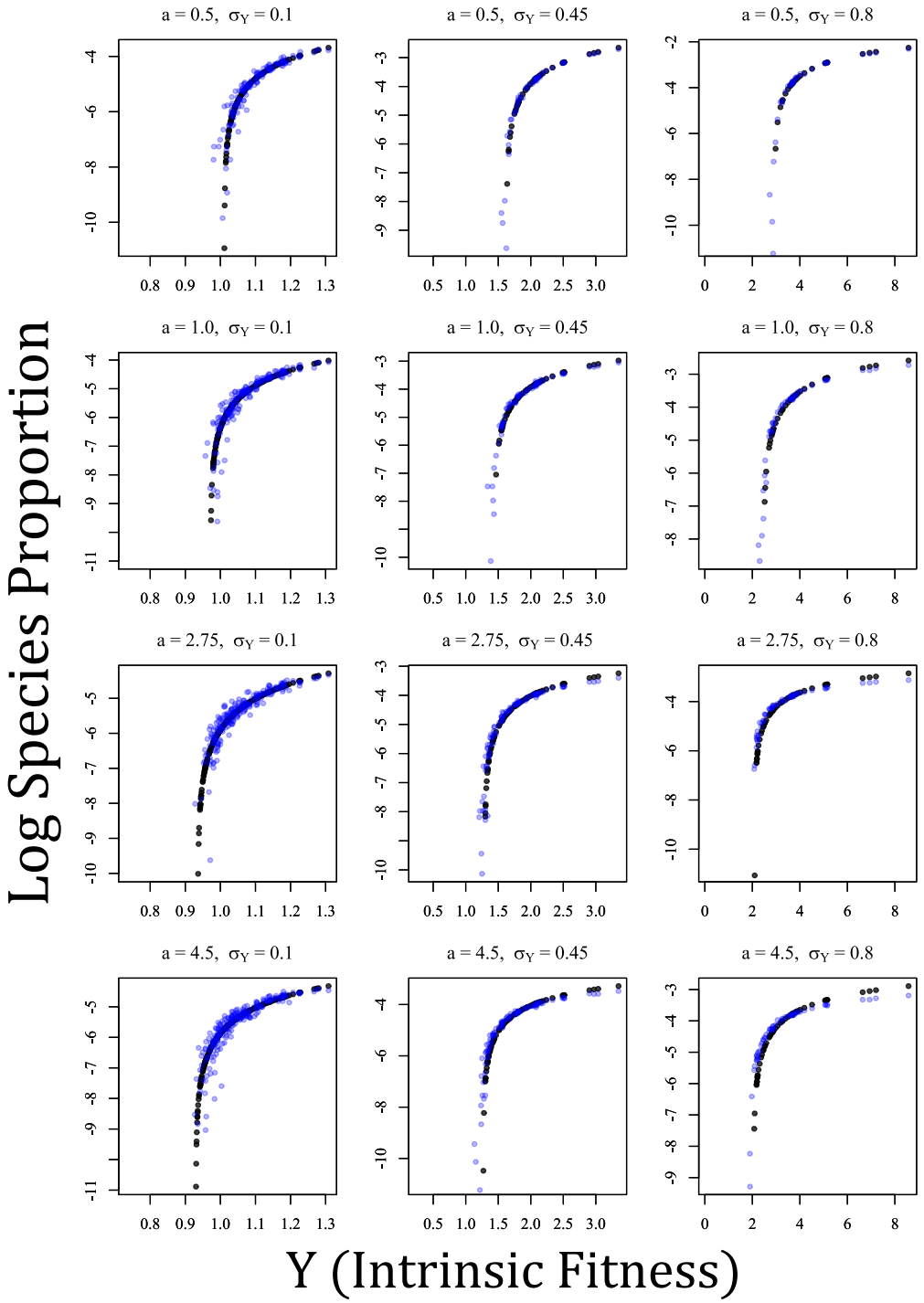

Figure 2.17: The same format as fig. 2.16, but with $E_F = 25$.

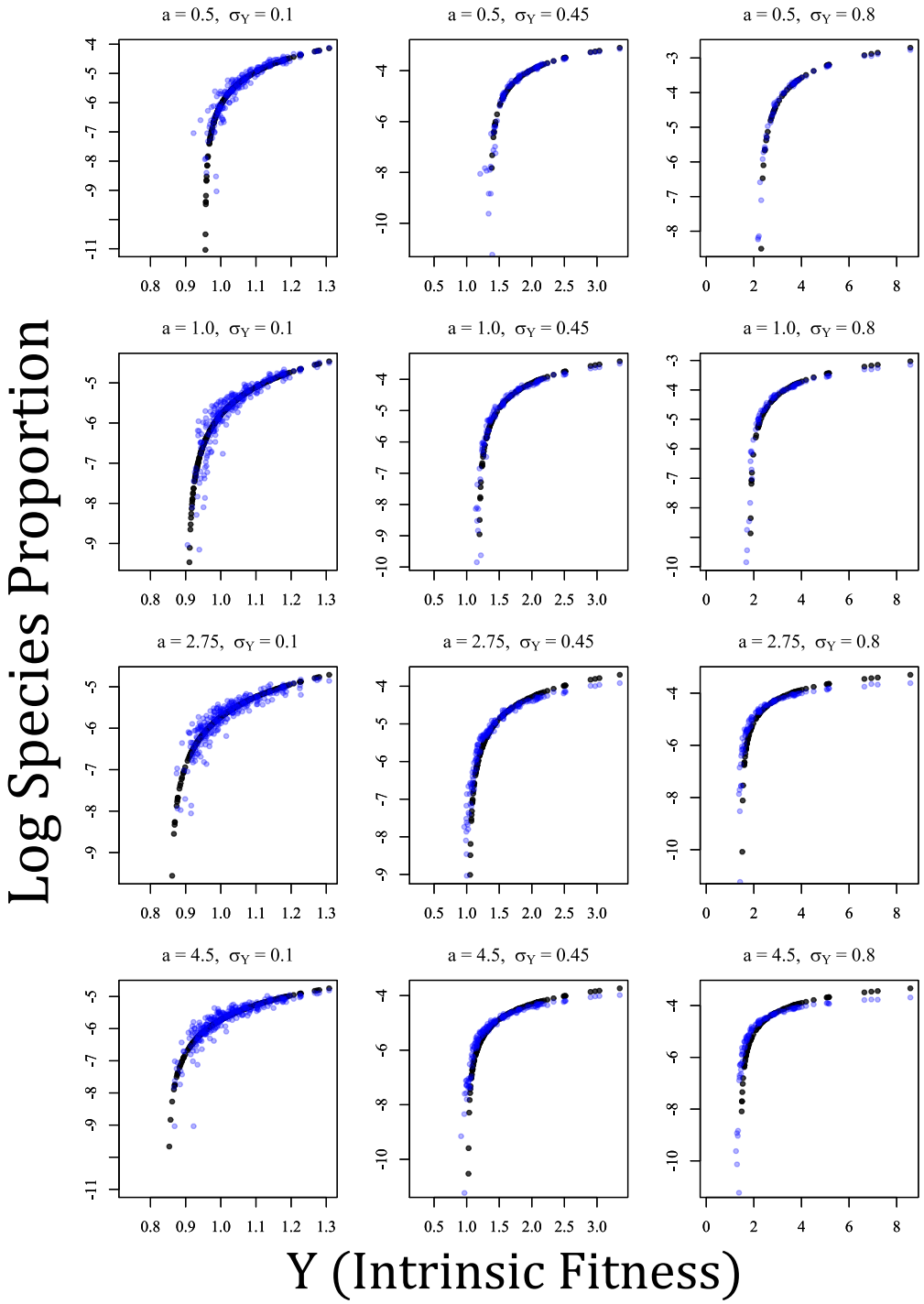

Figure 2.18: The same format as fig. 2.16, but with $E_F = 49$.

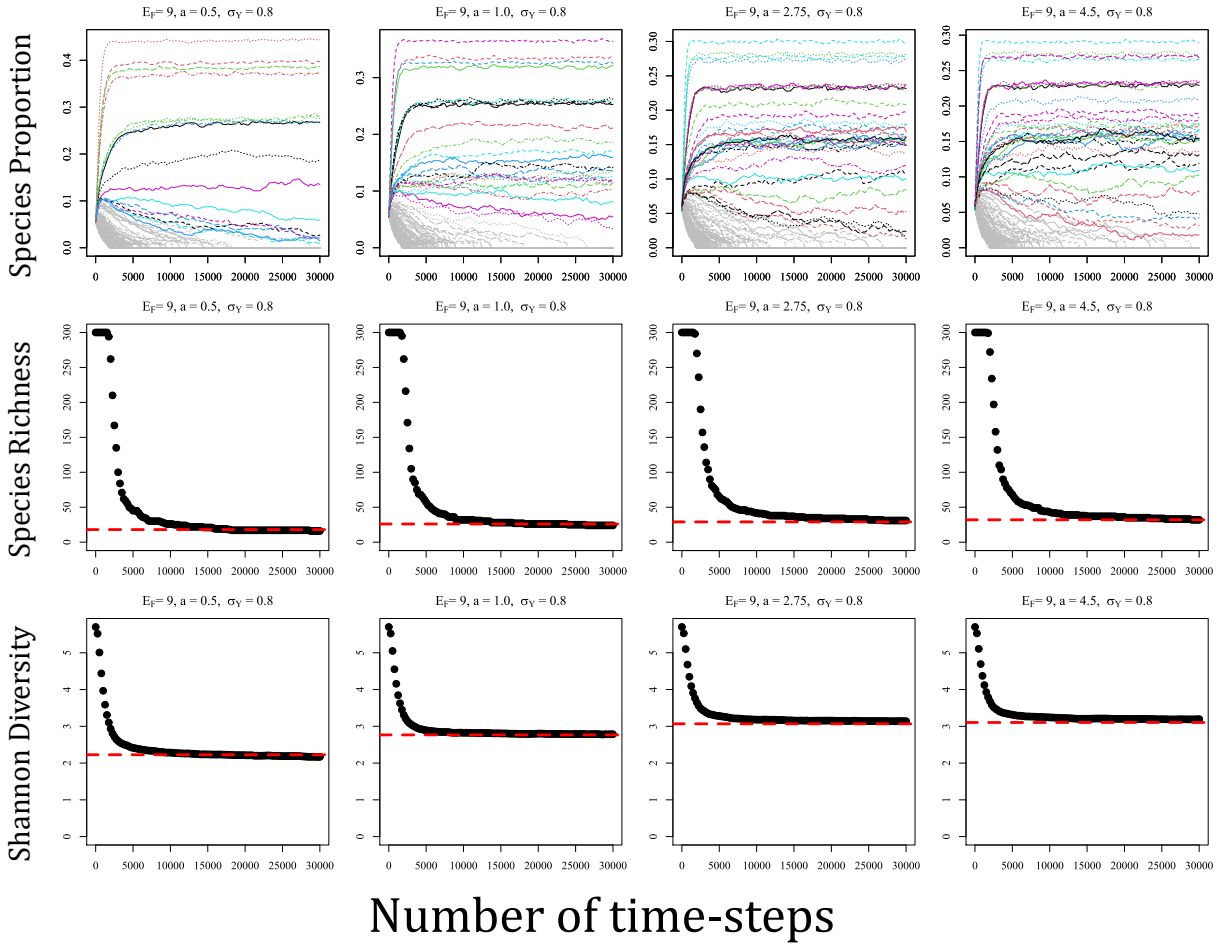

Figure 2.19: Examples of the SEM simulation time series outputs, species richness over time in the simulations, and Shannon diversity over time in the simulations. The top row shows examples of the time series outputs of the SEMs. The x-axis is time and the y-axis is each species' proportion. Proportions have been square-root transformed to aid visualization. Colored trajectories indicate species that persisted throughout the simulation; grey trajectories indicate species that went extinct. Parameters are listed on each plot. Dynamics as shown are typical examples from the SEMs. Most species settle into a relatively stable pseudo-equilibrium, while lower abundance species fluctuate due to drift. The second row shows the number of persisting species in the community as a function of time. Each panel corresponds to the plot above it. Most species that go extinct do so in the early stages of the dynamics. Therefore, the vast majority of persisting species likely persist deterministically. The dashed red line is the diversity maintained by the ODE under the same parameterization. All SEMs saturate, approximately, to the dashed line. The third row is the same as the second row, except it shows Shannon diversity instead of species richness.

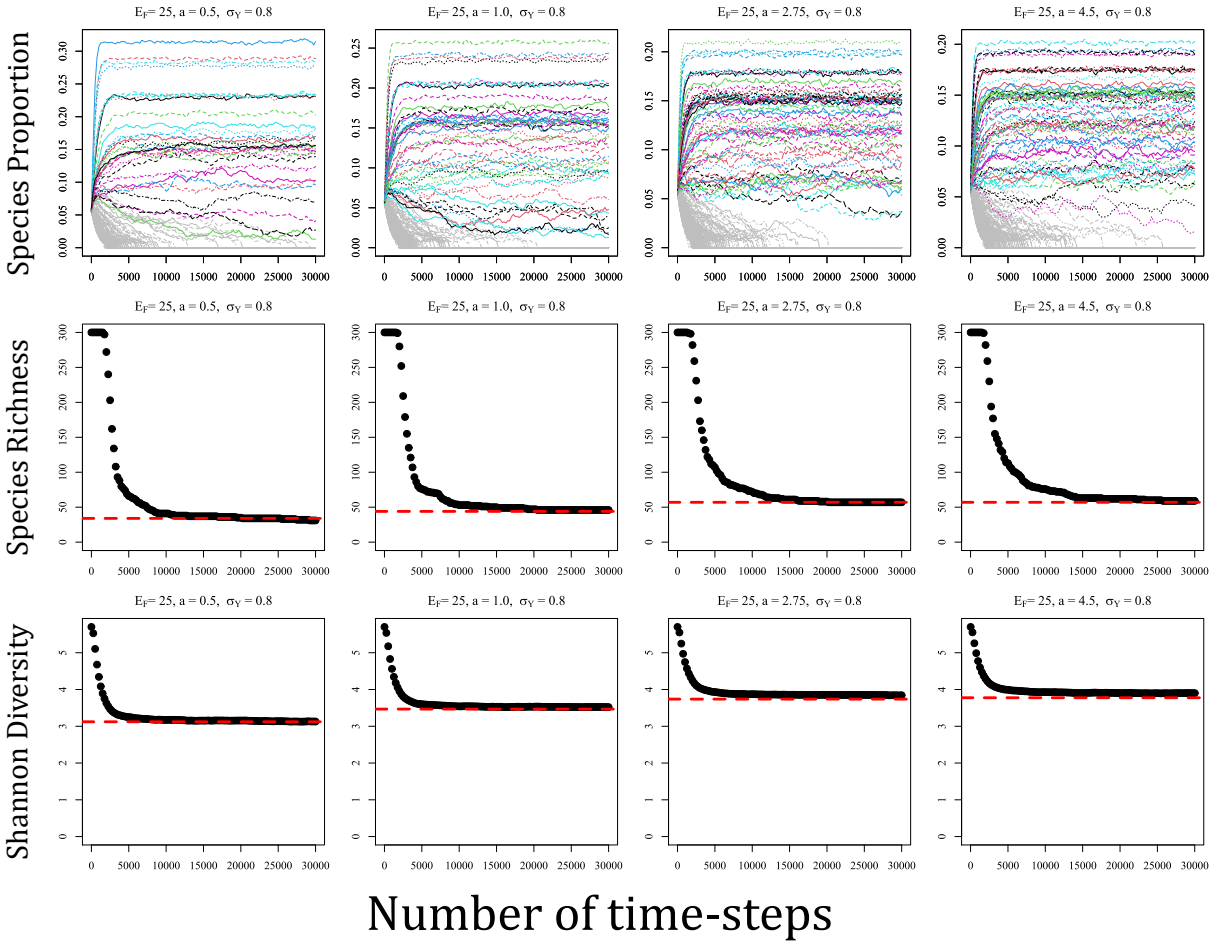

Figure 2.20: The same as fig. 2.19, but with $E_F = 25$.

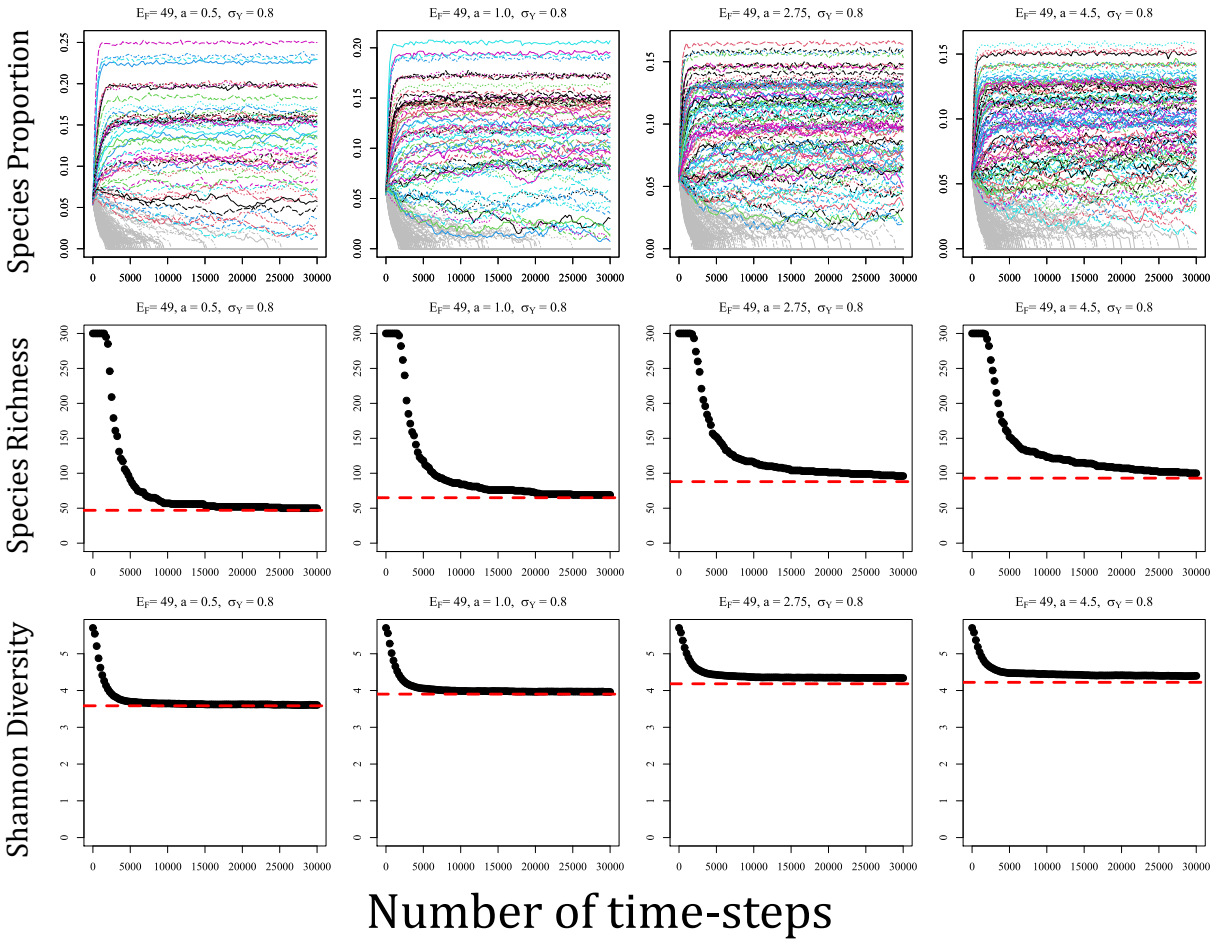

Figure 2.21: The same as fig. 2.19, but with $E_F = 49$.

Appendix A.3: Non-additive−Distance-decay SEM and ODE approximation

Introduction

In this Appendix, I analyze the Non-additive−Distance-decay (ND) model presented in the main text. This Appendix is composed of three main subsections: **(1)** I introduce a spatially explicit model (SEM) of the ND model. I then demonstrate that taking the expected offspring abundances on each patch yields the ODE model discussed in the main text. **(2)** I provide outputs of the ODE model and the SEM model under the same parameterizations. I show the outputs are very similar, hence demonstrating that the ODE is a sufficiently accurate approximation of the SEM. **(3)** I provide the derivation of the approximate invasion criteria of the ND model (Table 2.1 in the main text). The structure of this Appendix is identical to that of Appendices A and B.

Spatially Explicit Model and derivation of ODE approximation

In this subsection, I discuss the SEM, briefly review within-patch dynamics from the main text, and show the derivation of the ODE approximation. I assume the reader is familiar with the general model discussed in the main text.

SEM

I developed a spatially explicit model that integrates the non-additive−distance-decay functional form. The model consists of a community on a grid of $L \times L$ patches (M total patches, $M = L^2$) modeled as a torus to avoid edge effects. A single tree is present on every space on the grid. At each time-step, each tree dies with probability δ and tree replacement occurs via a lottery based on offspring abundances on each patch. The ND model assumes that predation pressure is non-additive and that predation pressure declines exponentially with

distance. As noted in the main text, offspring abundances on each patch type are equal to

$$\begin{aligned} S_{i,i}(x) &= Y_i\big[(1-D)+p_iD\big]J_{i,i}(x) \\ S_{i,k}(x) &= Y_i p_i D J_{i,k}(x) \\ S_{all,i}(x) &= \sum_{n=1}^{N} S_{n,i}(x) \end{aligned} \tag{2.62}$$

where $S_{A,B}(x)$ is the offspring abundance of species A on a patch occupied by species B at location x, $J_{i,i}(x)$ and $J_{i,k}(x)$ are how JCEs affect offspring surivorship, p_i is the proportion of species i in the population, Y_i is the intrinsic fitness of species i, and D is the dispersal proportion. For the ND model:

$$\begin{aligned} J_{i,i}(x) &= \exp\big[-a\big] \\ J_{i,k}(x) &= \exp\Big[-ae^{-\min(x_i)/v}\Big] \end{aligned} \tag{2.63}$$

where $\min(x_i)$ is distance between the focal patch and the closest individual of species i. Offspring abundances are determined by the following equations:

$$\begin{aligned} S_{i,i}(x) &= Y_i\big[(1-D)+p_iD\big]e^{-a} \\ S_{i,k}(x) &= Y_i p_i D\, \exp\Big[-ae^{-\min(x_i)/v}\Big] \\ S_{all,i}(x) &= Y_i\big[(1-D)+p_iD\big]e^{-a} + D\sum_{k\neq i} Y_k p_k\, \exp\Big[-ae^{-\min(x_k)/v}\Big] \end{aligned} \tag{2.64}$$

where $S_{A,B}(x)$ is the offspring abundance of species A on a patch occupied by species B at location x. v defines rate at which predataion declines with distance (higher v indicates a lower rate of predation decay). The lottery is determined by the relative abundance of offspring. Let $P_{A,B}(x)$ be the probability species A colonizes a patch previously occupied by species B at location x. Then, $P_{i,i}(x) = S_{i,i}(x)/S_{all,i}(x)$ and $P_{i,k}(x) = S_{i,k}(x)/S_{all,k}(x)$.

For the SEM, patch-specific JCEs are determined by the euclidean distance between patches. Distances are calculated between the center points of each patch and it is assumed offspring are at the center of each patch.

ODE Model

To derive the ODE model, I take approximations of the expected values of $P_{i,i}(x)$ and $P_{i,k}(x)$. To do so, I take the expected abundance of $S_{i,i}(x)$, $S_{i,k}(x)$, and $S_{all,i}(x)$ and then take their quotients. Expectations are taken with respect to space. Using this, I derive the the ODE approximation

$$\frac{dp_i}{dt} = \delta\left[\frac{\mathbb{E}[S_{i,i}(x)]}{\mathbb{E}[S_{all,i}(x)]}p_i + \sum_{k\neq i}\frac{\mathbb{E}[S_{i,k}]}{\mathbb{E}[S_{all,k}(x)]}p_k - p_i\right] \tag{2.65}$$

that captures the behavior of the SEM. See "Note" at the end of this Appendix for additional information about the assumptions of this approximation.

JCEs in the SEM are implemented using the spatial proximity of trees that, computationally, is stored in a matrix. The deterministic ODE model is spatially implicit. Therefore, it is necessary to use an approximation of the terms that do not require spatial information. In particular, the quantity $S_{i,k}(x)$, which contains the term

$$\exp\left[-ae^{-\min(x_i)/v}\right] \tag{2.66}$$

must be approximated as a spatially implicit term. To do so, I approximate the expected survival of each species' offspring on a random patch by evaluating

$$\mathbb{E}\left[\exp\left[-ae^{-\min(x_i)/v}\right]\right].$$

To evaluate this quantity, I use a Taylor Expansion to evaluate the first moment approx-

imation the function of $f(X) = \exp\big[-ae^{-X/v}\big]$. The approximation is defined by:

$$\begin{aligned}\mathbb{E}[f(X)] &\approx f(\mathbb{E}[X]) + \frac{1}{2}f''(\mathbb{E}[X])\,\mathbb{E}\left[(X-\mathbb{E}[X])^2\right] \\ &= f(\mathbb{E}[X]) + \frac{1}{2}f''(\mathbb{E}[X])\sigma_X^2\end{aligned} \tag{2.67}$$

where X is the a random variable of the nearest neighbor distribution in space (i.e. the probability distribution of $\min(x_i)$) and σ_X^2 is the variance of X. Assuming individuals are approximately randomly distributed in space, X follows a Rayleigh distribution with probability distribution function $f_X = 2\pi g p_i x e^{-gp_i\pi x^2}$ where x represents radial distance from a point in 2D space (Clark and Evans, 1954). Relevant to the approximation,

$$\begin{aligned}\mathbb{E}[X] &= \frac{1}{2\sqrt{p_i g}} \\ \sigma_X^2 &= \left(1-\frac{\pi}{4}\right)\frac{1}{\pi g p_i}\end{aligned} \tag{2.68}$$

for the Rayleigh distribution. In addition,

$$f''(X) = \frac{1}{v^2}ae^{-ae^{-\frac{X}{v}}}e^{-\frac{X}{v}}\left(ae^{-\frac{X}{v}}-1\right) \tag{2.69}$$

Putting it all together and doing some rearranging yields

$$\mathbb{E}[f(X)] \approx e^{-ae^{-\sqrt{\frac{\pi}{2E_D p_i}}}}\left(1+ae^{-\sqrt{\frac{\pi}{2E_D p_i}}}\left(ae^{-\sqrt{\frac{\pi}{2E_D p_i}}}-1\right)\left(1-\frac{\pi}{4}\right)\frac{1}{p_i E_D}\right) \tag{2.70}$$

where

$$E_D = 2\pi g v^2$$

Plugged into the appropriate offspring abundance equations, the approximation yields

$$\mathbb{E}[S_{i,i}(x)] = Y_i\big[(1-D)+p_iD\big]e^{-a}$$
$$\mathbb{E}[S_{i,k}(x)] = Y_iDp_ie^{-ae^{-\sqrt{\frac{\pi}{2E_Dp_i}}}}\left(1+ae^{-\sqrt{\frac{\pi}{2E_Dp_i}}}\left(ae^{-\sqrt{\frac{\pi}{2E_Dp_i}}}-1\right)\left(1-\frac{\pi}{4}\right)\frac{1}{p_iE_D}\right) \tag{2.71}$$

which are identical to the ND model offspring abundance expressions in the main text. $\mathbb{E}[S_{all,i}(x)] = \sum_{n=1}^{N}\mathbb{E}[S_{n,i}(x)]$.

Comparison between ODE model and SEM model

In this subsection, I describe simulations that compare the ODE model to the SEM. I demonstrate that the SEM and ODE model yield highly similar outputs of species abundance and species richness. I provide 36 comparisons of the SEM to the ODE (12 cases in which $v = 5$, 12 cases in which $v = 7.5$, and 12 cases in which $v = 10$). Parameter values were chosen to approximately encapsulate the range of parameters shown in the main text.

ODE and SEM parameterization

Each SEM simulation began with 300 species at equal abundance, with individuals randomly distributed throughout the community. Simulations were conducted on a 275×275 torus (thus containing 275^2 individual trees). I used the following parameters: $Y \sim \text{lognormal}[\mu = 0, \sigma_Y]$ with $\sigma_Y \sim \{0.1, 0.45, 0.8\}$ and $a \sim \{0.5, 1.0, 2.75, 4.5\}$. In all simulations, $g = 0.20$ and $D = 1$. I tested each of the 12 parameter combinations of σ_Y and a with $v \sim \{5, 7.5, 10\}$. This generated 36 outputs. Simulations were run for about 65 generations, sufficient time for the community to approximately reach equilibrium without drift dominating the dynamics of the lower abundance species. See Figs. 2.27-2.29 for typical outputs of the SEM time series dynamics.

A corresponding set of 36 ODE simulations were run using the same parameterizations as the SEM. I compared the outputs of the SEM and ODE model in terms of species diversity, species abundance, and Shannon diversity. I considered a species to be extinct if it had less than 1 individual at any point of the simulation. This was implemented directly in the SEM; for the ODE model, I assumed a species, i, to be extinct if $p_i^* < 1/275^2$ where p_i^* is the equilibrium proportion of species i. Note that these simulations do not attempt to demonstrate the long-term resistance against extinction due to drift. Rather, they demonstrate that the ODE model and SEM yield similar outputs of expected species abundance and richness given the same parameterization.

Results of comparison

ODE model and SEM produced very similar species richness and Shannon diversity (Figs. 2.22, 2.23). The ODE model and SEM also produced very similar species proportions (Figs. 2.24-2.26). To quantify the quality of the approximation, I calculated the mean difference in species richness between the ODE model and SEM, ΔR:

$$\Delta R = \frac{1}{S}\sum_{k=1}^{S}(R_{\text{SEM}}^k - R_{\text{ODE}}^k) \tag{2.72}$$

where S is the number of simulations, and R_{SEM}^k and R_{ODE}^k are the species richness of the k_{th} simulation of the SEM and ODE model, respectively. I also examined the r^2 (coefficient of determination) between SEM and ODE species richness. For the comparisons, $\Delta R = -3.37$ and $r^2 = 0.98$. Overall, the ODE provides a highly similar, albeit non-exact, estimation of species diversity. Error in which the ODE model predicted greater diversity than the SEM is most likely due to stochastic extinction due to drift. This is particularly likely when diversity is high, where the expected abundance of each species is correspondingly smaller. Cases in which the ODE model predicted lower species richness are likely due to incomplete transient

dynamics of the SEM.

Derivation of invasion criteria

In this subsection, I derive the approximate invasion criteria of the ND model when species experience inter-specific variation in intrinsic fitness (Y) with $D = 1$. Compared to the other subsections, the algebra of this is quite messy. Therefore, I provide a brief description of the steps. Interested readers can verify the abbreviated algebra or contact the author for details. For simplicity, let

$$\mathbb{E}[J(p_i)] = e^{-ae^{-\sqrt{\frac{\pi}{2E_D p_i}}}}\left(1 + ae^{-\sqrt{\frac{\pi}{2E_D p_i}}}\left(ae^{-\sqrt{\frac{\pi}{2E_D p_i}}} - 1\right)\left(1 - \frac{\pi}{4}\right)\frac{1}{p_i E_D}\right)$$

Then, the per capita growth rate of species i, substituting in the offspring abundance values, is

$$\begin{aligned}\frac{1}{p_i}\frac{dp_i}{dt} = r_i = \delta\Bigg[&\frac{Y_i\big[(1-D)+p_i d\big]e^{-a}\,\mathbb{E}[J(p_i)]}{Y_i\big[(1-D)+p_i D\big]e^{-a}J(p_i) + D\sum_{k\neq i}Y_k p_k\,\mathbb{E}[J(p_k)]} \\ &+ Y_i D\sum_{m\neq i}\frac{1}{Y_m\big[(1-D)+p_m D\big]e^{-a}\,\mathbb{E}[J(p_m)] + D\sum_{k\neq m}Y_k p_k\,\mathbb{E}[J(p_k)]}p_k - 1\Bigg]\end{aligned} \tag{2.73}$$

Species i can invade is this quantity if positive when it is rare ($p_i \to 0$). When $D = 1$ (the case of interest), the above reduces to

$$Y_i\sum_{m\neq i}\frac{1}{Y_m p_m e^{-a} + \sum_{k\neq m}Y_k p_k\,\mathbb{E}[J(p_k)]}p_m > 1 \tag{2.74}$$

To further simplify the above equation, I remove the term $Y_m p_m e^{-a}$ and substitute it with $Y_m p_m \, \mathbb{E}[J(p_m)]$ in the denominator of the summation. Doing so yields

$$Y_i \sum_{m \neq i} \frac{p_m}{\sum_{k \neq i} Y_k p_k \, \mathbb{E}[J(p_k)]} > 1 \tag{2.75}$$

This simplification is equivalent to making the species identity of the tree previously occupying a patch (the tree that dies) irrelevant (i.e., JCEs only result from trees nearby the patch rather than the previous occupant of the patch). As long as predation occurs over a non-trivial distance – that is, so long as v is not very small – this assumption should not meaningfully affect the invasion criteria.

With this simplification, the denominator of equation (2.75) is no longer directly dependent on m and equation (2.75) can be rewritten as

$$Y_i \Bigg(\sum_{m \neq i} p_m \Bigg) \Bigg(\frac{1}{\sum_{k \neq i} Y_k p_k \, \mathbb{E}[J(p_k)]} \Bigg) > 1 \tag{2.76}$$

Because $\sum_{m \neq i} p_m = 1$, the inequality can be written as

$$Y_i > \sum_{k \neq i} Y_k p_k \, \mathbb{E}[J(p_k)] \tag{2.77}$$

I then take the linearization of $p_k \, \mathbb{E}[J(p_k)]$ around the point $1/N$ where N is the number of species in the resident community yields a close approximation of the expression so long as inter-specific variation in p_k is not very large. This yields

$$p_k \, \mathbb{E}[J(p_k)] \approx \frac{1}{N} J\Bigg(\frac{1}{N} \Bigg) + J'\Bigg(\frac{1}{N} \Bigg) \Bigg(p_k - \frac{1}{N} \Bigg) \tag{2.78}$$

where $J'\Big(\frac{1}{N} \Big)$ is the derivative of $\mathbb{E}[J(p_k)]$ with respect to p_k at the point $1/N$. Plugging

this into the summation yields:

$$\frac{1}{N}J\left(\frac{1}{N}\right)\sum_{k\neq i}Y_k + J'\left(\frac{1}{N}\right)\sum_{k\neq i}Y_k p_k - J'\left(\frac{1}{N}\right)\frac{1}{N}\sum_{k\neq i}Y_k \tag{2.79}$$

The first and third summations in the above expression are easy to evaluate:

$$\frac{1}{N}J\left(\frac{1}{N}\right)\sum_{k\neq i}Y_k = J\left(\frac{1}{N}\right)\overline{Y} \tag{2.80}$$

and

$$-J'\left(\frac{1}{N}\right)\frac{1}{N}\sum_{k\neq i}Y_k = -J'\left(\frac{1}{N}\right)\overline{Y} \tag{2.81}$$

where $\overline{Y}$ is the mean fitness of the resident community.

The second summation term, which contains a $Y_k p_k$ term can be evaluated using the property

$$\frac{1}{N}\sum_{m=1}^{N}A_m B_m = \overline{A}\times\overline{B} + \mathrm{Cov}(A,B) \tag{2.82}$$

substituting A and B with p and Y. Ultimately, doing this procedure and rearranging terms yields:

$$J'\left(\frac{1}{N}\right)\sum_{k\neq i}Y_k p_k = J'\left(\frac{1}{N}\right)\left[\overline{Y} + N\mathrm{Cov}(p,Y)\right] \tag{2.83}$$

noting that $\overline{p} = 1/N$.

I then add all the summation terms together. Notably, the third summation term, $-J'\left(\frac{1}{N}\right)\overline{Y}$, and the $\overline{Y}$ term from the second summation term, $J'\left(\frac{1}{N}\right)\overline{Y}$, will cancel. After some algebra and substituting the correct values of $J\left(\frac{1}{N}\right)$ and $J'\left(\frac{1}{N}\right)$, the invasion criterion can be expressed as

$$
\begin{aligned}
Y_i > & \underbrace{\overline{Y} e^{-ae^{-\sqrt{\frac{\pi N}{2E_D}}}} \left(1 + ae^{-\sqrt{\frac{\pi N}{2E_D}}} \left(ae^{-\sqrt{\frac{\pi N}{2E_D}}} - 1\right)\left(1 - \frac{\pi}{4}\right)\frac{N}{E_D}\right)}_{\text{mean JCE-fitness term}} \\
& + N\text{Cov}(p, Y)\times \\
& e^{-ae^{-\sqrt{\frac{\pi N}{2E_D}}}} \Bigg[1 - \frac{\left(1 - \frac{\pi}{4}\right) a^3 N \sqrt{\frac{\pi N}{2E_D}} e^{-3\sqrt{\frac{\pi N}{2E_D}}}}{2E_D} + \\
& \underbrace{\frac{3\left(1 - \frac{\pi}{4}\right) a^2 N \sqrt{\frac{\pi N}{2E_D}} e^{-2\sqrt{\frac{\pi N}{2E_D}}}}{2E_D} - \frac{a\sqrt{\frac{\pi N}{2E_D}}\left(E_D + \left(1 - \frac{\pi}{4}\right) N\right) e^{-\sqrt{\frac{\pi N}{2E_D}}}}{2E_D}\Bigg]}_{\text{covariance-JCE term}}
\end{aligned}
\tag{2.84}
$$

which is identical to the expression in Table 2.1 in the main text with the covariance-JCE term added.

Note on ODE approximation

To derive the ODE model, I took approximations of the expected values of $P_{i,i}(x)$ and $P_{i,k}(x)$. To do so, I took the expected abundance of $S_{i,i}(x)$, $S_{i,k}(x)$, and $S_{all,i}(x)$ with respect to space and then examined their quotients. Note that this assumes $\mathbb{E}[S_{i,k}(x)/S_{all,i}(x)] \approx \mathbb{E}[S_{i,k}(x)]/\mathbb{E}[S_{all,k}(x)]$ (I take the expectation of the numerator and denominator and then take the quotient). Using a Taylor Expansion about the mean,

$$
\mathbb{E}\left[\frac{S_{i,k}(x)}{S_{all,i}(x)}\right] \approx \frac{\mathbb{E}[S_{i,k}(x)]}{\mathbb{E}[S_{all,k}(x)]} - \frac{\text{Cov}\big(S_{i,k}(x), S_{all,k}(x)\big)}{\mathbb{E}[S_{all,k}(x)]^2} + \text{Var}\big(S_{all,k}(x)\big)\frac{\mathbb{E}[S_{i,k}(x)]}{\mathbb{E}[S_{all,i}(x)]^3}
$$

Because there are many species in the community, $S_{all,i}(x) >> S_{i,k}(x)$. This implies that the covariance term and the term containing $\mathbb{E}[S_{all,i}(x)]^3$ are close to zero. Additionally, $\text{Var}\big(S_{all,i}(x)\big)$ is likely small because it is assumed that dispersal is uniform across the community. Therefore, $\mathbb{E}[S_{i,k}(x)/S_{all,i}(x)] \approx \mathbb{E}[S_{i,k}(x)]/\mathbb{E}[S_{all,k}(x)]$ is likely a good approxi-

mation. I rely on the quantitative similarity of the SEM and ODE model to validate this assumption.

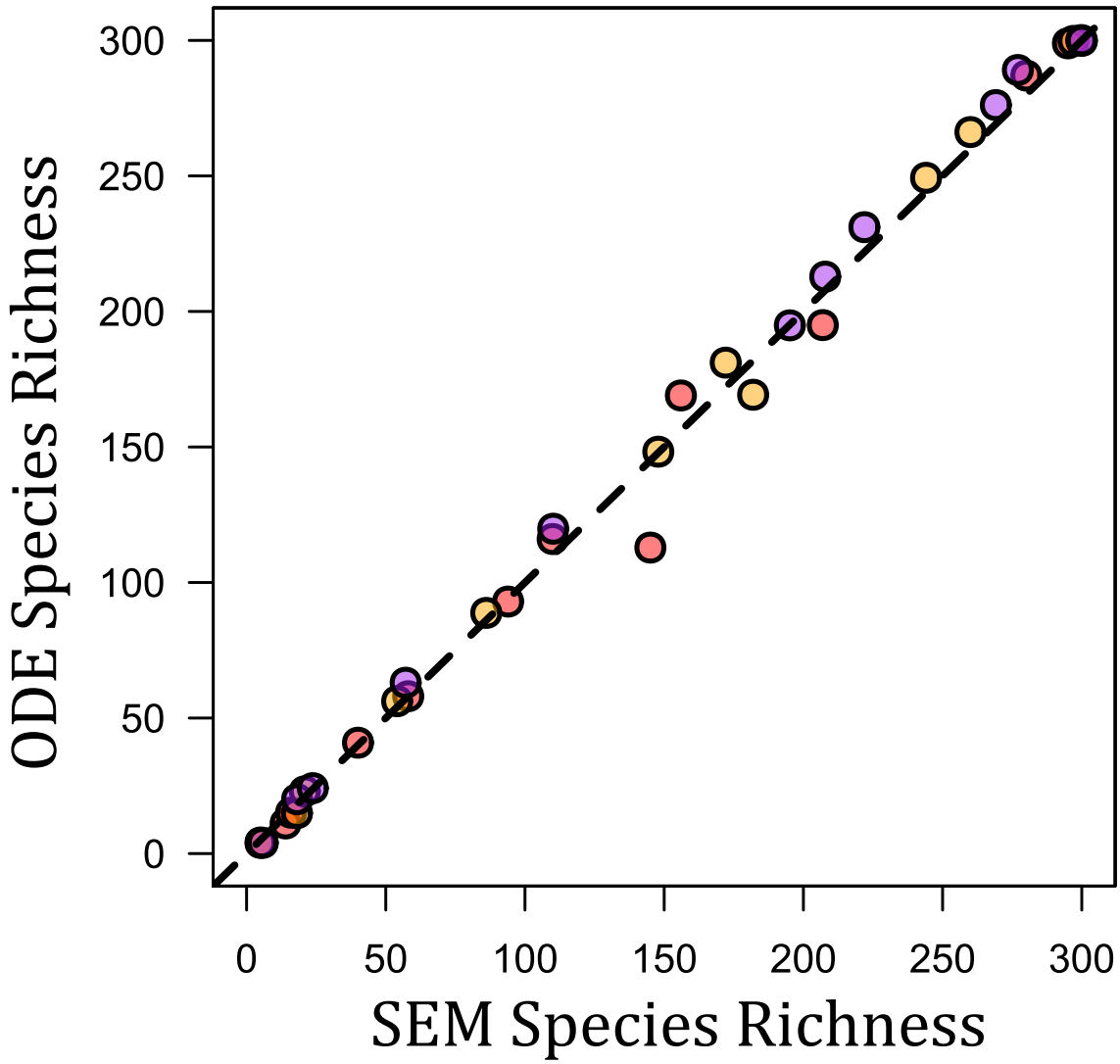

Figure 2.22: ODE model validation. The figure compares species richness between SEM and ODE model simulations under identical parameterizations. The dashed line is the one-to-one line (points on the line represent when the SEM and ODE yield the exact same diversity output). Red points are when $v = 5$, orange/yellow points are when $v = 7.5$, and purple points are when $v = 10$. To a first approximation, the ODE model yields the same output as the SEM.

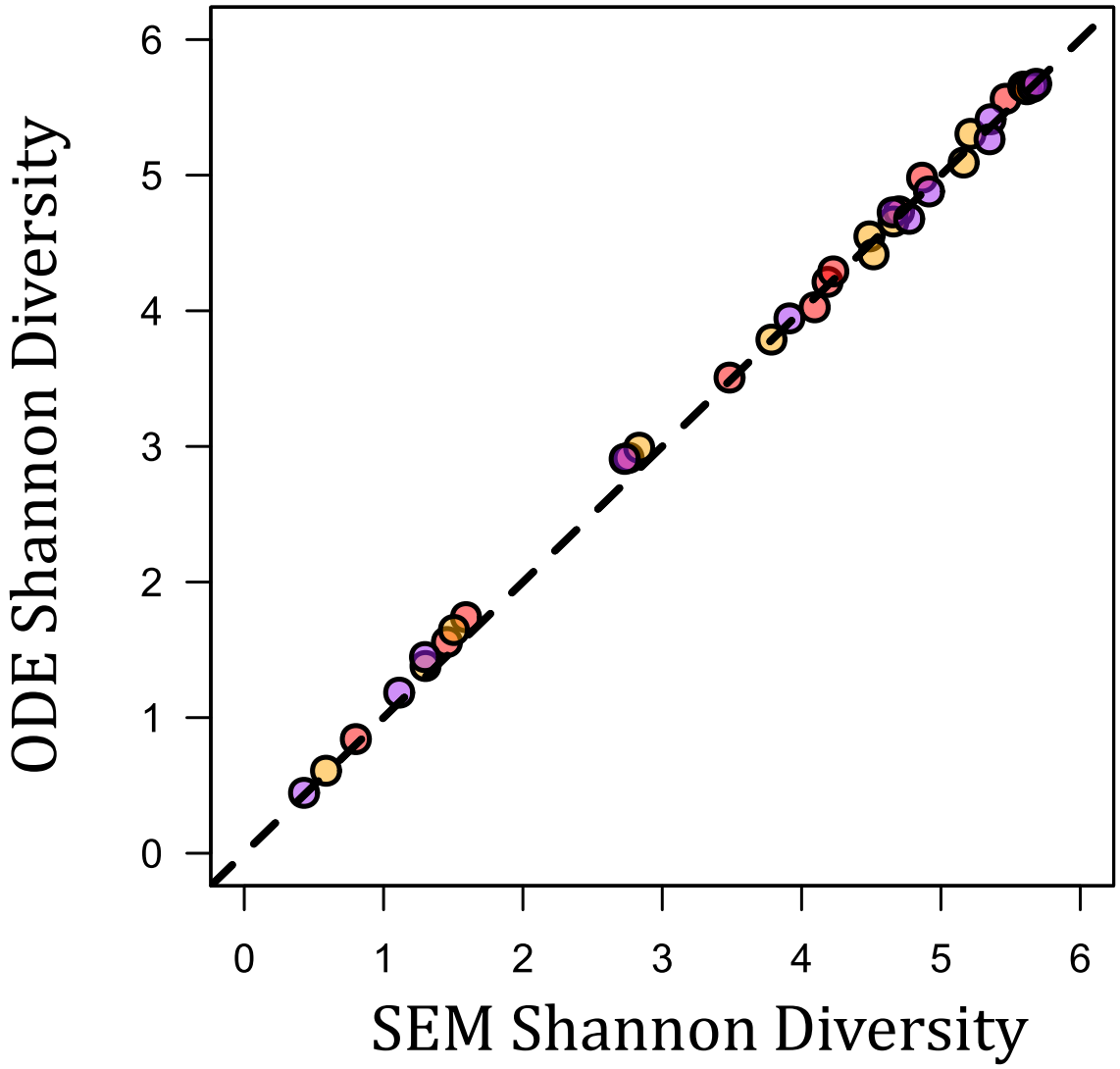

Figure 2.23: The same as the fig. 2.22, but showing Shannon Diversity instead of species richness. As in the above case, the SEM and ODE model yield very similar outputs.

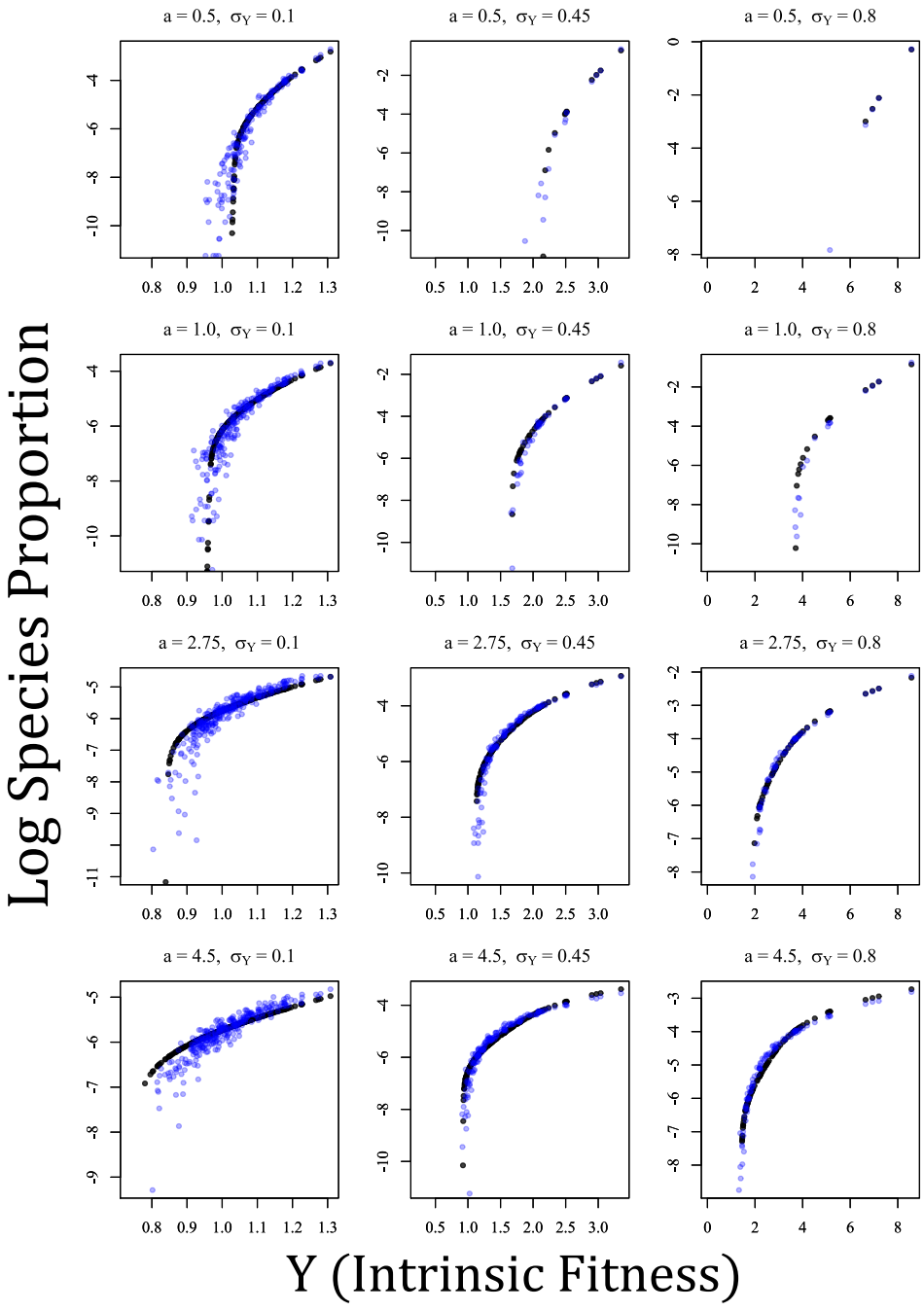

Figure 2.24: Comparisons between identical parameterizations of the ODE approximation (black) and SEM (blue) outputs under twelve parameter values when species vary in intrinsic fitness (Y). The y-axis depicts the log-proportion of each species and the x-axis depicts Y of each species. In all plots, $v = 5$, $g = 0.2$, and $D = 1.0$. Other relevant parameters are listed on each plot.

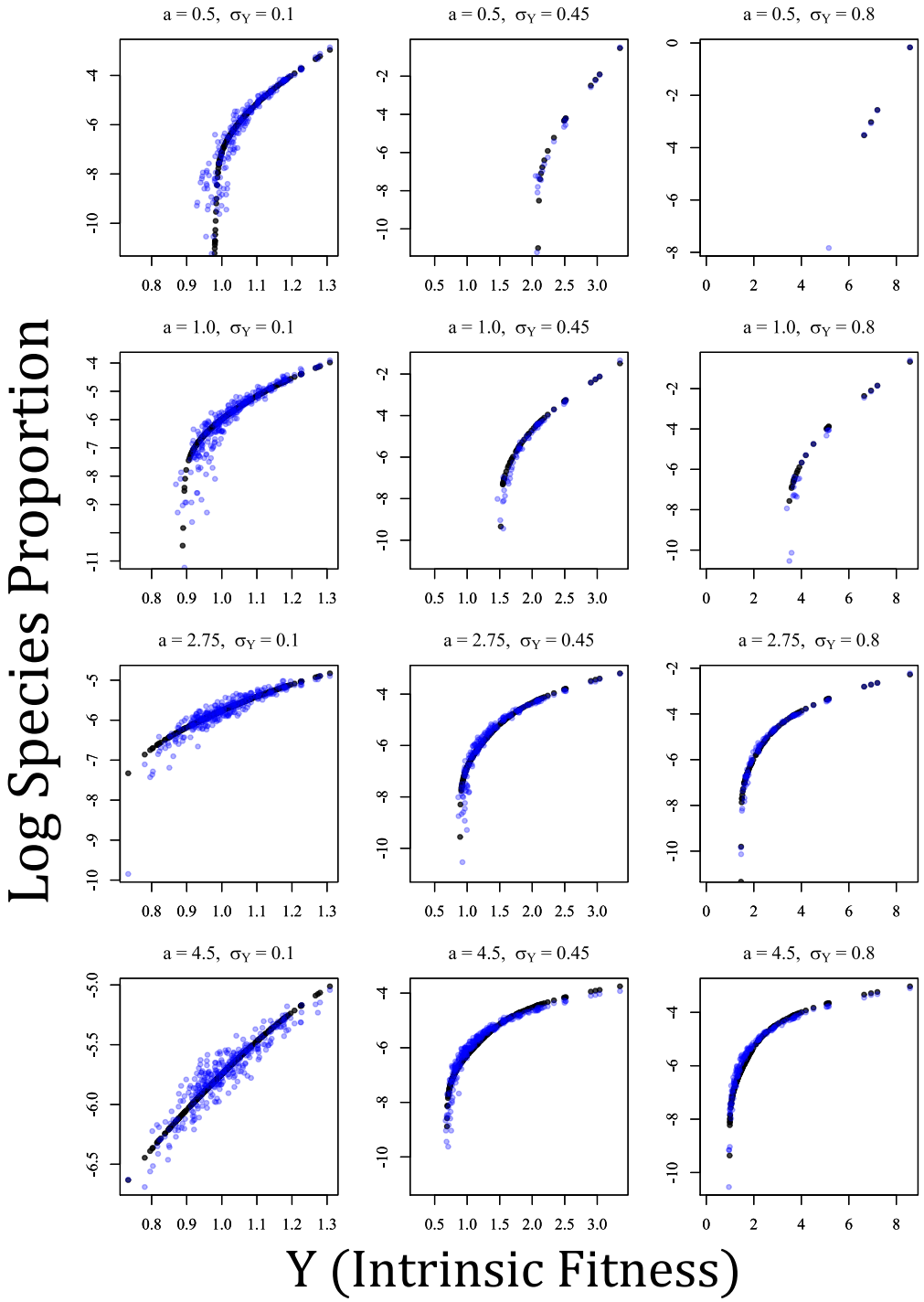

Figure 2.25: The same format as fig. 2.24, but with $v = 7.5$.

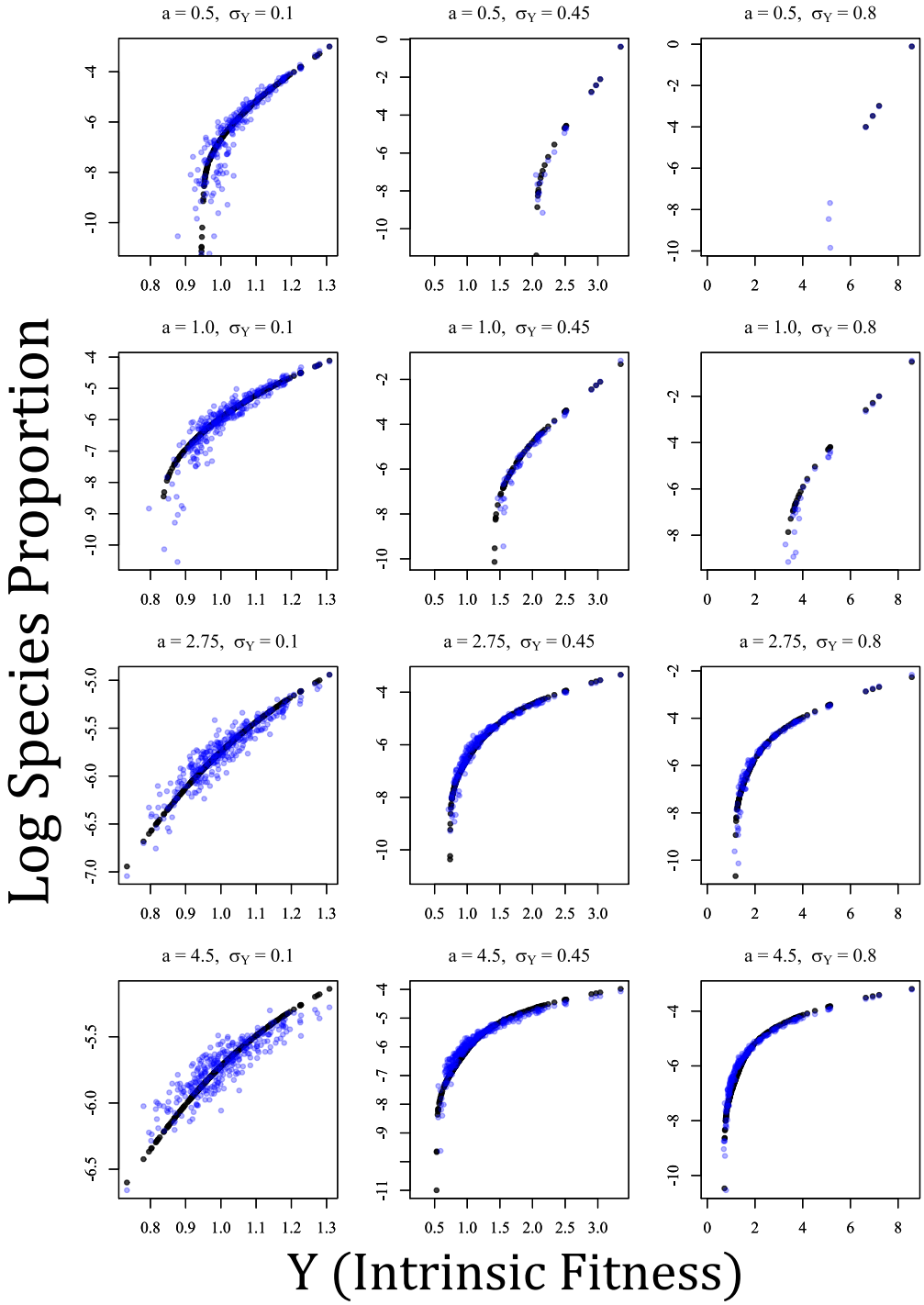

Figure 2.26: The same format as fig. 2.24, but with $v = 10$.

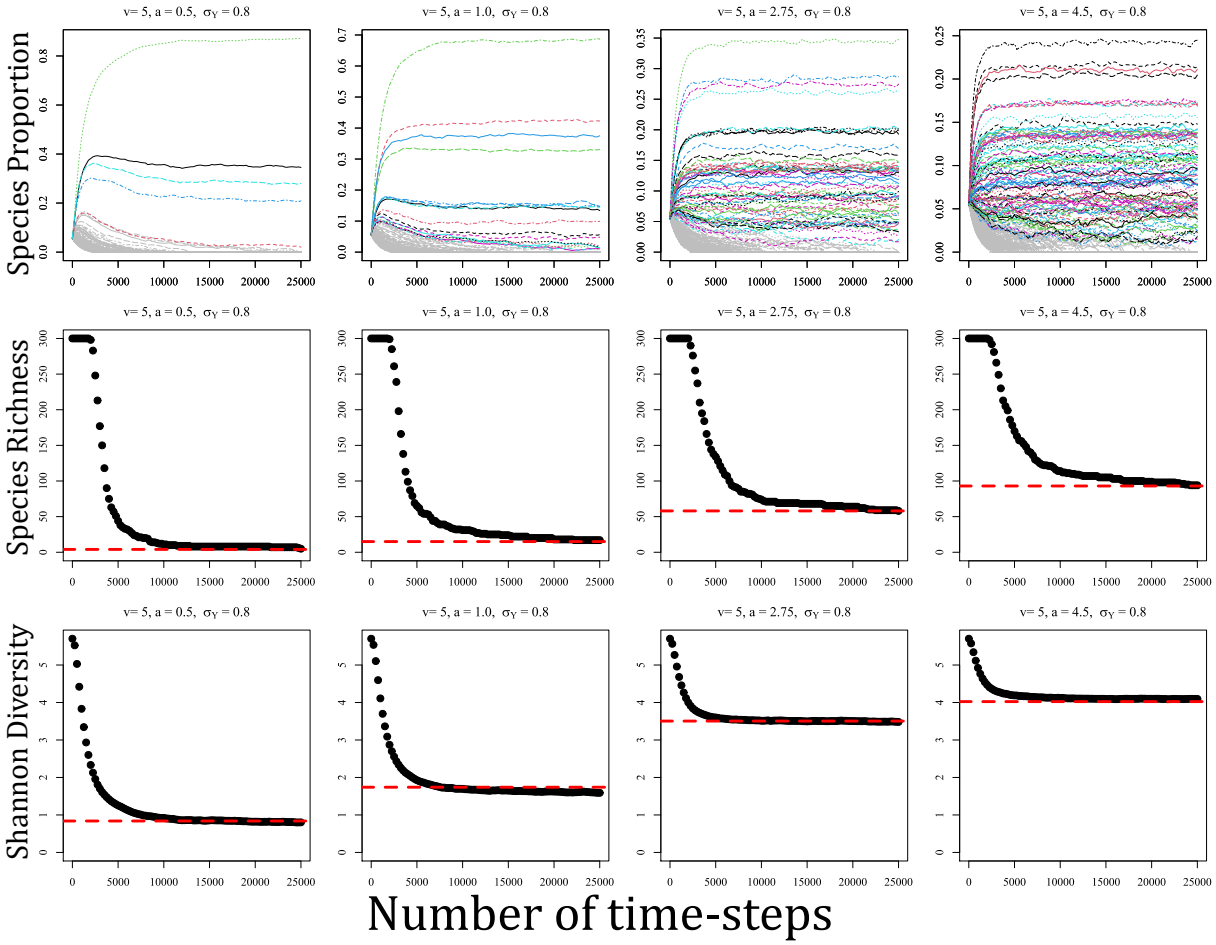

Figure 2.27: Examples of the SEM simulation time series outputs, species richness over time in the simulations, and Shannon diversity over time in the simulations. The top row shows examples of the time series outputs of the SEMs. The x-axis is time and the y-axis is each species' proportion. Proportions have been square-root transformed to aid visualization. Colored trajectories indicate species that persisted throughout the simulation; grey trajectories indicate species that went extinct. Parameters are listed on each plot. Dynamics as shown are typical examples from the SEMs. Most species settle into a relatively stable pseudo-equilibrium, while lower abundance species fluctuate due to drift. The second row shows the number of persisting species in the community as a function of time. Each panel corresponds to the plot above it. Most species that go extinct do so in the early stages of the dynamics. Therefore, the vast majority of persisting species likely persist deterministically. The dashed red line is the diversity maintained by the ODE under the same parameterization. All SEMs saturate, approximately, to the dashed line. The third row is the same as the second row, except it shows Shannon diversity instead of species richness.

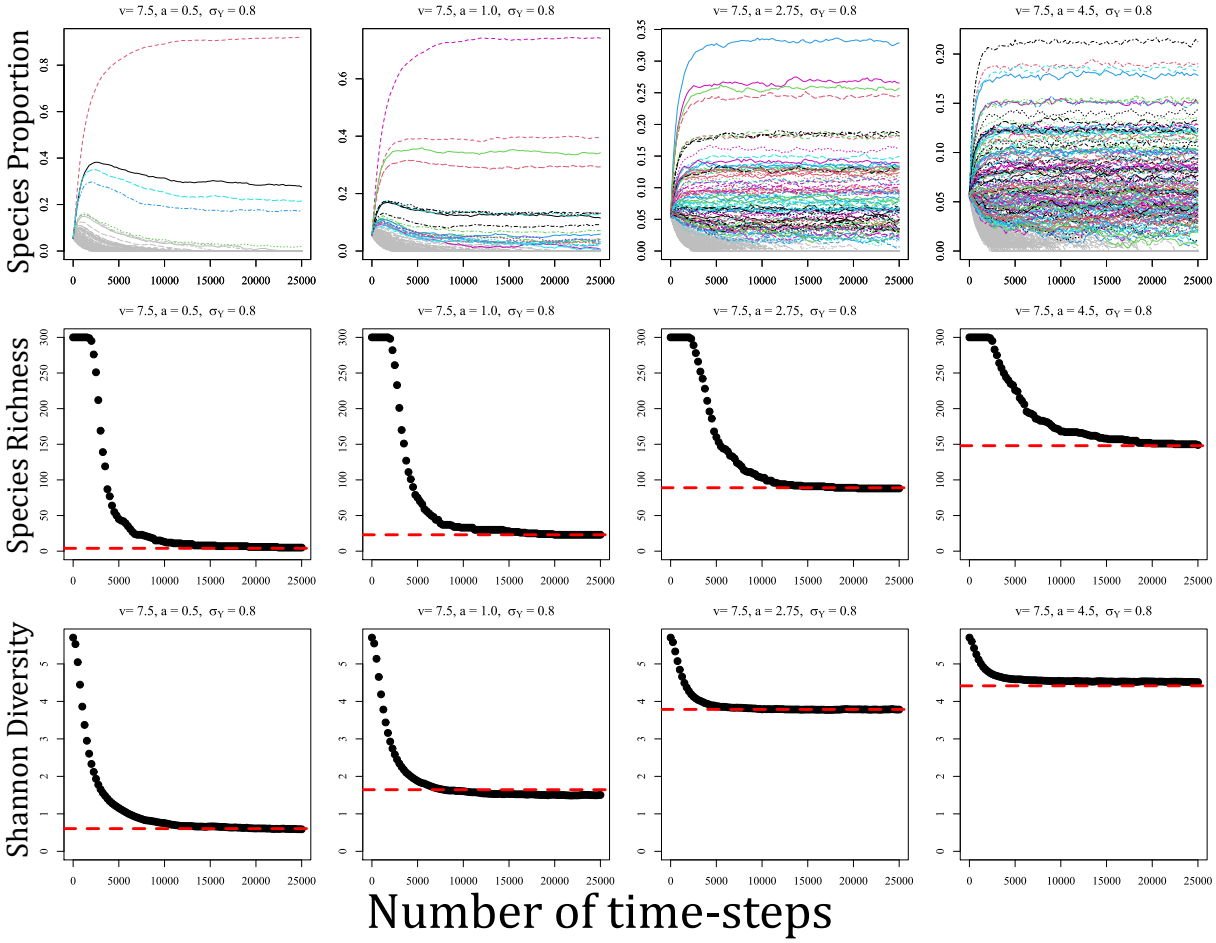

Figure 2.28: The same as fig. 2.27, but with $v = 7.5$.

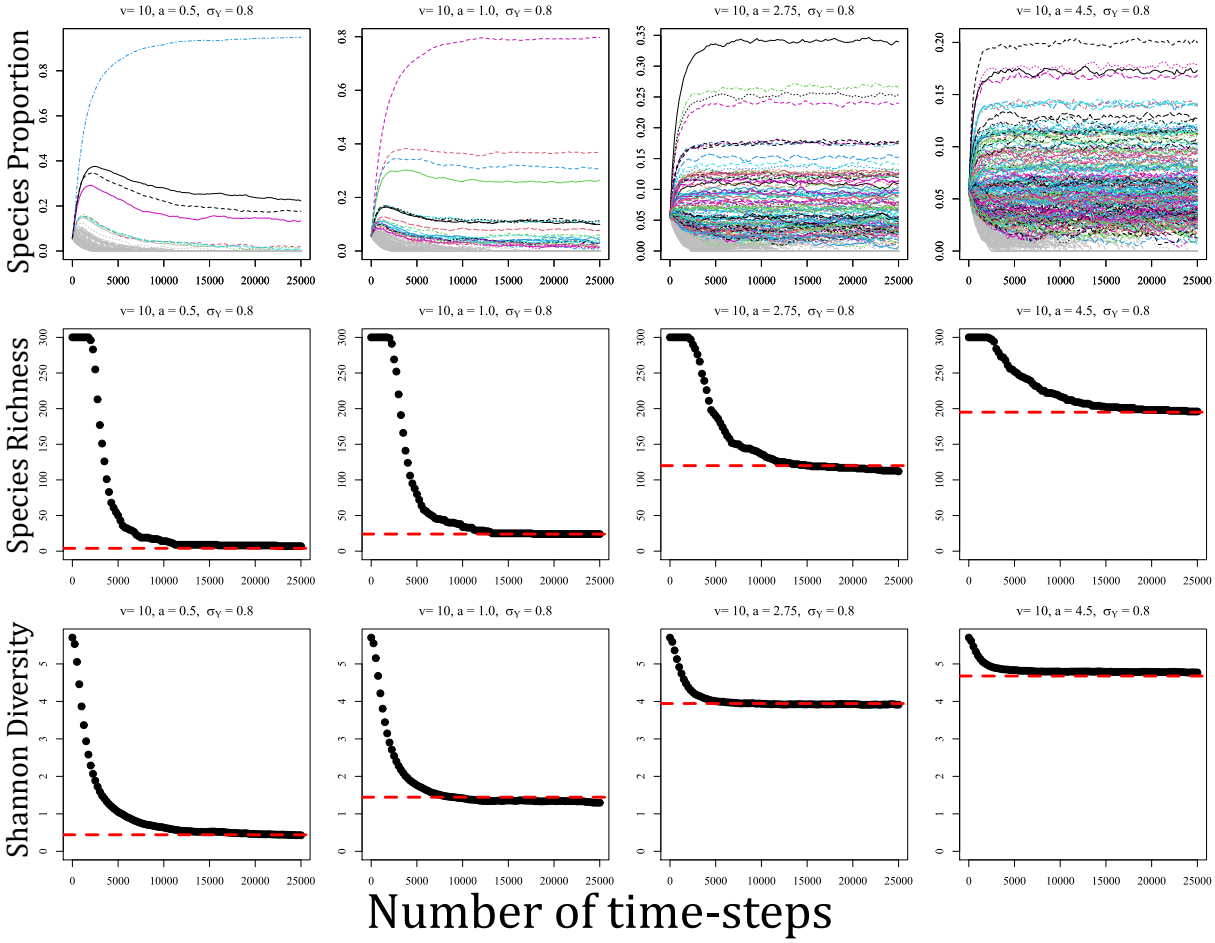

Figure 2.29: The same as fig. 2.27, but with $v = 10$.

Appendix A.4: Additive−Distance-decay model SEM and ODE approximation

Introduction

In this Appendix, I analyze the additive−distance-decay (AD) model presented in the main text. This Appendix is composed of three main subsections: **(1)** I introduce a spatially explicit model (SEM) for the AD model. I then demonstrate that taking the expected offspring abundances on each patch yields the Ordinary Differential Equation (ODE) model discussed in the main text. **(2)** I provide outputs of the ODE model and the SEM model under the same parameterizations. I show the outputs are very similar, hence demonstrating that the ODE is a sufficiently accurate approximation of the SEM. **(3)** I provide the derivation of the approximate invasion criteria for the AD model (Table 2.1 in the main text). The structure of this appendix is identical to that of appendices A-C.

Spatially Explicit Model and derivation of ODE approximation

In this subsection, I discuss the SEM, briefly reviewing within-patch dynamics from the main text. Then, I show the derivation of the ODE approximation. I assume the reader is generally familiar with the model discussed in the main text.

Spatially Explicit Model

I developed a Spatially Explicit Model (SEM) that incorporates additive predation pressure that decays with distance. The model consists of a community on a grid of $L \times L$ patches (M total patches, $M = L^2$) modeled as a torus to avoid edge effects. A single tree is present on every patch on the grid. At each time step, each tree dies with probability δ and tree replacement occur via a lottery based on seedling abundances on each patch. I assume predation pressure increases linearly as a function of conspecific density and that predation

induced by conspecific adults on a patch decreases exponentially with distance. As noted in the main text, offspring abundances are defined by

$$\begin{aligned} S_{i,i}(x) &= Y_i\big[(1-D)+p_iD\big]J_{i,i}(x) \\ S_{i,k}(x) &= Y_i p_i D J_{i,k}(x) \\ S_{all,i}(x) &= \sum_{n=1}^{N} S_{n,i,x} \end{aligned} \tag{2.85}$$

where $S_{A,B}(x)$ is the offspring abundance of species A on a patch occupied by species B at location x, $J_{i,i}(x)$ and $J_{i,k}(x)$ are how JCEs affect offspring surivorship, p_i is the proportion of species i in the population, Y_i is the intrinsic fitness of species i, and D is the dispersal proportion. For the AD model:

$$\begin{aligned} J_{i,i}(x) &= \exp\bigg[-a\bigg(1+\sum_{m=1}^{Mp_i} e^{-x_{i,m}/v}\bigg)\bigg] \\ J_{i,k}(x) &= \exp\bigg[-a\sum_{m=1}^{Mp_i} e^{-x_{i,m}/v}\bigg] \end{aligned} \tag{2.86}$$

Mp_i is the total number of individuals of species i in the community and $x_{i,m}$ is the distance between the m_{th} closest individual of species i and the focal patch at location x. $J_{i,i}(x)$ contains the $+1$ term because the focal patch contains an individual of species i. v defines rate at which predataion declines with distance (higher v indicates a lower rate of predation decay) and a is the baseline rate of predation pressure. Offspring abundances are then determined by the following equations:

$$
\begin{aligned}
S_{i,i}(x) &= Y_i\big[(1-D)+p_iD\big]\,\exp\bigg[-a\bigg(1+\sum_{m=1}^{Mp_i}e^{-x_{i,m}/v}\bigg)\bigg] \\
S_{i,k}(x) &= Y_ip_iD\,\exp\bigg[-a\sum_{m=1}^{Mp_i}e^{-x_{i,m}/v}\bigg] \\
S_{all,i}(x) &= Y_i\big[(1-D)+p_iD\big]\,\exp\bigg[-a\bigg(1+\sum_{m=1}^{Mp_i}e^{-x_{i,m}/v}\bigg)\bigg] \\
&\quad + D\sum_{k\neq i}Y_kp_k\,\exp\bigg[-a\sum_{m=1}^{Mp_k}e^{-x_{k,m}/v}\bigg]
\end{aligned}
\tag{2.87}
$$

As noted before, replacements are determined by a lottery model. The lottery is determined by the abundance of offspring. Let $P_{A,B}(x)$ be the probability species A colonizes a patch previously occupied by species B at location x. Then, $P_{i,i}(x) = S_{i,i}(x)/S_{all,i}(x)$ and $P_{i,k}(x) = S_{i,k}(x)/S_{all,k}(x)$. For the SEM, patch-specific JCEs are determined by the euclidean distances of adults surrounding each patch. The position of each patch is defined by its center point and it is assumed offspring are at the center of each patch.

ODE Model

To derive the ODE model, I take approximations of the expected values of $P_{i,i}(x)$ and $P_{i,k}(x)$. To do so, I take the expected abundance of $S_{i,i}(x)$, $S_{i,k}(x)$, and $S_{all,i}(x)$ and then take their quotients. Expectations are taken with respect to space. Using this, I derive the the ODE approximation

$$
\frac{dp_i}{dt} = \delta\bigg[\frac{\mathbb{E}[S_{i,i}(x)]}{\mathbb{E}[S_{all,i}(x)]}p_i + \sum_{k\neq i}\frac{\mathbb{E}[S_{i,k}]}{\mathbb{E}[S_{all,k}(x)]}p_k - p_i\bigg] \tag{2.88}
$$

that captures the behavior of the SEM. See "Note" at the end of this Appendix for additional information about the assumptions of this approximation.

Predation pressure in the SEM is implemented using the proximity trees in space that,

computationally, is stored in a matrix. The deterministic ODE model is spatially implicit. Therefore, it is necessary to use an approximation of the terms that does not require spatial information. Specifically, it is necessary to approximate $J_{i,i}(x)$ and $J_{i,k}(x)$ in spatially implicit terms. To do this, I evaluate

$$\mathbb{E}\left[J_{i,k}(x)\right] \tag{2.89}$$

noting that $J_{i,i}(x) = e^{-a} J_{i,k}(x)$ (in which case, it is sufficient to just compute $J_{i,k}(x)$).

To accomplish this, I evaluate the total mortality an individual of species i induces given the AD model. Then, I assume individuals (and thus, mortality induced) are randomly distributed in space. Then, I calculate the probability that mortality does not occur on a random patch. The total mortality induced by an individual of species i is equal to

$$\lambda = 2\pi g \int_0^\infty x\left(1 - e^{-ae^{-x/v}}\right)\mathrm{d}x \tag{2.90}$$

where x represents distance and $\left(1 - e^{-ae^{-x/v}}\right)$ is the proportion of offspring that do not survive x meters away from an adult of species i. The 2π term reflects that predation pressure occurs in 2D space. Therefore, λ then represents the sum of mortality induced by an individual of species i.

Species i is of proportion p_i in the population and I assume adults of species i are approximately randomly distributed in space. Then adults of species i are Poission distributed in 2D space and, by extension, mortality is also approximately Poisson distributed with rate parameter $p_i\lambda$. Then, the probability that no mortality event occurs on a random patch (i.e. the probability of survival) is relatively easy to define:

$$\mathrm{P}(\text{no mortality}) = \mathrm{P}(\mathrm{Poi}(p_i\lambda) \ = 0) \ = \frac{1^0 e^{-p_i\lambda}}{0!} = e^{-p_i\lambda}.$$

This yields:

$$\mathbb{E}[J_{i,k}(x)] = \exp\Bigg[- p_i \, 2\pi g \int_0^\infty x\Big(1 - e^{-ae^{-x/v}}\Big)\mathrm{d}x\Bigg]. \tag{2.91}$$

which is the quantity of interested (the probability of offspring survival). It is necessary to evaluate this quantity.

The integral (λ) is not trivial to evaluate. One approach is to take the Taylor series of $e^{-ae^{-x/v}}$. The expression becomes

$$2\pi g \int_0^\infty x\Big(1 - \sum_{n=0}^{\infty} \frac{(-ae^{-x/v})^n}{n!}\Big)\mathrm{d}x \tag{2.92}$$

When $n = 1$, $\frac{(-ae^{-x/v})^n}{n!} = 1$. Therefore, the above can be rewritten as

$$2\pi g \int_0^\infty x\Big(1 - \Big[1 + \sum_{n=1}^{\infty} \frac{(-ae^{-x/v})^n}{n!}\Big]\Big) = -2\pi g \int_0^\infty x \sum_{n=1}^{\infty} \frac{(-ae^{-x/v})^n}{n!}\mathrm{d}x \tag{2.93}$$

noting the change in the index of summation ($n = 1$). Then, changing the order of integration and summation and evaluating the integral yields

$$-2\pi g \sum_{n=1}^{\infty} \frac{v(nx+v)\left(-ae^{-x/v}\right)^n}{n^2 n!}\Bigg|_0^\infty \tag{2.94}$$

When all the constants are positive (as is the case for this expression) it is easy to show that

$$\lim_{x\to\infty} \frac{v(nx+v)\left(-ae^{-x/v}\right)^n}{n^2 n!} \to 0 \tag{2.95}$$

for all $n \geq 1$ on the basis that $\lim_{x\to\infty}(x + K_1)e^{-xK_2} \to 0$ if K_1 and K_2 are positive constants (which is the case for the equivalent terms involving v and n in the equation

above). Therefore,

$$-2\pi g \sum_{n=1}^{\infty} \frac{v(nx+v)\left(-ae^{-x/v}\right)^n}{n^2 n!}\Bigg|_0^{\infty} =$$
$$\lim_{x\to\infty}\left(-2\pi g \sum_{n=1}^{\infty} \frac{v(nx+v)\left(-ae^{-x/v}\right)^n}{n^2 n!}\right) + \lim_{x\to 0} 2\pi \sum_{n=1}^{\infty} \frac{v(nx+v)\left(-ae^{-x/v}\right)^n}{n^2 n!}$$
$$= 2\pi g v^2 a \sum_{n=1}^{\infty} \frac{(-a)^{n-1}}{n^2 n!} \tag{2.96}$$

after some small algebraic manipulations. Importantly, while the summation

$$\sum_{n=1}^{\infty} \frac{(-a)^{n-1}}{n^2 n!}$$

has no elementary solution I am aware of, it has all the properties of a Generalized Hypergeometric Function (henceforth, GHF). To see this, note that the summation follows the form

$$\sum_{n=1}^{\infty} \frac{(-a)^{n-1}}{n^2 n!} = 1 + \frac{1}{2^2 2!}(-a)^1 + \frac{1}{3^2 3!}(-a)^2 + ... + \frac{1}{n^2 n!}(-a)^{n-1} \tag{2.97}$$

Let β_n be the n_{th} coefficient of the summation (i.e. $\beta_0 = 1$, $\beta_1 = \frac{1}{2^2 2!}$, etc.). Therefore,

$$\frac{\beta_{n+1}}{\beta_n} = \frac{(n+2)^2(n+2)!}{(n+1)^2(n+1)!} = \frac{(n+2)^3}{(n+1)^2} \tag{2.98}$$

This yields the GHF

$$\sum_{n=1}^{\infty} \frac{(-a)^{n-1}}{n^2 n!} = {}_3F_3(1,1,1;2,2,2;-a) \tag{2.99}$$

(a result the interested reader can confirm using Wolfram Mathematica; (Wolfram Inc.,

2021). For simplicity, I use the notation

$$H(a) = {}_3F_3(1,1,1;2,2,2;-a) \tag{2.100}$$

from this point forward. Therefore, finally,

$$2\pi g \int_0^\infty x\left(1 - e^{-ae^{-x/v}}\right)\mathrm{d}x = 2a\pi g v^2 H(a) \tag{2.101}$$

in which case,

$$\mathbb{E}[J_{i,k}(x)] \approx e^{-2ap_i\pi g v^2 H(a)} \tag{2.102}$$

Substituting this into the offspring abundance equations

$$\begin{aligned}\mathbb{E}[S_{i,k}(x)] &= Y_i\big[(1-D) + p_i D\big]e^{-a}e^{-ap_i E_D H(a)} \\ \mathbb{E}[S_{i,k}(x)] &= Y_i p_i D e^{-ap_i E_D H(a)}\end{aligned} \tag{2.103}$$

where

$$E_D = 2\pi g v^2$$

and where $S_{all,i}(x) = \sum_{n=1}^{N} S_{n,i}(x)$. These expressions are identical to the AD model offspring abundance equations in the main text.

Comparison between ODE model and SEM model

In this subsection, I describe simulations that compare the ODE model to the SEM. I demonstrate that the SEM and ODE model yield highly similar outputs of species abundance and species richness. I provide 36 comparisons of the SEM to the ODE (12 cases in which $v = 5$, 12 cases in which $v = 7.5$, and 12 cases in which $v = 10$).

ODE and SEM parameterization

Each SEM simulation began with 300 species at equal abundance, with individuals randomly distributed throughout the community. Simulations were conducted on a 275×275 torus (thus containing 275^2 individual trees). I used the following parameters: $Y \sim \text{lognormal}[\mu = 0, \sigma_Y]$ with $\sigma_Y \sim \{0.1, 0.45, 0.8\}$ and $a \sim \{0.5, 1.0, 2.75, 4.5\}$. In all simulations, $g = 0.20$ and $D = 1$. I tested each of the 12 parameter combinations of σ_Y and a with $v \sim \{5, 7.5, 10\}$. This generated 36 outputs. Simulations were run for about 65 generations, sufficient time for the community to approximately reach equilibrium without drift dominating the dynamics of the lower abundance species. See Figs. 2.35-2.37 for typical outputs of the SEM time series dynamics.

A corresponding set of 36 ODE simulations were run using the same parameterizations as the SEM. I compared the outputs of the SEM and ODE model in terms of species diversity, species abundance, and Shannon diversity. I considered a species to be extinct if it had less than 1 individual at any point of the simulation. This was implemented directly in the SEM; for the ODE model, I assumed a species, i, to be extinct if $p_i^* < 1/275^2$ where p_i^* is the equilibrium proportion of species i. Note that these simulations do not attempt to demonstrate the long-term resistance against extinction due to drift. Rather, they demonstrate that the ODE model and SEM yield similar outputs of expected species abundance and richness given the same parameterization.

Results of comparison

ODE model and SEM produced very similar species richness and Shannon diversity (Figs. 2.30, 2.31). The ODE model and SEM also produced very similar species proportions (Figs. 2.32-2.34). To quantify the quality of the approximation, I calculated the mean difference in

species richness between the ODE model and SEM, ΔR:

$$\Delta R = \frac{1}{S}\sum_{k=1}^{S}(R^k_{\text{SEM}} - R^k_{\text{ODE}}) \tag{2.104}$$

where S is the number of simulations, and R^k_{SEM} and R^k_{ODE} are the species richness of the k_{th} simulation of the SEM and ODE model, respectively. I also examined the r^2 (coefficient of determination) between SEM and ODE species richness. For the comparisons, $\Delta R = -.52$ and $r^2 = 0.99$. Overall, the ODE provides a highly similar, albeit non-exact, estimation of species diversity. Error in which the ODE model predicted greater diversity than the SEM is most likely due to stochastic extinction due to drift. This is particularly likely when species richness is high, where the expected abundance of each species is correspondingly smaller. Cases in which the ODE model predicted lower species richness are likely due to incomplete transient dynamics of the SEM.

Derivation of invasion criteria

In this subsection, I derive the approximate invasion criteria of the additive−fixed-distance model when species experience inter-specific variation in intrinsic (Y) and $D = 1$. Recalling the derivations above,

$$\mathbb{E}[J_{k,i}(x)] = e^{-ap_iE_DH(a)} \tag{2.105}$$

and

$$\mathbb{E}[J_{i,i}(x)] = e^{-a}e^{-ap_iE_DH(a)} \tag{2.106}$$

The invasion criteria of an invader can be expressed as when the per capita growth rate as $p_i \to 0$. Using variables previous defined in this Appendix, the per capita growth rate of

species i (substituting in the seedling abundance values) is

$$\frac{1}{p_i}\frac{dp_i}{dt} = r_i = \delta\Bigg[\frac{Y_i\big[(1-D)+p_iD\big]}{Y_i\big[(1-D)+p_iD\big]\,\mathbb{E}[J_{i,i}(x)] + \sum_{k\neq i} Y_k p_k D\,\mathbb{E}[J_{k,i}(x)]} + Y_i D \sum_{m\neq i} \frac{1}{Y_m\big[(1-D)+p_mD\big]\,\mathbb{E}[J_{m,m}(x)] + \sum_{k\neq m} Y_k p_k D\,\mathbb{E}[J_{k,m}(x)]} p_m - 1\Bigg] \tag{2.107}$$

Species i can invade is this quantity if positive when it is rare ($p_i \to 0$). When $D = 1$ (the case of interest), the above reduces to

$$Y_i \sum_{m\neq i} \frac{p_m}{Y_m\,\mathbb{E}[J_{m,m}(x)]p_m + \sum_{k\neq m} Y_k p_k\,\mathbb{E}[J_{k,m}(x)]} > 1 \tag{2.108}$$

To simplify the above equation, I ignore the term $Y_m\,\mathbb{E}[J_{m,m}(x)]p_m$ in the denominator and incorporate an additional term representing species m into the summation, yielding:

$$Y_i \sum_{m\neq i} \frac{p_m}{\sum_{k\neq i} Y_k p_k\,\mathbb{E}[J_{k,i}(x)]} > 1 \tag{2.109}$$

This simplification is equivalent to making the species identity of the tree previously occupying a patch (the tree that dies) irrelevant (i.e., JCEs only result from trees nearby the patch rather than the previous occupant of the patch). As long as JCEs occur over a non-trivially small area (such that v is not very small) this assumption does not meaningfully affect the invasion criteria.

Importantly, the denominator of equation (2.109) is no longer directly dependent on m. That is, equation (2.109) can be rewritten as

$$Y_i\Bigg(\sum_{m\neq i} p_m\Bigg)\Bigg(\frac{1}{\sum_{k\neq i} Y_k p_k\,\mathbb{E}[J_{k,i}(x)]}\Bigg) > 1 \tag{2.110}$$

Because, by definition, $\sum_{m \neq i} p_m = 1$, the above equation can be rewritten as

$$Y_i > \sum_{k \neq i} Y_k p_k \, \mathbb{E}[J_{k,i}(x)] \tag{2.111}$$

Substituting the appropriate value for $\mathbb{E}[J_{k,i}(x)]$, the invasion criteria becomes

$$Y_i > \sum_{k \neq i} Y_k p_k e^{-a p_k E_D H(a)} \tag{2.112}$$

recalling that $E_D = 2\pi v^2 g$. I take the linearization of $p_k e^{-a p_k E_D H(a)}$ about the point $1/N$ where N is the number of species in the resident community (and thus, $1/N$ is the average abundance). This yields a close approximation of the expression so long as no species exhibits an abundance much greater than the mean abundance. For simplicity, let

$$J = a E_D H(a) \tag{2.113}$$

The, taking the linearization yields

$$p_k e^{-J p_k} \approx \frac{e^{-\frac{J}{N}}}{N} + \frac{e^{-\frac{J}{N}} \left(p_k - \frac{1}{N} \right)}{N} \left(1 - \frac{J}{N} \right) \tag{2.114}$$

Substituting this into the original expression, the summation can be rearranged and broken up into three parts:

$$e^{-\frac{J}{N}} \frac{1}{N} \sum_{k \neq i} Y_k + e^{-\frac{J}{N}} \left(1 - \frac{J}{N} \right) \sum_{k \neq i} Y_k p_k - e^{-\frac{J}{N}} \left(1 - \frac{J}{N} \right) \frac{1}{N} \sum_{k \neq i} Y_k \tag{2.115}$$

The first summation is straightforward to calculate:

$$e^{-\frac{J}{N}} \frac{1}{N} \sum_{k \neq i} Y_k = e^{-\frac{J}{N}} \overline{Y} \tag{2.116}$$

where $\overline{Y}$ is the mean intrinsic fitness of the community.

The second term can be expressed by using the property

$$\frac{1}{N}\sum_{m=1}^{N} A_m B_m = \overline{A} \times \overline{B} + \mathrm{Cov}(A, B) \tag{2.117}$$

I apply this property with respect to p and Y, noting that $\overline{p} = \frac{1}{N}$. Using this property and substituting A and B with p and Y for the first and second summations yields

$$\begin{aligned} e^{-\frac{J}{N}}\left(1-\frac{J}{N}\right)\sum_{k\neq i} p_k Y_k &= e^{-\frac{J}{N}}\left(1-\frac{J}{N}\right) N \frac{1}{N}\sum_{k\neq i} p_k Y_k \\ &= e^{-\frac{J}{N}}\left(1-\frac{J}{N}\right) N\left[\overline{Y}\frac{1}{N} + \mathrm{Cov}(p, Y)\right] \\ &= e^{-\frac{J}{N}}\left(1-\frac{J}{N}\right)\left[\overline{Y} + N\ \mathrm{Cov}(p, Y)\right] \end{aligned} \tag{2.118}$$

The third summation is easy to calculate:

$$-e^{-\frac{J}{N}}\left(1-\frac{J}{N}\right)\frac{1}{N}\sum_{k\neq i} Y_k = -e^{-\frac{J}{N}}\left(1-\frac{J}{N}\right)\overline{Y} \tag{2.119}$$

Adding all three summations together, the third summation term will cancel with the $\overline{Y}$ term of the second summation. Then, after some rearranging, I substitute $J = aE_D H(a)$ back into the equation. This yields:

$$Y_i > \underbrace{\overline{Y} e^{-aH(a)\frac{E_D}{N}}}_{\substack{\text{mean} \\ \text{JCE-fitness term}}} + \underbrace{N\mathrm{Cov}(p, Y)\left(1 - aH(a)\frac{E_D}{N}\right)e^{-aH(a)\frac{E_D}{N}}}_{\text{covariance-JCE term}} \tag{2.120}$$

which is identical to expression for the AD model in Table 2.1 of the main text.

Note on ODE approximation

To derive the ODE model, I took approximations of the expected values of $P_{i,i}(x)$ and $P_{i,k}(x)$. To do so, I took the expected abundance of $S_{i,i}(x)$, $S_{i,k}(x)$, and $S_{all,i}(x)$ with respect to space and then examined their quotients. Note that this assumes $\mathbb{E}[S_{i,k}(x)/S_{all,i}(x)] \approx \mathbb{E}[S_{i,k}(x)]/\,\mathbb{E}[S_{all,k}(x)]$ (I take the expectation of the numerator and denominator and then take the quotient). Using a Taylor Expansion about the mean,

$$\mathbb{E}\left[\frac{S_{i,k}(x)}{S_{all,i}(x)}\right] \approx \frac{\mathbb{E}[S_{i,k}(x)]}{\mathbb{E}[S_{all,k}(x)]} - \frac{\mathrm{Cov}\big(S_{i,k}(x), S_{all,k}(x)\big)}{\mathbb{E}[S_{all,k}(x)]^2} + \mathrm{Var}\big(S_{all,k}(x)\big)\frac{\mathbb{E}[S_{i,k}(x)]}{\mathbb{E}[S_{all,i}(x)]^3}$$

Because there are many species in the community, $S_{all,i}(x) >> S_{i,k}(x)$. This implies that the covariance term and the term containing $\mathbb{E}[S_{all,i}(x)]^3$ are close to zero. Additionally, $\mathrm{Var}\big(S_{all,i}(x)\big)$ is likely small because it is assumed that dispersal is uniform across the community. Therefore, $\mathbb{E}[S_{i,k}(x)/S_{all,i}(x)] \approx \mathbb{E}[S_{i,k}(x)]/\,\mathbb{E}[S_{all,k}(x)]$ is likely a good approximation. I rely on the quantitative similarity of the SEM and ODE model to validate this assumption.

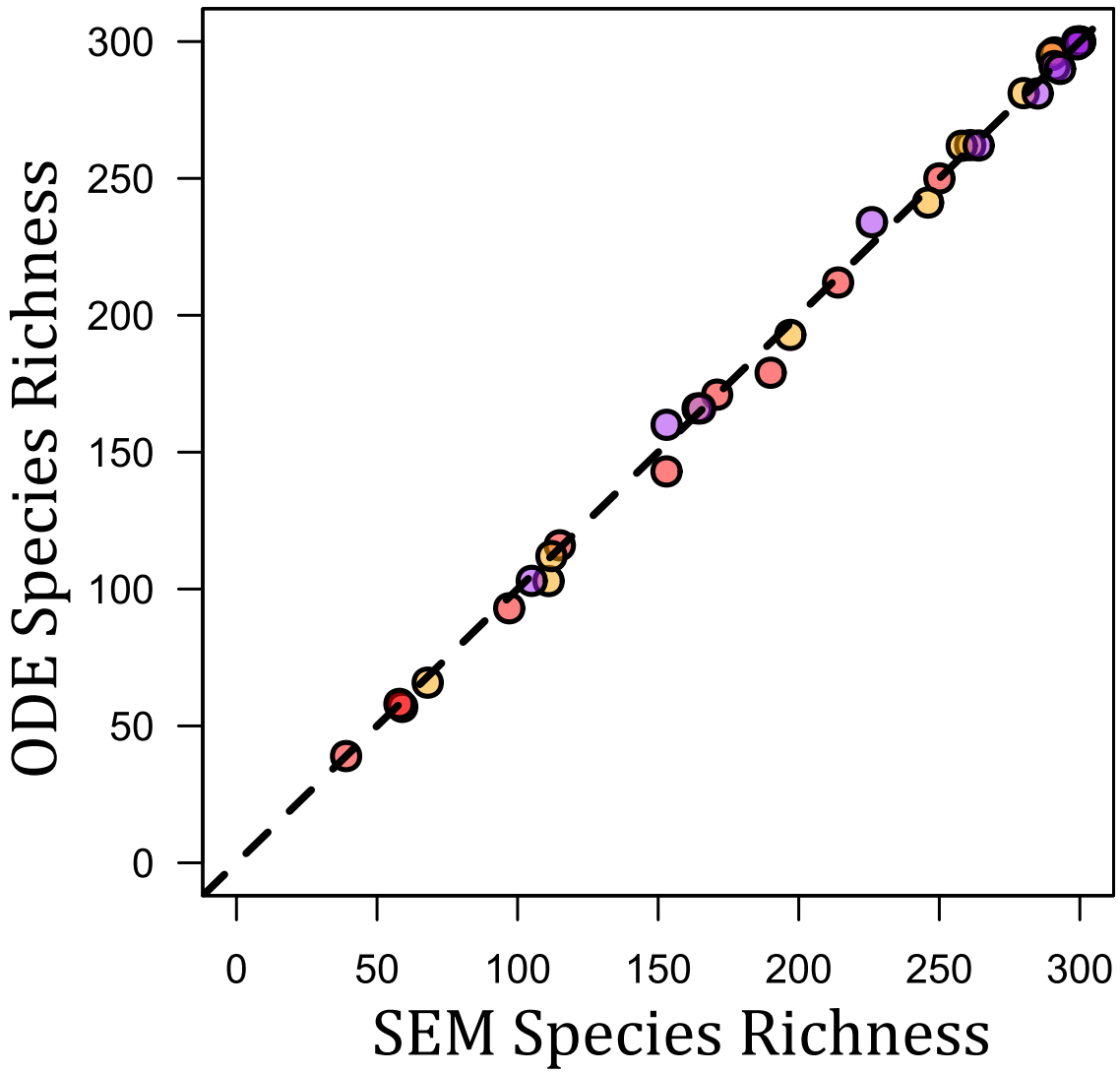

Figure 2.30: ODE model validation. The figures compare species richness between SEM and ODE model simulations under identical parameterizations.The dashed line is the one-to-one line (points on the line represent when the SEM and ODE yield the exact same diversity output). Red points are when $v = 5$, orange/yellow points are when $v = 7.5$, and purple points are when $v = 10$. To a first approximation, the ODE model yields the same output as the SEM. These parameter values span the most of the parameter space explored in Figs. 2 and 3 of the main text.

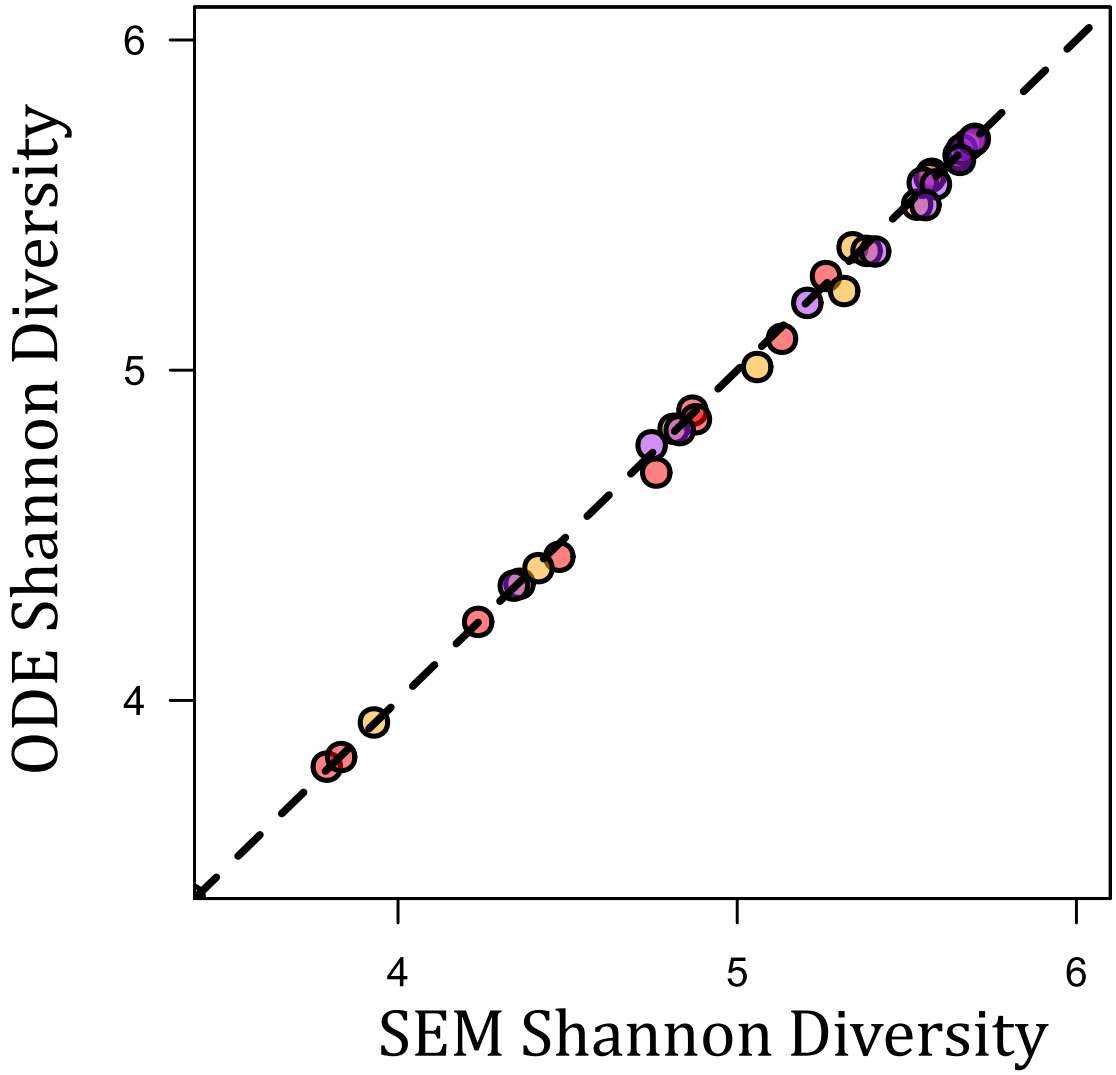

Figure 2.31: The same as the fig. 2.30, but showing Shannon Diversity instead of species richness. As in the above case, the SEM and ODE model yield very similar outputs.

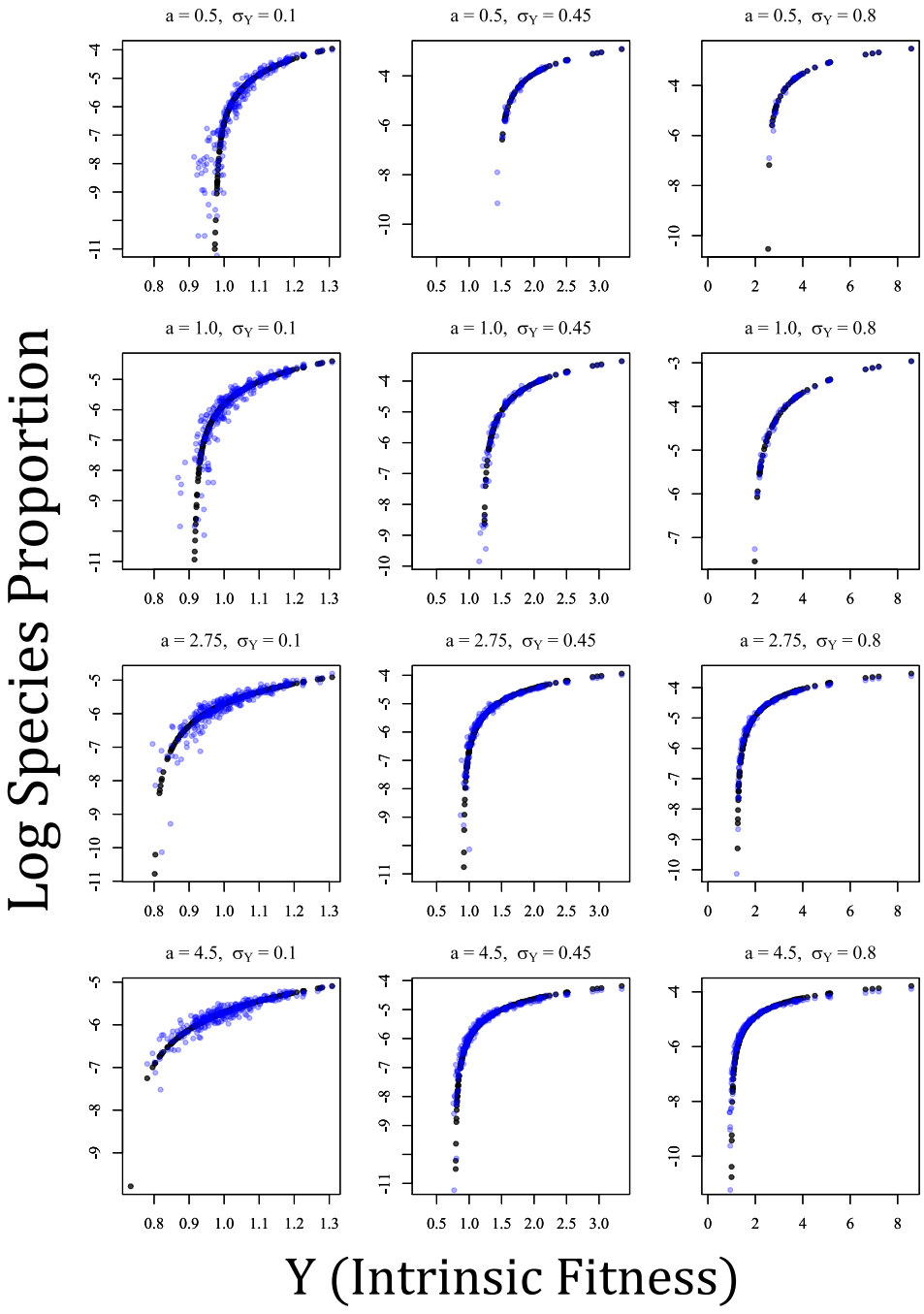

Figure 2.32: Comparisons between identical parameterizations of the ODE approximation (black) and SEM (blue) outputs under twelve parameter values when species vary in intrinsic fitness (Y). The y-axis depicts the log-proportion of each species and the x-axis depicts Y of each species. In all plots, $v = 5$, $g = 0.2$, and $D = 1.0$. Other relevant parameters are listed on each plot.

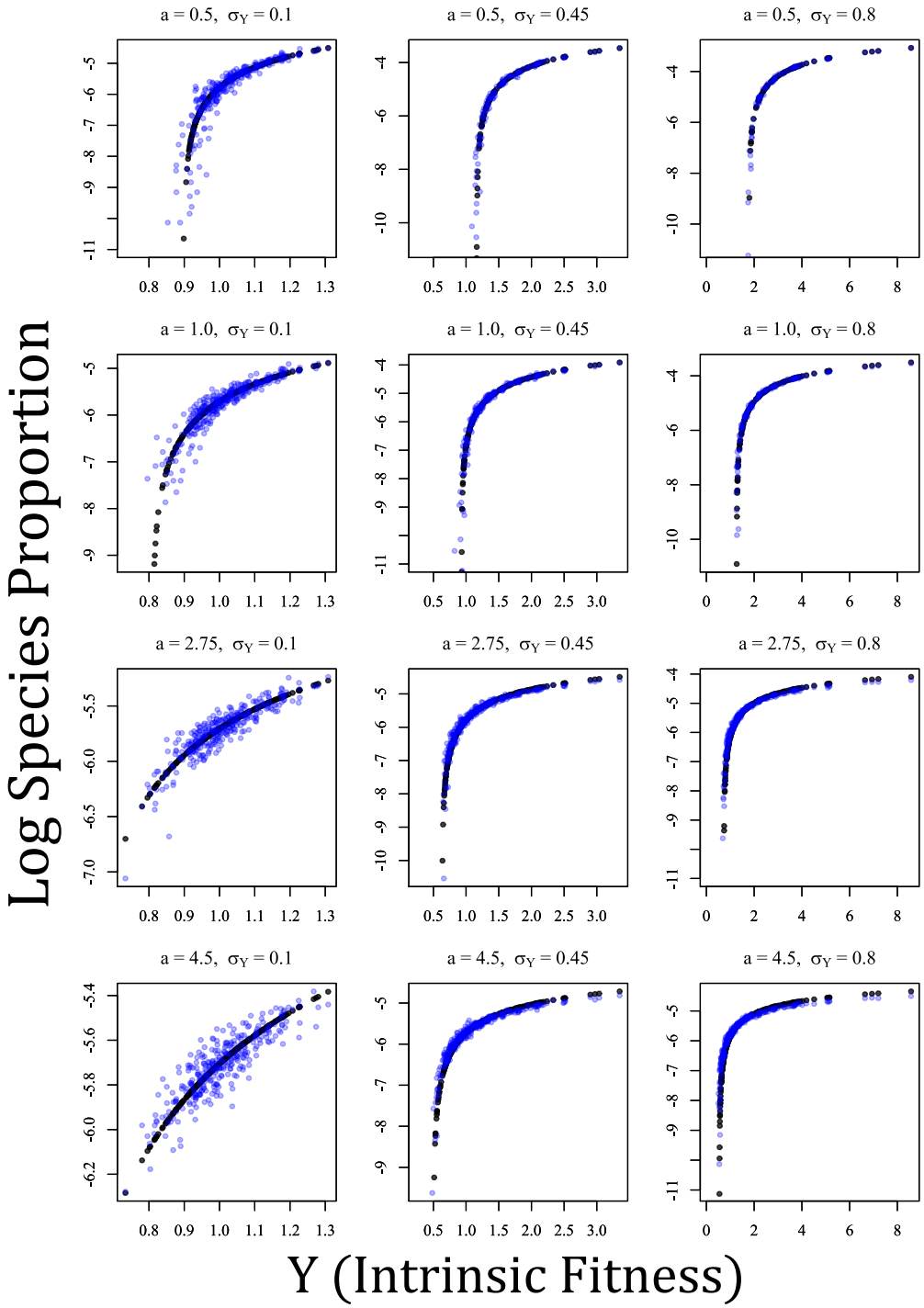

Figure 2.33: The same format as fig. 2.32, but with $v = 7.5$.

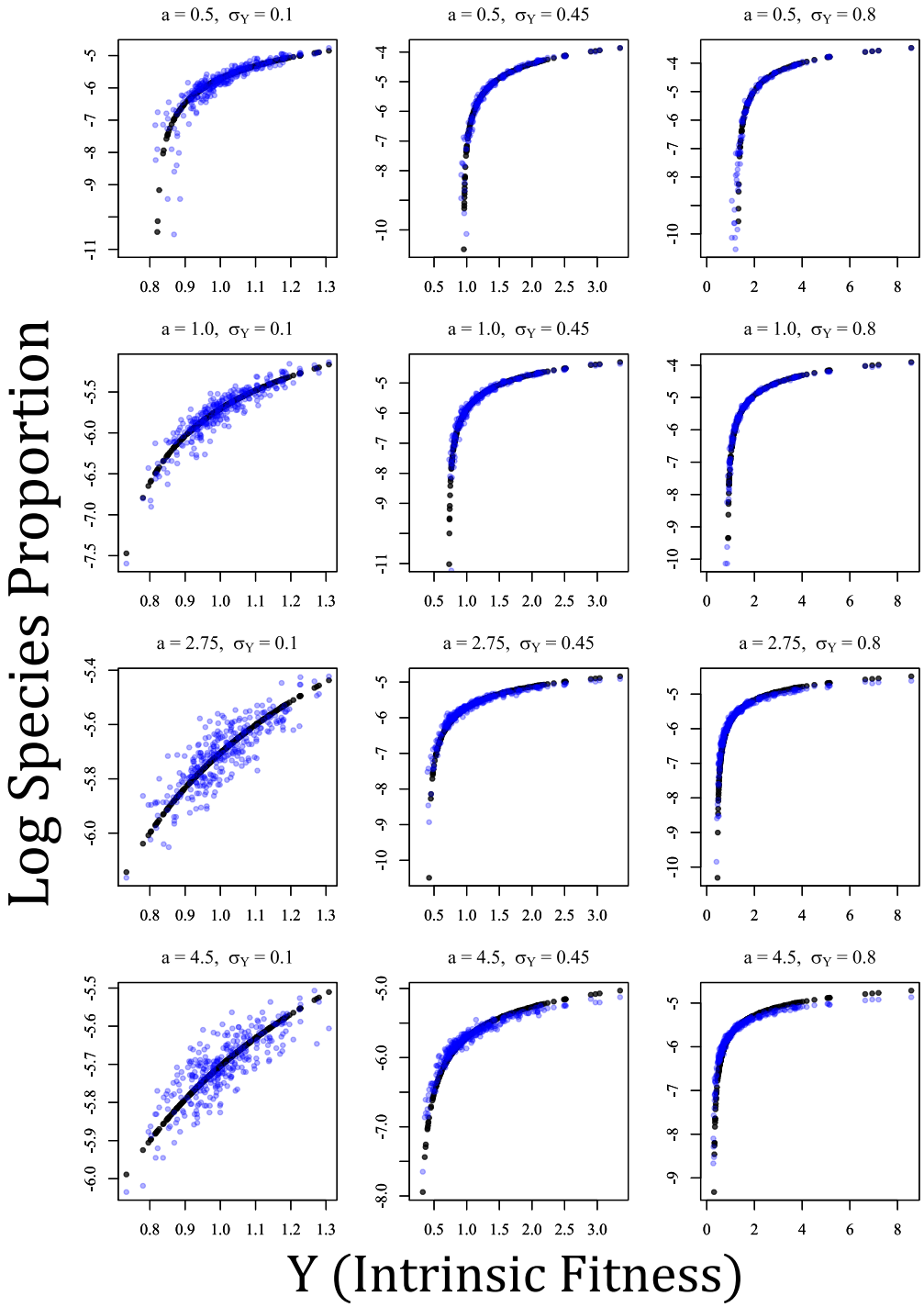

Figure 2.34: The same format as fig. 2.32, but with $v = 10$.

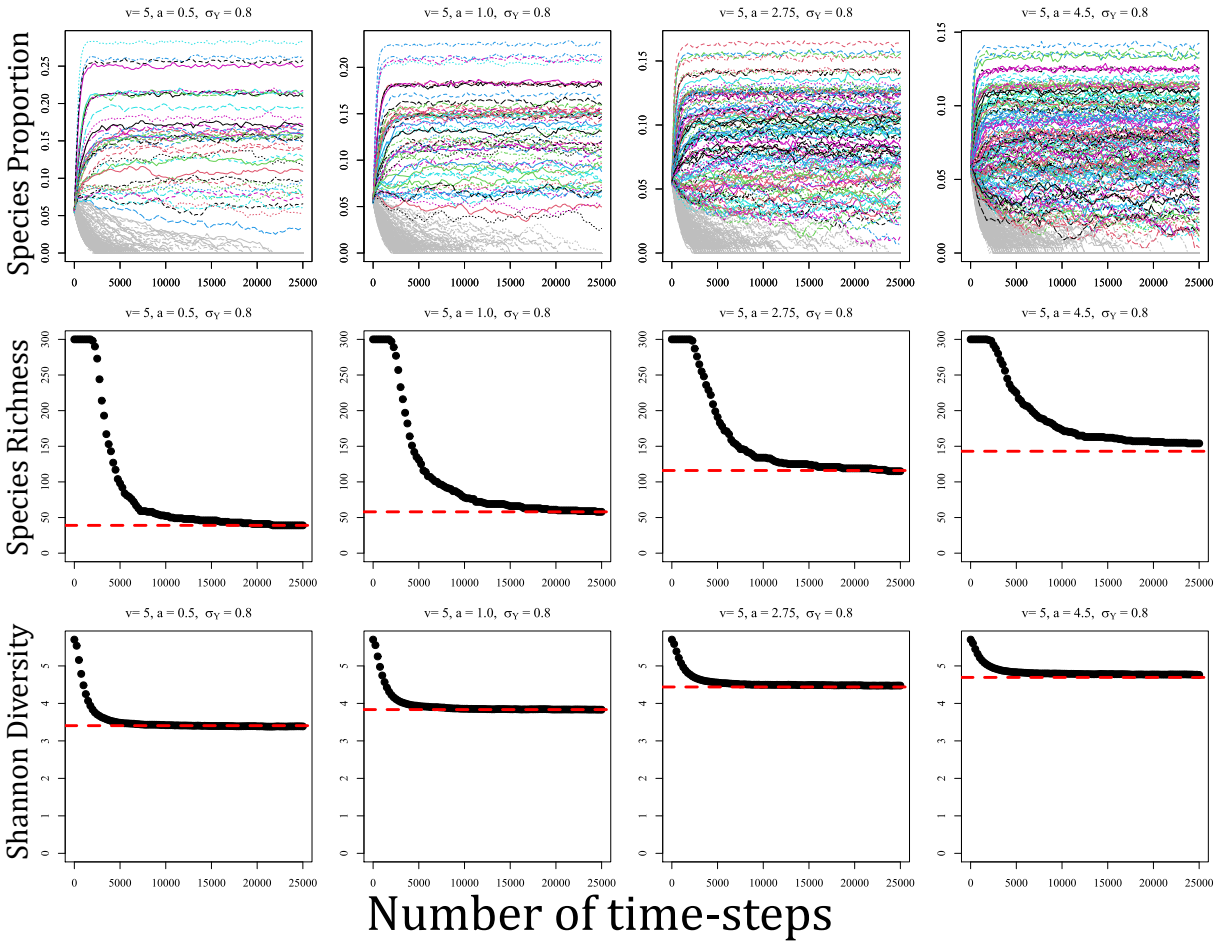

Figure 2.35: Examples of the SEM simulation time series outputs, species richness over time in the simulations, and Shannon diversity over time in the simulations. The top row shows examples of the time series outputs of the SEMs. The x-axis is time and the y-axis is each species' proportion. Proportions have been square-root transformed to aid visualization. Colored trajectories indicate species that persisted throughout the simulation; grey trajectories indicate species that went extinct. Parameters are listed on each plot. Dynamics as shown are typical examples from the SEMs. Most species settle into a relatively stable pseudo-equilibrium, while lower abundance species fluctuate due to drift. The second row shows the number of persisting species in the community as a function of time. Each panel corresponds to the plot above it. Most species that go extinct do so in the early stages of the dynamics. Therefore, the vast majority of persisting species likely persist deterministically. The dashed red line is the diversity maintained by the ODE under the same parameterization. All SEMs saturate, approximately, to the dashed line. The third row is the same as the second row, except it shows Shannon diversity instead of species richness.

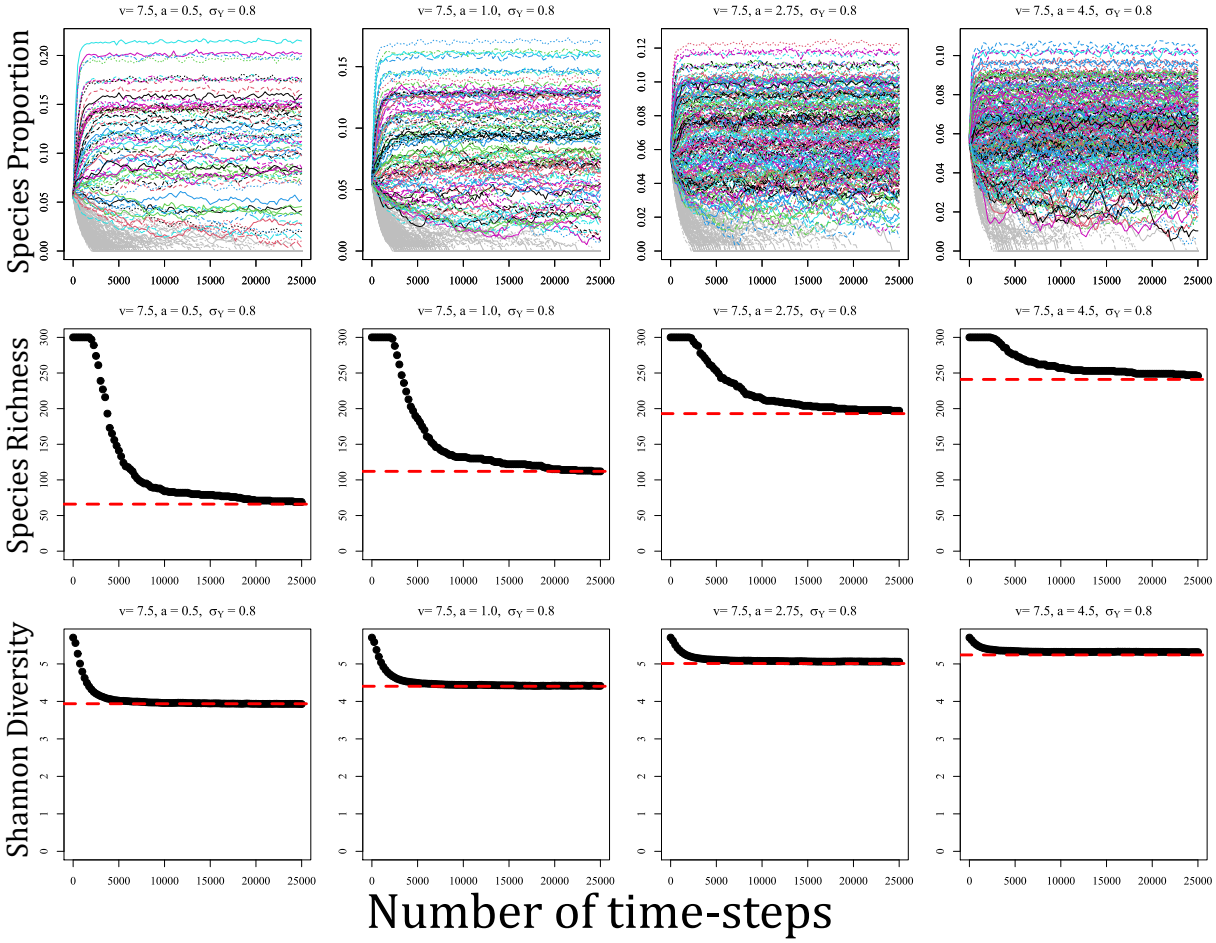

Figure 2.36: The same as fig. 2.35, but with $v = 7.5$.

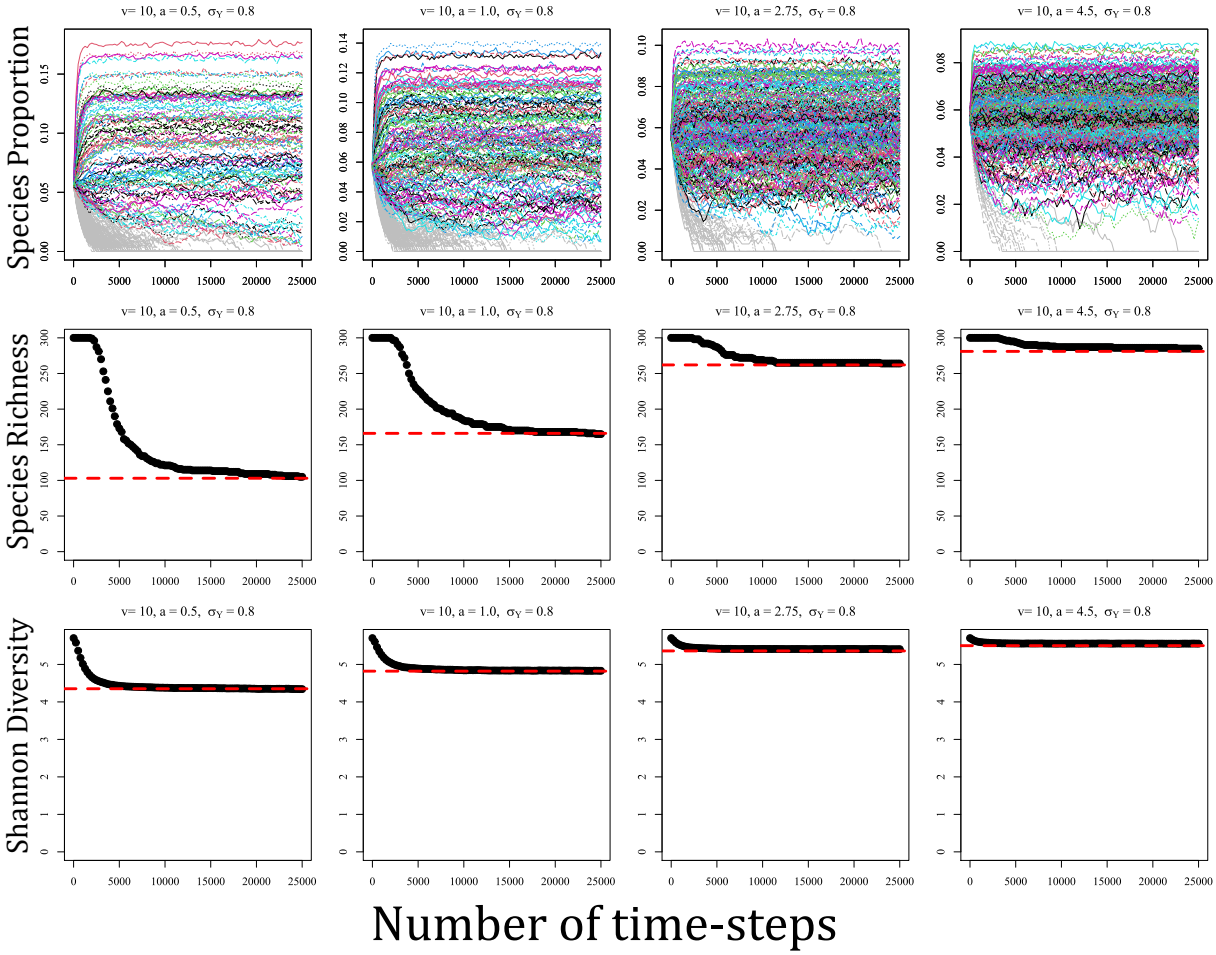

Figure 2.37: The same as fig. 2.35, but with $v = 10$.

Appendix A.5: Explanation of model formulation and normalizations

Introduction

In this Appendix, I explain the general conceptual and mathematical framework of the model in greater detail than is presented in the main text. Then, I provide detailed mathematical and conceptual explanations for the normalizations introduced in the main text. These normalizations are essential for the modeling comparisons, as they ensure the mean predation pressure offspring experience is identical between models.

General modeling framework

In this subsection, I provide an in-depth explanation of the within-patch dynamics and explicitly articulate how predation is incorporated into the model. Much of this first subsection is simply a re-iteration of content found in the main text, but in greater detail. The below descriptions are also relevant for motivating the inter-model normalizations.

The tree community model is conceptualized as having discrete time-steps. Each time-step, offspring of each species accumulate on each patch. Offspring abundance are determined in the following way: **(1)** each tree produces a set number of seeds each time-step, f_i. All trees uniformly disperse a portion of their seeds (D) among patches and retain the remaining portion of their seeds ($1 - D$) on the local patch. Therefore, if p_i is the proportion of trees of species i in the population, species i disperses $f_i p_i D$ seeds to each heterospecific patch and $f_i\big[(1 - D) + p_i D\big]$ seeds to each conspecific patch. **(2)** Offspring of species i at location x, after dispersal, experience density-independent mortality at rate m_i' and experience specialized predation pressure at rate $a' F_{i,k}(x)$. a' is a constant that defines the baseline rate of specialized predation pressure and $F_{i,k}(x)$ defines how the spatial distribution of adult trees of species i affects conspecific offspring predation on a patch occupied by species

k at location x. $F_{i,k}(x)$ is the functional form of specialized predation pressure which may be defined as the Additive−Distance-decay (AD) model, the Additive−Fixed-distance (AF) model, the Non-additive−Distance-decay (ND) model, or the Non-additive−Fixed-distance (NF) model. The reader may refer to the main text and Appendices A-D for more details on the models.

In any case, $F_{i,k}(x)$ is essentially a metric of the number of natural enemies at location x that attack species i. The key point is that $F_{i,k}(x)$ represents how the distance and density of conspecific trees affect the *rate* at which predation occurs. Let $S_{i,k}(x,t)$ represent the number of offspring of species i on a patch occupied by species k at location x and time t. Post dispersal,

$$\frac{dS_{i,k}(x,t)}{dt} = -S_{i,k}(x,t)\big(a'F(x) + m_i'\big) \tag{2.121}$$

Solving the ODE yields

$$S_{i,k}(x,\tau) = S_{i,k}(x,0)e^{-m_i}e^{-aF_{i,k}(x)} \tag{2.122}$$

in which $a = a'\tau$ and $m_i = m_i'\tau$ where τ is the time over which predation occurs (in essence, the time over which offspring develop and are susceptible to natural enemies and other sources of mortality) and $S_{i,k}(x,0)$ is the initial offspring abundance (at $t = 0$). If $k = i$

$$S_{i,i}(x,0) = f_i\big[(1-D) + p_iD\big] \tag{2.123}$$

such that

$$S_{i,i}(x,\tau) = \big[(1-D) + p_iD\big]f_ie^{-m_i}e^{-aF_{i,i}(x)} \tag{2.124}$$

If $k \neq i$,

$$S_{i,k}(x,0) = f_ip_iD. \tag{2.125}$$

such that

$$S_{i,k}(x,\tau) = p_i D f_i e^{-m_i} e^{-aF_{i,k}(x)} \tag{2.126}$$

Henceforth, I drop the τ from the notation such that

$$S_{i,i}(x) = \big[(1-D) + p_i D\big] f_i e^{-m_i} e^{-aF_{i,i}(x)} \tag{2.127}$$

and

$$S_{i,k}(x) = p_i D f_i e^{-m_i} e^{-aF_{i,k}(x)} \tag{2.128}$$

For both $S_{i,i}(x)$ and $S_{i,k}(x)$, offspring abundance is proportional to $f_i e^{-m_i}$. Therefore, "intrinsic fitness" is defined by

$$f_i e^{-m_i} = Y_i \tag{2.129}$$

Intrinsic fitness is then (explicitly) a compound trait of fecundity and survivorship, which represents the number of expected offspring in the absence of JCEs.

Finally, let $J_{i,i}(x) = e^{-aF_{i,i}(x)}$ and $J_{i,k}(x) = e^{-aF_{i,k}(x)}$. $J_{i,i}(x)$ and $J_{i,k}(x)$ are functions that describe the proportion of offspring of species i that survive JCEs on a patch occupied by species i and k, respectively ($i \neq k$) at location x. Putting it all together, the number of each species' offspring on each patch type are equal to

$$\begin{aligned} S_{i,i}(x) &= Y_i\big[(1-D) + p_i D\big] J_{i,i}(x) \\ S_{i,k}(x) &= Y_i p_i D J_{i,k}(x) \\ S_{all,i}(x) &= \sum_{n=1}^{N} S_{n,i}(x) \end{aligned} \tag{2.130}$$

where $i \neq k$. **(3)** If the adult in the focal patch at location x dies during the time step, then a lottery determines which species replaces the adult. If the adult occupying the patch does not die during the time-step, it is assumed all the offspring on the patch die. Equation

(2.130) is identical to equation (2.1) from the main text.

Normalizations

In this subsection, I discuss the inter-model normalizations in detail.

Normalization of distance-decay and fixed-distance functional forms

Two distance-dependent functional forms are considered in the main text of the model: the fixed-distance functional form (in which offspring experience predation pressure at a fixed rate up until a distance of r meters from a conspecific adult) and the distance-decay functional form (in which the predation pressure offspring experience from a conspecific adult decays exponentially with distance). To ensure model comparisons are fair, it is necessary to set equal the how each tree induces over space between functional forms. In other words, the predation a tree induces within the radius r under the fixed distance (AF and NF) models must be set equal to the predation over the scale set by v under the distance-decay (AD and ND) models. Conceptually, this is analogous to assuming that the number of natural enemies is maintained between distance-dependent functional forms, but are distributed in space differently.

Consider a single tree from which natural enemies disperse and induce predation pressure as defined by $G(x)$ (analogous to $F_{i,k}(x)$ in the above subsection, except from the perspective from the adult tree rather than the offspring; I use $G(x)$ instead of $F(x)$ to avoid confusion). $G(x)$, in essence, represents the relative density of natural enemies that disperse from a focal tree to a location x meters away from it. $G(x) \leq 1$ such that $G(x) = 1$ corresponds to maximum predation pressure induced by a single adult. For the fixed distance model, $G(x) = 1$ if $x \leq r$ and $G(x) = 0$ if $x > r$. For the distance-decay model, $G(x) = e^{-x/v}$. Predation pressure is induced in 2-dimensional space such that the total predation pressure

induced by a single adult is

$$g \int_0^\infty 2\pi x G(x) \mathrm{d}x \tag{2.131}$$

Note that the $2\pi x$ term reflects that fact that predation is equal to the sum (integral) of predation pressure spanned by the radius x in two dimensions.

For the fixed distance model:

$$\begin{aligned} g \int_0^\infty 2\pi x G(x) \mathrm{d}x &= g \int_0^r 2\pi x \mathrm{d}x \\ &= \pi g r^2 \end{aligned} \tag{2.132}$$

and, for the distance-decay model:

$$\begin{aligned} g \int_0^\infty 2\pi x G(x) \mathrm{d}x &= g \int_0^\infty 2\pi x e^{-x/v} \mathrm{d}x \\ &= 2\pi g v^2 \end{aligned} \tag{2.133}$$

Predation pressure is therefore equal if $g\pi r^2 = 2g\pi v^2$; canceling terms yields the relationship $r = v\sqrt{2}$. If this equality is satisfied, an individual tree induces the same total magnitude of predation pressure irrespective of how predation decays with distance (albeit distributed over space differently). Note that $g\pi r^2 = E_F$ and $2g\pi v^2 = E_D$. Therefore, this normalization is equivalent to setting $E_F = E_D$.

Note that a is not included in the normalization – predation pressure is proportional to a where JCEs occur, but a is not directly related to the distance-decay component of the functional form. Thus, the above should be interpreted as normalizing r with v.

Connection to previous literature

It is noted in the main text that previous papers such as Adler and Muller-Landau (2005) and Sedio and Ostling (2013) also normalize predation pressure using a mathematically (and conceptually) similar method. I briefly articulate the similarity here. Making some

modest simplifications and altering some notation for consistency, I describe how they model predation.

First, they introduce the function

$$h(x) = \frac{1}{2\pi v^2} e^{-x/v} \tag{2.134}$$

where $h(x)$ is the relative density of natural enemies at distance x from the focal tree and v is identical to v in the present study. $h(x)$ integrates to 1. Then, Adler and Muller-Landau (2005) and Sedio and Ostling (2013) assume that offspring survival on a patch is a hyperbolically decreasing function of distance-weighted adult density (defined by $h(x)$) such that:

$$\Pr[\text{Survival}] = \frac{1}{1 + \beta N \sum_{m=1}^{N_i} h(x_m)} \tag{2.135}$$

where N_i is the number of adults of species i in the population and x_m is the distance of the m_{th} individual of species i to the location x, β defines the strength of predication pressure, and N acts as a general density term such that morality increases with the total number of adults in the population. This is similar to the present study, in which survival is an exponentially decreasing function (rather than hyperbolic). However, the models are conceptually and mathematically very similar.

The key point is that Adler and Muller-Landau (2005) and Sedio and Ostling (2013) vary v between simulations. Because $h(x)$ is structured such that its integral over space sums to 1, it follows varying v does not change the total number of natural enemies. In this way, they normalize the distance-dependent component of their assumed functional form. In the present study, I do not normalize v between simulations. Rather, I compare the distance-decay and fixed-distance functional forms. In the present study, $h(x)$ is analogous to

$$G(x) = e^{-x/v} \tag{2.136}$$

for the distance-decay models, which integrates to $2\pi v^2$; for the fixed-distance models, $h(x)$ is analogous to

$$G(x) = \begin{cases} 1, & \text{if } r \leq x \\ 0, & \text{if } r > x \end{cases} \tag{2.137}$$

which integrates to πr^2. Therefore, setting $2\pi v^2 = \pi r^2$ serves the same function as ensuring that $h(x)$ integrates to 1 with respect to different values of v in Adler and Muller-Landau (2005) and Sedio and Ostling (2013). This, in turn, is identical to assuming that each distance-dependent functional form produces the same total number of natural enemies that disperse from adult trees, albeit distributed in space differently. Therefore, this normalization in the present study is biologically meaningful and consistent with previous literature.

It should be noted, however, that the coefficients that determine the baseline strength of predation pressure (a in the present study and β in Adler and Muller-Landau (2005) and Sedio and Ostling (2013)) have slightly different interpretations.

Normalization of additive and non-additive functional forms

In this subsection, I describe the process of normalizing predation pressure between the additive and non-additive functional forms. Because offspring experience mean greater predation pressure under the additive models than under the non-additive models, it is necessary to adjust the baseline predation pressure of the latter to compensate. I take the following approach: I calculate the mean predation pressure experienced by offspring in a community given that predation is additive. Then, I adjust the non-additive model such that both models exhibit the same mean predation pressure. Here, I present the normalization and then I justify it with reference to its implementation for the non-additive models (the non-additive−fixed-distance (NF) model and the non-additive−distance-decay (ND) model).

The normalization is as follows. Let a_{A} and a_{n} be the predation pressure for an additive model and non-additive model, respectively. Additionally, let E represent E_n or E_D

(recalling that these quantities are identical due to the normalization described in the above subsection). The additive−non-additive normalization sets a_{n} as

$$a_{\mathrm{n}} = a_{\mathrm{A}}\left(1 + \frac{E}{N}\right) \tag{2.138}$$

where N is the number of species in the community.

Now, I describe the logic behind this normalization in the context of the NF and ND models, respectively. For the NF model, if species i experiences JCEs on a given patch because it falls within the radius defined by r, it experiences predation pressure with intensity a. However, if predation pressure were additive, it would experience predation pressure additional predation pressure equal to the total number of conspecifics found within the effect radius, r. On average, one expects an additional $p_i E_F$ offspring to fall within the patch (on the basis that p_i is the proprotion of species i in the population and E_F is the expected number of trees in the effect area defined by r). Therefore, the expected additional predation pressure induced by species i due to additive predation is equal to

$$a_{\mathrm{A}} p_i E_F \tag{2.139}$$

in which case, the total expected predation pressure for species i on a patch in which it experiences JCEs is equal to

$$a_{\mathrm{A}}\left(1 + p_i E_F\right) \tag{2.140}$$

The $+1$ comes from the baseline predation pressure that species i experiences due to the first adult falling within r and the $p_i E_F$ is the expected additional predation due to additive effects. Thus, the above should be interpreted as "given offspring of species i experience JCEs on a patch, what is the expected total predation pressure it experiences when predation is additive?".

Then, the mean predation pressure within the community is equal to

$$\begin{aligned}\mathbb{E}\left[a_{\mathrm{A}}\left(1+p_i E_F\right)\right] &= \frac{1}{N}\sum_{i=1}^{N} a_{\mathrm{A}}\left(1+p_i E_F\right) \\ &= a_{\mathrm{A}}\left(1+\frac{E_F}{N}\right)\end{aligned} \tag{2.141}$$

noting that the above results comes from the fact that $\mathbb{E}\left[p_i\right] = 1/N$ (the mean proportion in a community of N species is $1/N$). Therefore, the normalization requires that

$$a_{\mathrm{n}} = a_{\mathrm{A}}\left(1+\frac{E_F}{N}\right) \tag{2.142}$$

recalling a_{n} is the normalized baseline predation pressure for non-additive models and a_{A} is the baseline predation pressure for the additive models.

Very similar logic applies for the ND model. On a given patch, the ND model induces predation pressure to offspring of species i on a given patch defined by the minimum distance between the patch and a conspecific adult. However, when predation is additive, the expected additional predation pressure experienced by offspring of species i is equal to $a_{\mathrm{A}} p_i E_D$. As before, the expected predation pressure due to additive predation is equal to

$$\begin{aligned}\mathbb{E}\left[a_{\mathrm{A}} p_i E_D\right] &= \frac{1}{N}\sum_{i=1}^{N} a_{\mathrm{A}} p_i E_D \\ &= a_{\mathrm{A}}\frac{E_D}{N}\end{aligned} \tag{2.143}$$

This yields the normalization

$$a_{\mathrm{n}} = a_{\mathrm{A}}\left(1+\frac{E_D}{N}\right) \tag{2.144}$$

I now describe how this is implemented comparing numerical simulations (ODEs) of the additive and non-additive models. I perform the following operations:

1. A simulation is run for one of the additive models with a given set of parameters (i.e.

σ_Y, g, a_A, D, and v or r.

2. The number of coexisting species for the additive model at the end of simulation (after reaching equilibrium) henceforth N_A, is recorded.

3. The predation pressure for the non-additive model is set to

$$a_\mathrm{n} = a_\mathrm{A}\left(1 + \frac{E}{N_\mathrm{A}}\right).$$

4. A simulation is run for the non-additive model and the number of coexisting species is recorded after the community reaches equilibrium.

With these steps, additive and non-additive models are compared under the condition that the *mean* predation pressure experienced by offspring is identical between simulations. More precisely, this probes the question: given an additive model maintains N_A species, how many species would be maintained under a non-additive model if offspring experience the same mean predation pressure non-additively?

Appendix A.6: Arguments related to dispersal-limited communities

Introduction

In this appendix, I outline several arguments related to dispersal limitation and species richness referenced in the main text.

The effects of large a

In the main text, it is noted that dispersal limitation does not matter if a (baseline predation pressure) is very large. To show this, consider the invasion criteria of species i (see Appendices A-D) which can be written as

$$\frac{Y_i(1-D)e^{-a}}{Y_i(1-D)e^{-a} + D\sum_{k\neq i} Y_k p_k \,\mathbb{E}[J_{k,i}(x)]} + Y_i D \sum_{m\neq i} \frac{1}{Y_m\big[(1-D)+p_m D\big]e^{-a}\,\mathbb{E}[J_{m,i}(x)] + D\sum_{k\neq m} Y_k p_k \,\mathbb{E}[J_{k,m}(x)]p_m} > 1 \tag{2.145}$$

noting that $\mathbb{E}[J_{m,m}(x)] = e^{-a}\,\mathbb{E}[J_{m,i}(x)]$ because local JCEs simply induce an addition e^{-a} mortality. In Appendices A-D, it is assumed that $D = 1$ and that the species identity of the tree previously occupying a patch does not matter such that $Y_m p_m e^{-a}\,\mathbb{E}[J_{m,i}(x)] \approx Y_m p_m\,\mathbb{E}[J_{m,i}(x)]$. Making these assumptions and doing some rearranging of equation (2.145) yields

$$Y_i \sum_{m\neq i} \frac{1}{\sum_{k\neq i} Y_k p_k \,\mathbb{E}[J_{k,i}(x)]} p_m > 1 \tag{2.146}$$

Now, I consider when there is dispersal limitation and a is large. I take the limit of

equation (2.145) as $a \to \infty$. Therefore, all terms containing e^{-a} will disappear. This yields

$$Y_i \sum_{m \neq i} \frac{1}{\sum_{k \neq i, k \neq m} Y_k p_k \, \mathbb{E}[J_{k,i}(x)]} p_m > 1 \tag{2.147}$$

Comparing Equations (2.146) and (2.147), the only difference is that species m is not included in the denominator for the latter equation (noting the difference in the indexes on the summations). In other words, only one less species' offspring are present on a given patch. Therefore, unless there are very few species or if one species is highly dominant, Equations (2.146) and (2.147) will be approximately the same value. Therefore, for large a such that $e^{-a} \approx 0$, the dispersal-limited case is approximately identical to that of the non-dispersal-limited case.

The effects of small a

In the main text, it is also claimed that dispersal limitation should not matter for small a. As $a \to 0$, no JCEs occur. Then, the system converges to a lottery model with no stabilizing effects (resulting in mono-dominance) in which case dispersal limitation is irrelevant. Taken with the above result, this implies that dispersal limitation is less important for both low a and very high a, consistent with fig. 2.2 from the main text (at least, for the non-additive models).

Expanded argument on dispersal limitation

In the Results and Discussion of the main text, I argue that the functional form of specialized predation (whether it is additive or non-additive) interacts with dispersal limitation. Here, I present an extended argument for why dispersal limitation leads to lower species richness when predation is non-additive but not when it is additive.

Consider when predation is additive and species experience dispersal limitation ($D < 1$).

Additionally, consider two conspecific adults nearby in space such that they induce predation pressure on each others patches. Each conspecific adult increases the offspring mortality of the locally dispersed offspring on each patch. More generally, as a species becomes more common in the community, its locally dispersed offspring experience greater and greater mortality due to additive predation. Therefore, dispersal limitation does not affect rare species advantage: although rare species lose some of their locally dispersed offspring to Janzen-Connell Effects (JCEs), they lose a smaller proportion than more common species lose.

In contrast, if predation is non-additive, then two conspecific adults close in proximity do not affect the survival of offspring on each others patches. More generally, as a species becomes more common in the community, the proportion of locally dispersed offspring that experience mortality due to JCEs does not change. As a result, the survival a rare species' locally dispersed offspring is exactly the same as that of common species. Thus, relative to when there is no dispersal limitation ($D = 1$, in which case rare species' offspring experience no JCE-induced mortality) rare species advantage is diminished.

Connection to Stump and Chesson (2015)

I now connect the above arguments to Stump and Chesson (2015). Stump and Chesson (2015) compare two JCE-related situations: (1) when JCEs are "local", occurring directly beneath adults (only on the local patch; identical to the NF model with $E = 0$) and (2) when JCEs are entirely "non-localized". For "non-localized" JCEs, predation occurs equally on every patch in the community such that the proportion of offspring of species i that die on every patch, J_i, is equal to:

$$J_i = \alpha p_i \tag{2.148}$$

where p_i is the proportion of species i in the community and α represents the strength of JCEs ($0 \leq \alpha \leq 1$). In comparing these models, Stump and Chesson (2015) find that

dispersal limitation reduces the stabilizing effects of JCEs for the "local" model, but not for the "non-local" model. They conclude that this is because locally dispersed offspring of rare species experience mortality in the "local" model, but not in the "non-local" model.

This is not incorrect, but the I argue that it's not the mortality of locally dispersed offspring that causes this result *per se*. Rather, the "non-local" model presented by Stump and Chesson (2015) is implicitly additive while their "local" model is non-additive. I aruge it is this distinction that truly underlies why dispersal limitation decreases the JCE stabilizing effect in Stump and Chesson (2015).

The "non-local" model in Stump and Chesson (2015) does not allow for any JCE-induced local offspring mortality of rare species ($J_i = \alpha p_i \to 0$ as $p_i \to 0$). In other words, all offspring of rare species always escape JCEs. Therefore, it is ambiguous in Stump and Chesson (2015) whether additive predation or the lack of local offspring mortality underlies why the "non-local" model decreases JCE stabilizing effect strength. The additive (AD and AF) models in the present paper allow for the co-occurrence dispersal limitation such that a rare species' locally dispersed offspring experience JCE-induced mortality and additive predation simultaneously. When $D < 1$ and predation is additive (AD and AF models), species richness is indistinguishable from the $D = 1$ case (main text, Fig. 2). When $D < 1$ and predation is non-additive (ND and NF models), species richness is lower than the $D = 1$ case. The additive models incorporate "local" predation as defined in Stump and Chesson (2015) (the survival of locally dispersed offspring of rare species is decreased by JCEs) yet species richness is unaffected by dispersal limitation. This implies that the nature of predation – whether it is additive or non-additive – determines whether dispersal limitation decreases the ability of JCEs to maintain species richness (rather than "local" vs. "non-local" predation *per se*). In other words, whether JCEs kill locally dispersed offspring of rare species does not affect whether dispersal limitation decreases the ability of JCEs to stabilize coexistence – rather, what matters is if the locally dispersed offspring of rare species

experience lower mortality *relative* to resident species.

Connection to other models

Despite the above insights, Muller-Landau and Adler (2007) find species richness can increase with dispersal limitation (particularly when predators disperse large distances). As their model incorporates additive predation, this seems to contradict the above results. Importantly, Muller-Landau and Adler (2007) examine spatially explicit models, using spatially explicit seed and predator dispersal kernels. I hypothesize the results from Muller-Landau and Adler (2007) reflect how the co-occurrence of spatially explicit seed and predator dispersal kernels modify the spatial structure of trees. Similarly, papers in which dispersal limitation increases species diversity (Detto and Muller-Landau, 2016; Wiegand et al., 2021) largely attribute this result to species aggregation. Aggregation is not possible under the model in this study (both in terms of how dispersal limitation is modeled and because the ODE assumes species are approximately randomly distributed in space). Therefore, further investigations of how dispersal and distance- and density-dependent are warranted, but beyond the scope of the present study.

Appendix A.7: Supplemental figures

In this Appendix, I present supplemental figure (most of which are referenced in the main text). Figure legends provide all necessary information to interpret the figures.

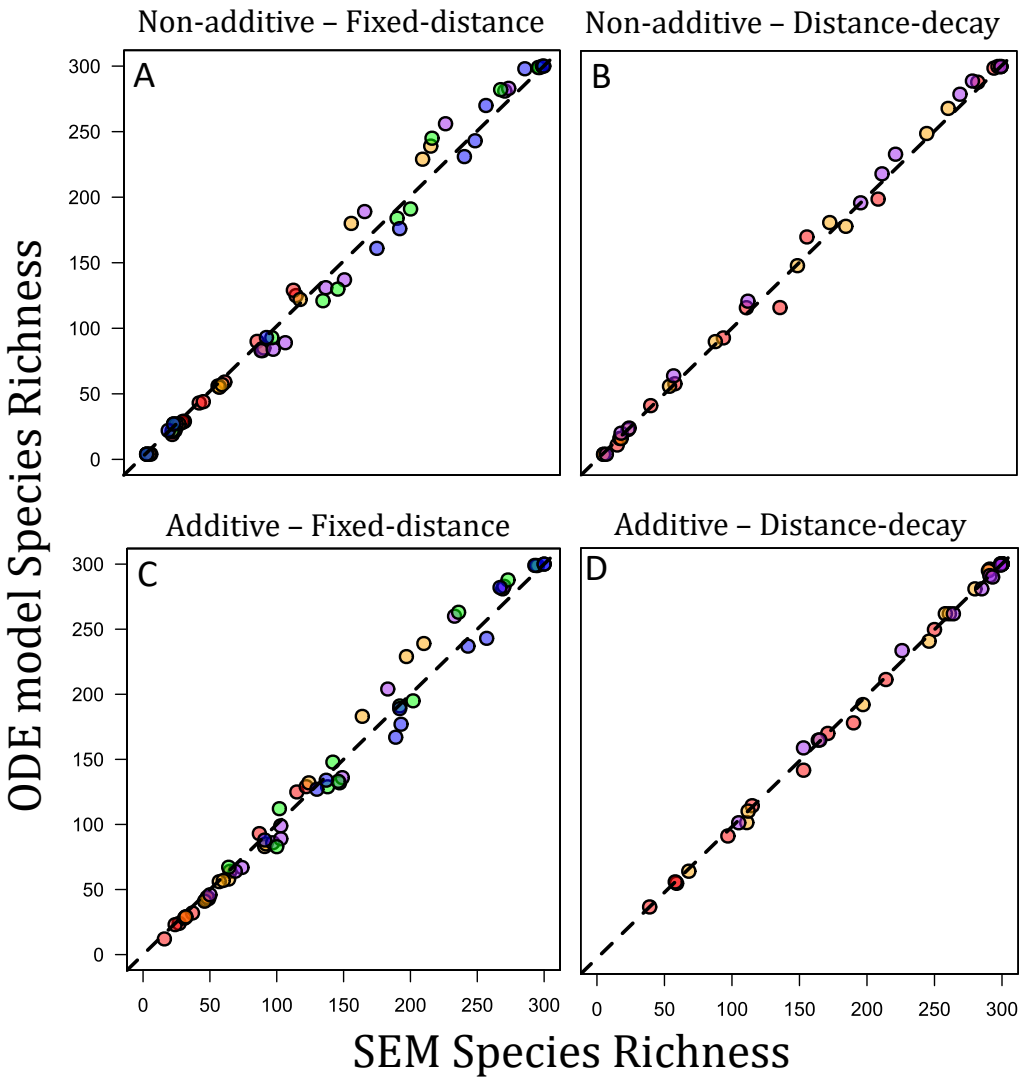

Figure 2.38: Ordinary Differential Equation (ODE) model validation. The figures compare species richness between Spatially Explicit Model (SEM) and ODE model simulations under identical parameterizations. Each panel shows a different model labeled by its functional form. The dashed line is the one-to-one line (points on the line represent when the SEM and ODE yield the exact same diversity output). For panels A and C (the fixed-distance models), red points depict a 3×3 Moore Neighborhood ($E_F = 9$), orange/yellow points depict a 5×5 Moore Neighborhood ($E_F = 25$), purple points depict a 7×7 Moore Neighborhood ($E_F = 49$), green points depict a 9×9 Moore Neighborhood ($E_F = 81$), and blue points depict an 11×11 Moore Neighborhood ($E_F = 121$). This approximately corresponds to r between 4.0 and 14. For panels B and D, red points are when $v = 5$, orange/yellow points are when $v = 7.5$, and purple points are when $v = 10$. To a first approximation, the ODE model yields the same species richness output as the SEM. See Appendices A-D for more details and summary statistics.

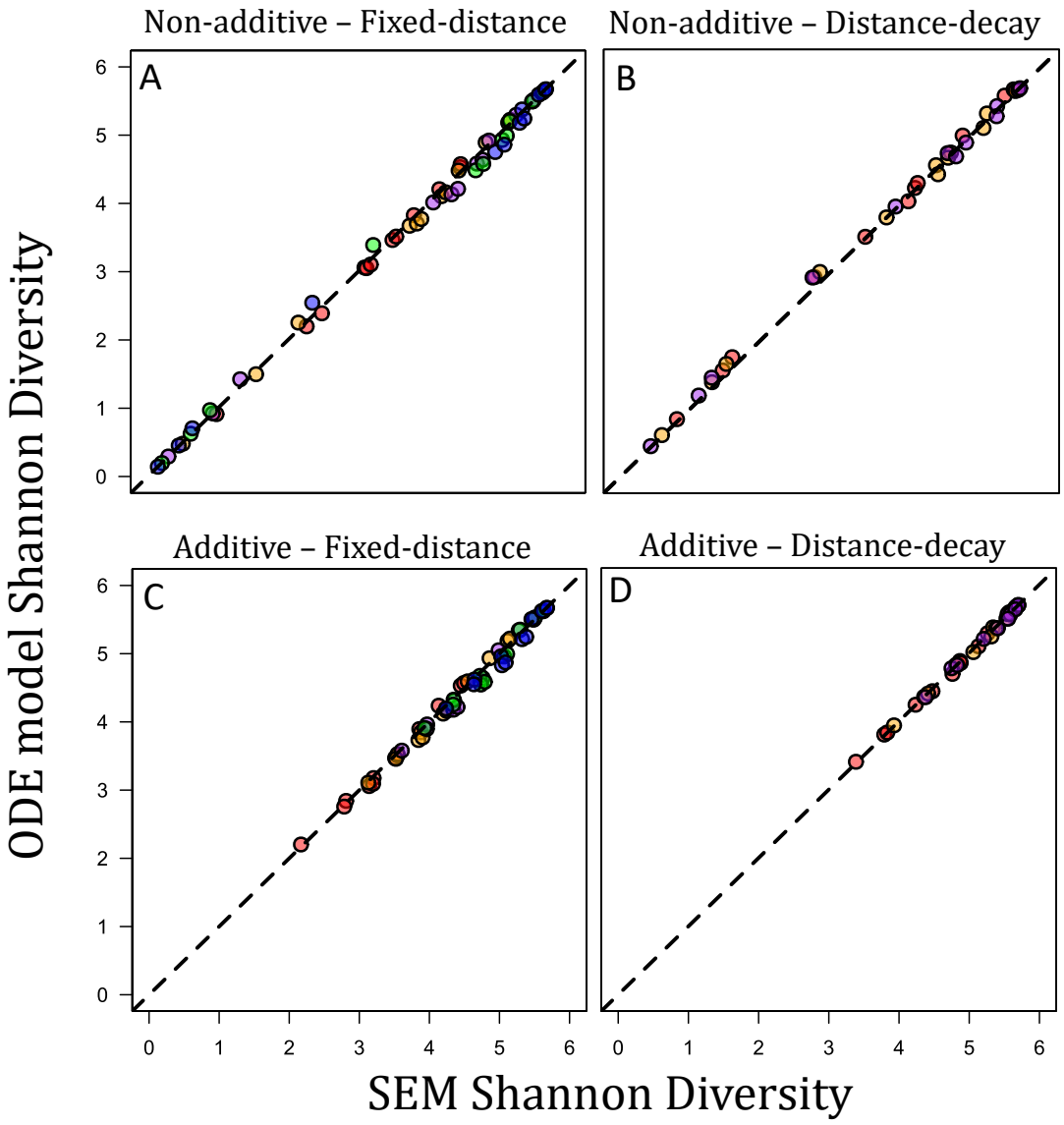

Figure 2.39: The same as fig. 2.37, but showing Shannon Diversity instead of species richness. SEM and ODE model outputs are highly similar.

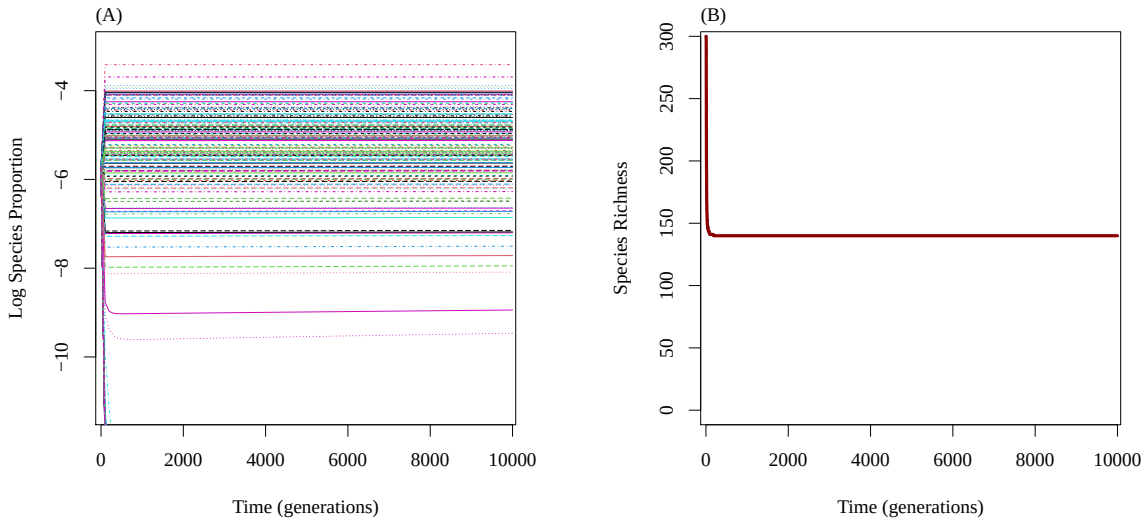

Figure 2.40: An example of a time-series output from the ODE model, showing the AD model. (A) shows the log-transformed proportion of each species as a function of time. Abundances stop changing relatively early into the simulation. (B) shows number of species persisting in the community as a function of time. This implies the transient dynamics have concluded and the system is at equilibrium. This is a typical example. Parameters are as follows: $v = 10$, $g = 0.172$, $1 - e^{-a} = 0.7$ ($a \approx 1.2$), $D = 1$, $\sigma_Y = 1.0$.

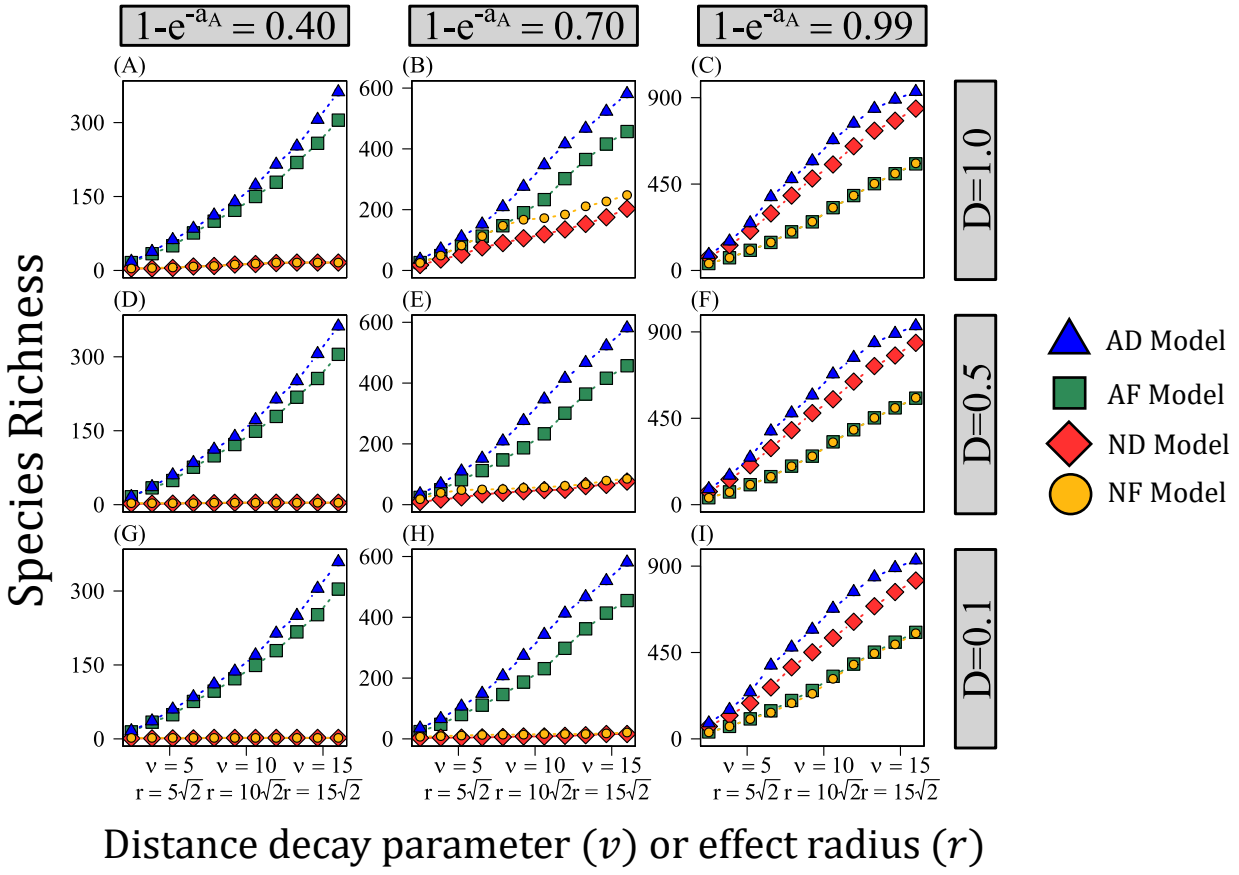

Figure 2.41: The same as fig. 2.2 from the main text, but with 1000 species in the initial community (instead of 300). In the main text, it is noted that model differences are more extreme for a larger initial species pool. In columns 1 and 2, the additive models can maintain hundreds of more species than the non-additive models. Similarly, in column 3, the species richness maintained by the distance-decay models is often several hundred greater than the fixed-distance models. For large a_A and large v, the species richness of the AD model is nearly 1000 species. As in fig. 2.2 of the main text, $g = 0.172$ and $\sigma_Y = 0.55$ ($Y \sim \text{lognormal}[\mu = 0, \sigma_Y]$). All other relevant parameters are noted on the figure.

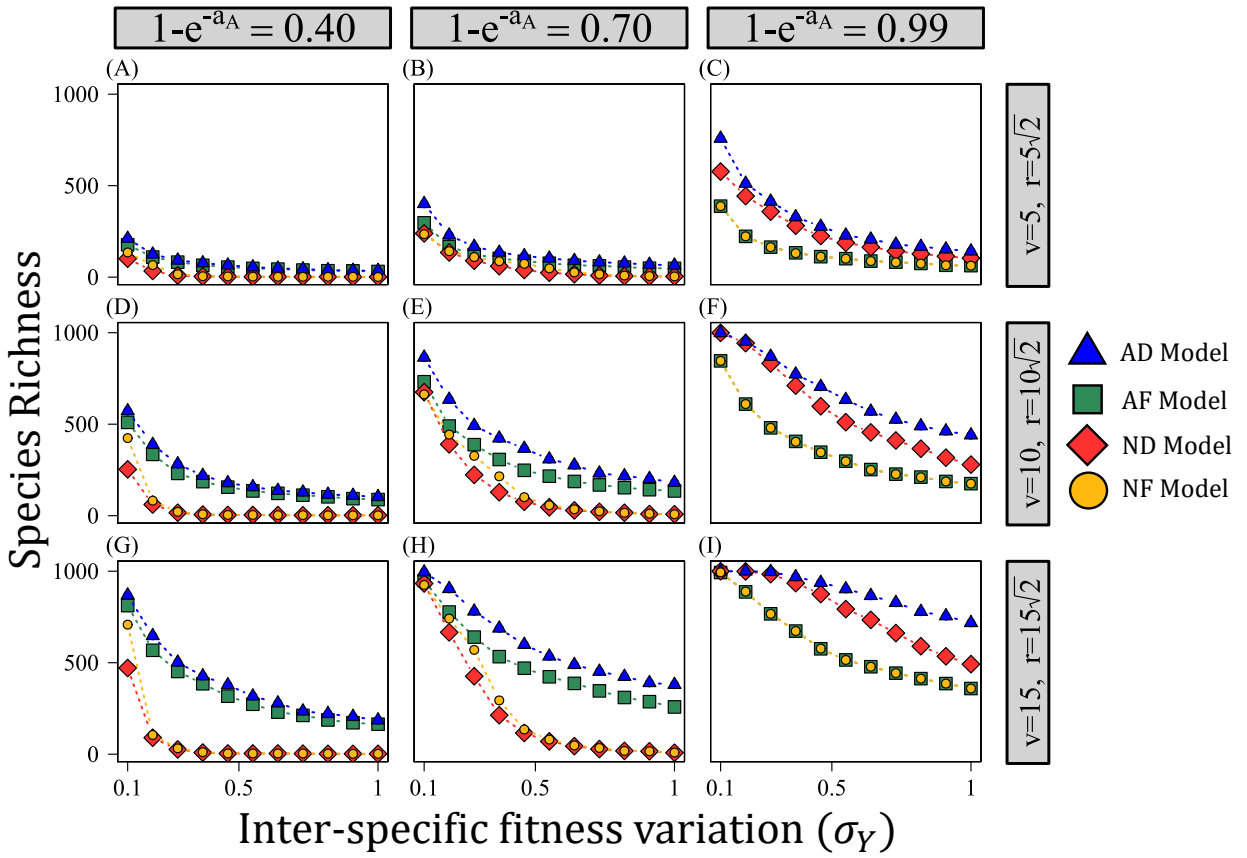

Figure 2.42: The same as fig. 2.3 from the main text, but with 1000 species in the initial community (instead of 300). As noted in the main text, results are qualitatively similar to the 300 species case, but the numerical difference in species richness maintained by models is larger. In particular, when JCEs extend over a large spatial scale (large v and r; rows 2 and 3) models differences are sometimes very large. The starkest contrast to fig. 2.3 of the main text is Panel (I) – in this case, the AD model maintains hundreds of more species than each other model. In the analogous plot in the main text (fig. 2.3, Panel (I)), all species maintain high species richness for all σ_Y. Therefore, when JCEs are very strong (large v or r and large a_{A}, as in Panel (I)), examining a larger species pool reveals the full extent to which the AD maintains greater species richness than the other models (particularly the fixed-distance models).

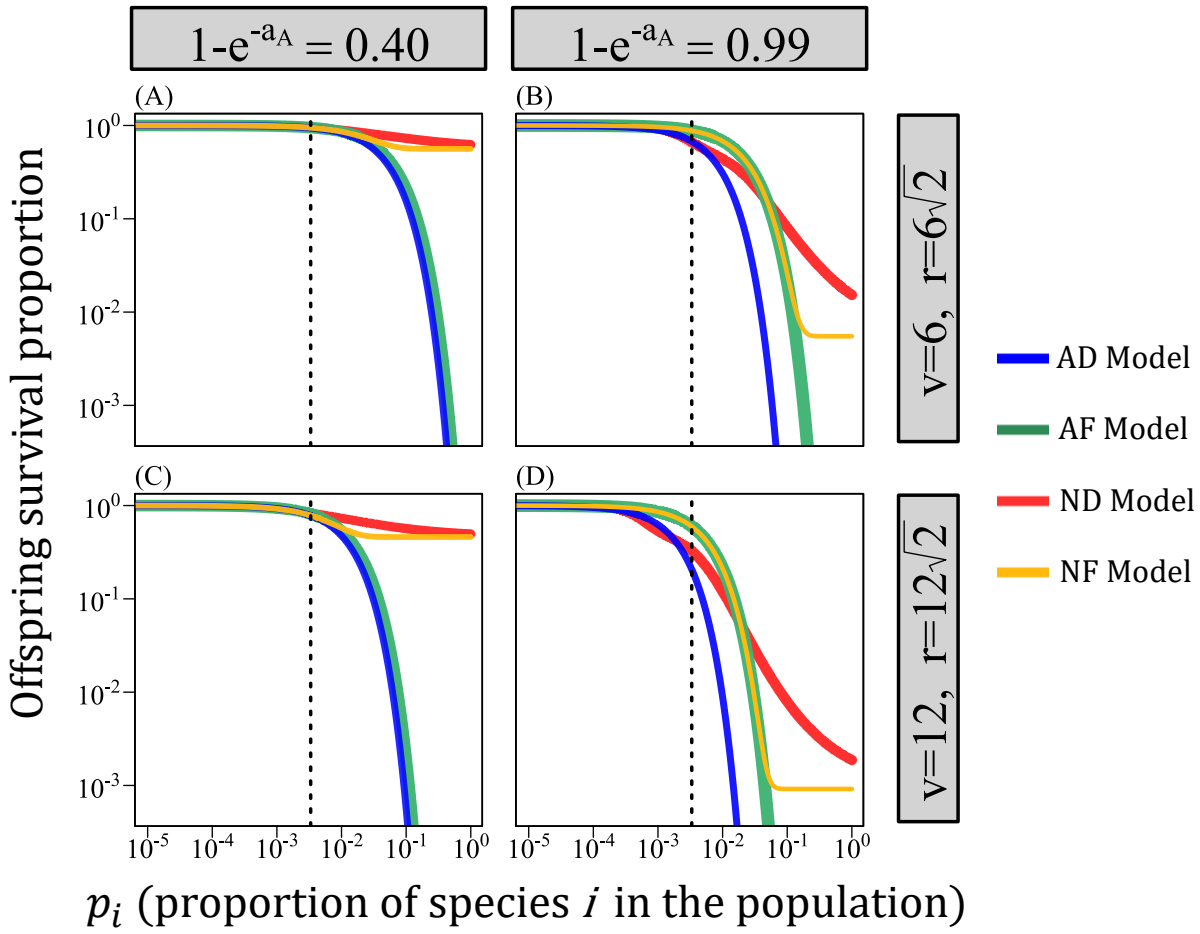

Figure 2.43: The same as fig. 2.4 from the main text, but both axes are log-scaled (rather than just the x-axis). This allows the observation that the additive models indeed produce stronger negative frequency dependence (lower offspring survival for large p_i) than the non-additive models in all cases, including (B) and (D) (which is difficult to see in fig. 2.4 of the main text). Parameters are as follows: $g = 0.172$, $D = 1.0$, $N = 300$, and $a_{\mathrm{N}} = a_{\mathrm{A}}\big(1+E/N\big)$ where $E = E_F = E_D = 2\pi v^2 g$.

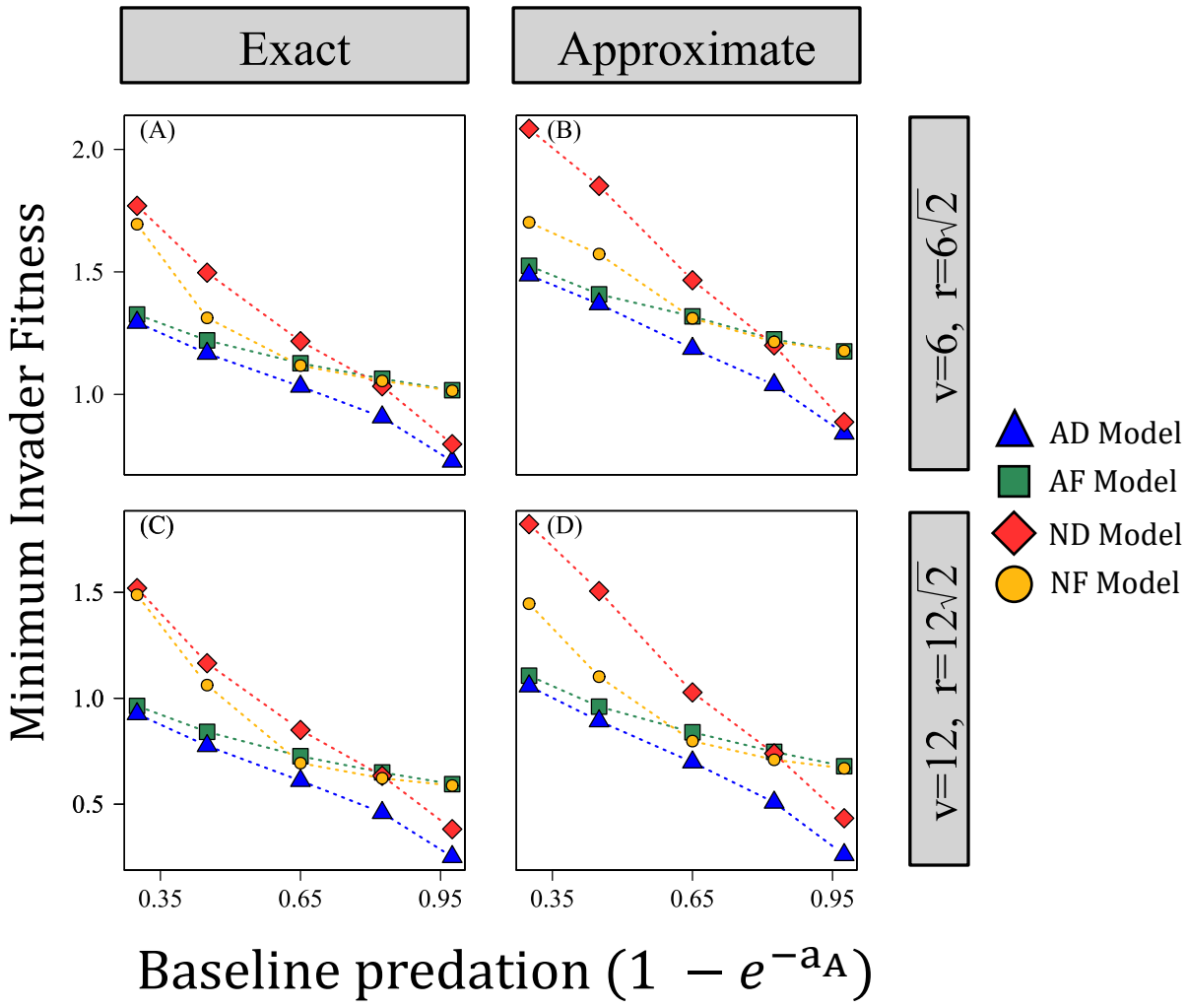

Figure 2.44: The approximate invasion criteria compared to the exact invasion criteria (the right-hand-side, "minimum invader fitness", of the invasion criteria shown in Table 2.1). (A, C) show the exact invasion criteria for each model and (B, D) show the approximate invasion criteria for each model. Results are qualitatively identical, although approximate invasion criteria tends produce larger values (which means the approximation underestimates stabilizing strength). Relevant parameters are as follows: $D = 1$, $g = 0.172$, and $\sigma_Y = 0.375$. Other parameters are listed on the figure.

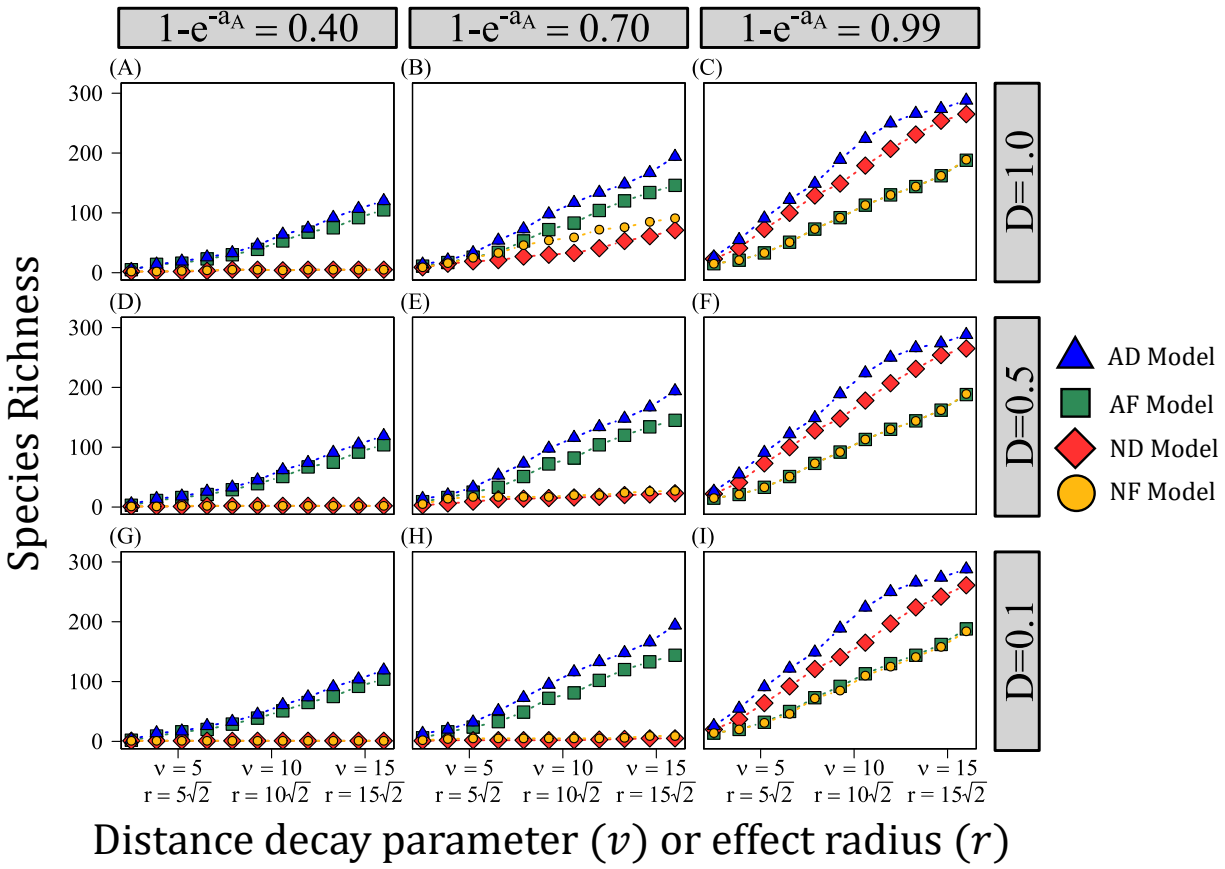

Figure 2.45: Species richness maintained by each JCE functional form under different values of baseline predation pressure (a_{A}), dispersal limitation (D), and the spatial scale of predation (v and r) at relatively low tree density ($g = 0.06$). In the main text, it is noted that lower g produces lower species diversity; this figure should be compared to Fig. 2.2 of the main text, as they are identical except for the value of g. For each plot, the x-axis depicts either v or r (depending on the JCE functional form) and the y-axis is species richness (the number of species maintained in the community at equilibrium). Models are differentiated by shape and color. Each column depicts a different value of a_{A} (the baseline predation pressure for the additive models) and each row shows a different value of D ($D = 1$, $D = 0.5$, and $D = 0.1$, respectively). The non-additive models are normalized such that $a_{\mathrm{N}} = a_{\mathrm{A}}(1 + E/N_{\mathrm{A}})$ where a_{N} is the normalized predation pressure for the non-additive models, N_{A} is the diversity maintained by the additive model to which the non-additive model is being compared and E is either E_F or E_D (which are equivalent). a_{N} was calculated based on the diversity maintained by the AD model for the additive – non-additive normalizations. Using the AF model outputs to quantify a_{N} yielded trivially similar results. All simulations were conducted with 300 species initially in the population. $g = 0.06$ and $\sigma_Y = 0.55$ ($Y \sim \mathrm{lognormal}[\mu = 0, \sigma_Y]$). All other relevant parameters are noted on the figure.

Chapter 3

On the interaction between Janzen-Connell effects and habitat partitioning in spatially structured environments

3.1 Abstract

Janzen-Connell Effects and Habitat Partitioning have both been proposed as potential stabilizing mechanisms in species-rich forest communities. Janzen-Connell Effects describe the process in which specialized predators are attracted to adult trees, which reduce the survivorship of nearby conspecific juveniles. Habitat Partitioning describes when species exhibit different fitness responses to spatially heterogeneous environmental factors, typically causing species to aggregate into favorable habitat types. Despite substantial evidence that both processes occur simultaneously in empirical systems, the theoretical implications of how their interactions shape species richness remain underdeveloped. Here, I examine a spatially explicit model that incorporates both processes. I show that Janzen-Connell Effects and Habitat Partitioning can act synergistically to promote coexistence when environmental spatial heterogeneity is positively autocorrelated. The results of this study highlight the need to explicitly model the interactions between co-occurring spatially dependent coexistence mechanisms to understand the role they play in the maintenance of species richness.

3.2 Introduction

The maintenance of species richness in forest communities has long captured the interest of ecologists. Janzen-Connell Effects (JCEs) and Habitat Partitioning (HP) are two leading hypotheses, both frequently invoked to explain the high diversity of tropical forests. However, their ability to promote diversity while operating simultaneously remains understudied.

JCEs are based on observation that host-specific natural enemies attracted to adult trees (insects, pathogens, fungi, etc.) reduce juvenile conspecific offspring survivorship (Janzen, 1970; Connell, 1971; Terborgh, 2012). JCEs are thought to maintain species richness by inducing negative frequency dependence: the more common a species is, the greater the proportion of the environment that is rendered inhospitable to its offspring. Many empirical systems show evidence of JCEs (e.g. Hyatt et al., 2003; Petermann et al., 2008; Mangan et al., 2010; Swamy and Terborgh, 2010; Zhu et al., 2010; Johnson et al., 2012, 2014; Comita et al., 2014; Bever et al., 2015); theoretical models evaluate the conditions under which JCEs can maintain species diversity (e.g. Adler and Muller-Landau, 2005; Muller-Landau and Adler, 2007; Stump and Chesson, 2015; Chisholm and Fung, 2020).

HP is based on the observation that species differ in their tolerances of environmental conditions that vary in space (Mouquet and Loreau, 2003; Hortal et al., 2009; Stein et al., 2014; Leibold and Chase, 2017). Environmental factors such as topography (e.g. elevation, convexity) and soil composition (e.g. soil moisture, pH, nutrient composition) have been observed to differentially affect species-specific demographic traits, often impacting seed and seedling survival in tree communities. HP can stabilize coexistence if species are sufficiently different in their environmental fitness associations (Chesson, 2000a; Snyder and Chesson, 2003). Empirical evidence strongly suggests that JCEs and HP co-occur in a variety of forest communities (e.g. Hubbell et al., 2001; Wright, 2002; Uriarte et al., 2004; Freckleton and Lewis, 2006; Queenborough et al., 2009; Chen et al., 2010; Bagchi et al., 2011; Bai et al., 2012; Piao et al., 2013; Lu et al., 2015; Wu et al., 2016; Pu et al., 2017; Yao et al., 2020; Magee

et al., 2021; Huang et al., 2022; Liu et al., 2022). Despite this, the theoretical implications of communities that experience both coexistence mechanisms are surprisingly underdeveloped (but see Stump and Chesson, 2015). Developing an understanding of their interactions is of particular importance given that recent work casts doubt on the ability of JCEs operating in isolation to maintain the high species richness observed in tropical forests (**?**Cannon et al., 2021).

Superficially, JCEs and HP seem to operate through opposing forces: HP allows for coexistence by aggregating species into favorable habitat types, whereas JCEs function because adults render nearby areas inhospitable to conspecifics. It is therefore important to elucidate how these seemingly countervailing forces affect diversity on the community level. The interaction between JCEs and HP likely depends on the spatial structure of the abiotic environment. Specifically, the degree of spatial autocorrelation (the tendency for more similar environmental types to neighbor each other) may impact the patches on which species experience JCEs (Fig. 3.1C) and modulate the extent to which it affects competitive outcomes. Current theory does not examine how interactions between JCEs, HP, and spatial structure affect species coexistence.

Previous work shows that JCEs alone are likely sufficient to maintain high species richness in an otherwise neutral community (Levi et al., 2019). However, this result is not robust to when communities exhibit realistic levels of inter-specific fitness variation (Chisholm and Fung, 2020) unless they occur over a fairly large spatial scale (Smith, 2022a). In this study, I explore the question: can the joint operation of JCEs and HP maintain high species richness in communities that experience realistically large inter-specific fitness variation in situations where a single mechanism is insufficient?

To address this question, I develop a simple spatially explicit model that incorporates JCEs and HP. I show that JCEs and HP have the potential to synergetically promote coexistence. Specifically, I find that level of richness maintained by the simultaneous operation

of JCEs and HP is considerably greater than the sum of their operation in isolation when abiotic spatial heterogeneity is positively autocorrelated. Then, I demonstrate that the interaction between JCEs and HP depends on a key metric, k_M, which describes the level of spatial autocorrelation on the spatial scale over which JCEs occur. Overall, the results of this study provide a simple framework to understand the factors determining how JCEs and HP interact and their subsequent effect on the maintenance of species richness.

3.3 Methods

3.3.1 Model description

I consider a discrete-time site occupancy model. The community consists of a $X \times X$ grid, upon which each cell represents a single patch that contains a single adult tree. First, I describe the offspring dynamics on each patch type.

Each time-step, species i disperses Y_i offspring uniformly throughout the environment. $i = 1, 2, .., N$ such that there are N species in the community. Y_i is a composite parameter of the fecundity and baseline density-independent mortality of species i's offspring (see Appendix B for details). I refer to Y_i as "intrinsic fitness". Because dispersal is global, the number of offspring species i disperses to a patch is equal to $p_i Y_i$, where p_i is the proportion of patches in the environment occupied by species i. The number of offspring of species i on a given patch is modified by (1) habitat type and (2) Janzen-Connell Effects (JCEs). Let x represent a location in space. In addition to spatial information, x indexes a value defied by its habitat type for which (for simplicity) $0 \leq x \leq 1$. Each patch (i.e. each discrete grid-cell) takes a single habitat value defined by x which I assume is constant through time. Similarly, let $H_i(x)$ be the probability that an offspring of species i survives on patch x as a function of habitat type (i.e. the relative fitness of species i on the habitat type of x). I assume fitness

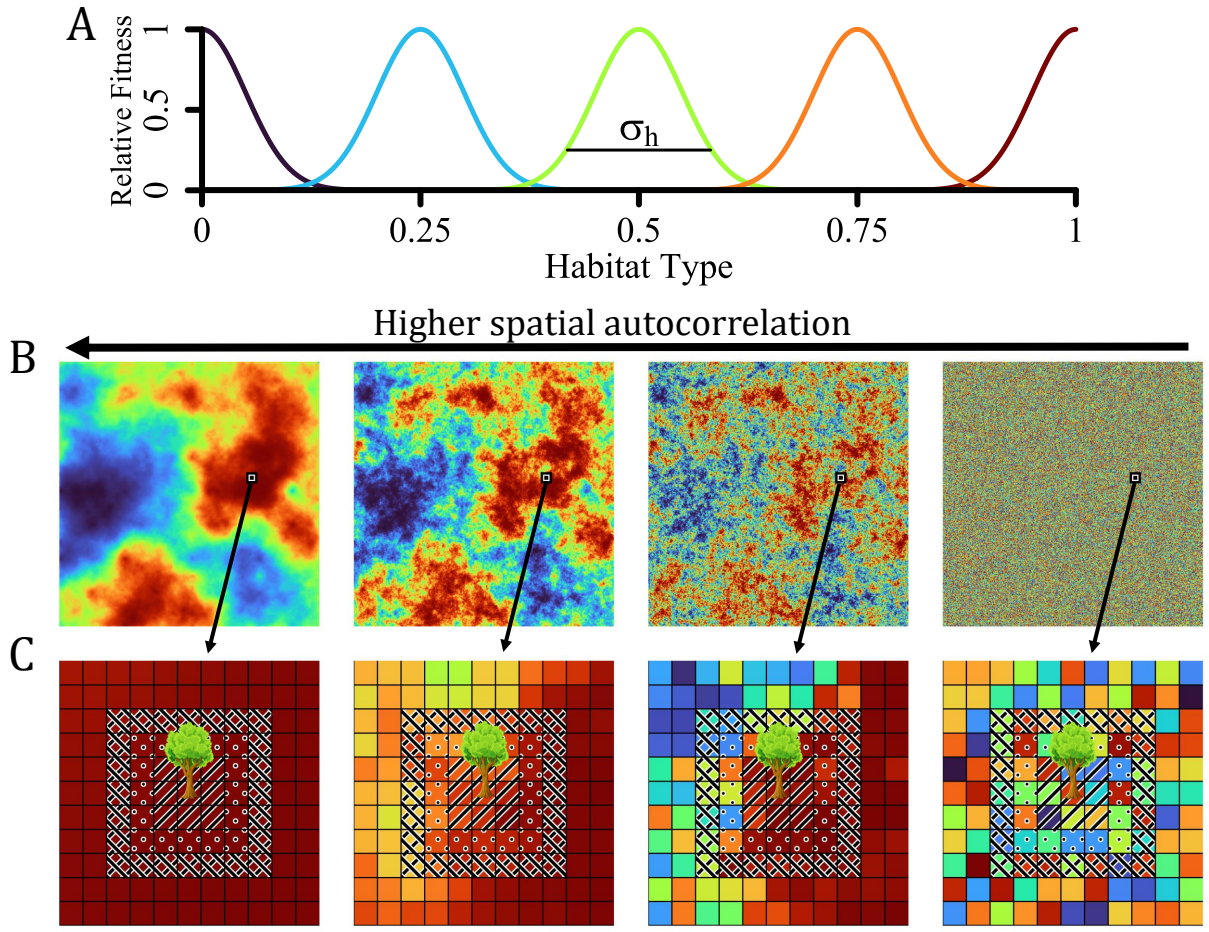

Figure 3.1: Visualization of species' responses to spatial environmental heterogeneity, habitat structure, and its potential interaction with Janzen-Connell Effects (JCEs). (A) shows how species-specific habitat associations are implemented in the model: fitness is a Gaussian function of habitat type (Equation 3.1) with response breadth defined by σ_h. Environmental type affects the probability a species' offspring (seeds and seedlings) survive on a patch. Responses depict when $\sigma_h = 0.05$. (B) shows the different landscapes examined, which vary in their level of spatial autocorrelation. Different colors represent a different value of an environmental variable, ranging from $0 - 1$. Environments range from highly positively autocorrelated (left hand side) to randomly distributed (zero autocorrelation; right hand side). (C) depicts a small portion of the habitat. Each grid-cell is a patch which contains a single adult tree; only a single tree is depicted for simplicity. Patterns around the tree depict the area over which JCEs occur, spanning a 3×3 Moore neighborhood (lines), a 5×5 Moore neighborhood (dots), and a 7×7 Moore neighborhood (crosshatches). If the focal tree has a preference for red habitat types, then the autocorrleation of the environment affects how many favorable (red) patches on which it induces JCEs. When autocorrelation is high, the tree induces JCEs almost entirely on favorable patches. When autocorrelation is low, the tree induces JCEs on relatively few favorable patches.

is a Gaussian function of habitat type:

$$H_i(x) = \exp(-(x - h_{\text{opt},i})^2/2\sigma_h^2) \tag{3.1}$$

where $h_{\text{opt},i}$ is the optimal patch type of species i ($0 \leq h_{\text{opt},i} \leq 1$) and σ_h is the breadth of environmental response (smaller σ_h means species are more specialized). See Fig. 3.1A for a visualization.

JCEs are implemented by assuming adult trees within the $M \times M$ Moore neighborhood around a patch (x) decrease the probability of conspecific offspring survival therein such that the probability of offspring survival is described by the function

$$J_i(x) = \exp\Bigg(- a \sum_{m=1}^{M(x)^2} \mathbf{1}_m(i) \Bigg) \tag{3.2}$$

noting that M^2 trees are contained within an $M \times M$ Moore neighborhood. $M(x)$ refers to the Moore Neighborhood around the patch located at x. a is a constant that defines the baseline strength of JCEs such that e^{-a} corresponds to the probability of offspring survival when a single conspecific adult is found within the Moore neighborhood. $\mathbf{1}_m(i)$ is an indicator function for which

$$\mathbf{1}_m(i) = \begin{cases} 1, & \text{if } m = i \\ 0, & \text{if } m \neq i \end{cases} \tag{3.3}$$

Therefore, offspring survival declines exponentially with the number of conspecific adult trees within the area of effect. The number of offspring of species i on patch x, $S_i(x)$, is then equal to:

$$S_i(x) = p_i Y_i H_i(x) J_i(x) \tag{3.4}$$

noting that this formulation of JCEs ($J_i(x)$) and the fitness response to the environment ($H_i(x)$) means that JCEs and HP are, at the patch level, entirely independent (see Appendix

B for more details). Therefore, interactions between JCEs and HP are emergent properties of how adults are distributed in space (i.e. both depend on x).

Now, I describe adult dynamics. Each time-step, each adult dies with probability δ. If the adult on a patch dies, the patch is immediately replaced by another individual. The identity of the species replacing the patch is determined by a lottery model (Chesson and Warner, 1981) where the probability species i "wins" the lottery and colonizes the patch is equal to the relative abundance of its offspring on a patch. That is:

$$\text{P(species } i \text{ colonizes patch } x) = \frac{S_i(x)}{\sum_{j=1}^{N} S_j(x)} \tag{3.5}$$

using the quantities from Equation 3.4 for each of the N species. Each time-step, all vacated patches are replaced according to Equation 3.5.

3.3.2 Spatially explicit simulations

Simulations were conducted on a 500×500 grid on which each grid-cell represents a patch containing a single adult tree (as noted above). The community was modeled on a torus to avoid edge effects. Landscapes (i.e. habitat structure; Fig. 3.1B) were generated by assigning a value between $0 - 1$ to each grid-cell, defining its habitat type. Autocorrelation was introduced using a midpoint displacement algorithm (Saupe, 1988) by modifying the value of the Hurst exponent using the [R] package NLMR (Sciaini et al., 2018). The resulting landscape was subsequently modified such that frequency of habitat types was uniformly distributed between $0 - 1$ throughout the entire community.

All simulations began with 300 species at equal abundance. Intrinsic fitness (Y) was log-normally distributed such that $Y \sim \text{lognormal}[\mu = 0, \sigma_Y = 1.0]$. These values were chosen on the basis that recent analyses at Barro Colorodo Island indicate inter-specific variation in low-density seedling recruitment is of approximately this order (Wright et al., 2005; Chisholm and

Fung, 2020). Each species was assigned a habitat preference, ($h_{\text{opt},i}$), with values regularly distributed between 0 and 1. Simulations examined $\sigma_h \sim \{.025, .05, .075., 0.10\}$ (the breadth of environmental response) and $M \times M \sim \{1 \times 1, 3 \times 3, 5 \times 5, 7 \times 7, 9 \times 9\}$ (the size of the Moore neighborhood). For simulations, I consider when $a = 0.5$, which implies that the presence of a single adult within the Moore neighborhood reduces offspring survivorship by approximately 40% (i.e. $e^{-a} \approx 0.60$). This value of a is generally consistent with meta-analyses assessing the strength of JCEs (if somewhat conservative; see Comita et al., 2014; Song et al., 2021a). However, I consider a more generally in analytical treatments of the model. Simulations were run for approximately 125 generations (equivalent to over 3×10^7 tree replacements), sufficiently long for the transient dynamics to end (with species richness and Shannon diversity in the community having approximately saturated to a constant number; see Appendix B, Figs. 3.9-3.16). All simulations were conducted in [R] (R Core Team, 2021).

Approximate invasion criterion

I derived an approximate invasion criterion that quantifies the condition under which a rare species deterministically increases in abundance within a community of N resident species. The derivation of the approximate invasion criterion and validation of its accuracy can be found in Appendix B.

3.3.3 Quantification of spatial autocorrelation

To examine how spatial autocorrelation mediates the interaction of JCEs and HP, I derive a metric of spatial autocorrelation of the habitat types (henceforth k_M) which quantifies the level of spatial autocorrelation of habitat types with respect to the size of the Moore neighborhood size (M) and the response breadth of habitat specialization (σ_h). To quantify

k_M, I consider the approximation

$$H_i(x) \approx \begin{cases} 1, & \text{if } h_{\text{opt},i} - \frac{1}{2}\sigma_h\sqrt{2\pi} \leq x \leq h_{\text{opt},i} + \frac{1}{2}\sigma_h\sqrt{2\pi} \\ 0, & \text{otherwise} \end{cases} \tag{3.6}$$

or, in words, species i experiences a relative fitness of 1 for the proportion of habitat types between $h_{\text{opt},i} - \frac{1}{2}\sigma_h\sqrt{2\pi}$ and $h_{\text{opt},i} + \frac{1}{2}\sigma_h\sqrt{2\pi}$ and 0 in other habitat types (Appendix B, Fig. 3.6). Therefore, a portion of approximately $\sigma_h\sqrt{2\pi}$ of the community is favorable to each species. k_M is then calculated with the following summation:

$$k_M = \frac{1}{\sigma_h\sqrt{2\pi}M^2} \sum_{x=1}^{X^2} \sum_{j \in M^2} \frac{\mathbf{1}\big[j < f(x)\big]}{X^2} \tag{3.7}$$

recalling X^2 is the number of patches in the community and where

$$\mathbf{1}\big[j < f(x)\big] = \begin{cases} 1, & x - \frac{1}{2}\sigma_h\sqrt{2\pi} \leq j \leq x + \frac{1}{2}\sigma_h\sqrt{2\pi} \\ 0, & \text{otherwise} \end{cases} \tag{3.8}$$

in which j represents the habitat type of one of the patches within the $M \times M$ around x ($j \in M^2$). Equation 3.7 is therefore highly similar to a discrete-space analogue to Ripley's K (Ripley, 1976).

k_M quantifies how the habitat types of patches at the $M \times M$ Moore neighborhood scale deviate from random (see Fig. 3.1C). Note that Equation 3.7 is divided by $1/\sigma_h\sqrt{2\pi}M^2$. If $k_M = 1$, it means that

$$\sum_{x=1}^{X^2} \sum_{j \in M^2} \frac{\mathbf{1}\big[j < f(x)\big]}{X^2} = \sigma_h\sqrt{2\pi}M^2 \tag{3.9}$$

which implies, on average, a proportion of $\sigma_h\sqrt{2\pi}$ of similar habitat types fall within M^2. This is identical to when patches are randomly distributed in the environment. Conversely, if $k_m = 1/\sigma_h\sqrt{2\pi}$, it follows that

$$\sum_{x=1}^{X^2} \sum_{j \in M^2} \frac{\mathbf{1}\big[j < f(h)\big]}{X^2} = M^2 \tag{3.10}$$

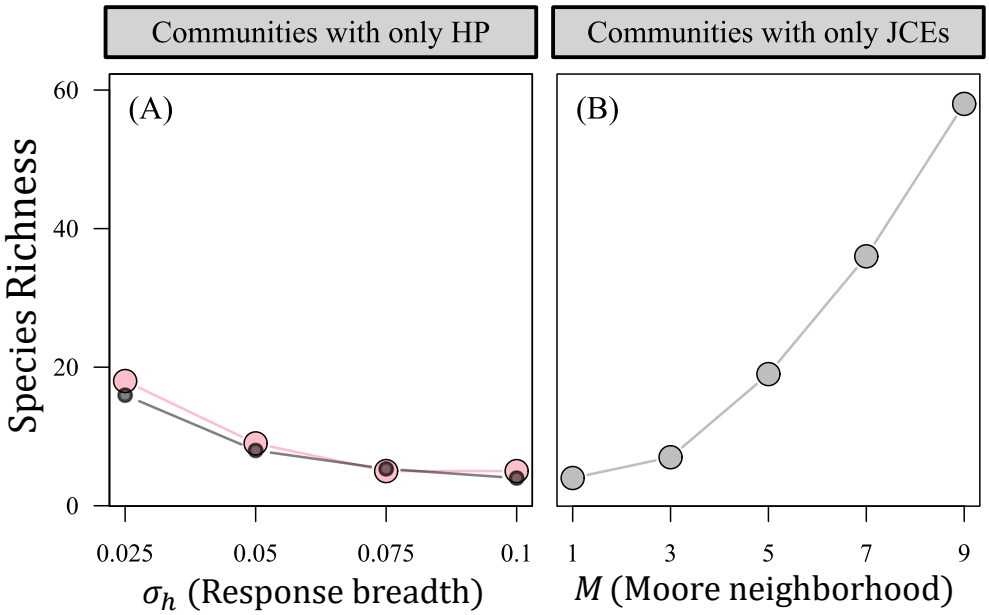

Figure 3.2: Species richness maintained by either Habitat Partitioning (HP) or Janzen-Connell Effects (JCEs) in isolation. (A) shows the diversity maintained by HP under different values of σ_h (the breadth of environmental response; Equation 3.82). Higher diversity is maintained for smaller σ_h because species are more specialized (more species can persist in the community because of relatively small niche overlap). The pink points show the exact values from model simulations. The grey points show the approximate predicted level species richness noted in the main text and Appendix B ($1/\sigma_h\sqrt{2\pi}$). (B) shows species richness when only JCEs are present for different Moore neighborhood sizes (M). Diversity increases with M. However, species richness is overall low: out of an initial pool of 300 species, up to 58 species are maintained.

which means all patches within M^2 are always of similar habitat types (high spatial autocorrelation). This is an upper bound to k_M. Therefore,

$$1 \leq k_M \leq \frac{1}{\sigma_h\sqrt{2\pi}} \tag{3.11}$$

ranging from randomly distributed habitat types to highly spatially autocorrelated. Negatively autocorrelated environments could yield $k_M < 1$, but I do not examine this case in the present study.

3.4 Results

3.4.1 Simulations

In the presence of a single coexistence mechanism (JCEs or HP only) a relatively small portion of the initial community persisted (often less than 10% of the initial community of 300 species; Fig. 3.2). When JCEs operated alone, species richness increased with increasing Moore neighborhood size (M). When HP operated alone, species richness increased with greater specialization (smaller σ_h, species habitat response breadth; Equation 3.1).

In communities with both JCEs and HP, species richness always increased relative to either mechanism in isolation. However, the degree of spatial autocorrelation dramatically affected the extent of this increase. For zero or low autocorrelation, the diversity maintained under JCEs and HP together only modestly increased diversity relative to either mechanism in isolation (Fig. 3.3, columns 3 and 4). The number of species maintained by JCEs and HP simultaneously under zero autocorrelation (red dots, Fig. 3.3, column 4) was similar to the sum of species maintained by each JCEs and HP in isolation (the sum of the dashed line and grey dots, Fig. 3.3) with their simultaneous operation increasing species richness by up to 32%. When spatial autocorrelation was high, the combination of JCEs and HP produced considerably greater diversity than either mechanism in isolation (Fig. 3.3, columns 1 and 2). Simultaneous operation HP and JCEs (red dots, Fig. **??**, column 1) maintained up to 277% greater species richness than the sum of species richness maintained by the mechanisms in isolation (the sum of the dashed line and grey dots, Fig. 3.3). Results were qualitatively identical when examining Shannon diversity (Appendix B, Fig. 3.17)

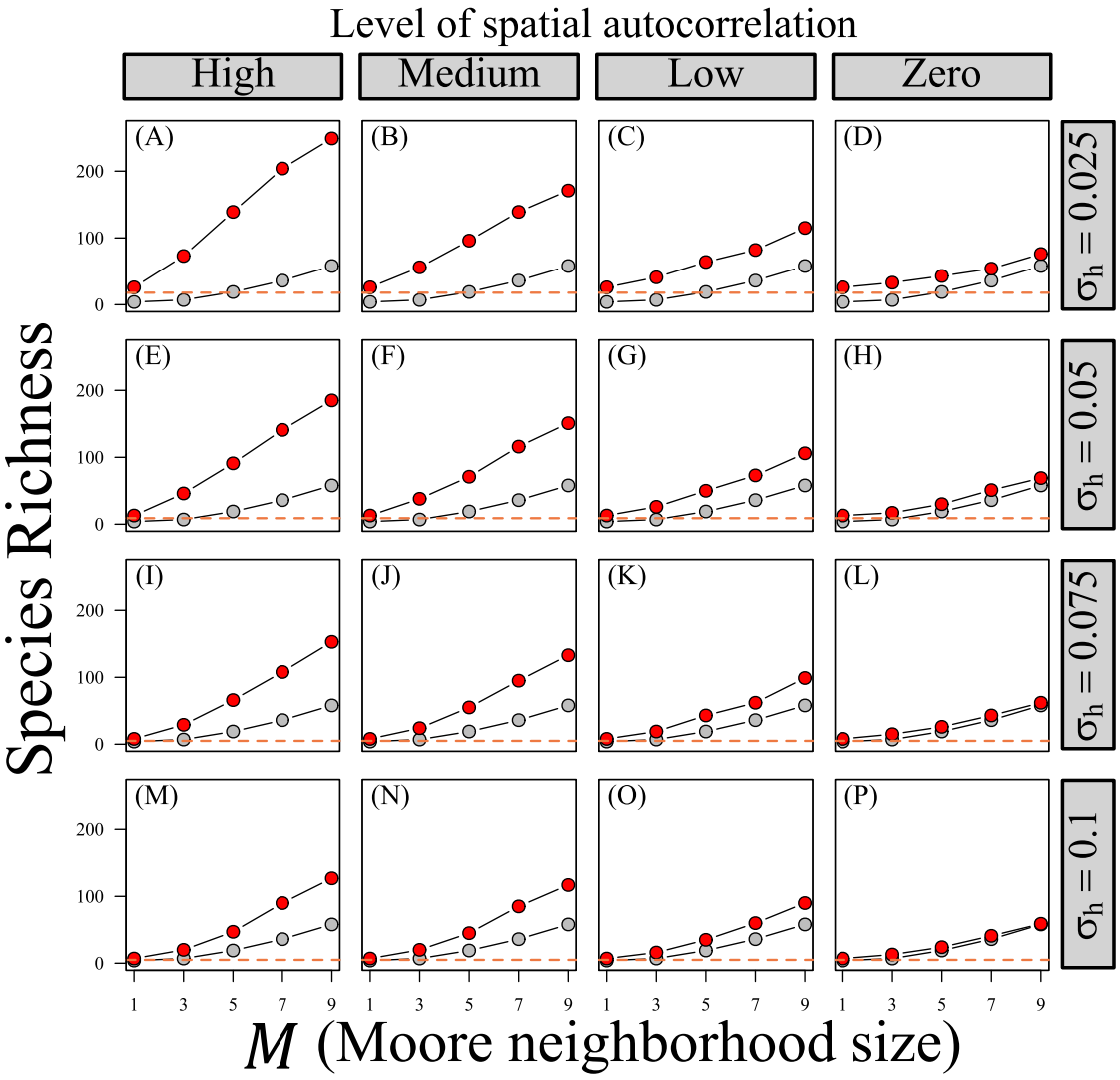

Figure 3.3: Species richness maintained by Janzen-Connell Effects (JCEs) and Habitat Partitioning (HP) operating simultaneously. Plots show how the level of spatial autocorrelation (columns), response breadth (σ_h; rows), and Moore neighborhood size (M; x-axis) affect species richness. The four levels of spatial autocorrelation are the same as those depicted in Fig. 3.1. Red points depict when JCEs and HP operate simultaneously, grey point depict when only JCEs are present, and dashed lines depict when only HP is present. As in the case of JCEs alone, species richness increases with increasing M and decreasing σ_h. The magnitude of this increase depends on the level of spatial autocorrelation. For zero and low autocorrelation, the species richness maintained at various Moore neighborhood sizes is very similar to that of the JCEs only case (grey points) regardless of σ_h. In contrast, when under medium and high spatial autocorrelation, diversity increases rapidly with M, particularly under lower σ_h. This indicates that the level of spatial autocorrelation mediates the interaction between JCEs and HP. Results were qualitatively identical examining Shannon diversity (Appendix B, Fig. 3.17).

3.4.2 Invasion analysis

To provide some insight into these results, I derived an approximate invasion criterion that quantifies the condition under which a rare species can invade a community of N resident species:

$$Y_i > \underbrace{\overline{Y}}_{\substack{\text{mean}\\ \text{intrinsic}\\ \text{fitness}}} \underbrace{\left(1+\text{Cov}(Y,p)\phi\right)}_{\substack{\text{relative}\\ \text{competition}\\ \text{term}}} \underbrace{R(\sigma_h,N)}_{\substack{\text{HP}\\ \text{term}}} \underbrace{e^{-(1-e^{-a})\frac{M^2}{N}R(\sigma_h,N)k_M}}_{\substack{\text{JCE}-\text{HP}\\ \text{term}}} \tag{3.12}$$

The left had side of Equation 3.12 represents the intrinsic fitness of a rare invading species. The right-hand side of Equation 3.12 can be interpreted as the mean fitness of the resident community at equilibrium, with smaller values more easily allowing a rare species to invade. The right-hand side consists of several key terms. $\overline{Y}$ is the mean intrinsic fitness of the resident community. The relative competition term (which is equal to or greater than 1) quantifies the degree to which invaders tend to compete against species of high fitness. The mean intrinsic fitness and relative competition terms are quantitatively important for determining invasion, but not qualitatively important concerning how JCEs and HP interact to shape affect invasion (see Appendix B). I henceforth focus on the HP and JCE−HP terms.

$R_i(\sigma_h, N)$, the HP term, quantifies the extent to which HP in isolation promotes invasion. If it is assumed species' habitat preferences are randomly distributed in trait space, it can be shown that

$$R(\sigma_h, N) \approx 1 - e^{-N\sigma_h\sqrt{2\pi}} \tag{3.13}$$

(see Appendix B). $R_i(\sigma_h, N)$ quantifies the expected proportion of habitat overlap between an invader (species i) and the N residents ($0 \leq R_i(\sigma_h, N) \leq 1$). $R_i(\sigma_h, N)$ increases with the number of species in the community, N, rapidly saturating to 1 (Fig. 3.4A). This reflects how unless species are highly specialized (σ_h is very small) potential habitat preferences (i.e. spatial niches) quickly saturate such that a species invading a diverse community is likely to compete against species with near-complete habitat preference overlap. Therefore, HP directly contributes to invasion when there are relatively few species in the community, but not when it is diverse. Under the assumption that species evenly partition the environment, (i.e. species' habitat optima are all equidistant in trait

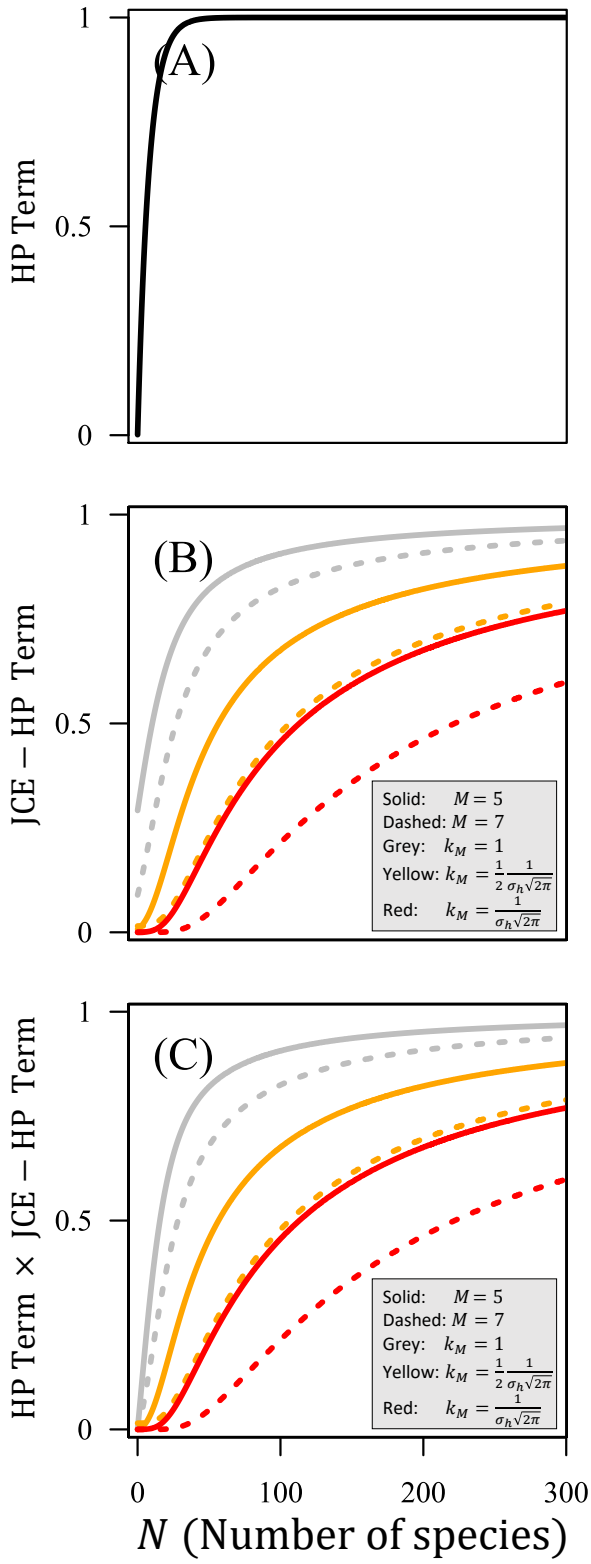

Figure 3.4: Visualization of the different components of the invasion criterion (Equation 3.12). The x-axis shows N, the number of species in the community. Note that N in this figure is a parameter input into the invasion criterion, not an output from a simulation. For all invasion criterion components (the y-axis of each plot) invasion is easier when the component is smaller; a value of 1 implies the component does not facilitate invasion (i.e. no stabilizing effect). (A) depicts the HP term, $R(\sigma_h, N)$. Invasion is made easier only for relatively small N; $R(\sigma_h, N)$ rapidly saturates to 1 as N increases. (B) shows the JCE−HP term under three different values of k_M (spatial autocorrelation) and two different values of M (Moore neighborhood size). Grey shows $k_M = 1$ (no autocorrelation), orange shows $k_M = 1/2\sigma_h\sqrt{2\pi}$ (moderate autocorrelation), and red shows $k_M = 1/\sigma_h\sqrt{2\pi}$ (high autocorrelation; the upper bound of k_M). Invasion becomes more difficult with increasing N, but less so when the spatial environment is highly autocorrelated. Solid curves show $M = 5$ and dashed curves show $M = 7$. While invasion becomes easier with larger M in all cases, the effect is much more pronounced under high autocorrelation (compare the difference between solid and dashed curves in grey to the difference between solid and dashed curves in red). This reflects how positive autocorrelation mediates a synergistic interaction between JCEs and HP. (C) shows the product of (A) and (B). (B) and (C) are almost identical, while different colored curves within each panel dramatically differ. Therefore, the effect of HP on species invasion through its mediation of JCEs (i.e. k_M) is often more quantitatively important than the direct of effect of HP alone ($R(\sigma_h, N)$). Parameters are as follows: $\sigma_h = 0.05$, $a = 0.5$.

space) it can be derived that approximately $1/(\sigma_h\sqrt{2\pi})$ species coexist in the community when HP operates in isolation (see Appendix B, Equation 3.73). Simulation outputs are roughly consistent with this approximation (Fig. 3.2).

The JCE−HP term quantifies how JCEs and their interactions with HP facilitate species invasion. Invasion becomes easier with larger $(1-e^{-a})\frac{M^2}{N}R(\sigma_h, N)k_M$, increasing species richness (Figs. 3.4 and 3.5). Larger values of a (baseline JCE strength) and M (Moore Neighborhood size) increase the baseline strength and spatial scale over which JCEs occur, respectively, which (unsurprisingly) facilitate invasion.

Species invasion also becomes easier with increasing k_M (Fig. 3.4). As noted above, k_M is a metric of the autocorrelation of habitat types at the $M \times M$ Moore neighborhood. $1 \leq k_M \leq 1/\sigma_h\sqrt{2\pi}$ for which $k_M = 1$ indicates zero autocorrelation and $k_M = 1/\sigma_h\sqrt{2\pi}$ indicates the upper bound of spatial autocorrelation. To understand the impact of k_M on invasion, first consider how HP affects the spatial composition of adult trees. For each species, a proportion of approximately $\sigma_h\sqrt{2\pi}$ of the environment is favorable (Equation 3.6) and, consequently, each of the resident species mainly inhabit patches favorable to them. Now consider a patch in the environment of habitat type x that is favorable to the invader, species i. Species i competes mainly against resident species that also have a positive habitat association with x. Species i experiences a competitive advantage colonizing the patch due to JCEs induced by the surrounding M^2 adult trees. However, species i benefits from these JCEs only when the surrounding adults have a positive habitat association with x. Because species tend to occupy favorable patches, JCEs most strongly promote invasion if species tend to neighbor favorable patches – i.e., if habitats types are positively autocorrelated (Fig. 3.1C). $k_M = 1$ corresponds to when all species are equally likely to neighbor all habitat types. In this case, JCE strength rapidly weakens with increasing N (the number of species in the community) because many resident species induce JCEs on unfavorable patches, which does not benefit invaders (Fig. 3.4B, grey curves). The upper bound to spatial autocorrelation (when $k_M = 1/\sigma_h\sqrt{2\pi}$) corresponds to when species only neighbor the (approximate) $\sigma_h\sqrt{2\pi}$ proportion of patches they find favorable. This reduces the diluting effect N has on JCE strength and species invasion because resident species induce JCEs only on favorable patches, which always benefits invaders (Fig. 3.4B,

red curves). Notably, for highly diverse communities (large N) in which $R(\sigma_h, N) \approx 1$ (i.e. habitat niche space is saturated) and there is zero autocorrelation ($k_M = 1$), the invasion criterion for the JCE and HP case (Equation 3.12) converges exactly to the invasion criterion of JCEs operating in isolation. Therefore, positive spatial autocorrelation is necessary for the interaction between JCEs and HP to boost invader growth rate in highly diverse communities. See Appendix B for details.

How HP promotes invasion through its mediation of JCEs (i.e. k_M) is potentially more quantitatively important than the direct effect of HP on invasion (i.e. Equation 3.13; see Fig. 3.4). Consistent with this, variation in species richness between simulations depicted in Fig. 3.3 are al-

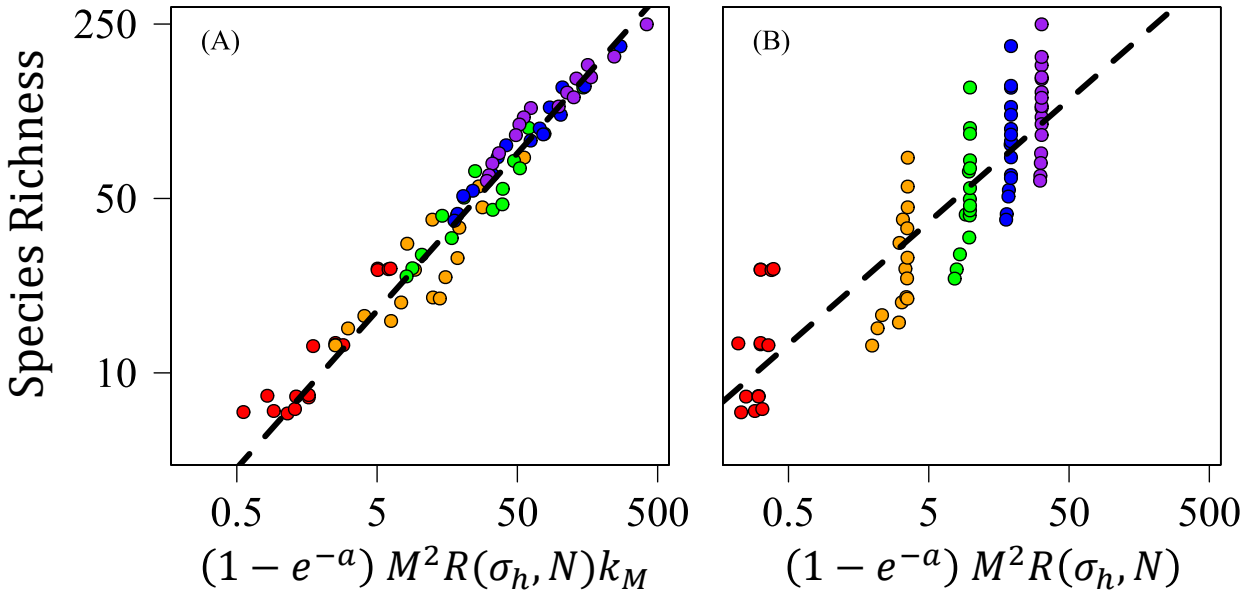

Figure 3.5: The relationship between species richness and the key metric from the JCE−HP term from Equation 3.52. In each plot, the color of each point represents a different value of M (Moore Neighborhood size). Red: $M = 1$, orange: $M = 3$, green: $M = 5$, : $M = 7$, purple: $M = 9$. Panel (A) shows consideration of the entire quantity, $(1-e^{-a})M^2R(\sigma_h, N)k_M$. Most of the variation in species richness is captured by this quantity. Panel (B) shows the same plot as (A) when one ignores spatial structure and spatial autocorrelation. That is, (B) shows the key metric from the JCE−HP term when it is assumed that habitat types (and, by extension, all trees) are randomly distributed in space (i.e. when $k_M = 1$). Taking into account spatial structure (Panel A) explains species richness far more precisely than it is ignored. In principle, considering spatial structure accounts for the number of *favorable* patches on which resident trees induce JCEs (proportional to M^2k_M). Ignoring spatial structure accounts for only the total number of patches on which resident trees induce JCEs (proportional to M^2). k_M was calculated using Equation 3.7 (Methods), M^2 and σ_h are parameters from each simulation; $a = 0.5$ in all simulations.

most entirely explained by the key quantity of the JCE−HP term, $(1 - e^{-a})M^2R(\sigma_h, N)k_M$ (Fig. 3.5A). Failing to account for spatial structure (modifying the invasion criterion such that species and patches are randomly distributed in space; i.e. $k_M = 1$), while still informative, yields a much poorer explanation of species richness (Fig. 3.5B).

3.5 Discussion

3.5.1 How Janzen-Connell Effects and Habitat Partitioning interact

Despite considerable theoretical attention given to both JCEs (e.g. Armstrong, 1989; Adler and Muller-Landau, 2005; Stump and Comita, 2018; Levi et al., 2019; Chisholm and Fung, 2020; Smith, 2022a) and HP (e.g. Chesson, 1985, 2000a; Amarasekare, 2003; Leibold et al., 2004; Snyder and Chesson, 2003; Shoemaker and Melbourne, 2016; Ben-Hur and Kadmon, 2020) in isolation and the strong evidence of their joint presence in numerous communities, their potential interactions have received relatively little theoretical attention. In this paper, I show that the interaction between JCEs and HP fundamentally depends on the spatial composition of abiotic heterogeneity: JCEs and HP synergistically interact to promote high species richness if habitat types exhibit positive spatial autocorrelation.

This result stems from how HP and autocorrelation modify the spatial composition of competitors and the patches they neighbor. First, consider the case of only JCEs: all species in the community compete equally (in that no habitat preferences exist) so the particular patches on which a species induces JCEs does not matter. This is not the case when HP is considered: species experience high fitness only on patches with suitable habitat types and compete primarily with species sharing similar habitat preferences. When there is little or no spatial autocorrelation, species do not tend to neighbor patches on which they experience high fitness (Fig. 3.1C) which means they induce JCEs on many patches they are already unlikely to colonize. When habitat types are positively autocorrelated, this is reversed: species tend to neighbor and induce JCEs on patches where they have high fitness. This increases the strength of frequency dependence, allowing for the maintenance of relatively high species richness (Fig. 3.3). In the extreme case – when there is high autocor-

relation and species are highly specialized (Fig. 3.3A) – the community approximately acts like it is structured with several sub-communities comprising primarily of competitors sharing habitat preferences. This increases species richness because the strength by which JCEs promote invasion is a decreasing function of the total number of species in the community (Equation 3.52). How the spatial scale over which spatial heterogeneity is autocorrelated compares to the spatial scale over which JCEs occur, k_M, defines the strength of this effect. Measuring k_M is therefore of key importance in determining the interaction between these mechanisms.

Notably, Stump and Chesson (2015) examine a similar model and find a lack of interaction between JCEs and HP. This discrepancy reflects the fact that their model treats space *implicitly*. In doing so, JCEs occur entirely locally at the patch level (i.e. JCEs occur only on the patch occupied by adults and no neighboring patches; equivalent to $M = 1$). While elegant, this simplification ignores the spatial composition of adults, which constitutes the key factor governing the interaction of JCEs and HP. Future modeling efforts should be cognizant of how explicit (as compared to implicit) treatments of space may qualitatively change how coexistence mechanisms interact.

3.5.2 Realism of the model and future avenues

This model makes several simplifying assumptions which may quantitatively modify the results. One limitation is that I considered a one-dimensional axis on which the spatial environment varies; in reality, species-specific adaptations to spatial environmental heterogeneity are multidimensional. Different spatially varying environmental factors may exhibit differing (and independent) levels of autocorrelation, which may factor into how JCEs and HP interact. In addition, I assumed no temporal variation in the habitats (habitat structure was invariant with time, sometimes called "pure spatial variation"; Chesson, 1985). However, some forms of spatial environmental heterogeneity emerge from short-term spatial-temporal fluctuations (e.g. flooding that occurs periodically and randomly at different locations) such that changes in the spatial environment are rapid. If habitat types change considerably faster than tree generation time, adults are no longer likely to neighbor favorable patches (even if spatial structure shows positive autocorrelation). This can undermine the synergistic interaction between JCEs and HP. More broadly, the interaction between JCEs

and HP (defined by k_M above) under spatial-temporal variation can be redefined by k_M scaled by the probability a patch changes between recruitment events (see Appendix B for details). Future empirical studies examining JCEs and HP should emphasize the time-scale of spatial-temporal variation in habitat types.

All species were assumed to have the same degree of habitat specialization, σ_h. However, the breadth of environmental tolerance varies between species. For example, larger seeded species tend to be tolerant of more stressful environmental conditions (large seeded species are thus habitat generalists with respect to stress; Moles et al., 2003; Moles and Westoby, 2004) and previous work shows that a trade-off between seed size and fecundity can maintain diversity in communities with spatial heterogeneity in environmental stress levels (the tolerance–fecundity trade-off; Muller-Landau, 2010). Future work explicitly integrating the effects of variable stress levels, the tolerance–fecundity trade-off, and the model presented here might be a fruitful avenue to examine how interactions between JCEs and HP manifest themselves in empirical communities. Empirical evidence also indicates large-seeded (and shade-tolerant) species are less sensitive to JCEs (e.g. Lebrija-Trejos et al., 2016), which offers a potential means of integrating JCEs into life history theory.

An intriguing spatially varying abiotic variable JCEs may interact with is light availability. Species differ in their shade tolerance and light capture strategies (Wright et al., 2003; Rüger et al., 2009; D'andrea et al., 2020). However, light availability is largely determined by biotic factors (e.g. the presence or absence of canopy trees). This makes JCEs (which are biotically induced) and spatial variation in light availability particularly likely to interact. In addition to providing insights about species coexistence, theoretically exploring these interactions may provide insights into the growing body of evidence showing light availability and species shade tolerance impacts measurements of JCE strength (Comita et al., 2009; Inman-Narahari et al., 2016; McCarthy-Neumann and Kobe, 2019; Brown et al., 2020; Song et al., 2021b; Holík et al., 2021; Magee et al., 2021).

There are several further interesting avenues for future studies to explore. The model assumes species are not seed-limited. However, seed limitation can reduce species richness (Hurtt and Pacala, 1995; Ben-Hur and Kadmon, 2020) and the parameter space over which coexistence mechanisms operate (Muller-Landau, 2010). An additional complication is dispersal limitation, which can in-

teract with both HP (Chesson, 2000a; Snyder and Chesson, 2003; Hart et al., 2017; Ben-Hur and Kadmon, 2020) and JCEs (Muller-Landau and Adler, 2007; Stump and Chesson, 2015; Chisholm and Fung, 2020). Furthermore, this study assumes distance and density-dependent effects are perfectly specialized. While measurements show JCEs are indeed highly specialized (e.g. Comita et al., 2014; Sarmiento et al., 2017; Gripenberg et al., 2019) specialization is not perfect and often exhibits taxonomic spillover (Ødegaard et al., 2005; Gilbert and Webb, 2007). Whether species that share natural enemies are also more likely than random chance to have similar habitat associations is an additional axis on which HP and JCEs can interact (Stump, 2017).

Overall, the assumptions of this model leave room for refined biological realism and integration into life history theory that likely quantitatively modify how the joint ability of JCEs and HP to maintain diversity. However, the main result – that the interaction between HP and JCEs is shaped by the degree of spatial autocorrelation in habitat types – is likely to qualitatively hold so long as additional assumptions do not disrupt the tendency of adults to neighbor (and induce JCEs on) favorable patches when spatial autocorrelation is high.

3.5.3 Relevance to empirical measurements

Many studies measure JCE strength by quantifying the probability of juvenile survival close to and distant from conspecific adults (e.g. references in Comita et al., 2014; Song et al., 2021a). Previous empirical and theoretical work notes that the co-occurrence of JCEs and HP can complicate measurements of the former (e.g. Comita et al., 2009; Piao et al., 2013; Stump and Chesson, 2015; Wu et al., 2016). This is because in heterogeneous environments where HP operates, juveniles near adults may inhabit favorable habitats while juveniles far from adults may persist in relatively unfavorable conditions. This can obscure measurements purely based on the relative survival probability of offspring near and far from conspecifics.

The scenario is further complicated when considering the interacting spatial scales of JCEs and autocorrelation of the abiotic environment (defined by k_M in the model). JCEs and HP are predicted to strongly interact under positive spatial autocorrelation; it therefore is necessary to parse out how both density-independent and density-dependent survival varies as a function of conspecific adult

proximity. There are several avenues to accomplish this. For example, recent papers use GLMMs to examine how conspecific (and heterospecific) distance and density-dependent effects and spatially varying abiotic factors (e.g. topography, elevation, and pH) affect species-specific seedling and sapling survival (Yao et al., 2020; Huang et al., 2022). Such measurements in concert with the spatial distribution of habitat types and spatial point analyses of adult trees (e.g. Wiegand and Moloney, 2013; Wiegand et al., 2021) offer a promising means of quantifying the strength of JCE-HP interactions and the stabilizing effect it generates.

Another option is to preform experiments that directly tease out density/distance-dependent and density-independent survival. As empirical evidence indicates that specialized natural enemies (often fungal pathogens) generate JCEs (Bagchi et al., 2010, 2014; Liu et al., 2012; Hazelwood et al., 2021), 2×2 factorial manipulation experiments comparing juvenile survivorship near and far from conspecific adults in fungicide-treated locations vs. untreated locations may provide insights. Such an experiment would measure four quantities: (1) density-independent (fungicide-treated) juvenile survival near conspecific adults ($S_{\mathrm{T}}^{\mathrm{N}}$), (2) density-independent (fungicide-treated) juvenile survival far from conspecific adults ($S_{\mathrm{T}}^{\mathrm{F}}$), (3) non-fungicide-treated juvenile survival near conspecific adults ($S_{\mathrm{U}}^{\mathrm{N}}$), and (4) non-fungicide-treated offspring survival far from conspecific adults ($S_{\mathrm{U}}^{\mathrm{F}}$). Importantly, JCEs and HP strongly interact when adults induce JCEs primarily on locations where offspring have high survivorship (Figs. 3.2, 3.3). Evidence for this interaction would be supported if both $S_{\mathrm{T}}^{\mathrm{N}} > S_{\mathrm{UT}}^{\mathrm{F}}$ (density-independent survival is greater near conspecific adults) and $S_{\mathrm{T}}^{\mathrm{N}}/S_{\mathrm{U}}^{\mathrm{N}} > S_{\mathrm{T}}^{\mathrm{F}}/S_{\mathrm{U}}^{\mathrm{F}}$ (the proportional decrease in juvenile survival near conspecific adults is greater than the decrease far from conspecific adults).

3.5.4 Broader significance

Results are relevant to conservation concerns. Previous work shows habitat fragmentation reduces species richness (Hanski, 2015; Fletcher Jr et al., 2018) though the ecological processes that facilitate this are contentious. The results of this study suggest that fragmentation may reduce diversity through its interaction with JCEs. The degree of spatial autocorrelation is related to the extent of environmental fragmentation: lower autocorrelation implies that similar habitats are more frag-

mented (or, at least, more homogenized) in space. Therefore, habitat fragmentation may have particularly severe consequences for the maintenance of diversity of sessile organisms in systems for which JCEs and HP jointly operate. Indeed, JCEs have been measured to decrease in strength in more fragmented environments (nearer to the forest edge; Krishnadas et al., 2018) which can reduce their ability to stabilize coexistence (Krishnadas and Stump, 2021). The results of this study provide a potential mechanism for these observations if fragmentation results in a reduction in the mean distance between patches on which juvenile trees experience relatively high fitness. Processes that homogenize the spatial composition of habitats would also reduce potential synergetic interactions between JCEs and HP, even if the total area of the habitat remains intact. Restoration efforts should therefore be cognizant of how the spatial composition of restored habitats affects distance and density-dependent processes.

3.5.5 Conclusion

JCEs and HP can work synergistically to promote species richness in spatially autocorrelated environments. This result highlights the need to carefully model the interactions between spatially-dependent stabilizing mechanisms. Precise examinations of spatial coexistence mechanisms that elucidate the conditions under which they work in series or parallel are necessary to explain the high diversity of tropical forests and pinpoint environmental variables of high conservation concern.

3.6 Acknowledgements

This research was funded by the National Science Foundation grant NSF OCE 1851489. I thank J. Timothy Wootton, Catherine A Pfister, Mercedes Pascual, Trevor Price, Zachary Miller, and the Wootton-Pfister lab for insightful discussion and feedback on the manuscript.

Appendix B

Introduction

This appendix is broken into several sections. First, I provide a more detailed general derivation of the model presented in the main text. Second, I derive the approximate invasion criterion from the main text. Third, I demonstrate that the JCE-HP (Janzen-Connell Effect - Habitat Partitioning) model converges to a model with HP alone when a community is highly diverse (large N) and there is no spatial autocorrelation ($k_M = 1$; as noted in the main text). Fourth, I discuss how spatial-temporal autocorrelation impacts the interaction between JCEs and HP. Fifth, I demonstrate the accuracy of the approximate invasion criterion. Sixth, and finally, I provide additional details on the simulations.

General model derivation

As noted in the main text, I consider a discrete-time site occupancy model. The community consists of a $X \times X$ grid, upon which each cell represents a single patch that contains a single adult tree. Here, I (in detail) describe the offspring dynamics on each patch type.

Each time-step, species i disperses K_i seeds uniformly throughout the environment. $i = 1, 2, .., N$ such that there are N species in the community. Dispersal is assumed to be global. Therefore, the number of offspring species i disperses to a each patch is equal to $p_i K_i$, where p_i is the proportion of patches in the environment occupied by species i. The number of offspring of species i dispersed to a given patch experience mortality due to (1) habitat type and (2) Janzen-Connell Effects (JCEs).

Let x represent a given patch in space. The dynamics of the abundance of offspring of species i dispersed at patch x at time t, henceforth $S_i(x,t)$, are described by the following ODE

$$\frac{dS_i(x,t)}{dt} = -h_i(x)S_i(x,t) - j_i(x,t)S_i(x,t) \tag{3.14}$$

where $h_i(x)$ is a function defining the density-independent mortality of offspring of species i on the patch at location x and $j_i(x,t)$ describes how the density of adults of species i influences mortality. Importantly, density-independent mortality ($h_i(x,t)$) and density-dependent mortality ($j_i(x,t)$) are entirely independent on the patch level. This means that interactions between JCEs and HP (described below) are emergent properties of the spatial composition of adults.

Solving for the ODE (noting the initial number of offspring dispersed to a patch is equal to p_iK_i) yields

$$S_i(x,\tau) = p_iK_i \exp\big(-h_i(x)\tau\big)\exp\big(-j_i(x)\tau\big) \tag{3.15}$$

where τ is the period over which offspring are vulnerable to density-independent and density-dependnet mortality. For simplicity, I use the notation $S_i(x)$ in place of $S_i(x,\tau)$.

For density-independent effects, I describe mortality as a Gaussian function of habitat type, which entails:

$$h_i(x)\tau = m_i + \frac{(x - h_{\text{opt},i})^2}{2\sigma_h^2} \tag{3.16}$$

therefore

$$\exp\big(-h_i(x)\tau\big) = \exp(-m_i)\exp\bigg(-\frac{(x - h_{\text{opt},i})^2}{2\sigma_h^2}\bigg) \tag{3.17}$$

The first term, $\exp(-m_i)$, is the baseline proportion of offspring that survive on a species' optimal patch type. The second term represents how patch type affects density-independent mortality where $h_{\text{opt},i}$ is the optimal patch type of species i ($0 \leq h_{\text{opt},i} \leq 1$) and σ_h is the breadth of environmental response (smaller σ_h means species are more specialized). Note that latter term implies that survival is a Gaussian function of habitat type. I henceforth let $H_i(x) = \exp\big(-\frac{(x-h_{\text{opt},i})^2}{2\sigma_h^2}\big)$.

JCEs, defined by $j_i(x)$, are implemented by assuming that offspring mortality increases linearly

with the number of adult trees within the $M \times M$ Moore neighborhood around a patch. Therefore,

$$j_i(x)\tau = a \sum_{m=1}^{M(x)^2} \mathbf{1}_m(i) \tag{3.18}$$

noting that M^2 trees are contained within an $M \times M$ Moore neighborhood. $M(x)$ refers to the Moore Neighborhood around the patch located at x. a is a constant that defines the baseline strength of JCEs over the time period of vulnerability, τ. $\exp(-a)$ represents the proportion of offspring that survive JCEs when a single adult falls within the Moore neighborhood. $\mathbf{1}_m(i)$ is an indicator function for which $\mathbf{1}_m(i) =$ if $m = i$ and $\mathbf{1}_m(i) = 0$ if $m \neq i$. Therefore,

$$\exp\big(-j_i(x)\tau\big) = \exp\bigg(-a \sum_{m=1}^{M(x)^2} \mathbf{1}_m(i)\bigg) \tag{3.19}$$

I henceforth let $J_i(x) = \exp\big(-a\sum_{m=1}^{M(x)^2} \mathbf{1}_m(i)\big)$.

Overall, then, $S_i(x) = K_i\exp\big(-m_i\big)H_i(x)J_i(x)$. Let $K_i\exp(-m_i) = Y_i$, in which case Y_i is a composite parameter of the fecundity and the baseline density-independent mortality of species i's offspring. I refer to Y_i as "intrinsic fitness". Then,

$$S_i(x) = p_i Y_i H_i(x) J_i(x) \tag{3.20}$$

as shown in the main text.

Derivation of approximate invasion criterion

In this section, I show the derivation of the approximate invasion criterion from the main text. This term quantifies to what extent Janzen-Connell Effects (JCEs) and Habitat Partitioning (HP) affect the ability of a rare species (a species at low proportion in the environment) to invade a community of N resident species. The following derivation assumes (1) the proportion of habitat types are uniformly distributed and (2) species fitness (and, hence, species abundance) is independent of habitat association.

Basic setup

As noted in the main text and above, the number of offspring of species i on patch x, $S_i(x)$, is equal to:

$$S_i(x) = p_i Y_i H_i(x) J_i(x) \tag{3.21}$$

where

$$H_i(x) = \exp(-(x - h_{\text{opt},i})^2 / 2\sigma_h^2) \tag{3.22}$$

and

$$J_i(x) = \exp\Bigg(- a \sum_{m=1}^{M(x)^2} \mathbf{1}_m(i) \Bigg) \tag{3.23}$$

wherein

$$\mathbf{1}_m(i) = \begin{cases} 1, & \text{if } m = i \\ 0, & \text{if } m \neq i \end{cases} \tag{3.24}$$

Each time-step, each adult dies with probability δ. If the adult on a patch dies, the patch is immediately replaced by another individual. The identity of the species replacing the patch is determined by a lottery model Chesson and Warner (1981) where the probability species i "wins" the lottery and colonizes the patch is equal to the relative abundance of its offspring on a patch. That is:

$$\text{P(species } i \text{ colonizes patch } x) = \frac{S_i(x)}{\sum_{j=1}^{N} S_j(x)} \tag{3.25}$$

using the quantities from Equation 3.21 for each of the N species.

Basic invasion criterion derivation

Using the above, the growth rate of species i is equal to

$$\delta \Bigg[\sum_{\text{all } x} \frac{S_i(x)}{\sum_{j=1}^{N} S_j(x)} g(x) - p_i \Bigg] \tag{3.26}$$

where δ is the proportion of adult trees that die each time-step. $g(x)$ is a probability mass function representing all patches in the community such that $\sum_{\text{all } x} g(x) = 1$. It is assumed that patch types

are uniformly distributed such that there are an equal number of each patch type.

A rare species, species i, can invade if

$$\delta\left[\sum_{\text{all } x}\frac{S_i(x)}{\sum_{k=1}^{N}S_k(x)}g(x)-p_i\right]>0 \tag{3.27}$$

I now substitute Equation 3.21 into Equation 3.27. If species i is rare in the population, it escapes JCEs on essentially all patches, in which case $J_i(x)\approx 1$. Therefore, species i can invade if

$$\delta p_i\left[Y_i\sum_{\text{all } x}\frac{H_i(x)}{\sum_{j=1}^{N}p_jY_jH_j(x)J_j(x)}g(x)-1\right]>0 \tag{3.28}$$

From here, I make several approximations in order to derive an analytical expression. Firstly, while species fitness is a Gaussian function (Equation 3.22) of habitat type for the numerical simulations, I make the approximation

$$H_i(x)\approx\begin{cases}1, & \text{if } h_{\text{opt},i}-\frac{1}{2}\sigma_h\sqrt{2\pi}\le x\le h_{\text{opt},i}+\frac{1}{2}\sigma_h\sqrt{2\pi}\\ 0, & \text{otherwise}\end{cases} \tag{3.29}$$

or, in words, species i experiences a relative fitness of 1 for the proportion of habitat types between $h_{\text{opt},i}-\frac{1}{2}\sigma_h\sqrt{2\pi}$ and $h_{\text{opt},i}+\frac{1}{2}\sigma_h\sqrt{2\pi}$ and 0 in other habitat types (Fig. 3.6). Note that this approximation maintains the total area underneath $H_i(x)$ (i.e. $\int_0^\infty H_i(x)=\sigma_h\sqrt{2\pi}$ for both the Gaussian function, Equation 3.22, and the approximation, Equation 3.29).

There are several implication to Equation 3.29 in relation to Equation 3.28. Firstly, species i experiences non-zero fitness on a proportion of $\sigma_h\sqrt{2\pi}$ patches, so patches in which species i has 0 fitness can be ignored. Therefore, I subset $\sum_{\text{all } x}$ such that x includes only patches for which species i has a positive fitness association – that is, a fitness of 1 (henceforth $\sum_{x\in H_i(x)=1}$). $\sum_{x\in H_i(x)=1}g(x)=\sum_{\text{all } x}g(x)\sigma_h\sqrt{2\pi}$.

Let $g'(x)$ be a new probability mass function that represents the distribution of patches favorable

to species i (in which $x \in H_i(x) = 1$). Then, species i can invade if

$$\delta p_i \left[Y_i \sigma_h \sqrt{2\pi} \sum_{x \in H_i(x)=1} \frac{1}{\sum_{j=1}^{N} p_j Y_j H_j(x) J_j(x)} g'(x) - 1 \right] > 0 \tag{3.30}$$

Then, with some further algebraic manipulations, this is equal to

$$\sum_{x \in H_i(x)=1} \frac{1}{1 - \left(1 - \sum_{j=1}^{N} p_j \big(Y_j / Y_i\big) \big(H_j(x) / \sigma_h \sqrt{2\pi}\big) J_j(x) \right)} g'(x) - 1 > 0 \tag{3.31}$$

Then, assuming the term in parentheses in the denominator is somewhat small, I take the linear term of the Maclaurin series, which gives

$$\sum_{x \in H_i(x)=1} g'(x) \left[1 + \left(1 - \sum_{j=1}^{N} p_j \big(Y_j / Y_i\big) \big(H_j(x) / \sigma_h \sqrt{2\pi}\big) J_j(x) \right) \right] - 1 > 0 \tag{3.32}$$

which, after canceling some terms and doing some rearranging, gives

$$Y_i > \sum_{x \in H_i(x)=1} \sum_{j=1}^{N} p_j Y_j \frac{H_j(x)}{\sigma_h \sqrt{2\pi}} J_j(x) g'(x) \tag{3.33}$$

noting that $\sum_{x \in H_i(x)=1} g'(x) = 1$ by the definition of $g'(x)$ as a probability mass function.

The summations can be reversed and the above can be rewritten as

$$Y_i > \sum_{j=1}^{N} p_j Y_j \sum_{x \in H_i(x)=1} \frac{H_j(x)}{\sigma_h \sqrt{2\pi}} J_j(x) g'(x) \tag{3.34}$$

Then, $H_j(x)$ can be broken into two parts, such the latter sum can be expressed as

$$\begin{aligned} \sum_{x \in H_i(x)=1} \frac{1}{\sigma_h \sqrt{2\pi}} H_j(x) J_j(x) g'(x) &= \frac{1}{\sigma_h \sqrt{2\pi}} \big(1 - R_{ji}\big) \sum_{x \in H_i(x)=1} 0 \times J_j(x) g'(x) \\ &\quad + \frac{R_{ji}}{\sigma_h \sqrt{2\pi}} \sum_{x \in H_i(x)=1} 1 \times J_j(x) g'(x) \\ &= \frac{R_{ji}}{\sigma_h \sqrt{2\pi}} \, \mathbb{E}\left[J_j(x) \right] \end{aligned} \tag{3.35}$$

where R_{ji} is the proportion of patches in which species j and species i both have positive habitat associations. That is, R_{ji} is the proportion of patches where for which $H_j(x) = H_i(x) = 1$ over patches favorable to species i.

The expectation, $\mathbb{E}\left[J_j(x)\right]$, is taken with respect to x. $\mathbb{E}[J_j(x)]$ should be interpreted as the expected probability of survival of species j's offspring due to JCEs on a *suitable* patch. This yields the expression

$$Y_i > \sum_{j=1}^{N} p_j Y_j \frac{R_{ji}}{\sigma_h \sqrt{2\pi}} \mathbb{E}\left[J_j(x)\right] \tag{3.36}$$

Evaluation of $\mathbb{E}[\boldsymbol{J_j(x)}]$ *and derivation of* $\boldsymbol{k_M}$

Now, I evaluate $\mathbb{E}[J_j(x)]$. Consider a patch in space. JCEs are induced on the patch by adult trees within the $M \times M$ Moore neighborhood surrounding it. The probability species j's offspring survive on patch x is equal to (as noted before)

$$J_j(x) = \exp\Bigg(- a \sum_{m=1}^{M(x)^2} \mathbf{1}_m(j) \Bigg) \tag{3.37}$$

where a is a constant that defines the baseline strength of JCEs and $\mathbf{1}_m(j)$ is an indicator function for which

$$\mathbf{1}_m(j) = \begin{cases} 1, & \text{if } m = j \\ 0, & \text{if } m \neq j \end{cases} \tag{3.38}$$

To approximate the expectation of $J_j(x)$, I assume species are approximately randomly distributed in space, with a caveat. Species j can only occupy patches for which it has a positive habitat association ($H_j(x) = 1$). If patches are randomly distributed in space, then (by independence) the probability that species i neighbors any patch follow a binomial distribution:

$$\mathrm{P}(y \text{ of the } M^2 \text{ neighbors are species } j) \sim \mathrm{Bin}\big(M^2,\ p_j\big) \tag{3.39}$$

noting that the probability that species j occupies an particular patch is equal to its proportion in the community.

The autocorrelation of the environment potentially modifies the number of individuals of species j nearby a favorable patch. Firstly, consider when patches are randomly distributed (zero autocorrelation). In this case, the probability species j neighbors any patch in the community is also random (which is what Equation 3.39 assumes). This changes if patches are positively autocorrelated in space. To see this, consider an extreme case of high spatial autocorrelation in which a patch favorable to species j is always neighbored only by patches that are also favorable to species j on the scale of the M^2-sized Moore neighborhood. Patches favorable to species j make up a proportion of $\sigma_h\sqrt{2\pi}$ of the community. If patches favorable to species j neighbor only patches that also favorable to species j, then the probability a random patch favorable to species j is neighbored by an adult of species j is equal to $p_j/(\sigma_h\sqrt{2\pi})$. For example, if species j occupies $1/2$ of all patches favorable to it, then $p_j = \frac{1}{2}\sigma_h\sqrt{2\pi}$ and $p_j/(\sigma_h\sqrt{2\pi}) = \frac{1}{2}$.

More realistically, patches may exhibit some level of autocorrelation that are between the above-mentioned extremes. Assuming habitat types range from zero autocorrelation to high autocorrelation, the number of individuals of species j neighboring a favorable patch is given by

$$\mathrm{P}(y \text{ of the } M^2 \text{ neighbors are species } j) \sim \mathrm{Bin}\big(M^2,\ p_j k_M\big) \tag{3.40}$$

where k_M defines the extent to which patches are positively autocorrelated. $k_M \approx 1$ if patches are randomly distributed and $k_M \approx 1/\sigma_h\sqrt{2\pi}$ if patches are highly correlated. Or, put simply,

$$1 \leq k_M \leq \frac{1}{\sigma_h\sqrt{2\pi}} \tag{3.41}$$

In theory, k_M could be less than 1 if habitat types are negatively spatially autocorrelated. However, I do not consider this possibility for the purposes of this paper. k_M is highly similar to Ripley's K (Ripley, 1976) in discrete space.

Then, to calculate $\mathbb{E}[J_j(x)]$, it is necessary to take the expectation of offspring survival. Recall that offspring survival decreases exponentially with the number of conspecific adults within the Moore neighborhood such that $\mathrm{P}(\text{offspring of species } j \text{ survive given } y \text{ adults of species } j) = e^{-ay}$.

Then,

$$\begin{aligned}\mathbb{E}[J_j(x)] &= \sum_{y=0}^{M^2} \mathrm{P}(y \text{ of the } M^2 \text{ neighbors are species } j) \times \\ &\qquad \mathrm{P}(\text{offspring of species } j \text{ survive given } y \text{ adults of species } j) \\ &\approx \sum_{y=0}^{M^2} \binom{M^2}{y} (p_j k_M)^y (1 - p_j k_M)^{M^2 - y} e^{-ay} \\ &= \left(1 - (1 - e^{-a}) p_j k_M\right)^{M^2}\end{aligned} \tag{3.42}$$

It is more convenient to work with the above expression by noting the property that $(1-x)^y \approx e^{-xy}$. Applying this to the above yields

$$\mathbb{E}[J_j(x)] \approx e^{-(1-e^{-a})M^2 k_M p_j} \tag{3.43}$$

and, overall, plugging this into the invasion criterion yields the expression

$$Y_i > \sum_{j=1}^{N} Y_j \frac{R_{ji}}{\sigma_h \sqrt{2\pi}} p_j e^{-(1-e^{-a})M^2 k_M p_j} \tag{3.44}$$

General invasion criterion derivation

I now evaluate the above summation. To do so, I first take the linearization of the terms in the summation with respect to p_j about the mean proportion in the population $\overline{p}$. This gives

$$p_j e^{-(1-e^{-a})M^2 k_M p_j} \approx \overline{p}\, e^{-(1-e^{-a})\overline{p} M^2 k_M} + e^{-(1-e^{-a})M^2 \overline{p}\, k_M} \left(1 - \overline{p}\, M^2 k_M (1 - e^{-a})\right)\left(p_j - \overline{p}\right) \tag{3.45}$$

Then, substituting the lineraization into the summation gives:

$$
\begin{aligned}
\sum_{j=1}^{N}\big(Y_j\frac{R_{ji}}{\sigma_h\sqrt{2\pi}}\big)p_j e^{-(1-e^{-a})M^2k_M p_j} &= N\frac{1}{N}\sum_{j=1}^{N}\big(Y_j\frac{R_{ji}}{\sigma_h\sqrt{2\pi}}\big)p_j e^{-(1-e^{-a})M^2k_M p_j} \\
&\approx N\frac{1}{N}\sum_{j=1}^{N} Y_j\,\overline{p}\,\frac{R_{ji}}{\sigma_h\sqrt{2\pi}}e^{-(1-e^{-a})M^2k_M\,\overline{p}} \quad + \\
&\qquad Y_j\frac{R_{ji}}{\sigma_h\sqrt{2\pi}}e^{-(1-e^{-a})\frac{M^2}{N}k_M}\big(1-\overline{p}\,M^2k_M(1-e^{-a})\big)\big(p_j-\overline{p}\big) \\
&= N\frac{1}{N}\sum_{j=1}^{N} Y_j\,\overline{p}\frac{R_{ji}}{\sigma_h\sqrt{2\pi}}e^{-(1-e^{-a})M^2k_M\,\overline{p}} \quad - \\
&\qquad N\frac{1}{N}\sum_{j=1}^{N}\overline{p}\;Y_j\frac{R_{ji}}{\sigma_h\sqrt{2\pi}}e^{-(1-e^{-a})M^2k_M\,\overline{p}}\big(1-\overline{p}\,M^2k_M(1-e^{-a})\big) \quad + \\
&\qquad N\frac{1}{N}\sum_{j=1}^{N}Y_jp_j\frac{R_{ji}}{\sigma_h\sqrt{2\pi}}e^{-(1-e^{-a})M^2k_M\,\overline{p}}\big(1-\overline{p}\,M^2k_M(1-e^{-a})\big)
\end{aligned}
\tag{3.46}
$$

Then, the above summations can be evaluated by using the property that $\frac{1}{N}\sum XY = \overline{X}\;\overline{Y} + \mathrm{Cov}(X,Y)$ where X and Y are random variables and $\overline{X} = \frac{1}{N}\sum X$ (i.e. it is the mean). Additionally, $\frac{1}{N}\sum(XY)Z = \overline{XY}\;\overline{Z} + \mathrm{Cov}(XY,Z)$.

In the above expression, there are three summations. The first two summations contains Y_j and R_{ji} terms, but no p_j terms. To evaluate these summations, I use the property that $\frac{1}{N}\sum Y_jR_{ji} = \overline{R_i}\;\overline{Y} + \mathrm{Cov}(R_i,Y)$. Because fitness is independent of habitat association, $\mathrm{Cov}(R_i,Y) = 0$. Thus, the first sum in the above equation gives

$$
N\frac{1}{N}\sum_{j=1}^{N}\overline{p}\;Y_j\frac{R_{ji}}{\sigma_h\sqrt{2\pi}}e^{-(1-e^{-a})M^2k_M\,\overline{p}} = N\overline{p}\;\overline{Y}\;\frac{\overline{R_i}}{\sigma_h\sqrt{2\pi}}\;e^{-(1-e^{-a})M^2k_M\,\overline{p}} \tag{3.47}
$$

and the second sum gives

$$
\begin{aligned}
N\frac{1}{N}\sum_{j=1}^{N}\overline{p}Y_j\frac{R_{ji}}{\sigma_h\sqrt{2\pi}}e^{-(1-e^{-a})M^2k_M}\,\overline{p}\big(1-\overline{p}\,M^2k_M(1-e^{-a})\big) = \\
N\overline{p}\;\overline{Y}\;\frac{\overline{R_i}}{\sigma_h\sqrt{2\pi}}\;e^{-(1-e^{-a})M^2k_M\,\overline{p}}\big(1-\overline{p}\,M^2k_M(1-e^{-a})\big)
\end{aligned}
\tag{3.48}
$$

respectively.

For the third summation, I use the property $\frac{1}{N}\sum(p_jY_j)R_{ji} = \overline{pY}\ \overline{R_i} + \mathrm{Cov}(p\ Y, R_i)$. For the purposes of this study, it can be assumed that $\mathrm{Cov}(p\ Y, R_i) \approx 0$. This is because habitat types are uniformly distributed and species fitness (Y_j) is independent of habitat association. p_jY_j is equal to the number of offspring species j disperses to each patch. Fitness (Y) is independent of habitat association and species proportion (p) is simply a function of the the relative fitness of species (i.e. species vary only in Y, so their proportion should only depend on Y). Because the number of patches of each habitat type is uniformly distributed, the number of offsrping that a species produces is therefore independent of habitat association (which implies $\mathrm{Cov}(p\ Y, R_i) = 0$). More formally, $p_j = F(Y_j)$ (i.e. p is a function of Y, as species vary only in Y, which ultimately determines their relative proportion in the population). Therefore, $pY = YF(Y) = G(Y)$ where G is a function. Then, $\mathrm{Cov}(p\ Y, R_i) = \mathrm{Cov}(G(Y), R_i) = 0$ so long R_i and Y are independent and Y is measurable (which is true on the basis fitness is randomly distributed, i.e., it is a random variable).

Additionally, using the same property, $\overline{pY} = \frac{1}{N}\sum p_jY_j = \overline{p}\ \overline{Y} + \mathrm{Cov}(p, Y)$ such that $\frac{1}{N}\sum(p_jY_j)R_{ji}$ $= \big(\overline{p}\ \overline{Y} + \mathrm{Cov}(p, Y)\big)\overline{R_i}$. With these simplifications, the summation can be evaluated as:

$$
\begin{aligned}
N\frac{1}{N}\sum_{j=1}^{N} Y_j \frac{R_{ji}}{\sigma_h\sqrt{2\pi}} p_j e^{-(1-e^{-a})M^2k_M\,\overline{p}}\big(1 - \overline{p}\,M^2k_M(1-e^{-a})\big) = \\
N\left[\overline{pY}\ \frac{\overline{R_i}}{\sigma_h\sqrt{2\pi}} + \frac{1}{\sigma_h\sqrt{2\pi}}\mathrm{Cov}(p\ Y, R)\right] e^{-(1-e^{-a})M^2k_M\,\overline{p}}\big(1 - \overline{p}\,M^2k_M(1-e^{-a})\big) \\
= N\left[\overline{p}\,\overline{Y} + \mathrm{Cov}(p, Y)\right]\left[\frac{\overline{R_i}}{\sigma_h\sqrt{2\pi}}\right] e^{-(1-e^{-a})M^2k_M\,\overline{p}}\big(1 - \overline{p}\,M^2k_M(1-e^{-a})\big) \\
= \left[N\ \overline{p}\frac{\overline{R_i}}{\sigma_h\sqrt{2\pi}}\ \overline{Y} + \frac{\overline{R_i}}{\sigma_h\sqrt{2\pi}}\ N\ \mathrm{Cov}(p, Y)\right] e^{-(1-e^{-a})M^2k_M\,\overline{p}}\big(1 - \overline{p}\,M^2k_M(1-e^{-a})\big)
\end{aligned}
\tag{3.49}
$$

Adding all three of the summations (adding the final terms of Equations 3.47, 3.48, and 3.49) yields expression

$$
\sum_{j=1}^{N} Y_j p_j e^{-(1-e^{-a})M^2k_M p_j} \approx \overline{Y}\big(1 + \mathrm{Cov}(p, Y)\phi\big) N\overline{p}\frac{\overline{R_i}}{\sigma_h\sqrt{2\pi}}\ e^{-(1-e^{-a})M^2k_M\,\overline{p}} \tag{3.50}
$$

where

$$\phi = \frac{1}{\overline{p}}\frac{1}{\overline{Y}}\left(1 - \overline{p}\, M^2 k_M (1 - e^{-a})\right) \tag{3.51}$$

In which case, the invasion criterion can be written as

$$Y_i > \overline{Y}\left(1 + \mathrm{Cov}(p, Y)\phi\right) N\overline{p}\frac{\overline{R_i}}{\sigma_h\sqrt{2\pi}}\, e^{-(1-e^{-a})M^2 k_M\, \overline{p}} \tag{3.52}$$

Simplification of $\overline{\boldsymbol{p}}$

Consider the term $\overline{p}$, which is present in Equation 3.52. If all patches in the community are occupied, then

$$\overline{p} = \frac{1}{N} \tag{3.53}$$

on the basis that the sum of the proportions of all patches in the community should add to 1 (therefore, $\overline{p} = \frac{1}{N}\sum_{j=1}^{N} p_j = \frac{1}{N}$). However, whether every patch in the community is filled depends on if the trait space of the resident community (all $h_{\mathrm{opt},j}$, $j = 1, 2, ..N$) comprise values that contain the entire habitat space (between 0 and 1). Under the approximation of Equation 3.29, some habitat types are completely unsuitable for species j. Therefore, if there are relatively few species in the community (low N), it is possible that there are portions of the habitat for which no species has a positive habitat association (at least, according the approximation). In this case, not all of the community is occupied and $\sum_{j=1}^{N} p_j < 1$. Conceptually, then:

$$\begin{aligned}\overline{p} &= \frac{1}{N} \times \Big(1 - \mathrm{P}\big(\text{a habitat type is unoccupied}\big)\Big) \\ &= \frac{1}{N}\mathrm{P}(\text{there is no unoccupied trait space between two species adjacent in trait space})\end{aligned} \tag{3.54}$$

To derive an expression for $\overline{p}$, I assume that traits ($h_{\mathrm{opt},j}$) of the N species in the resident community are randomly distributed in trait space (i.e. follow a uniform distribution). Trait vales ($h_{\mathrm{opt},j}$) are

between 0 and 1.

Let z represent a random point in trait space ($0 \leq z \leq 1$). In general, there will be species with optima greater than and less than z. Let x_1 be the closest value of a species' optimum to z for which $x_1 < z$. Similarly, let x_2 be the closest value of a species' optimum to z for which $x_2 > z$. x_1 and x_2 completely overlap z if $x_2 - x_1 \leq \sigma_h\sqrt{2\pi}$ (based on the approximation of Equation 3.29). The quantity of interest,P(there is no unoccupied trait space between two species adjacent in trait space), is then given by $\mathrm{P}\big(x_2 - x_1 \leq \sigma_h\sqrt{2\pi}\big)$. This is because each species' range of suitability extends $x_j \pm \frac{1}{2}\sigma_h\sqrt{2\pi}$, so there is complete overlap so long as $x_2 - x_1 \leq \sigma_h\sqrt{2\pi}$. This can be readily described using Order Statistics. Notably, the probability density function between adjacent order statistics given N events (x_2 and x_1 in this case) is given by

$$x_2 - x_1 \sim \mathrm{Beta}\big(1, N\big). \tag{3.55}$$

The desired quantity is $\mathrm{P}\big(x_2 - x_2 \leq \sigma_h\sqrt{2\pi}\big)$. This, by definition, can be evaluated using the CDF of the above probability distribution function. This can be evaluated analytically. Let $B(s, r)$ represent the Beta function. Then:

$$\begin{aligned}
\mathrm{P}\big(x_2 - x_2 \leq \sigma_h\sqrt{2\pi}\big) &= \frac{\int_0^{\sigma_h\sqrt{2\pi}} \big(1-t\big)^{N-1}\, dt}{B(1, N)} \\
&= \frac{\int_0^{\sigma_h\sqrt{2\pi}} \big(1-t\big)^{N-1}\, dt}{\int_0^{1} \big(1-t\big)^{N-1}\, dt} \\
&= 1 - \big(1 - \sigma_h\sqrt{2\pi}\big)^N
\end{aligned} \tag{3.56}$$

Noting that $\sigma_h\sqrt{2\pi}$ is relatively small (less than 1), one can make the approximation $1 - \big(1 - \sigma_h\sqrt{2\pi}\big)^N \approx 1 - e^{-N\sigma_h\sqrt{2\pi}}$ (which is a highly accurate for the values of σ_h considered). Then, overall, this yields

$$\mathrm{P}\big(x_2 - x_1 \leq \sigma_h\sqrt{2\pi}\big) \approx 1 - e^{-N\sigma_h\sqrt{2\pi}} \tag{3.57}$$

therefore,

$$\overline{p} = \frac{1}{N}\left(1 - e^{-N\sigma_h\sqrt{2\pi}}\right) \tag{3.58}$$

and

$$\begin{aligned} N\overline{p} &= N\left(\frac{1}{N} \times \left(1 - e^{-N\sigma_h\sqrt{2\pi}}\right)\right) \\ &= 1 - e^{-N\sigma_h\sqrt{2\pi}} \end{aligned} \tag{3.59}$$

Noting that this ignores edge cases in which a species' optima overlaps with trait space outside of the community (i.e. the above assumes that $\sigma_h\sqrt{2\pi} \leq z \leq 1 - \sigma_h\sqrt{2\pi}$).

This is an approximation – in principle (for the numerical simulations) Equation 3.22 assumes that all species have non-zero fitness on all patches such that all patches would be occupied. However, it is necessary to make this adjustment – because it is assumed that the rare species cannot colonize unfavorable patches (as defined by Equation 3.29) it must be also assumed that resident species cannot occupy unfavorable patches (at least, for the purpose of deriving the invasion criterion).

Evaluation of $\overline{\boldsymbol{R_i}}$ and simplification of approximate invasion criterion

The invasion criterion (Equation 3.52) defines the condition that allows the invasion of a rare species with a particular habitat association ($h_{\text{opt},i}$). While this is a potentially useful quantity, a more useful metric would be to quantify how easy, on average, it is for a species to invade the community with an arbitrary habitat association. To derive such a quantity, I take the expectation of Equation 3.52 with respect to different habitat preferences (i.e., all different values of $h_{\text{opt},i}$, from 0 to 1).

That is, I take the following expectation:

$$\mathbb{E}\left[Y_i\right] > \mathbb{E}\left[\overline{Y}\left(1 + \text{Cov}(p, Y)\phi\right)N\overline{p}\frac{\overline{R_i}}{\sigma_h\sqrt{2\pi}}\, e^{-(1-e^{-a})M^2 k_M \overline{p}}\right] \tag{3.60}$$

which can be rewritten as

$$\mathbb{E}\left[Y_i\right] > \mathbb{E}\left[\overline{Y}\ N\overline{p}\,\frac{\overline{R_i}}{\sigma_h\sqrt{2\pi}}\ e^{-(1-e^{-a})M^2k_M\,\overline{p}}\right] + \mathbb{E}\left[\frac{\overline{R_i}}{\sigma_h\sqrt{2\pi}}\mathrm{Cov}(p,Y)\phi' e^{-(1-e^{-a})M^2k_M\,\overline{p}}\right] \tag{3.61}$$

where

$$\phi' = \left(1 - \frac{M^2k_M}{N}(1-e^{-a})\right) \tag{3.62}$$

By independence, the above can be simplified to

$$\mathbb{E}\left[Y_i\right] > \left(\mathbb{E}\left[\overline{Y}\right]\ \mathbb{E}\left[\frac{\overline{R_i}}{\sigma_h\sqrt{2\pi}}\right]\mathbb{E}\left[N\overline{p}\right] + \mathbb{E}\left[\frac{\overline{R_i}}{\sigma_h\sqrt{2\pi}}\right]\mathbb{E}\left[\mathrm{Cov}(p,Y)\phi'\right]\right)\ \mathbb{E}\left[e^{-(1-e^{-a})M^2k_M\,\overline{p}}\right] \tag{3.63}$$

which is equal to

$$Y_i > \left(\overline{Y}\ \mathbb{E}\left[\frac{\overline{R_i}}{\sigma_h\sqrt{2\pi}}\right]N\overline{p} + \mathbb{E}\left[\frac{\overline{R_i}}{\sigma_h\sqrt{2\pi}}\right]\mathrm{Cov}(p,Y)\phi\right)\ e^{-(1-e^{-a})M^2k_M\,\overline{p}} \tag{3.64}$$

The above separation of terms can be done because (1) intrinsic fitness is independent of habitat association and (2) JCE strength is independent of habitat association. Overall, then, the quantity $\mathbb{E}\left[\overline{R_i}/\sigma_h\sqrt{2\pi}\right]$ must be evaluated.

Consider the term $\overline{R_i}/\sigma_h\sqrt{2\pi}$. Recall that $\overline{R_i}$ represents the average proportion of the environment favorable to species i that competitors also experience as favorable (the mean proportion for which $H_j(x) = H_i(x) = 1$). Thus, $(1/\sigma_h\sqrt{2\pi})\,\mathbb{E}\left[\overline{R_i}\right]$ is the mean proportion of the environment favorable to species i that competitors also experience as favorable. Again assuming species are randomly distributed in trait space (i.e. can be described by a Poisson process) I calculate the expected overlap between species i with the N resident species. Let $O_{j,i}$ be the overlap in habitat preference between species i with species j. Then, letting $d_j = |h_{\mathrm{opt},j} - h_{\mathrm{opt},i}|$,

$$O_{j,i} = \begin{cases} 1 - \frac{d_j}{\sigma_h\sqrt{2\pi}} & \text{if } d_j < \sigma_h\sqrt{2\pi} \\ 0 & \text{Otherwise} \end{cases} \tag{3.65}$$

noting the above is derived from Equation 3.29. Then, $\mathbb{E}\left[\frac{\overline{R_i}}{\sigma_h\sqrt{2\pi}}\right]$ is given by:

$$\begin{aligned}
\frac{1}{\sigma_h\sqrt{2\pi}}\mathbb{E}\left[\overline{R_i}\right] &= \frac{1}{\sigma_h\sqrt{2\pi}}\frac{1}{N}\mathbb{E}\left[\sum_{\text{all } j} O_{j,i}\right] \\
&= \frac{2}{\sigma_h\sqrt{2\pi}}\frac{1}{N}\mathbb{E}\left[\sum_{j\in\sigma_h\sqrt{2\pi}} 1 - \frac{d_j}{\sigma_h\sqrt{2\pi}}\right] \qquad \text{by symmetry} \\
&= \frac{2}{\sigma_h\sqrt{2\pi}}\frac{1}{N}\left(\mathbb{E}\left[\sum_{j\in\sigma_h\sqrt{2\pi}} 1\right] - \mathbb{E}\left[\sum_{j\in\sigma_h\sqrt{2\pi}} \frac{d_j}{\sigma_h\sqrt{2\pi}}\right]\right) \\
&= \frac{2}{\sigma_h\sqrt{2\pi}}\frac{1}{N}\left(N\sigma_h\sqrt{2\pi} - \frac{1}{\sigma_h\sqrt{2\pi}}\mathbb{E}\left[\sum_{j\in\sigma_h\sqrt{2\pi}} d_j\right]\right)
\end{aligned} \tag{3.66}$$

noting that the expression is multiplied by 2 because the sum must consider species that have optima greater than or less than species i's optima (i.e. the resident species' optima are distributed symmetrically around $h_{\text{opt},i}$).

d_j is simply the waiting time of the j_{th} event within the span of $t = \sigma_h\sqrt{2\pi}$ of a Poisson process. Therefore, $\mathbb{E}\left[\sum_{j\in\sigma_h\sqrt{2\pi}} d_j\right]$ is equal to the expected sum of Poisson waiting times (a well-known problem). Let $X(t)$ represent the Poisson process at rate $\lambda = N$ occurring over the "time period" $t = \sigma_h\sqrt{2\pi}$. Additionally, let Z represent the sum of waiting times over t (that is, $Z = \sum_{j\in\sigma_h\sqrt{2\pi}} d_j$). This gives

$$\begin{aligned}
\mathbb{E}\left[\sum_{j\in\sigma_h\sqrt{2\pi}} d_j\right] &= \mathbb{E}\left[Z\right] \\
&= \mathbb{E}\left[\mathbb{E}\left[Z|X(t)=n\right]\right] \\
&= \mathbb{E}\left[\frac{1}{2}tX(t)\right] \qquad \text{because } n \text{ Poisson events occurring within } t \\
&\qquad\qquad\qquad\qquad \text{are uniformly distributed} \\
&= \frac{1}{2}\lambda t^2 \\
&= \frac{1}{2}N\left(\sigma_h\sqrt{2\pi}\right)^2
\end{aligned} \tag{3.67}$$

in which case,

$$\begin{aligned}\frac{1}{\sigma_h\sqrt{2\pi}}\mathbb{E}\left[\overline{R_i}\right] &= \frac{2}{\sigma_h\sqrt{2\pi}}\frac{1}{N}\left(N\sigma_h\sqrt{2\pi} - \frac{1}{\sigma_h\sqrt{2\pi}}\frac{1}{2}N\left(\sigma_h\sqrt{2\pi}\right)^2\right) \\ &= 1\end{aligned} \tag{3.68}$$

Then, putting things together, let

$$\begin{aligned}R(\sigma_h, N) &= N\overline{p}\frac{1}{\sigma_h\sqrt{2\pi}}\mathbb{E}\left[\overline{R_i}\right] \\ &= 1 - e^{-N\sigma_h\sqrt{2\pi}}\end{aligned} \tag{3.69}$$

as shown in the main text. This also implies that

$$\overline{p} = \frac{1}{N}R(\sigma_h, N) \tag{3.70}$$

$R(\sigma_h, N)$ is therefore a simple metric of the extent of habitat overlap. In words, $R(\sigma_h, N)$ is the probability a random habitat type in the environment falls within the range of habitat suitability of at least one of the resident species. More nuanced metrics are possible, but this is sufficient for the purposes of the present study. Note that the above derivations make the implicit approximation of ignoring "edge cases" for which the invader's or resident species' habitat range overlaps with values not in the environment (i.e., it is assumed that $\sigma_h\sqrt{2\pi} \leq h_{\text{opt},i} \leq 1 - \sigma_h\sqrt{2\pi}$). Accounting for these cases would likely result in small quantitative differences in the above expressions, but no qualitative changes.

Plugging Equations 3.69 and 3.70 into Equation 3.52 yields the invasion criterion:

$$Y_i \gtrsim \underbrace{\overline{Y}}_{\substack{\text{mean}\\ \text{intrinsic}\\ \text{fitness}}} \underbrace{\left(1 + \text{cov}(Y, p)\phi\right)}_{\substack{\text{relative}\\ \text{competition}\\ \text{term}}} \underbrace{R(\sigma_h, N)}_{\substack{\text{HP}\\ \text{term}}} \underbrace{e^{-(1-e^{-a})\frac{M^2}{N}R(\sigma_h,N)k_M}}_{\substack{\text{JCE}-\text{HP}\\ \text{term}}} \tag{3.71}$$

for which

$$\phi = \frac{N}{R(\sigma_h, N)\overline{Y}}\left(1 - R(\sigma_h, N)\frac{M^2}{N}k_M(1 - e^{-a})\right) \tag{3.72}$$

noting that Equation 3.71 is identical to invasion criterion presented in the main text.

Interpretation of invasion criterion

Here, I provide several notes on the interpretation of Equations 3.71 and 3.72 that are not provided in the main text. Generally, invasion becomes easier as the HP and JCE−HP terms decrease. The HP term defines how HP in isolation make invasion easier (reduces the mean fitness encountered by an invader) and the JCE−HP term quantifies how the interaction of JCEs and HP affect species invasion.

$R(\sigma_h, N)$ appears twice in the invasion criterion – once in the "HP term" and once in the "JCE−HP term". The HP term declines as $R(\sigma_h, N)$ decreases while the JCE-HP term increases as $R(\sigma_h, N)$ decreases. This implies a tension between HP and JCE mechanisms. This can be understood as follows. JCEs make invasion easier insomuch as they reduce the survival of the resident species' offspring that share habitat associations with the invader. $R(\sigma_h, N)$ quantifies the proportion of the environment in which the invader faces competitors. Therefore, the stabilizing effect of JCEs decreases for small $R(\sigma_h, N)$ because there are fewer species that may induce JCEs on patches favorable to species i (the invader). This becomes unimportant for large N (when there are a large number of species in the community).

The "relative competition term" (Equation 3.72) quantifies how the relative abundance of the resident species affects species invasion. The relative competition term depends on $\text{Cov}(Y, p)$. If $\text{Cov}(Y, p)$ is positive, invasion becomes more difficult. This will always be true ($\text{Cov}(Y, p) > 0$) in the case examined in this model, as species vary only in Y (and species with higher Y are more fit). $\text{Cov}(Y, p)$ quantifies the degree to which species with relatively high fitness are also relatively abundant – if highly fit species are also relatively abundant, then the invader experiences stronger competition relative to when species abundance is unrelated to fitness (i.e. when $\text{Cov}(Y, p) = 0$ and the relative competition term = 1). ϕ is a constant that, in effect, quantifies how the JCEs (as mediated by the JCE−HP term) reduce the fitness of relatively abundant species.

Upper bound to $\boldsymbol{R(\sigma_h, N)}$

If it assumed that species' trait optima are *regularly* distributed (meaning species' optima are equidistant in trait space) then

$$R(\sigma_h, N) \approx \begin{cases} N\sigma_h\sqrt{2\pi} & N \leq \frac{1}{\sigma_h\sqrt{2\pi}} \\ 1 & N > \frac{1}{\sigma_h\sqrt{2\pi}} \end{cases} \tag{3.73}$$

which represents an upper bound to $R(\sigma_h, N)$. An interesting implication of Equation 3.73 is that it implies that the stabilizing effect of HP alone disappears if $N \geq \frac{1}{\sigma_h\sqrt{2\pi}}$, which suggests that no more than $\frac{1}{\sigma_h\sqrt{2\pi}}$ species should coexist when HP operates alone. This is therefore a lower bound to species richness. Fig. 3.2 from the main text suggests this lower bound is a good approximation (at least under high fitness variation, the situation examined in this paper).

Invasion criteria when only JCEs operate

In the main text, it is noted that in highly diverse communities (large N) for which $R(\sigma_h, N) \approx 1$ (i.e. habitat niche space is saturated) in which there is zero autocorrelation ($k_M = 1$) the invasion criterion for the JCE and HP case (Equation 3.71) converges exactly to the invasion criterion for which JCEs operate in isolation. Here, I provide a short proof of this claim.

Notably, Smith (2022a) shows that the invasion criterion of a rare species in a model almost identical to that of this study without HP is approximately equal to

$$Y_i > \underbrace{\overline{Y}e^{-\left(1-e^{-a}\right)\frac{M^2}{N}}}_{\substack{\text{mean} \\ \text{JCE-fitness term}}} + \underbrace{N\text{Cov}(p, Y)\left(1 - \left(1 - e^{-a}\right)\frac{M^2}{N}\right)e^{-\left(1-e^{-a}\right)\frac{M^2}{N}}}_{\text{covariance-JCE term}} \tag{3.74}$$

with modifications to the notation in Smith (2022a) made for consistency. Setting $R(\sigma_h, N) = 1$ and $k_M = 1$ in Equations 3.71 and 3.72, substituting the latter into the former, and doing some rearranging yields an expression identical to Equation 3.74. Hence, the invasion criteria for the JCE-HP case and the JCE-only cases are identical when N is large and habitats are randomly

distributed in space at the patch level.

JCE-HP interactions under spatial-temporal variation

In the main text, it is noted that if habitat types change over time considerably faster than tree generation time (i.e. fast relative to recruitment events), the synergistic interaction between JCEs and HP is reduced. Here, I provide a simple analytical argument demonstrating this result.

In the above section "Evaluation of $\mathbb{E}[J_j(x)]$ and derivation of k_M", I argue that the probability y individuals of species j neighbor a random favorable patch is equal to

$$\mathrm{P}(y \text{ of the } M^2 \text{ neighbors are species } j) \sim \mathrm{Bin}\big(M^2,\ p_j k_M\big) \tag{3.75}$$

where k_M defines the extent to which patches are positively autocorrelated such that $1 \leq k_M \leq \frac{1}{\sigma_h \sqrt{2\pi}}$. This conceptualization of k_M, however, relies on the assumption that habitat types do not change over time. If this assumption is relaxed, then k_M must be modified to account for the fact that a species initially near favorable patches may no longer neighbor them when recruitment occurs.

Consider patches of type x such that x is favorable to species j. Let $\mathrm{P}(\Delta x)$ represent the probability a patch *remains* favorable to species j between recruitment events. Conversely, a patch changes from favorable to unfavorable for species j between recruitment events with probability $1 - \mathrm{P}(\Delta x)$. For simplicity, I assume that the level of spatial autocorrelation is unaffected by spatial-temporal variation in habitat types (although a generative model would need to be specified to implement this into simulations). Then, for a random patch x favorable to species j, the probability a given neighbor within M^2 is of species j is equal to

$$\mathrm{P}(\Delta x) k_M + \big(1 - \mathrm{P}(\Delta x)\big) \tag{3.76}$$

It then follows that

$$\mathrm{P}(y \text{ of the } M^2 \text{ neighbors are species } j) \sim \mathrm{Bin}\Big(M^2,\ p_j\big[\mathrm{P}(\Delta x)k_M + \big(1-\mathrm{P}(\Delta x)\big)\big]\Big) \tag{3.77}$$

from which the invasion criterion can be calculated in exactly the same way as the previous sections. Therefore, the invasion criterion for a community with spatial-temporal variation is:

$$Y_i \gtrsim \underbrace{\overline{Y}}_{\substack{\text{mean}\\ \text{intrinsic}\\ \text{fitness}}} \underbrace{\Big(1+\mathrm{cov}(Y,p)\phi\Big)}_{\substack{\text{relative}\\ \text{competition}\\ \text{term}}} \underbrace{R(\sigma_h,N)}_{\substack{\text{HP}\\ \text{term}}} \underbrace{e^{-(1-e^{-a})\frac{M^2}{N}R(\sigma_h,N)\left(\mathrm{P}(\Delta x)k_M+\left(1-\mathrm{P}(\Delta x)\right)\right)}}_{\substack{\text{JCE}-\text{HP}\\ \text{term}}} \tag{3.78}$$

for which

$$\phi = \frac{N}{R(\sigma_h,N)\overline{Y}}\Big(1-R(\sigma_h,N)\frac{M^2}{N}(1-e^{-a})\big(\mathrm{P}(\Delta x)k_M+\big(1-\mathrm{P}(\Delta x)\big)\Big) \tag{3.79}$$

I now highlight two limiting cases. If $\mathrm{P}(\Delta x) = 1$ (patch types are very unlikely to change between generations), then Equation 3.77) collapses to Equation 3.75 and, by extension, Equation 3.78 collapses to Equation 3.71. This is the case examined in the main text and the previous sections. Conversely, if $\mathrm{P}(\Delta x) = 0$ (patch types always change between generations), then $\mathrm{P}(\Delta x)k_M + \big(1 - \mathrm{P}(\Delta x)\big) \to 1$. In this case, Equations 3.77 and 3.78 converge to the cause of zero autocorrleation ($k_M = 1$). In this case, there is no synergistic interaction between JCEs and HP.

More broadly, one should consider when $0 < \mathrm{P}(\Delta x) < 1$. The closer $\mathrm{P}(\Delta x)$ is to 1, the stronger the synergistic interaction between JCEs and HP. Realistically, patches likely do not change entirely randomly between types. Rather, the probability a patch of type x_1 changes to type x_2 between recruitment events is likely a decreasing function of $|x_1 - x_2|$. Future models should explicitly explore how specific regimes of spatial-temporal fluctuations impact the interaction between JCEs and HP.

Approximate invasion criterion validation and calculation of k_M

Previously, I derived the approximate invasion criterion from the main text. In this section, I derive an expression that yields an "exact invasion criterion". I then use simulations outputs to parameterize the approximate and exact invasion criteria. I demonstrate that the exact and approximate invasion criteria yield quantitatively similar outputs (Figs. 3.7 and 3.8) validating the usefulness of Equation 3.71 in interpreting the simulation outputs. Additionally, I show how k_M is calculated (which is necessary for quantifying the approximate invasion criterion). This calculation of k_M is also shown in the main text.

Comparison between approximate and exact invasion criteria

Numerically, species i will have a positive invader growth rate if

$$\delta\left[\frac{1}{X^2}\sum_{\text{all } x}\frac{S_i(x)}{\sum_{k=1}^{N}S_k(x)} - p_i\right] > 0 \tag{3.80}$$

where X^2 is all the patches in the community. Therefore, $1/X^2$ is the proportion each patch takes up in the community. Substituting $S_i(x) = Y_i H_i(x) p_i$, dividing each side by p_i (such that *per capita* growth rate is examined) and doing some re-arranging yields:

$$Y_i > \frac{X^2}{\sum_{\text{all } x}\frac{H_i(x)}{\sum_{k=1}^{N}S_k(x)}} \tag{3.81}$$

noting that

$$H_i(x) = \exp(-(x - h_{\text{opt},i})^2/2\sigma_h^2) \tag{3.82}$$

Now consider Equation 3.71, the approximate invasion criterion. Equation 3.71 was derived by taking the expectation of the invasion criterion with respect to different optima (different values of

$h_{\text{opt},i}$). The equivalent expression for Equation 3.81 is

$$Y_i > \int_0^1 \frac{X^2}{\sum_{\text{all } x} \frac{\exp(-(x-h)^2/2\sigma_h^2)}{\sum_{j=1}^{N} S_j(x)}}\, dh \tag{3.83}$$

where h is the habitat preference of the invader (with notation reduced for simplicity). However, this can be computationally intense to calculate. Therefore, numerically, I examine

$$Y_i > \frac{1}{S}\sum_{h=1}^{S} \frac{X^2}{\sum_{\text{all } x} \frac{\exp(-(x-h/S)^2/2\sigma_h^2)}{\sum_{j=1}^{N} S_j(x)}} \tag{3.84}$$

for which S is a constant, Note that Equation 3.84 converges to Equation 3.83 as $S \to \infty$ by the definition of a Riemann sum – thus, using a sufficiently large finite value of S allows for a close numerical approximation of Equation 3.83.

Importantly, the left hand side of Equation 3.71 is identical to that of Equation 3.84. Therefore, the quality of the approximation can be estimated by comparing the right hand sides of Equation 3.84 and Equation 3.71. I refer to the right hand side of Equations 3.84 and 3.71 as the "exact invasion metric" and the "approximate invasion metric", respectively.

I numerically compared the exact and approximate invasion metrics. For each of the simulations depicted in Fig. 3.3 of the main text, I numerically calculated Equations 3.84 and 3.71 using the $X \times X$ community produced by the simulation (i.e. the community after the final time-step). Equation 3.84 was computed directly under the condition that $S = 25$. For Equation 3.71, I calculated k_M for each parameter combination (each combination of σ_h and M) using the method explained below (and in the main text). Equation 3.71 was then evaluated using the values of p, Y, σ_h, N, k_M, and $R(\sigma_h, N)$ from the persisting community for each case in Fig. **??**. Comparisons indicate that Equation 3.71 yields a highly accurate approximation in most cases (Figs. 3.7 and 3.8). Therefore, Equation 3.71 serves as an appropriate tool to explain the theoretical results. Both values of $R(\sigma_h, N)$ (that is, Equations 3.69 and 3.73) yielded highly accurate approximations.

Calculation of k_M

Equation 3.71 requires the calculation of k_M, the metric of the autocorrelation of the environment at the $M \times M$ Moore neighborhood scale. As explained in the Methods and Materials of the main text,

$$k_M = \frac{1}{\sigma_h \sqrt{2\pi} M^2} \sum_{x=1}^{X^2} \sum_{j \in M^2} \frac{\mathbf{1}\big[j < f(x)\big]}{X^2} \tag{3.85}$$

where x indicates a single patch in the community and X^2 is the number of patches in the community. $\mathbf{1}\big[j < f(x)\big]$ is an indicator function that describes the number of patches of similar type to x within the $M \times M$ Moore neighborhood about x:

$$\mathbf{1}\big[j < f(x)\big] = \begin{cases} 1, & x - \frac{1}{2}\sigma_h\sqrt{2\pi} \leq j \leq x + \frac{1}{2}\sigma_h\sqrt{2\pi} \\ 0, & \text{otherwise} \end{cases} \tag{3.86}$$

where j represents the habitat type of one of the patches within the $M \times M$ around x ($j \in M^2$). k_M is therefore highly similar to Ripley's K Ripley (1976).

Note that Equation 3.85 is divided by $\frac{1}{\sigma_h \sqrt{2\pi} M^2}$. With this, if $k_m = 1$, it implies that

$$\sum_{x=1}^{X^2} \sum_{j \in M^2} \frac{\mathbf{1}\big[j < f(x)\big]}{X^2} = \sigma_h \sqrt{2\pi} M^2 \tag{3.87}$$

which means, on average, a proportion of $\sigma_h\sqrt{2\pi}$ of similar habitat types fall within M^2. This is identical to when patches are randomly distributed in the environment. Conversely, if $k_m = \frac{1}{\sigma_h\sqrt{2\pi}}$, it follows that

$$\sum_{x=1}^{X^2} \sum_{j \in M^2} \frac{\mathbf{1}\big[j < f(h)\big]}{X^2} = M^2 \tag{3.88}$$

which means all patches within M^2 are always of similar habitat types (high spatial autocorrelation). This is an upper bound to k_M. Therefore,

$$1 \leq k_M \leq \frac{1}{\sigma_h\sqrt{2\pi}} \tag{3.89}$$

as noted above and in the main text.

Additional simulation details

All simulations use the following parameters: $X = 500$ (a 500×500 patch community), $a = 0.5$, and intrinsic fitness (Y) was log-normally distributed such that $Y \sim \text{lognormal}[\mu = 0, \sigma_Y = 1.0]$. Each simulation was run for 125 generations (equivalent to over 3×10^7 tree replacements). Each simulation is characterized by an initial period of extinction, after which species richness approximately converges to a constant value. Figs. 3.9-3.12 show time series plots from each simulation, depicting species richness as a function of time. While future extinctions due to drift may continue to occur, the majority of remaining species in each case likely persist deterministically. This conclusion is strongly supported by Figs. 3.13-3.16, which show exp(Shannon diversity) – "effective species richness" – which clearly saturate to a constant value.

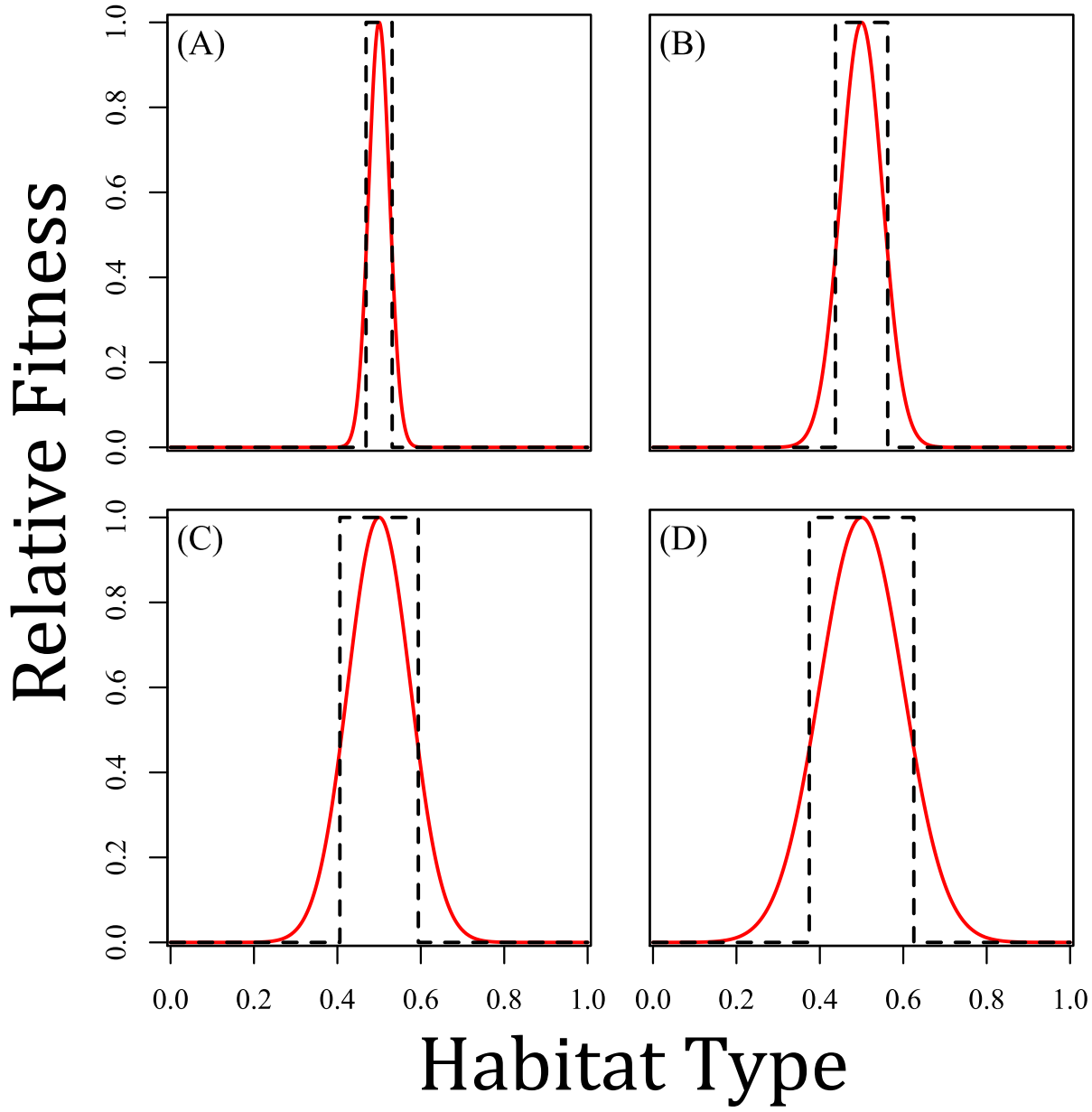

Figure 3.6: Examples of how the Guassian function that quantifies the fitness response to habitat type (Equation 3.22) is approximated for the purpose of deriving the approximate invasion criterion with Equation 3.29. (A) shows $\sigma_h = 0.025$, (B) shows $\sigma_h = 0.05$, (C) shows $\sigma_h = 0.075$, and (D) shows $\sigma_h = 0.10$. $h_{\text{opt},i} = 0.5$ in all cases.

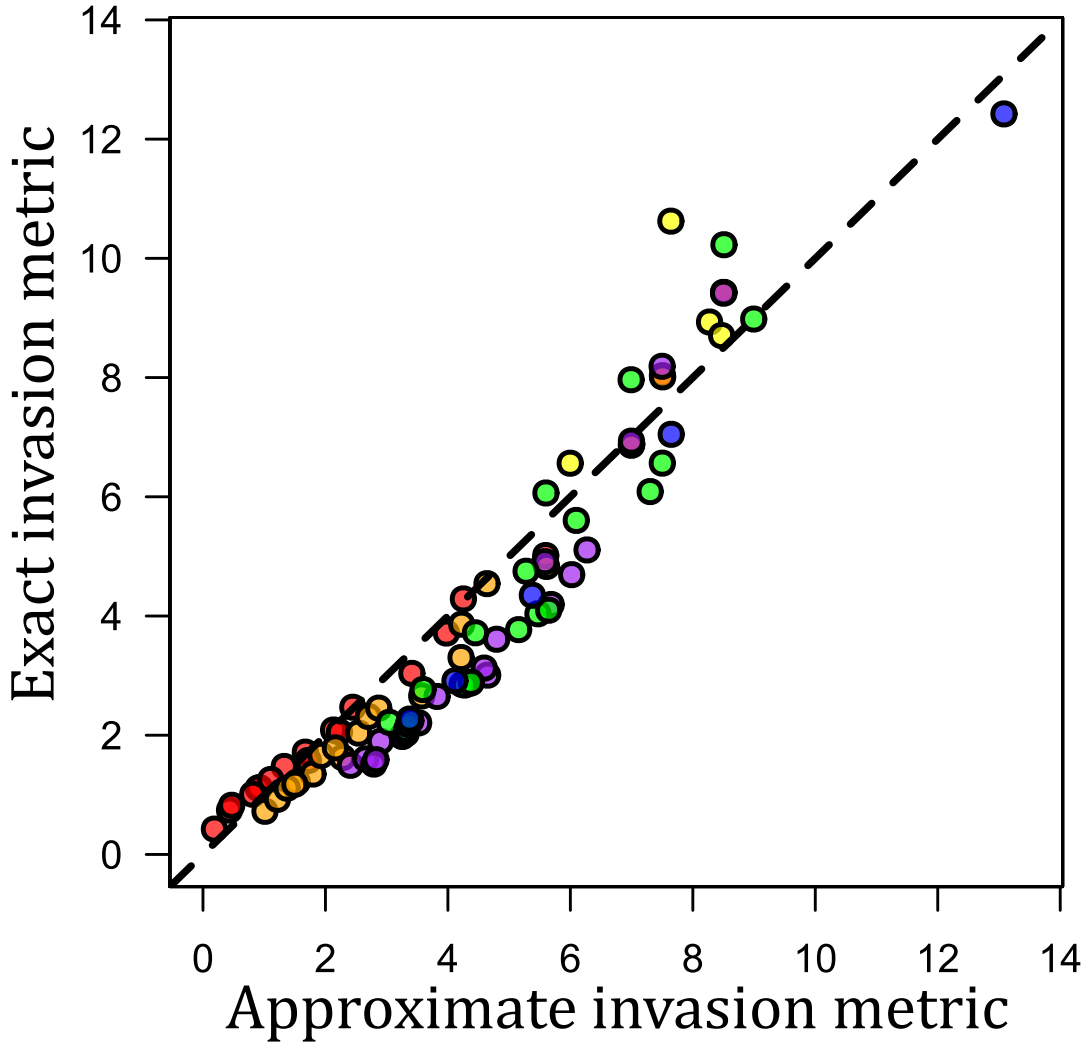

Figure 3.7: Comparisons between the approximate invasion criterion (Equation 3.71) and the "exact" invasion criterion (Equation 3.84). The x-axis shows the right-hand-side of Equation 3.71 and the y-axis show the right-hand-side of Equation 3.84. The black dashed is the one-to-one line (which depicts when the approximation and exact yield the same exact quantity). Different colored points depict different cases. Blue depicts JCEs alone, yellow depicts HP alone, red depicts JCEs and HP with high autocorrelation, orange depicts JCEs and HP with medium autocorrelation, purple depicts JCEs and HP with low autocorrelation, and green depicts JCEs and HP with zero autocorrelation. These cases depict all the values depicted in Fig. **??** of the main text. Generally, the approximate invasion criterion accurately captures the exact quantity. Points tend to fall below the dotted line, which indicates the approximation is somewhat conservative – points below the line are when the approximate invasion metric is greater than the exact invasion metric; the larger the invasion metric, the larger Y_i must be for species i to invade (and, thus, the more "difficult" invasion is).

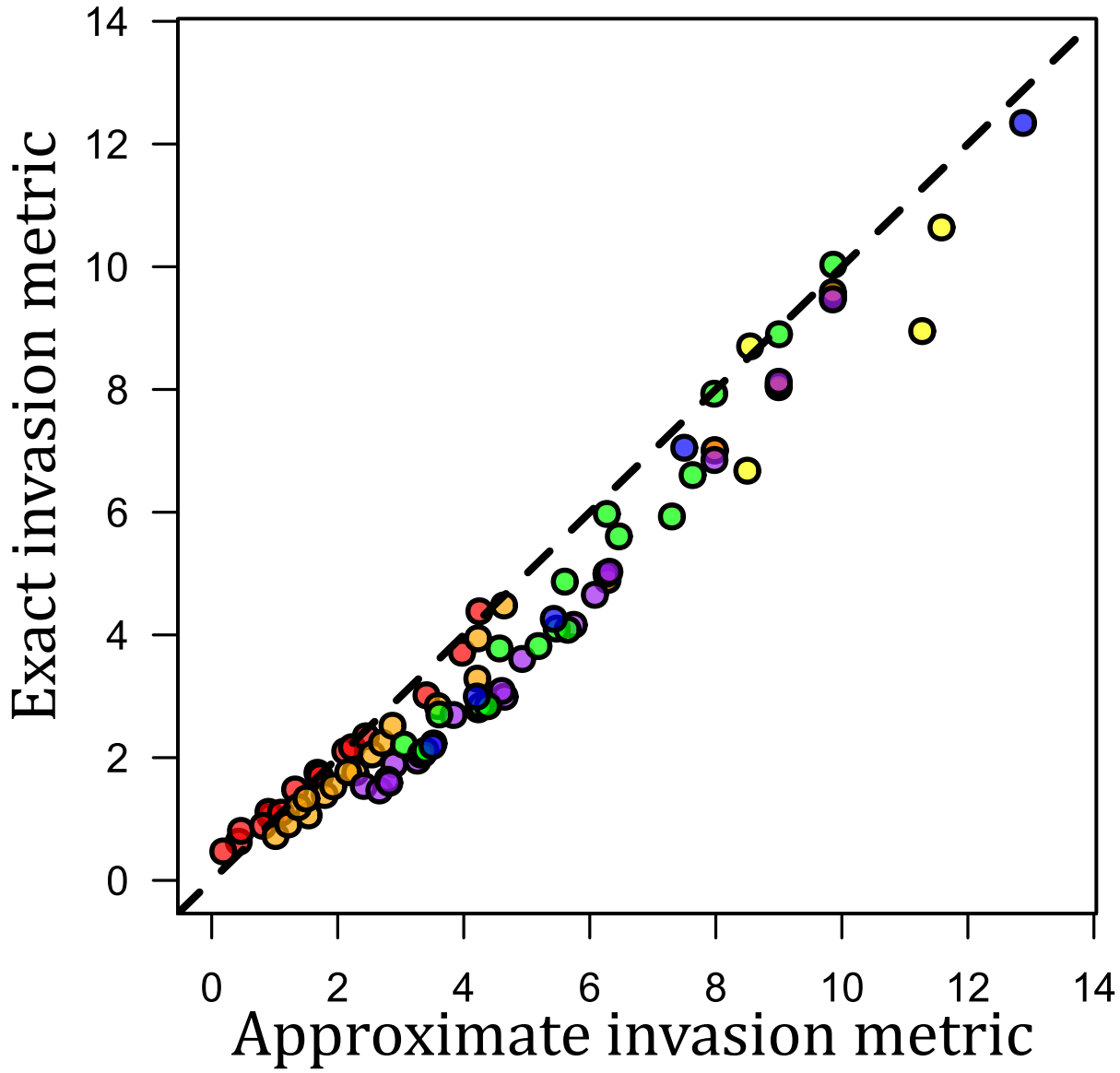

Figure 3.8: The same as the previous figure, but using the upper bound of $R(\sigma_h, N)$ (Equation 3.73).

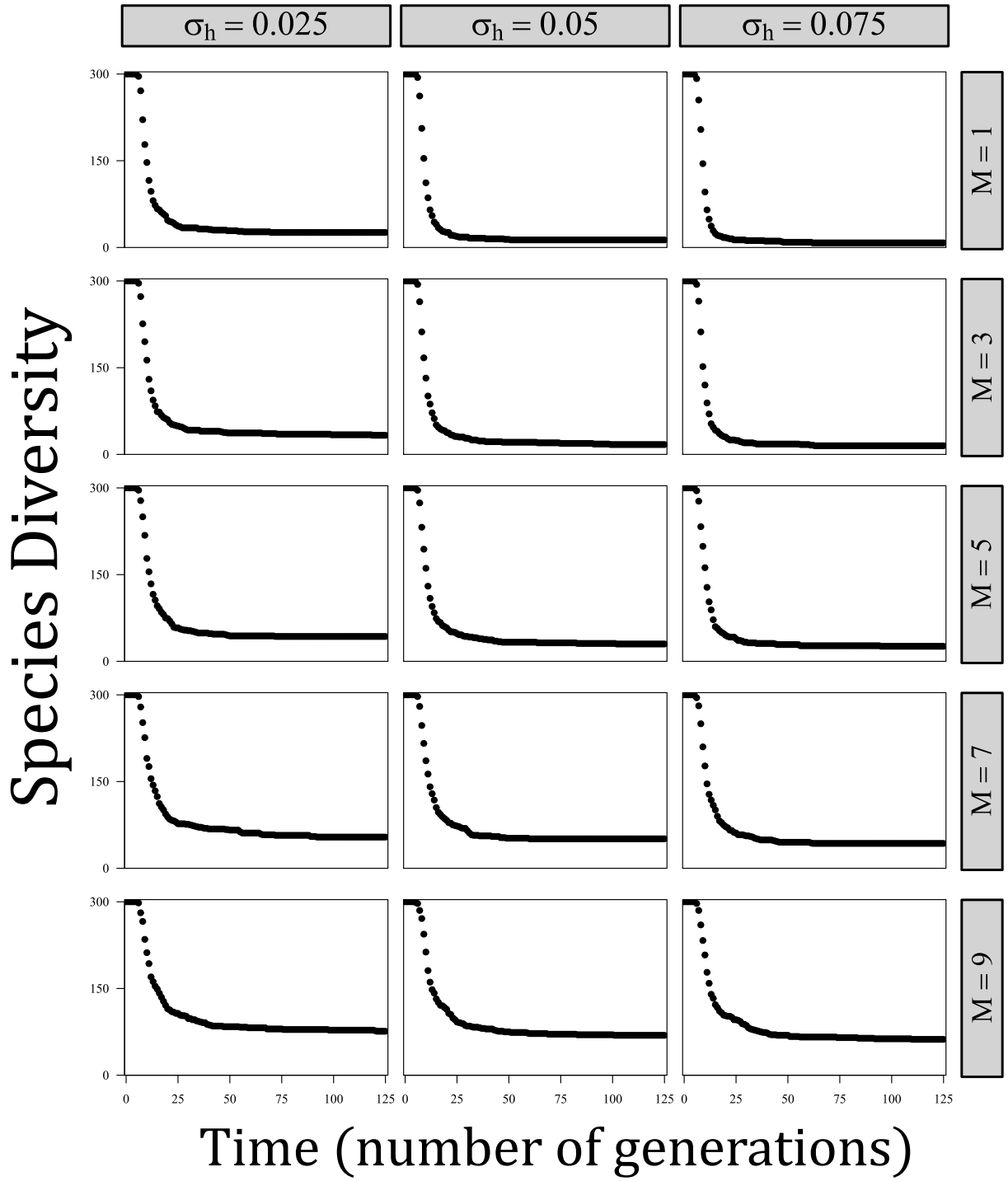

Figure 3.9: Species diversity (the number of species in the community) as a function of time (in generations). Parameters are as follows: $a = 0.5$. This plot shows when habitat types are randomly distributed (zero spatial autocorrelation).

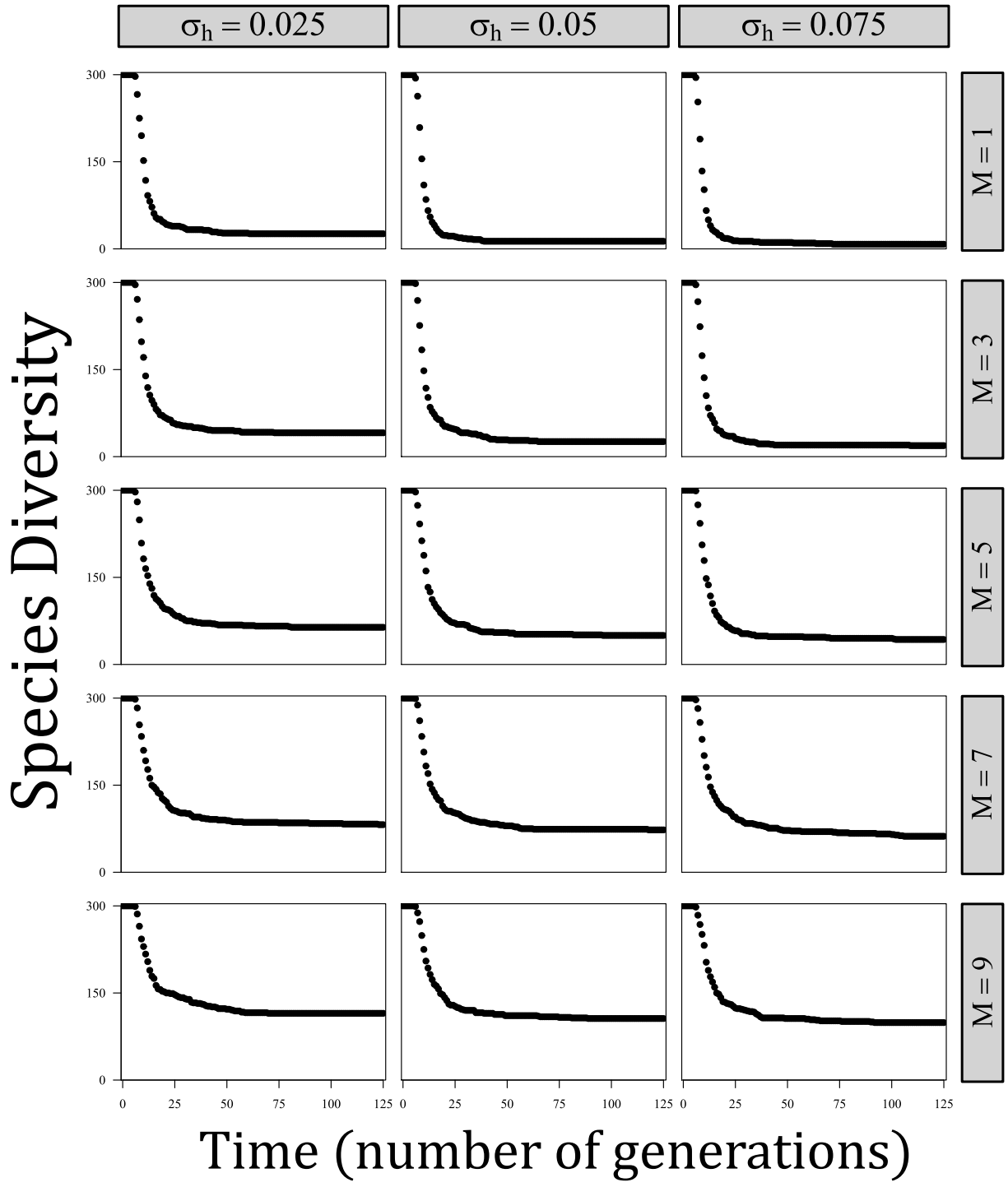

Figure 3.10: The same as the previous figure, but with low spatial autocorrelation.

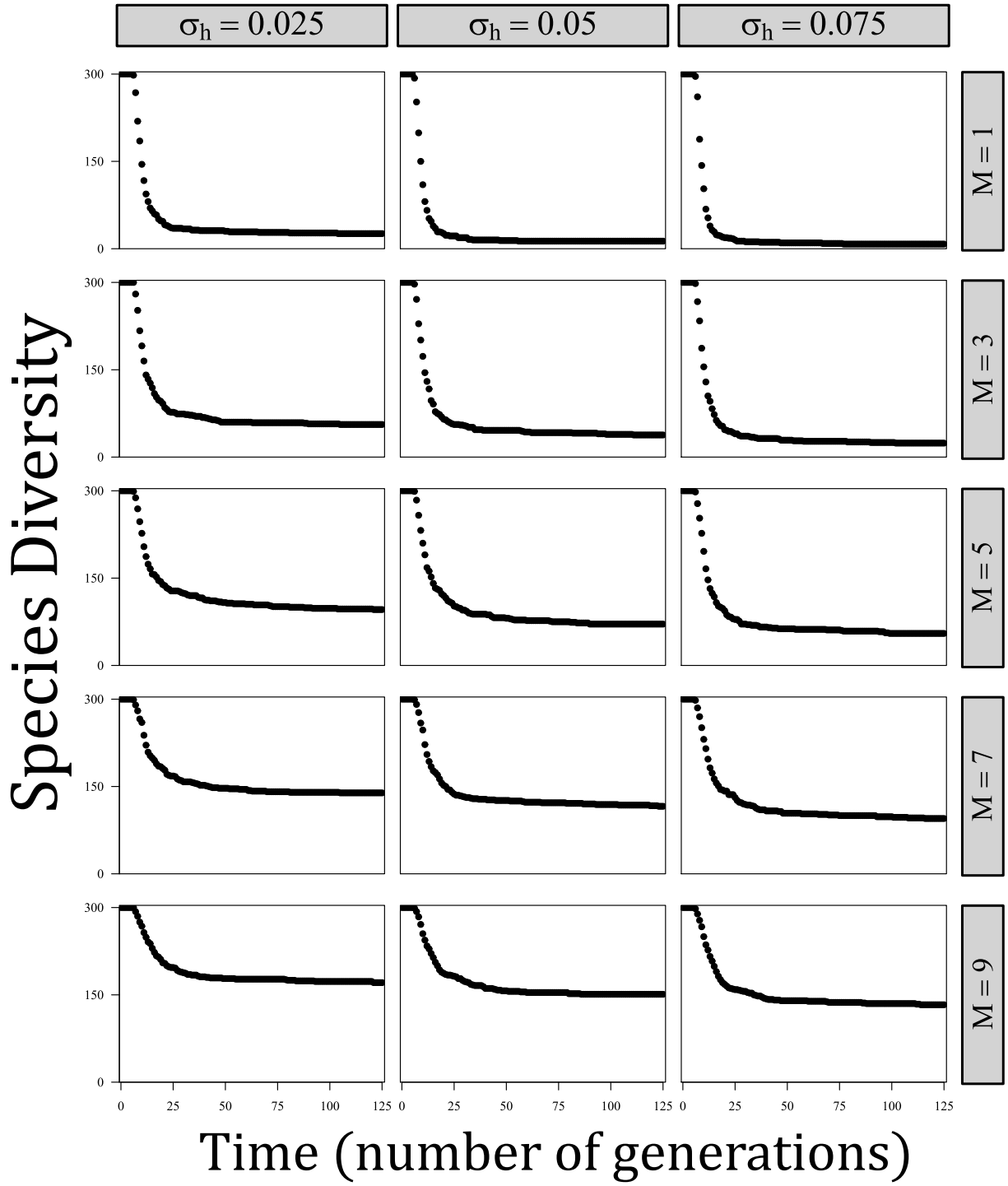

Figure 3.11: The same as the previous figure, but with medium spatial autocorrelation.

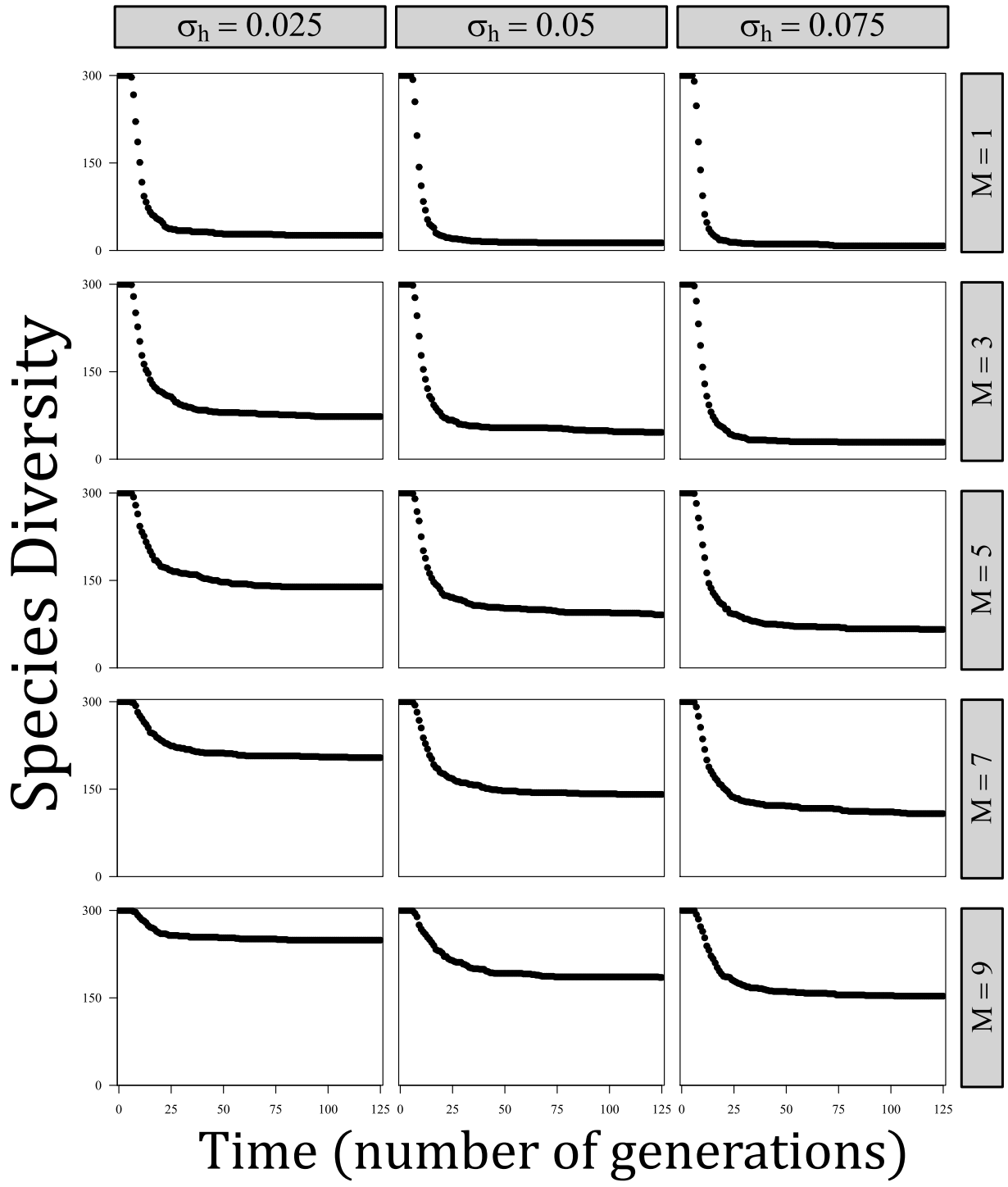

Figure 3.12: The same as the previous figure, but with high spatial autocorrelation.

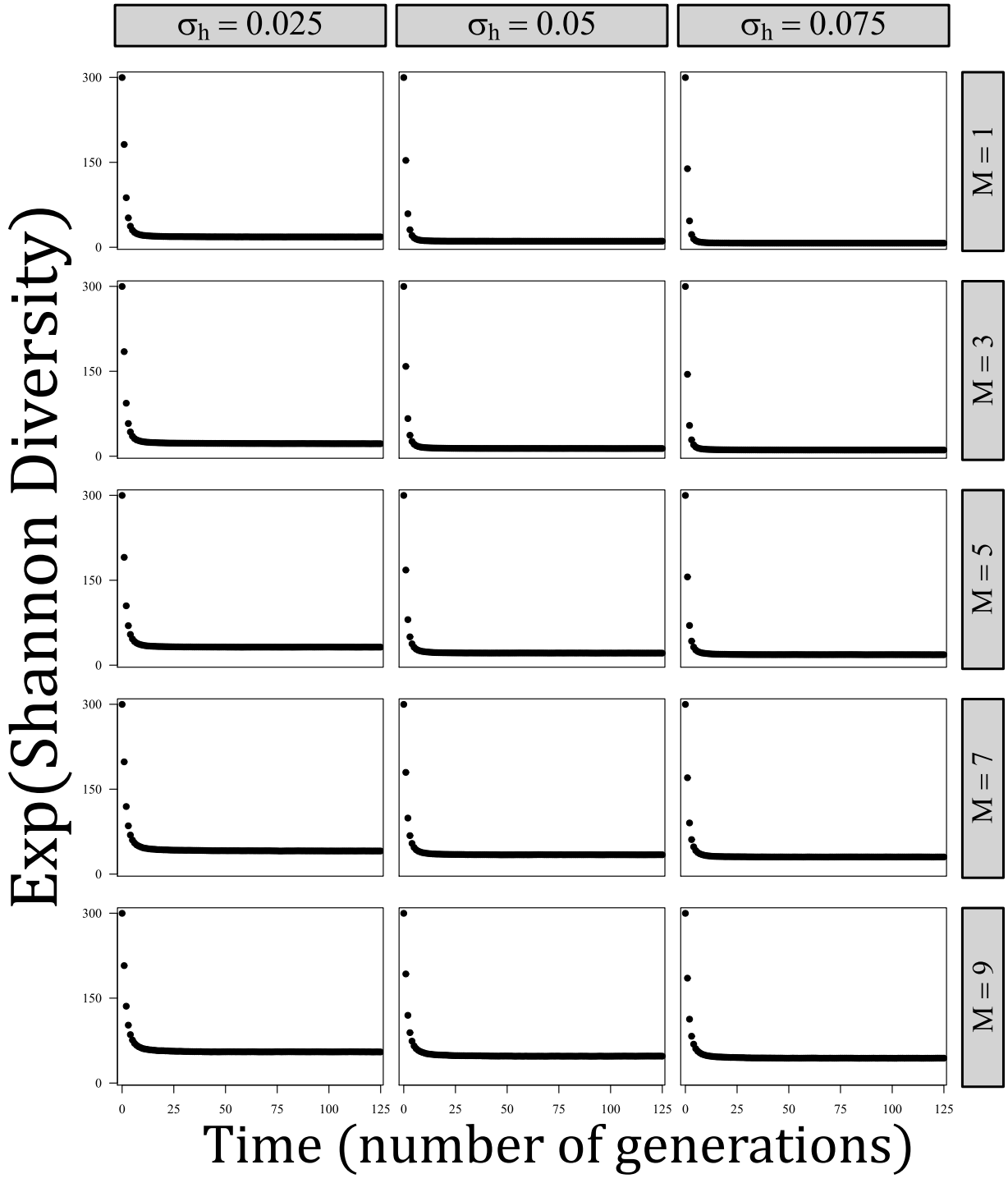

Figure 3.13: Exp(Shannon diversity) – that is, "effective species richness", as a function of time (in generations). Parameters are as follows: $a = 0.5$. This plot shows when habitat types are randomly distributed (zero spatial autocorrelation).

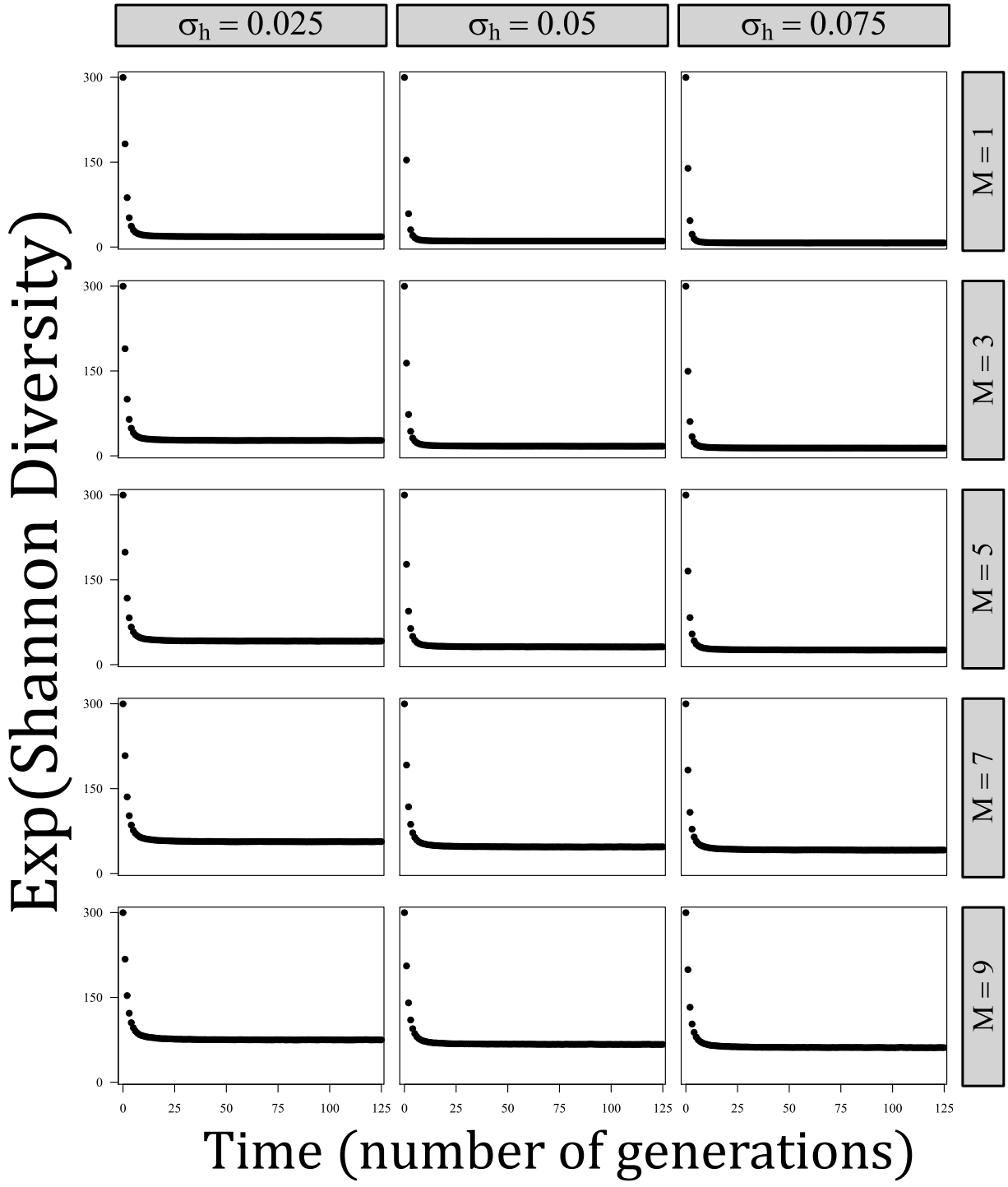

Figure 3.14: The same as the previous figure, but with low spatial autocorrelation.

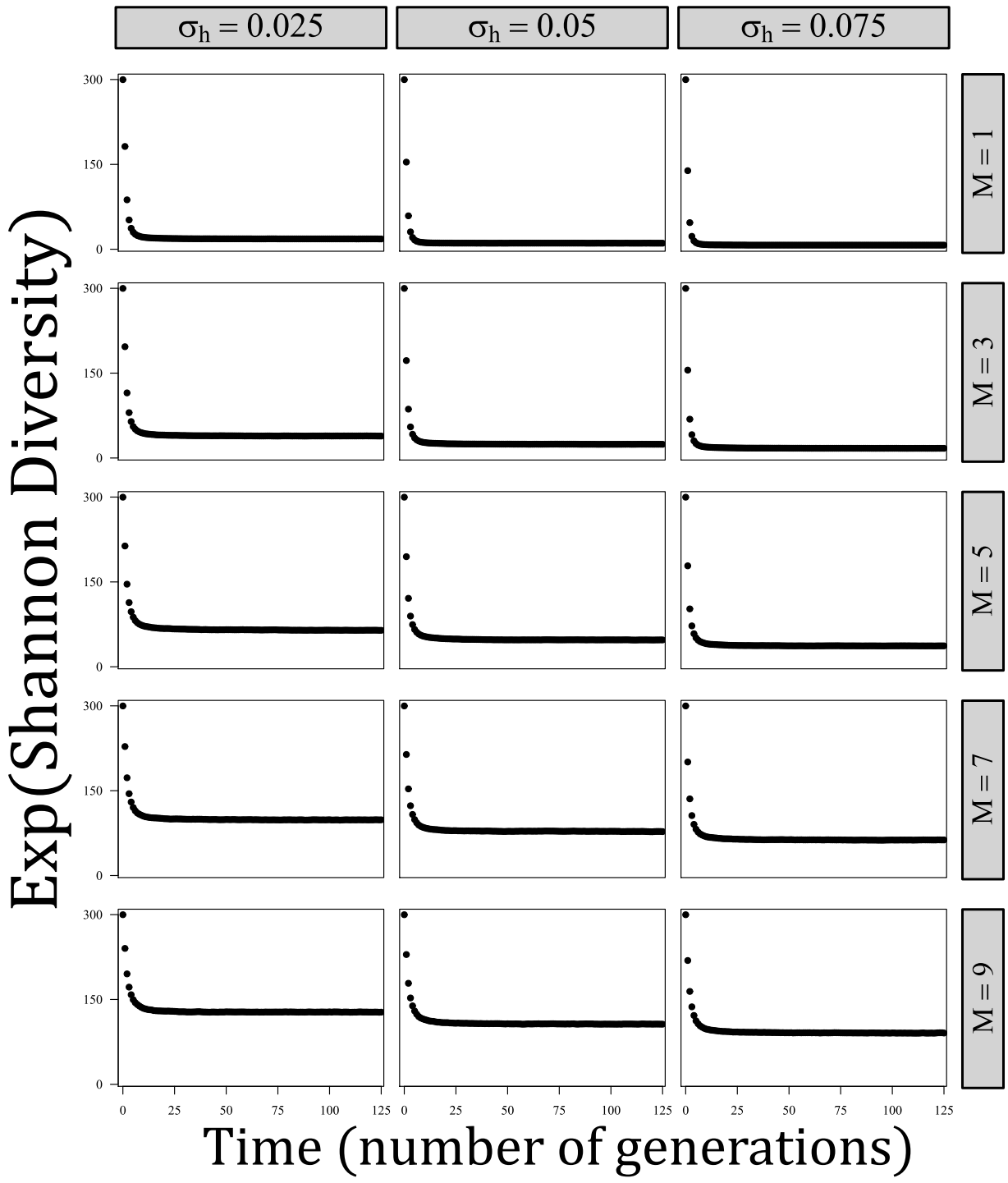

Figure 3.15: The same as the previous figure, but with medium spatial autocorrelation.

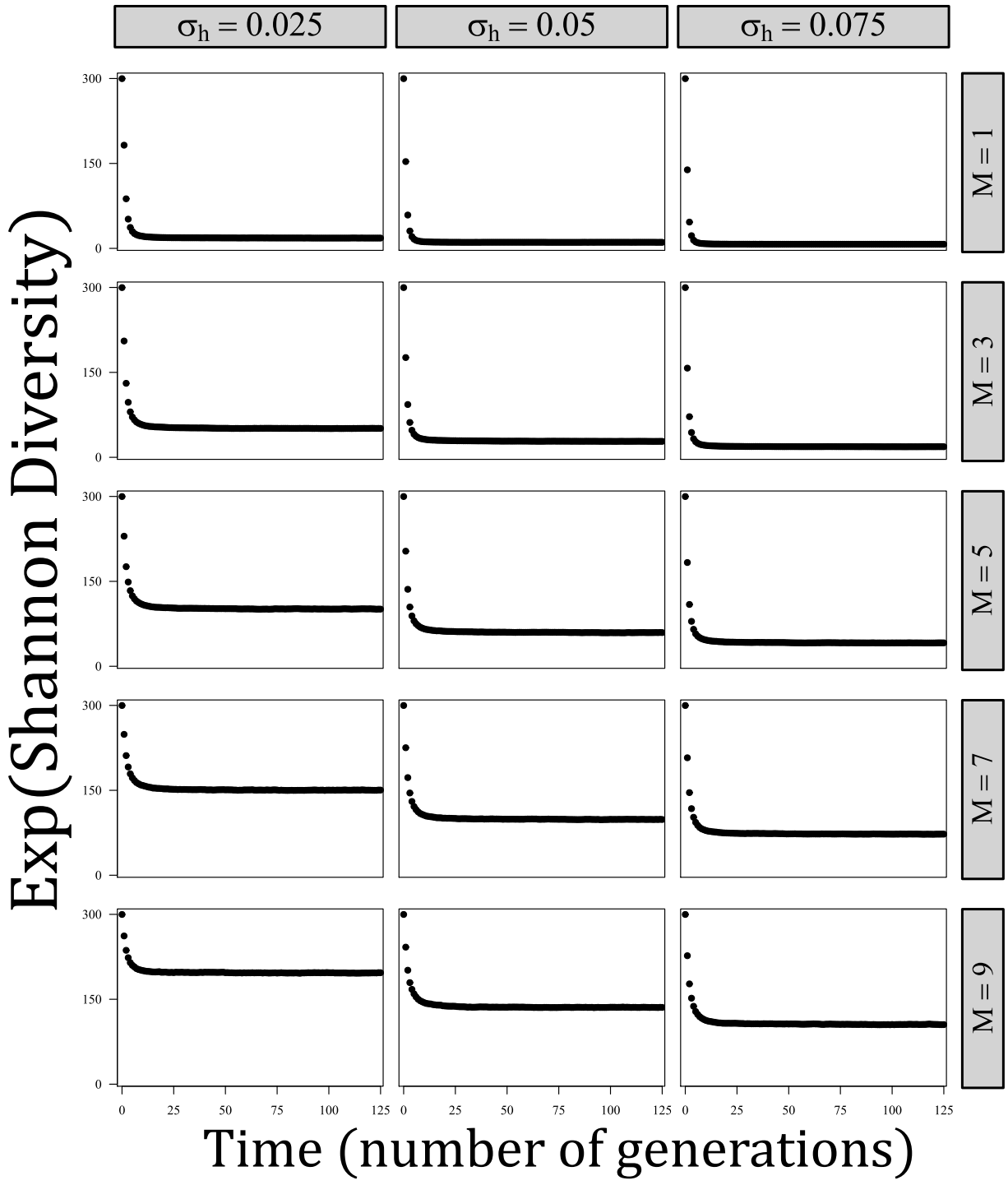

Figure 3.16: The same as the previous figure, but with high spatial autocorrelation.

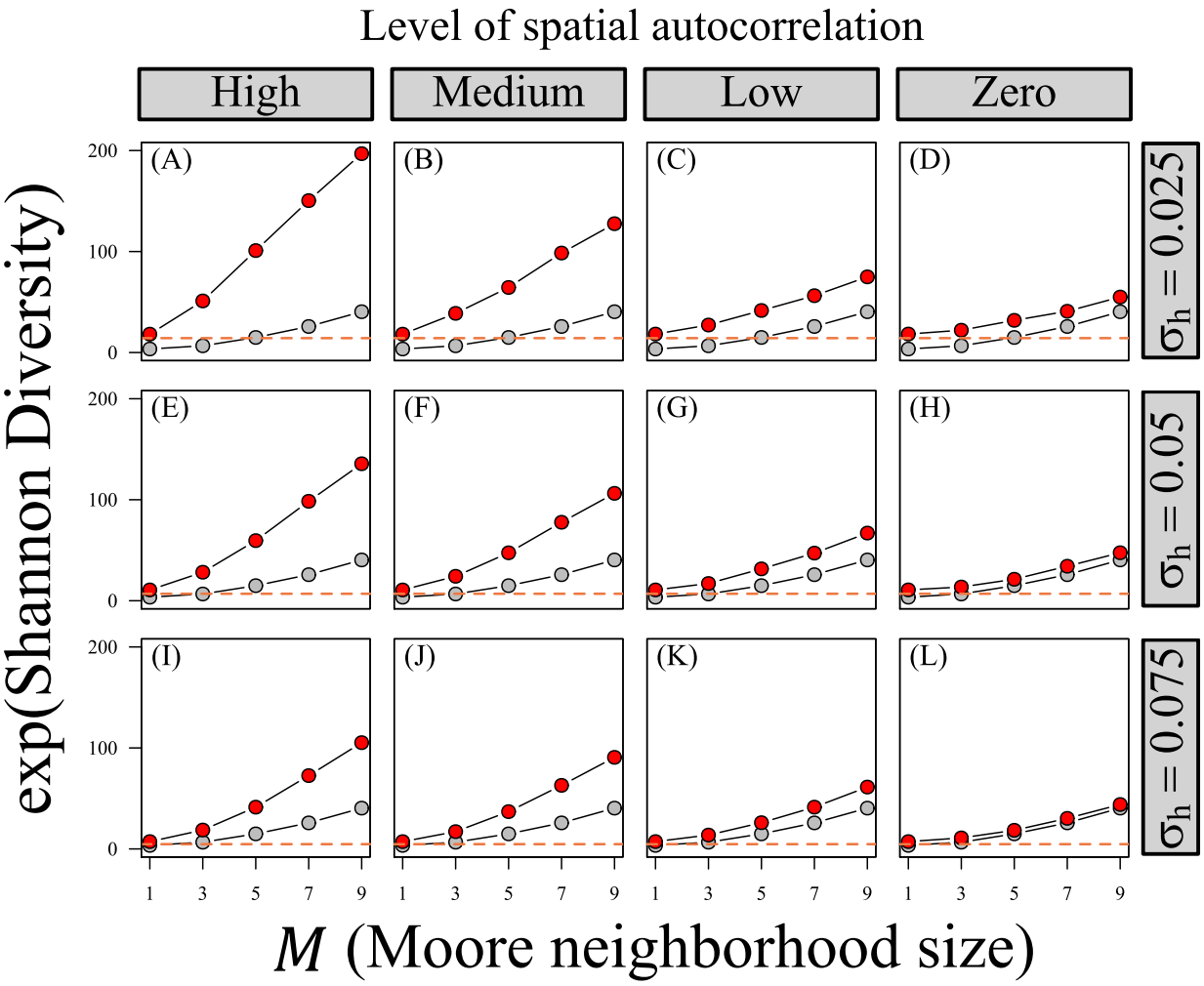

Figure 3.17: Similar to Fig. 3.3 in the main text, but showing exp(Shannon diversity) ("effective species richness") instead of species richness. Results are qualitatively identical to Fig. 3.3.

Chapter 4

How demography affects conspecific negative density dependence

4.1 Abstract

Conspecific Negative Density Dependence (CNDD) is thought to be an important driver of plant diversity. Empirical studies demonstrate that CNDD varies between species, life history strategy, and environmental conditions. While past theoretical studies examine how CNDD strength affects species coexistence, previous theory does not investigate how demographic traits (which are strongly influenced by environmental variables and life history trade-offs) affect CNDD strength and measurement. In this paper, I use a simple demographic model that highlights how key demographic traits (e.g. seed production rate, juvenile growth rate, and density-independent mortality rate) affect CNDD. I demonstrate that density-independent demographic traits strongly impact CNDD strength, even when explicit trade-offs between CNDD susceptibility and demographic traits are not assumed. I then show how these results provide insight into published CNDD measurements. Finally, I incorporate the demographic model into a simple multi-species competition model, demonstrating the density-independent factors which influence CNDD measurement have population level implications for the ability of CNDD to stabilize coexistence. Overall, the results of this paper provide a theoretical framework to examine how life history strategies and environmental conditions affect CNDD strength and its subsequent impact on species richness.

4.2 Introduction

Conspecific Negative Density Dependence (CNDD) is a leading theory for how tree species coexist. CNDD describes the empirical observation that juvenile trees experience decreased survival in locations of high conspecific density. This phenomenon is often attributed to specialized natural enemies (e.g. pests and pathogens) that are attracted to areas of high host abundance (Janzen, 1970; Connell, 1971; Comita et al., 2014; Bever et al., 2015). If species experience CNDD, the offspring of common species will tend to experience higher mortality than those of rare species – this may give rise to rare species advantage and play a role in maintaining species diversity (Chesson, 2000a).

A growing body of theoretical work examines how CNDD affects species richness (e.g. Adler and Muller-Landau, 2005; Muller-Landau and Adler, 2007; Chisholm and Muller-Landau, 2011; Stump and Chesson, 2015; Stump and Comita, 2018; Chisholm and Fung, 2020; Smith, 2022a). However, an overlooked aspect of CNDD in the literature pertains to the factors that mediate its strength. In these theoretical studies, CNDD is generally defined with a single parameter that quantifies the probability a juvenile dies in an area of high conspecific density or nearby a conspecific adult. This conceptualization is highly useful for exploring how CNDD might affect species abundance and richness under the assumption it is present at a defined level. However, this methodology cannot be used to examine the variables that influence density-dependent feedbacks and, consequently, CNDD measurements.

This gap in the literature is most evident when considering the many factors that influence CNDD strength. Firstly, there is robust empirical evidence CNDD varies with environmental conditions. Non-exhaustively, tree species experience greater CNDD in moister soils (Swinfield et al., 2012; LaManna et al., 2016; Magee et al., 2021; Zang et al., 2021) and/or greater precipitation (Comita et al., 2014; Bachelot et al., 2015; Uriarte et al., 2018; Song et al., 2018; Milici et al., 2020). Studies also find stronger CNDD at lower elevations (Fibich et al., 2021; LaManna et al., 2022; Xu et al., 2022), in more pH neutral (less acidic) soils (LaManna et al., 2016), and in more productive environments (LaManna et al., 2017a). CNDD varies with light availability (Inman-Narahari et al., 2016; McCarthy-Neumann and Ibáñez, 2013; McCarthy-Neumann and Kobe, 2019; Song et al., 2021b; Holík et al., 2021; Magee et al., 2021), soil nutrient composition (McCarthy-Neumann and

Kobe, 2019; Zang et al., 2021), interanuual climate variability and temperature (Song et al., 2018; Xu et al., 2022), and small-scale environmental conditions (Brown et al., 2021). Additionally, habitat fragmentation has been found to decrease CNDD strength (CNDD is weaker nearer to the forest edge; Krishnadas et al., 2018; Krishnadas and Stump, 2021).

In short, an accumulating body of evidence suggests CNDD is an emergent property of multiple interacting abiotic and biotic processes. Several arguments have been put forward to explain these results. Some use explanations based on biotic interactions. For example, LaManna et al. (2016) suggest resource-rich environments may produce stronger CNDD by increasing the intensity of host-specific natural enemy pressure or intra-specific competition; Milici et al. (2020) discuss how greater precipitation and humidity might enhance phytopathogen transmission and host specificity. However, others have argued that abiotic (density-independent) factors may simply be of relatively high importance in determining juvenile survival where relatively weak CNDD is measured, in which case direct environmental impacts on biotic interactions need not be invoked (Comita, 2017) . While both reasonable, these different perspectives have not been explored theoretically. Similarly, measurements of CNDD strength vary between species (e.g. Klironomos, 2002; Petermann et al., 2008; Comita et al., 2010; Mangan et al., 2010; Johnson et al., 2017; Murphy et al., 2017; Song et al., 2021a) variation that is sometimes associated with life history strategy (e.g. Zhu et al., 2018; Brown et al., 2020; Song et al., 2021b; Qin et al., 2022). While it is often assumed CNDD variation reflects inter-specific variation in susceptibility to natural enemies or sensitivity to intra-specific competition, current theory does not evaluate how demographic processes affect the measurements underlying said variation.

In addition, empirical studies examine the impact of conspecific density on juveniles through measurements of differing vital rates. While the majority of studies examine how conspecific density affects juvenile mortality, other studies observe impacts on juvenile growth rate (i.e. growth rate decreases with conspecific density; e.g. Ramage et al., 2017; Hazelwood et al., 2021; LaManna et al., 2022; Pu et al., 2022; Wei et al., 2022). While conspecific effects on each vital rate seem likely to impact fitness, we lack a theoretical framework elucidating how they interact with juvenile plant demography to shape recruitment probability. A further complication is that conspecific

density is sometimes lumped into a single variable. However, it is unclear (for example) if density-dependent mortality over the seed to seedling transition is primarily driven by (1) the number of seeds at a location (2) the number of individuals undergoing the seed-to-seedling transition, or (3) the number of established seedling recruits (Fig. 4.1). These factors may impact how density-dependent feedbacks shape CNDD strength. Relevant to these distinctions, previous work highlights that the functional form of CNDD – how the abundance of recruits responds to the initial abundance of conspecific seeds – may be important in understanding its effect on species richness (Freckleton and Lewis, 2006; Münkemüller et al., 2009; Bagchi et al., 2010, see Fig. 4.2). CNDD may be under-compensating (recruit abundance increases with initial seed abundance, but sub-linearly), compensating (recruit abundance is a saturating function of initial seed abundance), or over-compensating (recruit abundance decreases as a function of initial seed abundance at high density). Previous theory does not examine how the idiosyncrasies of juvenile tree demography and density-dependent feedbacks therein might give rise to these distinctive patterns.

In this paper, I present a simple stage-structured model that elucidates how demographic factors affect the strength of CNDD. I report several key results. (1) Density-independent demographic traits, the life history stage that induces negative density dependence, and the vital rate conspecific density impacts all interact to regulate the strength of CNDD measurements and its functional form. Crucially, these results stem from how demographic traits modulate the densities and subsequent interactions of the life history stages experiencing and generating negative density dependence – the impact of density-independent demographic traits on CNDD strength emerges without assuming life history trade-offs. (2) I show that demographic processes influence a common statistical method of measuring CNDD which I use to interpret the measurements in Krishnadas and Stump (2021). (3) I implement the stage-structured demographic model into a multi-species competition model, through which I show that the aforementioned demographic factors strongly influence the ability of CNDD to stabilize species coexistence.

4.3 Methods and Model

4.3.1 Demographic Model

I consider a stage-structured model consisting of three life history stages: seed (S), seed undergoing the seed-to-seedling transition (T), and seedling recruits R. See Fig. 4.1 for a visualization of the model. All individuals persist on a discretely defined patch. The community consists of X patches, in which each patch potentially contains a single adult tree. Each patch is indexed by a location, x. Adults of species i ($i = 1, 2, ..., N$) produce seeds at rate f_i and disperse seeds according to a dispersal kernel. The relative density of seeds dispersed to location x is defined by D_{ix}, which contains spatial information of all adult trees of species i relative to location x (D_{ix} defines how the spatial distribution of all adults of species i influences the number of seeds found at x – this is more convenient than defining the dispersal kernel of individual trees). I refer to D_{ix} as "seed rain density". I assume no long-term seed bank. On patch x, seeds of species i (S_{ix}) die at density-independent mortality at rate $m_{\mathrm{S}i}$ (deaths per unit time) and begin the seed-to-seedling-transition at growth rate $g_{\mathrm{S}i}$ (i.e. the rate at which seeds of species i begin germination per unit time, upon which they enter the Transitioning class, T_{ix}). Transitioning juveniles of species i experience density-independent mortality at rate $m_{\mathrm{T}i}$ and transition into established seedling recruits (R_{ix}) at rate $g_{\mathrm{T}i}$. Seedling recruits experience density-independent mortality at rate $m_{\mathrm{R}i}$. I allow each life history stage to (1) increase the mortality of juveniles undergoing the seed-to-seedling-transition and/or (2) decrease the rate at which individuals transition into seedling recruits (i.e. reduce g_{T}). I depict these dynamics using Ordinary Differential Equations:

$$\begin{aligned}
\frac{d\mathrm{S}_{ix}(t)}{dt} &= f_i D_{ix}(t) - m_{\mathrm{S}i}\mathrm{S}_{ix}(t) - g_{\mathrm{S}i}\mathrm{S}_{ix}(t) \\
\frac{d\mathrm{T}_{ix}(t)}{dt} &= g_{\mathrm{S}i}\mathrm{S}_{ix}(t) - \mathrm{T}_{ix}(t)M\big(\mathrm{S}_{ix}(t), \mathrm{T}_{ix}(t), \mathrm{R}_{ix}(t)\big) - m_{\mathrm{T}i}\mathrm{T}_{ix}(t) \\
&\qquad - g_{\mathrm{T}i}\mathrm{T}_{ix}(t)G\big(\mathrm{S}_{ix}(t), \mathrm{T}_{ix}(t), \mathrm{R}_{ix}(t)\big) \\
\frac{d\mathrm{R}_{ix}(t)}{dt} &= g_{\mathrm{T}i}\mathrm{T}_{ix}(t)G(\mathrm{S}_{ix}(t), \mathrm{T}_{ix}(t), \mathrm{R}_{ix}(t)\big) - m_{\mathrm{R}i}\mathrm{R}_{ix}(x)
\end{aligned} \tag{4.1}$$

where $M(\mathrm{S}_{ix}(t), \mathrm{T}_{ix}(t), \mathrm{R}_{ix}(t))$ and $G(\mathrm{S}_{ix}(t), \mathrm{T}_{ix}(t), \mathrm{R}_{ix}(t))$ quantify how conspecific density impacts transitioning juvenile mortality and growth rate, respectively. In this paper, I assume these equations take a very simple form:

$$\begin{aligned} M(\mathrm{S}_{ix}(t), \mathrm{T}_{ix}(t), \mathrm{R}_{ix}(t)) &= a_{\mathrm{S}i}\mathrm{S}_{ix}(t) + a_{\mathrm{T}i}\mathrm{T}_{ix}(t) + a_{\mathrm{R}i}\mathrm{R}_{ix}(t) \\ G(\mathrm{S}_{ix}(t), \mathrm{T}_{ix}(t), \mathrm{R}_{ix}(t)) &= \frac{1}{1 + a'_{\mathrm{S}i}\mathrm{S}_{ix}(t) + a'_{\mathrm{T}i}\mathrm{T}_{ix}(t) + a'_{\mathrm{R}i}\mathrm{R}_{ix}(t)} \end{aligned} \tag{4.2}$$

where $a_{\mathrm{S}i}$, $a_{\mathrm{T}i}$, and $a_{\mathrm{R}i}$ are constants that define the baseline strength of density-dependence. The apostrophe ($'$) delineates between effects on mortality and growth (indicating the latter). As an example, consider when $a_{\mathrm{T}i} > 0$ and $a_{\mathrm{S}i} = a_{\mathrm{R}i} = 0$. If CNDD is the consequence of soil pathogens, this would imply it is the density of individuals transitioning from seed-to-seedling *per se* that results in the local accumulation of pathogens (which increase the mortality of transitioning individuals). More realistic methods of implementing this process are possible, but equation (4.2) is sufficient for the purpose of examining how demographic traits affect the strength of CNDD (the main goal of this paper).

I assume all negative density dependence occurs over the seed-to-seedling-transition. I make this simplification for two reasons. Firstly, the seed-to-seedling-transition represents a key bottleneck in tree demography (Poorter, 2007; Green et al., 2014). Secondly, the key feature I aim to parse out is the consequence of negative density dependence experienced by a focal life history stage (juveniles undergoing the seed-to-seedling-transition, T) that is potentially affected by conspecific density of an earlier life history stage (seeds, S), conspecific density of the focal life history stage (T), or a later life history stage (seedling recruits, R). Therefore, the qualitative results of this study can be extended to other important bottlenecks in the plant regenerative pathway (i.e. the seedling-to-adult transition).

4.3.2 Demographic analyses

I conduct analytical and numerical analyses of equation (4.1) to examine how CNDD strength is impacted by (1) density-independent demographic rates (2) which life history stage induces negative

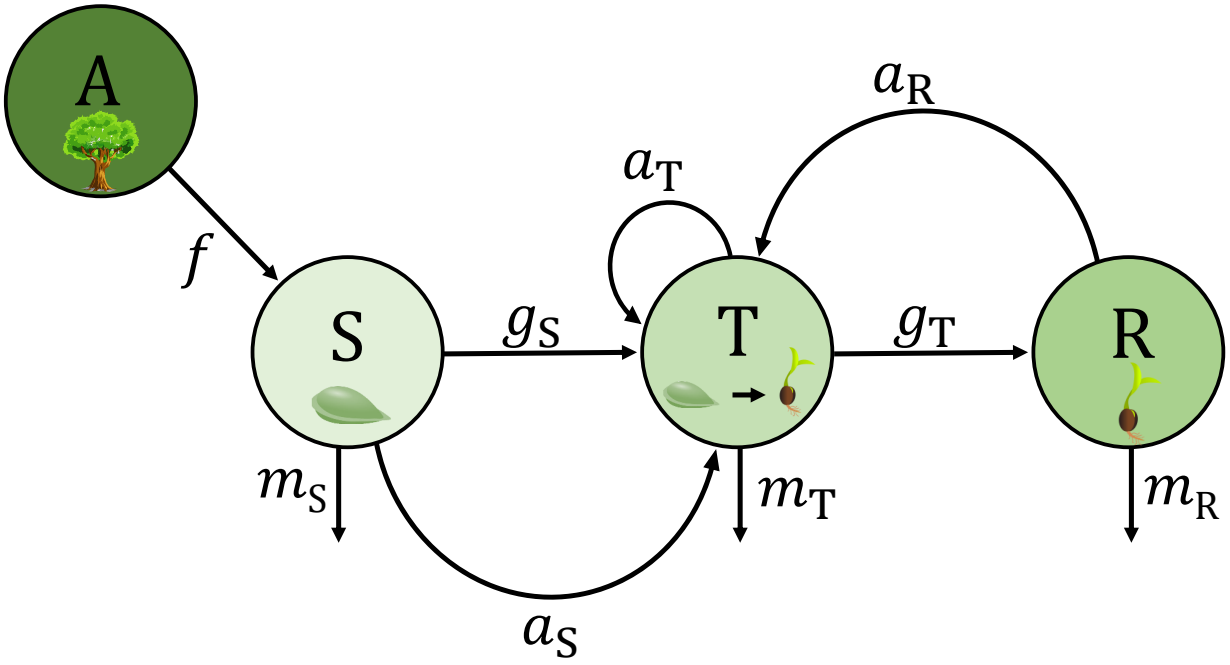

Figure 4.1: Visualization of the demographic model. Adults A produce seeds at rate f. Seeds (S) experience independent-mortality at rate m_S and begin the seed-to-seedling transition (i.e. begin germination) at rate g_S. Transitioning individuals (T) experience density-independent mortality at rate m_S and transition into successful seedling recruit at rate g_T. Seedling recruits (R) experience density-independent mortality at rate m_R. Seeds density, transitioning individual density, and seedling recruit density all potentially affect the vital rates of transitioning individuals (depicted with a_S, a_T, and a_R).

density-dependence, and (3) which vital rate conspecific density impacts (mortality or growth). For these analyses, I assume the system of Ordinary Differential Equations in equation (4.1) are at equilibrium at every patch (denoted by S^*_{ix}, T^*_{ix}, and R^*_{ix} where $*$ indicates equilibrium). This assumes seed-to-seedling-recruit dynamics occur at a timescale considerably faster than tree replacement. I define CNDD strength as the proportion of recruits that survive the seed-to-seedling transition relative to the absence of negative density-dependence at equilibrium. Let $R^{*\prime}_{ix}$ represent equilibrium recruit abundance when all coefficients in equation (4.2) (a_{Si}, a_{Ti}, a_{Ri}, etc.) are set equal to zero (i.e. no CNDD). Then, CNDD strength is defined as $R^*_{ix}/R^{*\prime}_{ix}$ for which a value of 1 indicates no CNDD and values closer to zero indicate stronger CNDD.

How demographic traits impact a common method of CNDD measurement

Empirical studies often measure CNDD strength by censusing multiple seed traps; the number of seeds in each trap are compared to the number of conspecific seedlings that recruit nearby (Harms et al., 2000; Bagchi et al., 2014; LaManna et al., 2016; Fricke and Wright, 2017; Krishnadas and Stump, 2021). This is achieved by fitting the equation:

$$R_{ix} = \alpha_i S_{ix}^{\beta_i} \tag{4.3}$$

where R_{ix} and S_{ix} represent newly emerged seedling recruit and seeds abundances of species i at location x, respectively, α_i represents the baseline proportion of seeds of species i that survive the seed-to-seedling transition, and β_i is a metric of the strength of CNDD of species i ($\beta_i = 1$ implies no CNDD and $\beta_i < 1$ implies species i experiences CNDD). Note that this measure of CNDD differs from as the metric described in the previous section. To examine how demographic factors affect fits of equation (4.3), I implement the demographic model (equation (4.1)) into a spatially explicit model. I randomly distribute adult trees throughout the environment. I assume each tree produces an initial number of seeds that disperse throughout the community according to an exponential dispersal kernel (defined by D_{ix}). After dispersal, juveniles follow the dynamics described by equation (4.1) until all seeds on each patch either successfully transition to a seedling

recruit or die before recruitment. I then fit equation (4.3) using the initial number of seeds and newly emerged seedlings on each patch as S_{ix} and R_{ix}, respectively, with a non-linear regression. Given a fixed initial density of seeds, I examine how different demographic rates impact fits of β and α. I use this approach instead of assuming equation (4.1) is at equilibrium because it is more consistent with how empirical studies make measurements; assuming equilibrium yielded qualitatively identical results. Krishnadas and Stump (2021) examined the impact of habitat fragmentation on CNDD strength for 17 species in an Indian forest. They fit equation (4.3) to each species at four different locations defined by their proximity to the forest edge ("Forest edge", "Near-edge", "Intermediate", and "Interior") finding that CNDD strength and baseline seed-to-seedling survival both decline with proximity to the forest edge (β is larger and α is smaller closer to the forest edge; Fig. 4.5A). Krishnadas and Stump (2021) also find that within fragmentation zones, species with higher seed-to-seedling survival tend to experience weaker CNDD strength (species with large β tend to have large α; Fig. 4.5A). I investigate the question: might these two qualitative trends reflect different underlying demographic processes?

4.3.3 Competition model and species richness analysis

I examine how demographic traits and CNDD impact species richness using a simple multi-species competition model. As before, I consider a community of X patches, on which each patch contains an adult tree. Adult trees disperse a fixed proportion of their seeds, D, uniformly throughout the environment and disperse the remaining $1 - D$ seeds on the local patch (x). This simplification allows relatively straightforward analytical of the model and is consistent with previous work (Stump and Chesson, 2015; Stump and Comita, 2018; Smith, 2022a). Therefore, x now indexes the identity of the tree occupying the patch. Let D_{ii} and D_{ij} represent the proportion of seeds of species i dispersed to patches occupied by species i and j, respectively ($i \neq j$). Then, $D_{ii} = 1 - D + p_i D$ and $D_{ij} = p_i D$ where p_i is the proportion of patches occupied by species i. Adults of each species die at rate δ. When an adult dies, it is replaced by a randomly selected individual in the plot weighted by a species-specific competitive ability parameter, C (a lottery model). Let R^*_{ik} represent the equilibrium recruit abundance of species i on a patch occupied by species k. Then, the probability

species i replaces a patch occupied by species k is: $\mathrm{R}^*_{ik}C_i/\sum_{\text{all } j} R^*_{jk}C_j$.

I examine the deterministic behavior of this model. The simplified form of dispersal limitation allows the model to be described spatially implicitly (patches can be described by just their occupant). I assume that the timescale of juvenile (seed-to-recruit) dynamics is much faster than tree mortality such recruits abundances always equilibrate between adult replacement events. Then, adult dynamics (each species' frequency, p_i, $i = 1, 2, .., N$) can be described by the following system of Ordinary Differential Equations:

$$\frac{dp_i}{dt} = \delta\left[\frac{\mathrm{R}^*_{ii}C_i}{\sum_{\text{all } j}\mathrm{R}^*_{ji}C_j}p_i + \sum_{k\neq i}\frac{\mathrm{R}^*_{ik}C_i}{\sum_{\text{all } j}\mathrm{R}^*_{jk}C_j}p_k - p_i\right] \tag{4.4}$$

noting that δ is on the outside of the equation because it is assumed all adults die at an equal rate. To analyze the model, I derive an approximate invasion criteria (the condition allowing a species to increase from rarity in a community of N residents) and provide outputs of numerical simulations. I conducted analyses in which species vary in their demographic traits (specified later) and, therefore, vary in fitness. Species coexist when the strength of CNDD is sufficiently strong to compensate for these fitness difference (i.e. stabilizing effects are stronger that fitness differences; Chesson, 2000b; Barabás et al., 2018). All simulations began with 50 species at equal proportion in the population. Simulations were run until equilibrium (greater than 10^4 generations) after which the remaining species were assumed to be coexisting. Simulations were run in [R] (R Core Team, 2022) using the package deSolve (Soetaert et al., 2010).

4.4 Results

4.4.1 How does demography influence the functional form of CNDD?

Strong CNDD can occur irrespective of the life history stage inducing density dependence or the vital rate it affects (i.e. whether density affects mortality or growth rate as specified in equation (4.2)). The functional form CNDD exhibits depends on both which life history stage induces density dependence and which vital rate density dependence affects (Fig. 4.2). When recruits induce

density dependence, an under-compensating pattern always emerges (Fig. 4.2C). Density dependence induced by transitioning individuals yields an under-compensating pattern when impacting mortality (black curve) and a compensating pattern when impacting either growth rate or both vital rates (Fig. 4.2B). When seeds induce density dependence, CNDD exhibits a compensating functional form when seed density impacts a single vital rate and an over-compensating functional form when impacting both vital rates (Fig. 4.2A).

These results reflect how density-dependent feedbacks are dictated by the developmental position of the life history stage inducing density dependence relative to the life history stage experiencing density dependence (those undergoing the seed-to-seedling transition). For example, seeds (the first life history stage) are unaffected by density-dependent processes (density dependence occurs over

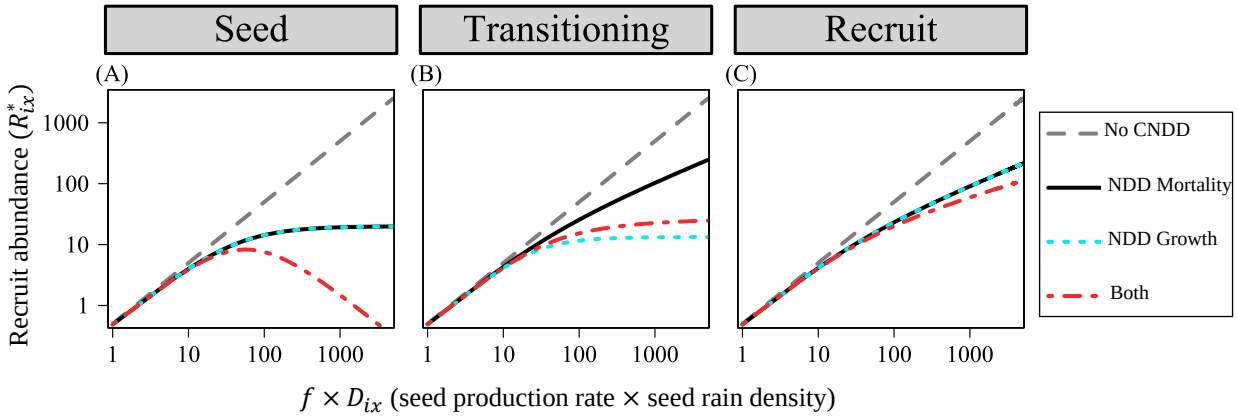

Figure 4.2: Equilibrium seedling recruits as a function of seed rain density. Labels on each column indicate the life history stage that induces density dependence *per se*. The x-axis shows $f \times D_{ix}$, which quantifies the rate a which seeds of species i disperse to location x. The y-axis shows the resulting number of seedling recruits (R^*_{ix}). The dashed grey lines shows when there is no CNDD, the black curves show when density dependence directly induces mortality, the teal dotted curves show when CNDD decreases growth rate over the seed-to-seedling transition, and red curves depict when CNDD affects both vital rates. The vital rate (mortality and/or growth rate) and the life history stage inducing density dependence both determine the functional form of CNDD, which may be under-compensating, compensating, or over-compensating. Parameters are as follows. Density-independent parameters: $m_{\mathrm{S}} = 1$, $g_{\mathrm{S}} = 1$, $m_{\mathrm{T}} = 1$, $g_{\mathrm{T}} = 1$. For each column indicating the life history stage inducing CNDD, a_{S} or $a'_{\mathrm{S}} = 0.025$, a_{T} or $a'_{\mathrm{T}} = 0.04$, a_{R} or $a'_{\mathrm{R}} = 0.1$ when CNDD affects a single vital rate. When CNDD affects both vital rates, each coefficient is set equal to half the above values (for example, $a_{\mathrm{S}} = a'_{\mathrm{S}} = 0.025 \times 0.5$).

the seed-to-seedling transition, not affecting seeds *per se*). When seeds induce density dependence, greater seed rain density always increases negative density dependence over the seed-to-seedling transition – this can give rise to compensating or over-compensating patterns. In contrast, when seedling recruits induce density dependence on juveniles undergoing the seed-to-seedling transition (Fig, 1C), the strength of density dependence depends on the number of individuals that have already successfully transitioned. As a result, CNDD can only ever be under-compensating.

4.4.2 The impact of demographic traits on CNDD strength

Assuming seed abundances are not very high (i.e. not in the high abundance region depicted in Fig. 4.2), it can derived from equation (4.1) that equilibrium seedling recruit abundance is equal to:

$$\mathrm{R}^*_{ix} \approx \underbrace{D_{ix}\frac{f_i}{m_{\mathrm{S}i}+g_{\mathrm{S}i}}\frac{g_{\mathrm{T}i}\,g_{\mathrm{S}i}}{m_{\mathrm{R}i}(m_{\mathrm{T}i}+g_{\mathrm{T}i})}}_{\text{Baseline recruit density}}\underbrace{\frac{1}{1+D_{ix}\rho_i}}_{\text{CNDD strength}} \tag{4.5}$$

where "Baseline recruit density" is the number of recruits that would be found at location x in the absence of CNDD and "CNDD strength" is the proportion of recruits that survive CNDD. Note that R^*_{ix} in equation (4.5) is exact when seeds induce density dependence and is an approximation for the other two cases (see Appendix C for details).

CNDD strength is determined by the constant ρ (Table 4.1). Unsurprisingly and trivially, baseline strength of density-dependence (a_{S}, a_{T}, and a_{R}) increases ρ and, by extension, CNDD strength (Table 4.1; Fig. 4.2, column 1). More interestingly, ρ strongly depends on density-independent demographic traits. How each trait affects ρ strongly depends on the vital rate affected by density dependence and the life history stage that induces it (Table 4.1). This is because each of these factors modulates how feedbacks between life history stages impact the seed-to-seedling transition.

I highlight several illuminating results. First, higher seed production rate (larger f) and lower seed mortality (lower m_{S}) increase CNDD strength in all cases (Table 4.1; Fig. 4.3, columns 2-3). Higher seed production and lower seed mortality lead to greater average densities, in which case density-dependent effects are more important. Faster seed growth rate (g_{S}) increases CNDD

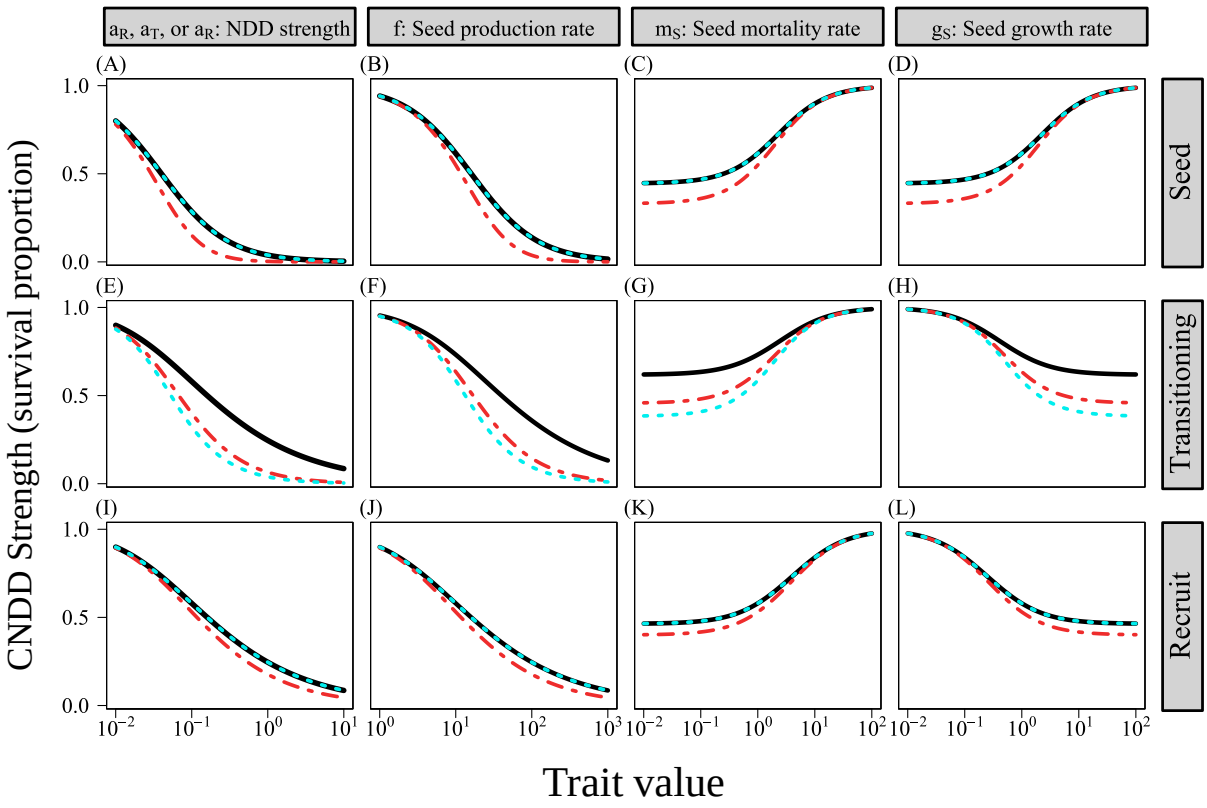

Figure 4.3: The impact of demographic traits on CNDD strength. The x-axis shows trait values; the y-axis shows CNDD strength (the proportion of recruits that survive CNDD relative to when CNDD is absent). The value of D_{ix} is identical between plots – therefore, the plots show how demographic traits impact CNDD strength at location x given a fixed seed rain density. The black curves show when density dependence directly induces mortality, the teal dotted curves show when CNDD decreases growth rate over the seed-to-seedling transition, and red curves depict when both vital rates are affected by CNDD. Each row is labeled by the life history stage that induces density dependence and each column shows a different demographic trait, in which every other demographic trait is held constant. Exact values (rather than approximations) are used in the plots. Non-specified parameters are as follows. Density-independent parameters: $f = 100$, $m_S = 1$, $g_S = 1$, $m_T = 1$, $g_T = 1$. For each column indicating the life history stage inducing CNDD, a_S or $a_S^{'} = 0.025$, a_T or $a_T^{'} = 0.04$, a_R or $a_R^{'} = 0.1$ when CNDD affects a single vital rate. When CNDD affects both vital rates, each coefficient is set equal to half the above values (for example, $a_S = a_S^{'} = 0.025 \times 0.5$).

strength when transitioning juveniles or seedling recruits induce density dependence ($a_{\mathrm{T}} > 0$ or $a_{\mathrm{R}} > 0$; Figs. 4.3H, 4.3L) but decreases CNDD strength when seeds induce density dependence ($a_{\mathrm{S}} > 0$; Fig. 4.3D). In the first cases ($a_{\mathrm{T}} > 0$ and $a_{\mathrm{R}} > 0$), larger g_{S} means that individuals more rapidly (and therefore, at higher densities) enter into the life history stages that induce density dependence, which increase its effect strength. When $a_{\mathrm{S}} > 0$, the opposite is true – individuals more rapidly exit the life history stage that induces density dependence (seeds), leading to a decrease in CNDD strength.

The impact of density-independent transitioning mortality rate (m_{T}) on CNDD is highly contingent on the vital rate affected by density dependence (Fig. 4.4, column 1). If density dependence increases mortality rate, lower m_{T} always increases CNDD strength. This can be understood as follows: CNDD strength is quantified by the increase in the probability of mortality due to density-dependent effects. Therefore, all else kept equal, the higher density-independent mortality is, the less important density-dependent mortality is by comparison. Thus, lower density-independent mortality leads to stronger CNDD. When density dependence decreases growth rate, the impact of m_{T} on CNDD depends on the life history stage that induces it. If seeds induce density dependence ($a'_{\mathrm{S}} > 0$), greater m_{T} yields stronger CNDD (Fig. 4.4A, blue curve). Greater seed density leads to individuals spending more time in the seed-to-seedling transition (in the T stage) – thus, the

		Life history stage inducing negative density dependence		
		Seed (S)	Transitioning (T)	Seedling Recruit (R)
Vital rate	Mortality	$\frac{a_{\mathrm{S}}}{m_{\mathrm{T}}+g_{\mathrm{T}}}\frac{f}{m_{\mathrm{S}}+g_{\mathrm{S}}}$	$\frac{a_{\mathrm{T}}g_{\mathrm{S}}}{(m_{\mathrm{T}}+g_{\mathrm{T}})^2}\frac{f}{m_{\mathrm{S}}+g_{\mathrm{S}}}$	$\frac{a_{\mathrm{R}}g_{\mathrm{S}}g_{\mathrm{T}}}{m_{\mathrm{R}}(m_{\mathrm{T}}+g_{\mathrm{T}})^2}\frac{f}{m_{\mathrm{S}}+g_{\mathrm{S}}}$
	Growth	$\frac{a'_{\mathrm{S}}m_{\mathrm{T}}}{m_{\mathrm{T}}+g_{\mathrm{T}}}\frac{f}{m_{\mathrm{S}}+g_{\mathrm{S}}}$	$\frac{a'_{\mathrm{T}}g_{\mathrm{S}}m_{\mathrm{T}}}{(m_{\mathrm{T}}+g_{\mathrm{T}})^2}\frac{f}{m_{\mathrm{S}}+g_{\mathrm{S}}}$	$\frac{a'_{\mathrm{R}}g_{\mathrm{S}}g_{\mathrm{T}}m_{\mathrm{T}}}{m_{\mathrm{R}}(m_{\mathrm{T}}+g_{\mathrm{T}})^2}\frac{f}{m_{\mathrm{S}}+g_{\mathrm{S}}}$

Table 4.1: Values of ρ from equation (4.5). Each column shows the life history stage that induces density dependence and each row indicates the vital rates it affects. Parameters are as follows. f: seed production rate (fecundity); m_{S}: seed mortality rate; g_{S} seed growth (germination) rate; m_{T}: transitioning mortality rate; g_{T}: transitioning growth rate; m_{R}: seedling recruit mortality rate; a_{S}, a_{T} and a_{R}: seed, transitioning, and seedling recruit density-dependent effects, respectively. a $'$ indicates density dependence affects growth rather than mortality

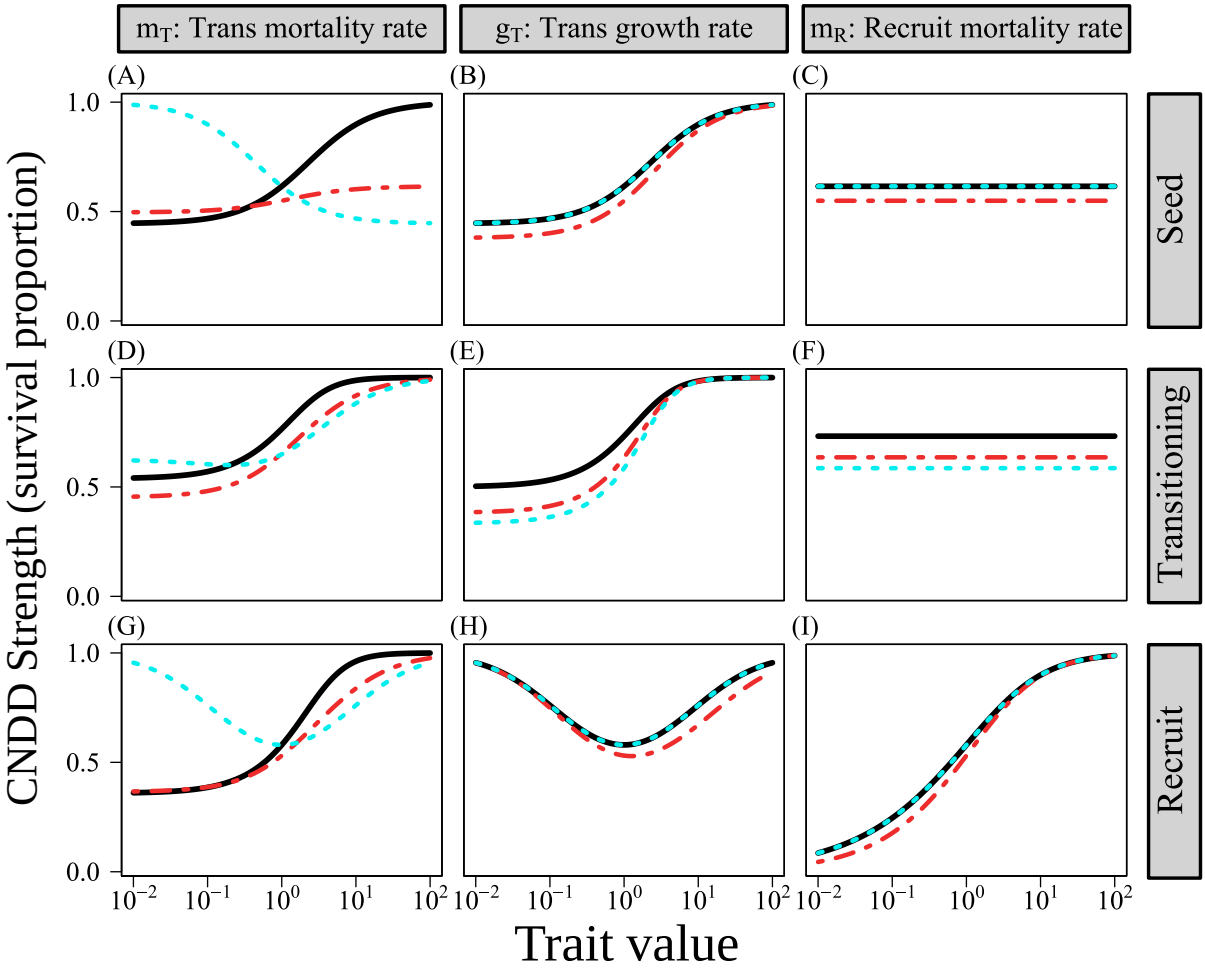

Figure 4.4: The same as Fig. 4.3, but showing different traits.

larger m_T is, the greater the increase in mortality due to density dependence. The other cases ($a'_T > 0$ or $a'_R > 0$) are less straightforward. For example, when recruits induce density dependence, CNDD strength is a unimodal function of m_T. Larger m_T increases the mortality of individuals over the seed-to-seedling transition – while this potentially increases CNDD strength for the same reason as the $a'_S > 0$, larger m_T also decreases how many recruits accumulate on the patch. Since density-dependent feedbacks explicitly depend on the number of recruits, this can decrease CNDD strength. These two factors create a tension such that peak CNDD strength occurs at an intermediate mortality level (precisely, when $m_T = g_T$). Similar logic applies to the impact of seed-to-seedling transition growth rate (g_T) on CNDD strength (Fig. 4.4H).

An additional illuminating result is that seeding recruit mortality rate (m_R) affects CNDD strength only when recruits induce density dependence ($a_R > 0$; Fig. 4.4, column 3). Smaller m_R allows more seedling recruits to accumulate – this feeds back into stronger CNDD if recruits induce density dependence (Fig. 4.4I) but does not impact CNDD strength if density dependence is driven by a prior life history stage (Fig. 4.4C, 4.4F).

4.4.3 How demographic traits impact an empirical method of CNDD measurement

Demographic traits strongly affect β (CNDD strength) and α (baseline survival) in fits of equation (4.3) to data. Fig. 4.5 shows several representative cases in which transitioning individuals induce density-dependent mortality ($a_T > 0$; Figs 4B, 4C). Importantly (and relevant to Krishnadas and Stump (2021)) demographic parameters can generate either a positive or a negative relationship between β and α when varied between fits of equation (4.3). For example, a positive relationship between β and α (meaning that CNDD strength is negatively correlated with baseline survival; Fig. 4.5B) occurs under fits of variable baseline density-dependence (a_T) and seed-to-seedling transition growth rate (g_T). This pattern is consistent with the results reported in Krishnadas and Stump (2021) within sites (inter-specific variation in CNDD measurements at set distances from the forest edge; Fig. 4.5A). Conversely, a negative relationship between β and α emerges when fitting variable

levels of density-independent seed-to-seedling transition mortality rate (m_T) or seed growth rate (g_S; Fig. 4.5C). This pattern is consistent with the between-site results reported in Krishnadas and Stump (2021) (Fig. 4.5A).

4.4.4 How CNDD affects species richness

Now I examine how the above results (in particular, the results highlighted in Figs. 4.3 and 4.4) species affect coexistence. Applying invasion analysis to the competition model (equation 4.4),

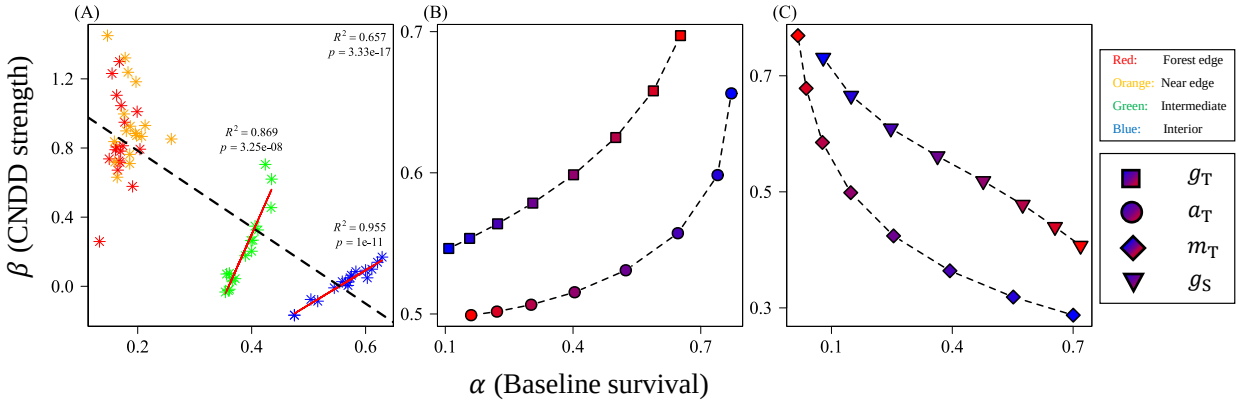

Figure 4.5: How demographic traits impact fits of equation (4.3) with reference to Krishnadas and Stump (2021). Panel (A) shows data from Krishnadas and Stump (2021). Each point indicates a fit of equation (4.3) of one of 17 different species fit at four different proximities to the forest edge. Red indicates "forest edge" (0-5 m from the edge), orange indicates "near-edge" (20-30 m from the edge), green indicates "intermediate" (50-60 m from the edge), and blue indicates the forest "interior" (90-100 m from the edge). Visible statistics show significant fits between the fit parameters of equation (4.3), showing positive relationships of fits of α and β between species within the intermediate and interior regions and a negative relationship between α and β between proximities (top-right). Panels (B) and (C) show the impact of demographic traits on fits of α and β in a spatially explicit simulated community under the assumptions that (1) seeds are dispersed according to an exponential dispersal kernel and (2) transitioning individuals (T) induce CNDD by increasing mortality rate (i.e. $a_T > 0$). The shape of each point indicates which demographic trait is varied between fits. Each trait is colored based on its relative value. Red indicates a higher value and blue indicates a lower value. For example, diamonds (panel C) depict density-independent transitioning mortality rate (m_T) – smaller values of m_T (lower density-independent mortality; bluer diamonds) yield fits of stronger CNDD (lower β) and higher baseline survival (higher α).

species i deterministically increases from rarity in a community of N residents species if:

$$r_i \approx \underbrace{\Delta Y_i + \Delta\rho_i}_{\substack{\text{Fitness}\\ \text{differences}}} + \underbrace{P_i}_{\text{Stabilization}} > 0 \tag{4.6}$$

where r_i is the growth rate of species i when rare. The terms in r_i are:

$$\begin{aligned}
\Delta Y_i &= D(2-D)\big(\log Y_i - \overline{\log Y}\big)\\
\Delta\rho_i &= D(1-D)\bigg(\log\big(1+(1-D)\rho_i\big) - \overline{\log\big(1+(1-D)\rho\big)}\bigg)\\
P_i &= D^2(3-2D)\bigg(\frac{\overline{\rho}}{N} + \mathrm{Cov}(p,\rho)\bigg)
\end{aligned} \tag{4.7}$$

noting that several approximations are necessary to evaluate r_i. See Appendix C for a derivation. Y_i defines species i's intrinsic fitness (the expected number of recruits a single tree is expected to produce in the absence of CNDD when recruits are at equilibrium, multiplied by its competitive ability): $Y_i = C_i \frac{f_i}{g_{\mathrm{S}_i}+m_{\mathrm{S}_i}} \frac{g_{\mathrm{S}_i} g_{\mathrm{T}_i}}{g_{\mathrm{T}_i}+m_{\mathrm{T}_i}}$. Overlines (e.g. $\overline{\log Y}$) indicate the average value of the resident community (e.g. $\overline{\log Y} = \frac{1}{N}\sum_{k=1}^{N} \log Y_k$). ρ_i (noting ρ should not be confused with p) is the CNDD coefficient previously noted (Table 4.1). The "fitness differences" terms quantify how factors unrelated to species abundances (p) affect the ability of species i to invade. ΔY_i quantifies intrinsic fitness differences (fitness differences induced by inter-specific variation in density-independent traits) – the larger Y_i relative to the mean ($\overline{Y}$), the easier invasion is. $\Delta\rho_i$ quantifies fitness differences induced by CNDD (specifically, fitness differences related to how CNDD affects the proportion of locally dispersed offspring, $1-D$). If species i experiences above-average CNDD strength ($\rho_i > \overline{\rho}$), invasion is more difficult. "Stabilization", P_i, is a positive term that quantifies the increase in species i's growth rate due to CNDD experienced by the resident species (species with $p > 0$; specifically, how the non-zero abundances of the resident species increase CNDD-induced mortality of their offspring). A rare species can invade if the stabilization term (P_i) is sufficiently large to compensate for fitness differences ($\Delta Y_i + \Delta\rho_i$).

It is most interesting to interpret these results in the context of demographic trait values. The

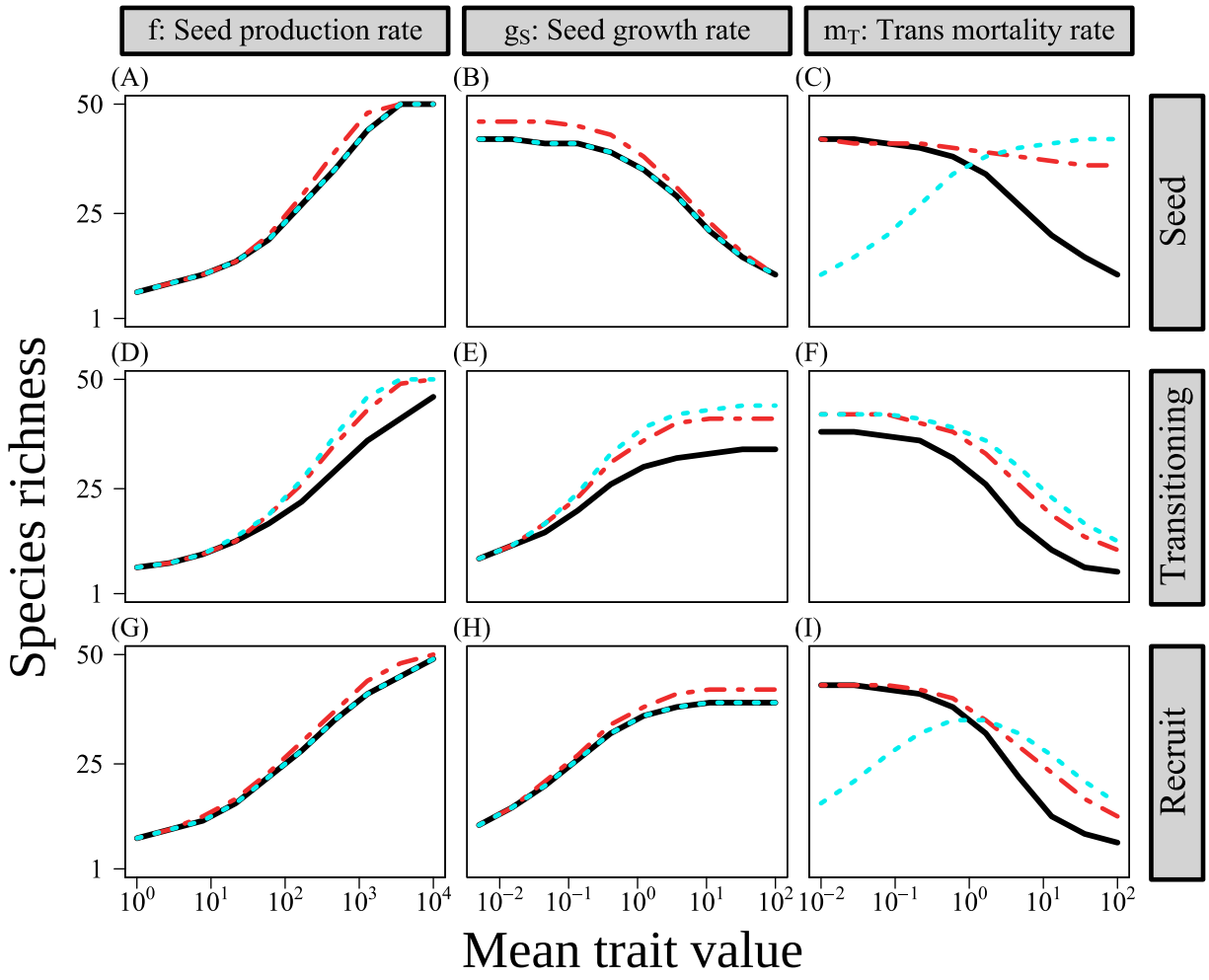

Figure 4.6: How density-independent demographic traits impact the species richness maintained by CNDD. The x-axis shows trait values; the y-axis shows species richness from simulations of equation (4.4). As in Figs. 4.3 and 4.4, the black curves show when density dependence directly induces mortality, the teal dotted curves show when CNDD decreases growth rate over the seed-to-seedling transition, and red curves depict when CNDD affects both vital rates. Each row is labeled by the life history stage that induces density dependence. Each column shows a different demographic trait that is varied between simulations (with all other demographic traits held constant). The species richness maintained by CNDD show the same qualitative patterns indicated in Figs. 4.3 and 4.4. Inter-specific fitness variation is incorporated by assuming competitive ability, C, varies between species for which $C \sim U[1, 10]$. Non-specified parameters are as follows. Density-independent parameters: $f = 100$, $m_S = 1$, $g_S = 1$, $m_T = 1$, $g_T = 1$. For each column indicating the life history stage inducing CNDD, a_S or $a_S^{'} = 0.025$, a_T or $a_T^{'} = 0.04$, a_R or $a_R^{'} = 0.1$ when CNDD affects a single vital rate. When CNDD affects both vital rates, each coefficient is set equal to half the above values (for example, $a_S = a_S^{'} = 0.025 \times 0.5$).

strength of stabilization, the ability of rare species to invade, and species richness increases with $\overline{\rho}$ – therefore, demographic traits that lead to higher ρ (see Table 4.1) increase the strength of stabilization. Given a fixed amount of inter-specific intrinsic fitness variation, the species richness maintained in a community qualitatively mirrors the patterns for CNDD strength (depicted in Figs. 4.3-4.4). For example, larger mean seed production rate ($\overline{f}$) always increases species richness (Fig. 4.6, column 1); larger $\overline{g_{\mathrm{S}}}$ increases species richness when transitioning individuals or seedling recruits induce density dependence, but reduces species richness when seeds induce density dependence (Fig. 4.6, column 2); how m_{T} affects species richness is highly dependent on which vital rate CNDD affects and the life history stage inducing density dependence (Fig. 4.6, column 3).

Which demographic trait underlies intrinsic fitness differences impacts the strength of stabilization relative to fitness differences. For example, compare when inter-specific fitness variation is driven by variation in seed production rate (f) versus seed growth rate (g_{S}) under the assumption that seeds induce density dependence ($a_{\mathrm{S}} > 0$). Given the same amount of initial fitness variation (as quantified by inter-specific variation in Y), inter-specific variation in g_{S} leads to a much larger reduction in species richness (Fig. 4.7A). Species with larger f have greater fitness (larger Y), but also experience stronger CNDD (larger ρ); less fit species with smaller f experience relatively weak CNDD (smaller ρ). Consequently, from the perspective of a relatively unfit invader, $\Delta Y_i < 0$ (which makes invasion more difficult; Fig. 4.7C) but $\Delta\rho_i > 0$ (which makes invasion easier; Fig. 4.7B). CNDD therefore acts as a fitness equalizing mechanism. Additionally, relatively fit species (species with high f and, consequently, high ρ) tend to be more abundant than less fit species. Therefore, $\mathrm{Cov}(p, \rho) > 0$, which increases the strength of the stabilizing effect (P_i; Fig. 4.7D). The opposite occurs when inter-specific fitness variation is primarily driven by g_{S}. Species with larger g_{S} have both higher intrinsic fitness and lower ρ (experience weaker CNDD). Consider an invading species with low fitness (low g_{S}): $\Delta Y_i < 0$ by the same exact amount as the fecundity case (Fig. 4.7C) *and* $\Delta\rho_i < 0$. Additionally, fitter species (species with larger g_{S} and smaller ρ) tend to be more relatively high in abundance. As a result, $\mathrm{Cov}(p, \rho) < 0$, which decreases the strength of stabilization (Fig. 4.7D). These differences exacerbate fitness differences and decrease the stabilizing effect relative to the fecundity case, leading to a reduction in species richness (Fig. 4.7A).

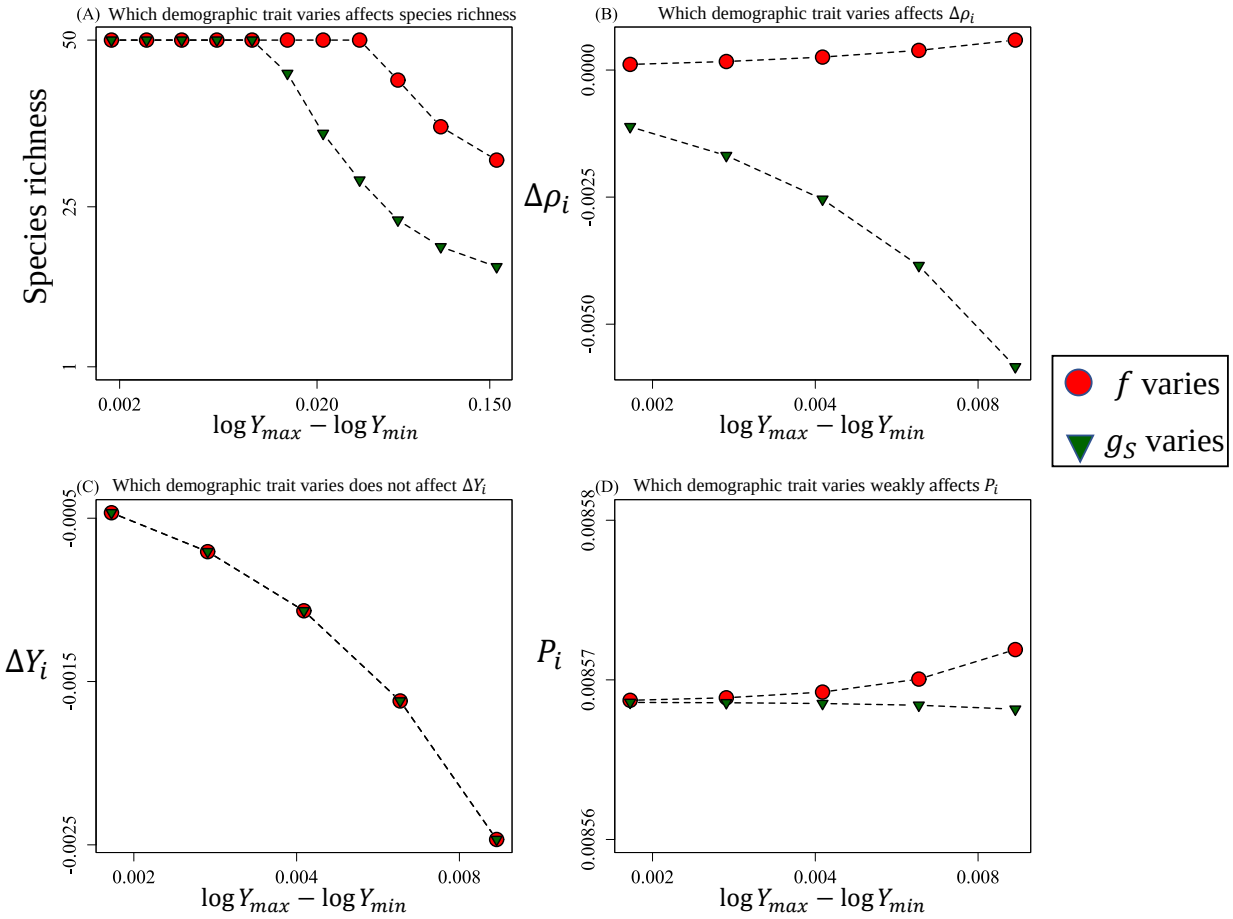

Figure 4.7: How the demographic trait inducing inter-specific variation in intrinsic fitness impacts the ability of CNDD to maintain species richness. Plots examine when species experience inter-specific variation in intrinsic fitness (Y) is driven by variation in seed production rate (f; red circles) and seed growth rate (g_{S}; green triangles). Each point on each plot shows a different simulation, with each simulation differentiated by the degree of inter-specific fitness variation. The x-axis on each plot shows the maximum log-difference in intrinsic fitness of the community at the start of the simulation (before any species went extinct; $\log Y_{\max} - \log Y_{\min}$). Panel (A) shows species richness as a function of fitness variation. Panel (B) shows $\Delta\rho_i$, panel (C) shows ΔY_i, and panel (D) shows P_i where i indicates the species with the lowest intrinsic fitness (the poorest competitor). Note that panels (B)-(D) only show the cases in all species coexist. Parameters are as follows: $m_{\mathrm{S}} = 0.1$, $m_{\mathrm{T}} = 0.5$, $g_{\mathrm{T}} = 0.05$, $D = 0.3$, $a_{\mathrm{S}} = 1$, $a'_{\mathrm{S}} = 0$, $a_{\mathrm{T}} = a'_{\mathrm{T}} = 0$, $a_{\mathrm{R}} = a'_{\mathrm{R}} = 0$.

4.5 Discussion

Previous theoretical work does not directly model how the stage-structured demographic processes of juvenile trees may influence Conspecific Negative Density Dependence (CNDD). Here, I present a first attempt at filling this gap by presenting a simple stage-structured model. Broadly, results indicate that CNDD strength and measurement are strongly modulated by density-independent demographic processes (Figs. 4.2 and 4.5) which may strongly influence the efficacy of CNDD in maintaining species richness (Figs. 4.6-4.7).

4.5.1 Interspecific variation in CNDD

Tree species vary in their density-independent demographic traits (e.g. seed production rate, juvenile mortality rate, growth rate, etc.). How demographic traits impact CNDD is, in turn, affected by the vital rate density dependence impacts (mortality and/or growth rate) and the life history stage that induces density dependence (Figs. 4.3-4.4). These factors also likely vary between species. Consequently, observations of inter-specific CNDD strength may emerge from multiple mechanisms. This is directly relevant with respect to how CNDD measurements can be interpreted – explanations that assume variation in CNDD is driven by inter-specific variation in intra-specific competition sensitivity or natural enemy susceptibility (variation in a_{S}, a_{T}, or a_{R}; e.g. LaManna et al., 2016, 2017b) must be weighed against other demographic-based explanations.

This is particularly interesting to think about in terms of life history theory. For example, several studies indicate slow-growing (often shade-tolerant) species tend to experience weaker CNDD than faster growing species (Lebrija-Trejos et al., 2016; Zhu et al., 2018; Zang et al., 2021; Song et al., 2021b). This relationship is often attributed to a defense-growth trade-off (a hypothesis that enjoys a degree of empirical support; e.g. Coley, 1980; McCarthy-Neumann and Kobe, 2008). However, I show that this pattern can come about as a result of development rate impacting density-dependent feedbacks between life history stages without assuming a trade-off (Figs. 4.3H, 4.3L, 4.4H). Therefore, it is necessary to distinguish these kinds of signals. In general, the result that density-independent demographic rates modify CNDD strength reflects how traits modify the den-

sity of individuals inducing negative density dependence. For example, if transitioning seedlings induce density dependence ($a_{\mathrm{T}} > 0$) faster seed germination rate (g_{S}) leads to a higher density of transitioning individuals accumulating within the transition class (T) at the same time, which generates stronger CNDD (Fig. 4.3H). This is distinctive from how larger a_{T} increases CNDD (larger a_{T} simply increases *per capita* density-dependent effect strength). When comparing CNDD between species, density manipulation experiments that control for the number of simultaneously transitioning seedlings may help to distinguish between these alternative mechanisms.

It is also relevant to develop baseline theoretical expectations for how trade-offs between density-independent life history traits affect CNDD strength. For example, plant species with faster growth rates also tend to have greater density-independent mortality rates (e.g. Kobe et al., 1995; Wright et al., 2010). How trade-offs between density-independent demographic traits (i.e. growth rate and density-independent mortality) influence CNDD strength in the context of the different forms of density-dependent feedbacks highlighted in this study (i.e. which vital rate density dependence impacts; which life history stage induces density dependence) is an interesting and non-trivial question. Future theoretical work should explore these questions with evolutionary models: how density-dependence influences the evolution of growth-mortality trade-offs (or *vice versa*) will lead to a better understanding of how CNDD fits into the broader picture of life history theory.

4.5.2 CNDD strength and environmental conditions

Environmental conditions unquestionably affect tree demographic traits such as seed production rate (f), growth rate (g_{S}, g_{T}), and juvenile mortality rate (m_{S}, m_{T}, m_{R}). I show that these traits strongly impact CNDD strength (Figs. 4.3-4.4). This provides a simple explanation for the growing body of literature showing environmental conditions affect CNDD.

This result also has implications for how CNDD varies along environmental gradients. For example, while some evidence suggests specialized predation pressure does not vary on latitudinal gradients (Novotny et al., 2002; Novotny and Basset, 2005; Moles et al., 2011; Chen and Moles, 2018) abiotic conditions housed by different environments strongly impact juvenile tree demographic traits, which may in turn alter density-dependent feedbacks. For example, recent studies show CNDD

decreases on elevational gradients (Fibich et al., 2021; LaManna et al., 2022). If environmental conditions increase in harshness as a function of elevation by raising seed or seedling mortality rate, this would decrease CNDD strength (Figs. 4.3-4.4) and provide a mechanism for these observation. Similarly, a recent analysis shows seed abundance exhibits a 250-fold increase between cool-dry and warm-moist climates, driven largely by a 100-fold increase in seed production rate (Journé et al., 2022). This is akin to a 100-fold increase of the parameter f in the demographic model, which leads to dramatically stronger CNDD and higher species richness (Fig. 4.3, Fig. 4.6). Therefore, even if *per capita* density-dependent effects (i.e. a_{S}, a_{T}, and/or a_{R}) do not vary at all between environments, warmer and moister conditions may still give rise to relatively strong CNDD. This may explain why relatively strong CNDD is measured in such environments (Comita et al., 2014; Bachelot et al., 2015; LaManna et al., 2016; Song et al., 2018; Milici et al., 2020; Magee et al., 2021).

4.5.3 Interpretation of CNDD measurements

Overall, it is important to parse out whether variation in density-dependent biological interaction strength (e.g. a_{T}, which may be mediate by pathogens) or density-independent demographic rates (e.g. m_{T}, which may be mediated by abiotic factors) underlie the relative strength of CNDD measurements. Fitting equation (4.3) to a simulated community indicates that the specific demographic trait or traits underlying CNDD variation may give rise to distinctive patterns with respect to the fits of the CNDD strength parameter (β) and baseline survival parameter (α). Applying these results to Krishnadas and Stump (2021) provides some insight into the mechanism of how habitat fragmentation modifies CNDD strength. Krishnadas and Stump (2021) show CNDD strength decreases (β increases) and baseline survival decreases (smaller α) with proximity to the forest edge. I find that this pattern can occur if proximity to the forest edge increases density-independent mortality or decreases seed growth rate but is unlikely to fundamentally reflect a decrease in baseline density dependence strength (a_{T}, which may correspond to factors such as intra-specific competition strength, natural enemy abundance, or natural enemy susceptibility; see Fig. 4.5B). Notably, the environment of sites closer to the forest edge differ from those of interior (e.g., they may be hotter, drier, and receive more light; see Asbjornsen et al., 2004; Arroyo-Rodríguez et al., 2017) which may

affect innter-site demographic trait variation and the resulting CNDD measurements in Krishnadas and Stump (2021). This result is encouraging, as it implies relatively simple CNDD metrics may still provide some insight into the demographic processes underlying CNDD measurements. This is also relevant for conservation planning – whether habitat fragmentation decreases CNDD strength and species diversity via modification of density-dependent or density-independent demographic rates may inform restoration efforts.

More broadly, empirical CNDD measurements take a variety of forms that are difficult to directly compare. Many studies fit equation (4.3) (e.g. Harms et al., 2000; Bagchi et al., 2014; LaManna et al., 2016; Fricke and Wright, 2017; Krishnadas and Stump, 2021); a number of studies calculate the probability of juvenile survival in an area of relatively high density versus an area of low density (e.g. see references in Comita et al., 2014; Song et al., 2021a); other studies fit a generalized linear mixed model (often with a logit link function) to quantify the effect of conspecific density on the probability of seedling and/or sapling survival (e.g. Comita et al., 2010; Zhu et al., 2018; Xu et al., 2022). It is unclear if the CNDD metrics derived by each method relay the same information. Future work should aim to conceptually and quantitatively bridge these various metrics by their mutual implementation into simulated communities that incorporate mechanistic demographic processes. This will allow for more robust interpretations of empirical measurements of CNDD and more meaningful parameterizations of theoretical models.

4.5.4 CNDD strength and species richness

Results also indicate that density-independent demographic rates can shape the efficacy of CNDD in maintaining species richness (Figs. 4.6-4.7). This implies that a robust understanding of tree juvenile demographic processes is necessary to determine whether CNDD is an important coexistence mechanism.

It is illuminating to consider this result in the context of previous theoretical CNDD-related work. There are two related differences between the model of this study and previous models. Previous studies (1) implement intrinsic fitness as a simplified composite parameter of fecundity and density-independent juvenile mortality rate (often called "yield") to define inter-specific fitness

differences without explicitly modeling the demographic processes that comprise it and (2) assume that CNDD effects are entirely independent of the demographic traits that comprise intrinsic fitness (e.g. Adler and Muller-Landau, 2005; Chisholm and Muller-Landau, 2011; Stump and Chesson, 2015; Stump and Comita, 2018; Chisholm and Fung, 2020; Smith, 2022a,b). These differences may affect conclusions on the efficacy of CNDD as a coexistence mechanism. For example, recent studies that examine realistic levels of inter-specific variation in seed production rate (i.e. fecundity) in communities experiencing CNDD argue the resulting inter-specific fitness differences can largely erode species richness (Chisholm and Fung, 2020; Smith, 2022a). However, the aforementioned simplifications these studies make miss two crucial features. Firstly, species with higher seed production rate also tend to experience stronger CNDD (Fig. 4.3) which can equalize fitness differences (Fig. 4.7B). Secondly, these studies only consider *relative* seed production rate rather than absolute seed rain (which f represents). While the absolute (mean) level of seed production does not matter if intrinsic fitness and CNDD are treated independently, it is crucial in determining the strength of CNDD and its ability to maintain diversity when demographic structure is explicitly modeled (Fig. 4.3, column 2; Fig. 4.6, column 1). Therefore, more precise empirical estimates of the absolute level of seed production rate (as well as other key demographic traits) are warranted before conclusions can be drawn on whether CNDD is strong enough to overcome inter-specific fitness differences. In particular, it is important to ask if inter-specific variation in intrinsic fitness is driven by demographic traits that cause CNDD to exacerbate or mitigate fitness differences (Fig. 4.7B).

4.5.5 Caveats and Future Directions

There are a number of simplifications this model makes. First, CNDD is generally thought to be the result of natural enemies that congregate to areas of high density. Future models should directly incorporate these interactions. Models that examine insect predators can build on Nathan and Casagrandi (2004); pathogen-motivated models can expand on Mordecai (2015). Second, I assumed density-dependent effects on seed-to-seedling transition mortality to be linear (equation (4.2)). However, these effects may exhibit non-linearities (Detto et al., 2019). Incorporating non-linearities could further complicate how each demographic trait impacts CNDD.

Third, I examined when seeds, transitioning individuals, or seedling recruits induce density dependence – however, empirical measurements indicate that it may be the density of adult trees themselves that increase conspecific mortality. I made this simplification because it allows examination of all sources of density dependence within the same framework (i.e. without the need of defining how adult effects on juveniles decay with distance; see Smith, 2022a).

Additionally, I only examined when a single life history stage induces density dependence. However, the densities of multiple life history stages likely affect density-dependent processes. Similarly, while empirical measurements indicate species experience CNDD over multiple life history stages, I only examined when CNDD occurs over the seed-to-seedling transition. These simplifications make the model examined in this study tractable, but may ignore key features affecting density-dependent feedbacks. Future models should allow for CNDD to be induced and experienced by juveniles throughout the entirety of development. This could be directly accomplished with the implementation of actor based models that index juvenile individuals and their interactions based on their size or age.

4.5.6 Conclusion

The key finding of this study is that density independent demographic traits play a key role in determining CNDD strength. Therefore, empirical studies should explicitly consider how density-independent demographic processes result in (1) inter-specific variation in CNDD measurements and (2) CNDD variation along environmental gradients. More generally, vestments of CNDD vary between sites and/or between species, variation in density-independent demographic processes should be thought of as an alternative hypothesis to variation in natural enemy susceptibility (noting these mechanisms are not mutually exclusive). Future theoretical should work toward integrating CNDD into life history theory, which may allow for the development of predictions on how CNDD strength and trait associations evolve.

4.6 Acknowledgements

This research was funded by the National Science Foundation grant NSF OCE 1851489. I thank J. Timothy Wootton, Catherine A Pfister, Mercedes Pascual, Trevor Price, and the Wootton-Pfister lab for insightful discussion and feedback on the manuscript.

Appendix C

Introduction

In this Appendix, I provide details on (1) approximations for recruit abundances, (2) spatially explicit simulations and fits of the power regression model (equation 4.3 in the main text), and (3) the derivation of the approximate invasion criterion in the main text.

Equilibrium Derivations and Approximations

In the main text, equation (5) breaks equilibrium recruit abundance into two terms:

$$\mathrm{R}^*_{ix} \approx \underbrace{D_{ix}\frac{f_i}{m_{\mathrm{S}i}+g_{\mathrm{S}i}}\frac{g_{\mathrm{T}i}\,g_{\mathrm{S}i}}{m_{\mathrm{R}i}(m_{\mathrm{T}i}+g_{\mathrm{T}i})}}_{\text{Baseline Recruit density}}\ \underbrace{\frac{1}{1+D_{ix}\rho_i}}_{\text{CNDD strength}} \tag{4.8}$$

"Baseline recruit density" is the number of recruits that would be found at location x in the absence of CNDD and "CNDD strength" is the proportion of recruits that survive CNDD. When seeds induce NDD, this expression is exact; when transitioning individuals or seedling recruits induce NDD, R^*_{ix} is an approximation. Here, I briefly show the derivations of R^*_{ix}.

Broadly, this expression is derived from setting each ODE from equation 4.1 in the main text,

$$\begin{aligned}
\frac{d\mathrm{S}_{ix}(t)}{dt} &= f_i D_{ix}(t) - m_{\mathrm{S}i}\mathrm{S}_{ix}(t) - g_{\mathrm{S}i}\mathrm{S}_{ix}(t) \\
\frac{d\mathrm{T}_{ix}(t)}{dt} &= g_{\mathrm{S}i}\mathrm{S}_{ix}(t) - \mathrm{T}_{ix}(t)M\big(\mathrm{S}_{ix}(t), \mathrm{T}_{ix}(t), \mathrm{R}_{ix}(t)\big) - m_{\mathrm{T}i}\mathrm{T}_{ix}(t) \\
&\qquad - g_{\mathrm{T}i}\mathrm{T}_{ix}(t)G\big(\mathrm{S}_{ix}(t), \mathrm{T}_{ix}(t), \mathrm{R}_{ix}(t)\big) \\
\frac{d\mathrm{R}_{ix}(t)}{dt} &= g_{\mathrm{T}i}\mathrm{T}_{ix}(t)G(\mathrm{S}_{ix}(t), \mathrm{T}_{ix}(t), \mathrm{R}_{ix}(t)\big) - m_{\mathrm{R}i}\mathrm{R}_{ix}(x)
\end{aligned} \tag{4.9}$$

to their non-trivial equilibria.

Notably, I examine the following cases:

$$\begin{aligned}
M\big(\mathrm{S}_{ix}(t), \mathrm{T}_{ix}(t), \mathrm{R}_{ix}(t)\big) &= a_{\mathrm{S}i}\mathrm{S}_{ix}(t) \\
M\big(\mathrm{S}_{ix}(t), \mathrm{T}_{ix}(t), \mathrm{R}_{ix}(t)\big) &= a_{\mathrm{T}i}\mathrm{T}_{ix}(t) \\
M\big(\mathrm{S}_{ix}(t), \mathrm{T}_{ix}(t), \mathrm{R}_{ix}(t)\big) &= a_{\mathrm{R}i}\mathrm{R}_{ix}(t)
\end{aligned} \tag{4.10}$$

for which $G(\mathrm{S}_{ix}(t), \mathrm{T}_{ix}(t), \mathrm{R}_{ix}(t)\big) = 1$ and

$$\begin{aligned}
G\big(\mathrm{S}_{ix}(t), \mathrm{T}_{ix}(t), \mathrm{R}_{ix}(t)\big) &= \frac{1}{1 + a'_{\mathrm{S}i}\mathrm{S}_{ix}(t)} \\
G\big(\mathrm{S}_{ix}(t), \mathrm{T}_{ix}(t), \mathrm{R}_{ix}(t)\big) &= \frac{1}{1 + a'_{\mathrm{T}i}\mathrm{T}_{ix}(t)} \\
G\big(\mathrm{S}_{ix}(t), \mathrm{T}_{ix}(t), \mathrm{R}_{ix}(t)\big) &= \frac{1}{1 + a'_{\mathrm{R}i}\mathrm{R}_{ix}(t)}
\end{aligned} \tag{4.11}$$

for which $M(\mathrm{S}_{ix}(t), \mathrm{T}_{ix}(t), \mathrm{R}_{ix}(t)\big) = 0$.

In each of these cases, the equilibrium for seed abundance is identical:

$$\mathrm{S}^*_{ix} = D_{ix}\frac{f_i}{m_{\mathrm{S}i} + g_{\mathrm{S}i}} \tag{4.12}$$

from which, T^*_{ix} and R^*_{ix} can be calculated (either exactly or approximately).

Seeds induce NDD

$M\big(S_{ix}(t),\, T_{ix}(t), R_{ix}(t)\big) = a_{Si} S_{ix}(t)$

It is trivial to solve the equilibrium for both T^*_{ix} and R^*_{ix}. A little algebra yields:

$$\begin{aligned} \mathrm{T}^*_{ix} &= \frac{g_{\mathrm{S}i}\mathrm{S}^*_{ix}}{m_{\mathrm{T}i} + g_{\mathrm{T}i} + a_{\mathrm{S}i}\mathrm{S}^*_{ix}} = \frac{D_{ix} g_{\mathrm{S}i} \frac{f_i}{m_{\mathrm{S}i}+g_{\mathrm{S}i}}}{m_{\mathrm{T}i} + g_{\mathrm{T}i} + D_{ix} a_{\mathrm{S}i} \frac{f_i}{m_{\mathrm{S}i}+g_{\mathrm{S}i}}} \\ \mathrm{R}^*_{ix} &= D_{ix} \frac{f_i}{m_{\mathrm{S}i} + g_{\mathrm{S}i}} \frac{g_{\mathrm{T}i}\, g_{\mathrm{S}i}}{m_{\mathrm{R}i}(m_{\mathrm{T}i} + g_{\mathrm{T}i})} \frac{1}{1 + D_{ix} \frac{a_{\mathrm{S}i}}{m_{\mathrm{T}i}+g_{\mathrm{T}i}} \frac{f_i}{m_{\mathrm{S}i}+g_{\mathrm{S}i}}} \end{aligned} \tag{4.13}$$

$G\big(S_{ix}(t),\, T_{ix}(t), R_{ix}(t)\big) = \frac{1}{1+a^{'}_{Si} S_{ix}(t)}$

The solution for the growth rate case (when negative density dependence affects growth rate) is almost identical to the above case:

$$\begin{aligned} \mathrm{T}^*_{ix} &= \frac{g_{\mathrm{S}i}\mathrm{S}^*_{ix}(1 + a^{'}_{\mathrm{S}i}\mathrm{S}^*_{ix})}{m_{\mathrm{T}i} + g_{\mathrm{T}i} + a^{'}_{\mathrm{S}i}\mathrm{S}^*_{ix}} = \frac{D_{ix} g_{\mathrm{S}i} \frac{f_i}{m_{\mathrm{S}i}+g_{\mathrm{S}i}} \left(1 + a^{'}_{\mathrm{S}i} D_{ix} \frac{f_i}{m_{\mathrm{S}i}+g_{\mathrm{S}i}}\right)}{m_{\mathrm{T}i} + g_{\mathrm{T}i} + D_{ix} a^{'}_{\mathrm{S}i} m_{\mathrm{T}i} \frac{f_i}{m_{\mathrm{S}i}+g_{\mathrm{S}i}}} \\ \mathrm{R}^*_{ix} &= D_{ix} \frac{f_i}{m_{\mathrm{S}i} + g_{\mathrm{S}i}} \frac{g_{\mathrm{T}i}\, g_{\mathrm{S}i}}{m_{\mathrm{R}i}(m_{\mathrm{T}i} + g_{\mathrm{T}i})} \frac{1}{1 + D_{ix} \frac{a^{'}_{\mathrm{S}i}}{m_{\mathrm{T}i}+g_{\mathrm{T}i}} \frac{f_i}{m_{\mathrm{S}i}+g_{\mathrm{S}i}}} \end{aligned} \tag{4.14}$$

noting that in this case and the above case, I skip the derivation – this is because these quantities can be derived by directly setting each expression in the system of Ordinary Differential Equation in equation 4.9 to zero and solving for the equilibrium.

Transitioning individuals induce NDD

$M\big(S_{ix}(t),\, T_{ix}(t), R_{ix}(t)\big) = a_{Ti} T_{ix}(t)$

First, consider the dynamics of transitioning individuals with the above value inserted. Rearranging terms slightly, the equilibrium is obtained by solving the following equation:

$$\frac{d\mathrm{T}_{ix}(t)}{dt} = g_{\mathrm{S}i}\mathrm{S}^*_{ix} - \mathrm{T}^*_{ix}\big(a_{\mathrm{T}i}\mathrm{T}^*_{ix} + m_{\mathrm{T}i} + g_{\mathrm{T}i}\big) = 0 \tag{4.15}$$

However, directly solving this yields a quadratic that is somewhat unpleasant to work with. To analyze this is the same framework as the seed case, I perform a linearization. To do so, I first divide each side of the equation by $a_{\mathrm{T}i}\mathrm{T}^*_{ix} + m_{\mathrm{T}i} + g_{\mathrm{T}i}$. With some rearranging, this gives:

$$\frac{1}{m_{\mathrm{T}i} + g_{\mathrm{T}i}} \frac{g_{\mathrm{S}i}\,\mathrm{S}^*_{ix}}{1 + \mathrm{T}^*_{ix}\frac{a_{\mathrm{T}i}}{m_{\mathrm{T}i}+g_{\mathrm{T}i}}} - \mathrm{T}^*_{ix} = 0 \tag{4.16}$$

I then take the first order term of the geometric series of $\frac{g_{\mathrm{S}i}\mathrm{S}^*_{ix}}{1+\mathrm{T}^*_{ix}\frac{a_{\mathrm{T}i}}{m_{\mathrm{T}i}+g_{\mathrm{T}i}}}$, noting that $1/(1+r) \approx 1-r$ if r is fairly small. This then gives

$$\frac{1}{m_{\mathrm{T}i} + g_{\mathrm{T}i}} \big(g_{\mathrm{S}i}\,\mathrm{S}^*_{ix}\big) \left(1 - \mathrm{T}^*_{ix}\frac{a_{\mathrm{T}i}}{m_{\mathrm{T}i} + g_{\mathrm{T}i}}\right) - \mathrm{T}^*_{ix} = 0 \tag{4.17}$$

then, solving for T^*_{ix} and using the equilibrium, T^*_{ix}, to solve for R^*_{ix} (which is straight-forward) gives:

$$\begin{aligned}
\mathrm{T}^*_{ix} &\approx \frac{g_{\mathrm{S}i}\mathrm{S}^*_{ix}}{m_{\mathrm{T}i} + g_{\mathrm{T}i} + \mathrm{S}^*_{ix}\frac{a_{\mathrm{S}i}}{m_{\mathrm{T}i}+g_{\mathrm{T}i}}} = \frac{D_{ix} g_{\mathrm{S}i} \frac{f_i}{m_{\mathrm{S}i}+g_{\mathrm{S}i}}}{m_{\mathrm{T}i} + g_{\mathrm{T}i} + D_{ix}\frac{a_{\mathrm{S}i}g_{\mathrm{S}i}}{m_{\mathrm{T}i}+g_{\mathrm{T}i}}\frac{f_i}{m_{\mathrm{S}i}+g_{\mathrm{S}i}}} \\
\mathrm{R}^*_{ix} &\approx D_{ix}\frac{f_i}{m_{\mathrm{S}i} + g_{\mathrm{S}i}} \frac{g_{\mathrm{T}i}\, g_{\mathrm{S}i}}{m_{\mathrm{R}i}(m_{\mathrm{T}i} + g_{\mathrm{T}i})} \frac{1}{1 + D_{ix}\frac{a_{\mathrm{S}i}g_{\mathrm{S}i}}{(m_{\mathrm{T}i}+g_{\mathrm{T}i})^2}\frac{f_i}{m_{\mathrm{S}i}+g_{\mathrm{S}i}}}
\end{aligned} \tag{4.18}$$

$G\big(S_{ix}(t),\, T_{ix}(t), R_{ix}(t)\big) = \frac{1}{1+a^{'}_{Ti}T_{ix}(t)}$

Similar to above, linearizations are performed to produce a relatively simple expression for T^*_{ix}. The Ordinary Differential Equation gives:

$$\frac{d\mathrm{T}_{ix}(t)}{dt} = g_{\mathrm{S}i}\mathrm{S}^*_{ix} - m_{\mathrm{T}i}\mathrm{T}^*_{ix} - g_{\mathrm{T}i}\mathrm{T}^*_{ix}\frac{1}{1 + a^{'}_{\mathrm{S}i}\mathrm{T}^*_{ix}} = 0 \tag{4.19}$$

for which I make two simplifications. First, I take the geometric expansion: $\frac{1}{1+a^{'}_{\mathrm{S}i}\mathrm{T}^*_{ix}} \approx 1 - a^{'}_{\mathrm{S}i}\mathrm{T}^*_{ix}$. Then, the above can be expressed as:

$$g_{\mathrm{S}i}\mathrm{S}^*_{ix} - \mathrm{T}^*_{ix}\big(m_{\mathrm{T}i} + g_{\mathrm{T}i} - a^{'}_{\mathrm{S}i}\mathrm{T}^*_{ix}\big) = 0 \tag{4.20}$$

Then, dividing each side of the equation by $m_{\mathrm{T}i} + g_{\mathrm{T}i} - a_{\mathrm{S}i}^{'}\mathrm{T}_{ix}^{*}$ and doing so rearranging yields

$$\frac{1}{m_{\mathrm{T}i} + g_{\mathrm{T}i}} \frac{g_{\mathrm{S}i}\mathrm{S}_{ix}^{*}}{1 - \frac{a_{\mathrm{S}i}^{'}\mathrm{T}_{ix}^{*}}{m_{\mathrm{T}i}+g_{\mathrm{T}i}}} - \mathrm{T}_{ix}^{*} = 0 \tag{4.21}$$

Taking the geometric series of the right had expression (as in the above section) yields

$$\frac{1}{m_{\mathrm{T}i} + g_{\mathrm{T}i}} g_{\mathrm{S}i}\mathrm{S}_{ix}^{*}\left(1 + \frac{a_{\mathrm{S}i}^{'}\mathrm{T}_{ix}^{*}}{m_{\mathrm{T}i} + g_{\mathrm{T}i}}\right) - \mathrm{T}_{ix}^{*} = 0 \tag{4.22}$$

With these simplifications, it is straightforward to solve for T_{ix}^{*} and R_{ix}^{*}, which ultimately yields

$$\begin{aligned}
\mathrm{T}_{ix}^{*} &\approx \frac{g_{\mathrm{S}i}\mathrm{S}_{ix}^{*}}{m_{\mathrm{T}i} + g_{\mathrm{T}i} - \mathrm{S}_{ix}^{*}\frac{a_{\mathrm{S}i}}{m_{\mathrm{T}i}+g_{\mathrm{T}i}}} = \frac{D_{ix}g_{\mathrm{S}i}\frac{f_i}{m_{\mathrm{S}i}+g_{\mathrm{S}i}}}{m_{\mathrm{T}i} + g_{\mathrm{T}i} + D_{ix}\frac{a_{\mathrm{T}i}g_{\mathrm{S}i}}{m_{\mathrm{T}i}+g_{\mathrm{T}i}}\frac{f_i}{m_{\mathrm{S}i}+g_{\mathrm{S}i}}} \\
\mathrm{R}_{ix}^{*} &\approx D_{ix}\frac{f_i}{m_{\mathrm{S}i} + g_{\mathrm{S}i}} \frac{g_{\mathrm{T}i}\, g_{\mathrm{S}i}}{m_{\mathrm{R}i}(m_{\mathrm{T}i} + g_{\mathrm{T}i})} \frac{1}{1 + D_{ix}\frac{a_{\mathrm{TS}i}^{'}m_{\mathrm{T}i}g_{\mathrm{S}i}}{(m_{\mathrm{T}i}+g_{\mathrm{T}i})^2}\frac{f_i}{m_{\mathrm{S}i}+g_{\mathrm{S}i}}}
\end{aligned} \tag{4.23}$$

Seedling recruits induce NDD

$M\big(S_{ix}(t), T_{ix}(t), R_{ix}(t)\big) = a_{Ri}R_{ix}(t)$

Solving for T_{ix}^{*} is straightforward and can be done exactly. This yields

$$\mathrm{T}_{ix}^{*} = \frac{1}{m_{\mathrm{T}i} + g_{\mathrm{T}i}} \frac{g_{\mathrm{S}i}\mathrm{S}_{ix}^{*}}{1 + \frac{a_{\mathrm{R}i}\mathrm{R}_{ix}^{*}}{m_{\mathrm{T}i}+g_{\mathrm{T}i}}} = \frac{1}{m_{\mathrm{T}i} + g_{\mathrm{T}i}} \frac{D_{ix}g_{\mathrm{S}i}\frac{f_i}{m_{\mathrm{S}i}+g_{\mathrm{S}i}}}{1 + \frac{a_{\mathrm{R}i}\mathrm{R}_{ix}^{*}}{m_{\mathrm{T}i}+g_{\mathrm{T}i}}} \tag{4.24}$$

and then, the ODE describing recruit abundance is at equilibrium when

$$\frac{d\mathrm{R}_{ix}(t)}{dt} = g_{\mathrm{T}i}\frac{1}{m_{\mathrm{T}i} + g_{\mathrm{T}i}} \frac{g_{\mathrm{S}i}\mathrm{S}_{ix}^{*}}{1 + \frac{a_{\mathrm{R}i}\mathrm{R}_{ix}^{*}}{m_{\mathrm{T}i}+g_{\mathrm{T}i}}} - m_{\mathrm{R}i}\mathrm{R}_{ix}^{*} = 0 \tag{4.25}$$

This equation can be solved directly. However, it yields a simpler expression to take the first term of the geometric expansion of $\frac{1}{1+\frac{a_{\mathrm{R}i}\mathrm{R}_{ix}}{m_{\mathrm{T}i}+g_{\mathrm{T}i}}}$, which gives

$$g_{\mathrm{T}i}\frac{1}{m_{\mathrm{T}i} + g_{\mathrm{T}i}} g_{\mathrm{S}i}\mathrm{S}_{ix}^{*}\left(1 - \frac{a_{\mathrm{R}i}\mathrm{R}_{ix}^{*}}{m_{\mathrm{T}i} + g_{\mathrm{T}i}}\right) - m_{\mathrm{R}i}\mathrm{R}_{ix}^{*} = 0 \tag{4.26}$$

which is straightforward to solve. This gives

$$\mathrm{R}^*_{ix} \approx D_{ix} \frac{f_i}{m_{\mathrm{S}i} + g_{\mathrm{S}i}} \frac{g_{\mathrm{T}i}\, g_{\mathrm{S}i}}{m_{\mathrm{R}i}(m_{\mathrm{T}i} + g_{\mathrm{T}i})} \frac{1}{1 + D_{ix} \frac{a_{\mathrm{R}i} g_{\mathrm{S}i} g_{\mathrm{T}i}}{(m_{\mathrm{T}i} + g_{\mathrm{T}i})^2} \frac{f_i}{m_{\mathrm{S}i} + g_{\mathrm{S}i}}} \tag{4.27}$$

$G\big(S_{ix}(t),\, T_{ix}(t),\, R_{ix}(t)\big) = \frac{1}{1 + a^{'}_{Ri} R_{ix}(t)}$

As in the above section, solving for T^*_{ix} is straightforward and can be done exactly. This yields

$$\mathrm{T}^*_{ix} = \frac{1}{m_{\mathrm{T}i} + g_{\mathrm{T}i}} \frac{g_{\mathrm{S}i} \mathrm{S}^*_{ix} \big(1 + a^{'}_{\mathrm{R}i} \mathrm{R}^*_{ix}\big)}{1 + \frac{a^{'}_{\mathrm{R}i} m_{\mathrm{T}i} \mathrm{R}^*_{ix}}{m_{\mathrm{T}i} + g_{\mathrm{T}i}}} = \frac{1}{m_{\mathrm{T}i} + g_{\mathrm{T}i}} \frac{D_{ix} g_{\mathrm{S}i} \frac{f_i}{m_{\mathrm{S}i} + g_{\mathrm{S}i}} \big(1 + a^{'}_{\mathrm{R}i} \mathrm{R}^*_{ix}\big)}{1 + \frac{a^{'}_{\mathrm{R}i} m_{\mathrm{T}i} \mathrm{R}^*_{ix}}{m_{\mathrm{T}i} + g_{\mathrm{T}i}}} \tag{4.28}$$

and then, the ODE describing recruit abundance is at equilibrium when

$$\frac{d\mathrm{R}_{ix}(t)}{dt} = g_{\mathrm{T}i} \frac{1}{m_{\mathrm{T}i} + g_{\mathrm{T}i}} \frac{g_{\mathrm{S}i} \mathrm{S}^*_{ix} \big(1 + a^{'}_{\mathrm{R}i} \mathrm{R}^*_{ix}\big)}{1 + \frac{a^{'}_{\mathrm{R}i} \mathrm{R}^*_{ix} m_{\mathrm{T}i}}{m_{\mathrm{T}i} + g_{\mathrm{T}i}}} \frac{1}{\big(1 + a^{'}_{\mathrm{R}i} \mathrm{R}^*_{ix}\big)} - m_{\mathrm{R}i} \mathrm{R}^*_{ix} = 0 \tag{4.29}$$

Firstly, the term $1 + a^{'}_{\mathrm{R}i} \mathrm{R}^*_{ix}$ will cancel. This equation can be solved directly, but (once again) it yields a simpler expression to take the first term of the geometric expansion of $\frac{1}{1 + \frac{a^{'}_{\mathrm{R}i} \mathrm{R}^*_{ix}}{m_{\mathrm{T}i} + g_{\mathrm{T}i}}}$. This gives

$$g_{\mathrm{T}i} \frac{1}{m_{\mathrm{T}i} + g_{\mathrm{T}i}} g_{\mathrm{S}i} \mathrm{S}^*_{ix} \left(1 - \frac{a^{'}_{\mathrm{R}i} m_{\mathrm{T}i} \mathrm{R}^*_{ix}}{m_{\mathrm{T}i} + g_{\mathrm{T}i}}\right) - m_{\mathrm{R}i} \mathrm{R}^*_{ix} = 0 \tag{4.30}$$

which is straightforward to solve. This gives

$$\mathrm{R}^*_{ix} \approx D_{ix} \frac{f_i}{m_{\mathrm{S}i} + g_{\mathrm{S}i}} \frac{g_{\mathrm{T}i}\, g_{\mathrm{S}i}}{m_{\mathrm{R}i}(m_{\mathrm{T}i} + g_{\mathrm{T}i})} \frac{1}{1 + D_{ix} \frac{a^{'}_{\mathrm{R}i} g_{\mathrm{S}i} g_{\mathrm{T}i} m_{\mathrm{T}i}}{(m_{\mathrm{T}i} + g_{\mathrm{T}i})^2} \frac{f_i}{m_{\mathrm{S}i} + g_{\mathrm{S}i}}} \tag{4.31}$$

Seed-to-Seedling Transition Analysis for Regression Fit

In the main text, I describe a spatially explicit model for which fits of the equation

$$\mathrm{R}_{ix} = \alpha_i \mathrm{S}^{\beta_i}_{ix} \tag{4.32}$$

are performed. R_{ix} and S_{ix} represent seed and newly emerged seedling recruit abundance of species i at location x, respectively, α_i represents baseline seed-to-seedling survival of species i, and β_i is a metric of the strength of CNDD of species i ($\beta_i = 1$ implies no CNDD and $\beta_i < 1$ implies species i experiences CNDD). Here, I provide additional details on the simulations and the assumptions therein.

General simulation details

I generate a 200×200 grid on which each grid-cell contains a single adult tree. I randomly assign each grid-cell a value between 1 and 20, which indexes a species. Arbitrarily, I examine species 1. Species 1 distributes seeds in space. The number of seeds species i disperses to location x is given by $S_0 \times D_{ix}$ where S_0 is the total seeds eachh adult disperses and D_{ix} is the seed rain density of species i at location x (reflecting the location of nearby adults; see the below section). With regards to equation 4.9, $S_0 \times D_{ix}$ serves as the initial abundance of seeds of species i at patch x. Similarly, I assume $f_i = 0$ (all seeds at location x come from the initially dispersed seeds) and $m_{\mathrm{R}i} = 0$ (all individuals that successfully recruit are counted). This more realistically reflects measurements, which examine the number of seedling recruits that emerge from an initial pool of seeds counted in nearby seed traps.

Dispersal kernel

In this section, I show the details of the term D_{ix} (seed rain density) that is used for the spatially explicit and fits of equation 4.32. I define the dispersal kernel similarly to Stump and Comita (2020).

For computational efficiency, I work with Manhattan distances rather than Euclidean distances (i.e. the distance between two points (a_1, b_1) and (a_2, b_2) is $|a_1 - a_2| + |b_1 - b_2|$ rather than $\sqrt{(a_1 - a_2)^2 + (b_1 - b_2)^2}$. Simulations indicate this assumption does not affect results (particularly because all that matters for the fits is that patches exhibit variation in the initial number of seeds). I assume distances between patches are defined by the Manhattan distance between their centers.

I model dispersal with a discrete approximation of a 2-Dimensional exponential distribution using the function:

$$E_i(z) = 2\pi z \frac{1}{2\pi\sigma_{Di}^2} e^{-z/\sigma_{Di}} \tag{4.33}$$

where $E_i(z)$ defines the probability that a seed of species i lands a distance of z meters away and σ_{Di} defines how dispersal of species i declines with distance. Note that $2\pi z$ is on the numerator (algebraically, the 2π terms cancel, but I leave things in this format because it is easier to understand this way). As noted by Stump and Comita (2020), this formulation of $E_i(z)$ defines the probability an adult of species i disperses a seed anywhere a distance of z meters away.

Using this, I calculate the probability of seed dispersal to a given distance z meters away. Let L represent the distance between the center-points of patches in meters, and let v represent the number of patch centers between locations. For computational efficiency, I assume trees disperse no seeds farther than 50 patch-lengths away (I ignore when $v > 50$). Under the parameterizations of this study, this accounts for over 99.9% of seeds a tree produces. Then, the probability a seed of species i lands on an individual patch v spaces away (henceforth $d_i(z)$) is equal to

$$d_i(z) = \begin{cases} \int_0^{0.5\,L} E_i(s)ds & v = 0 \\ \frac{1}{4v}\int_{L(v-0.5)}^{L(v+0.5)} E_i(s)ds & 1 \leq v \leq 50 \\ 0 & v > 50 \end{cases} \tag{4.34}$$

Integrals are taken in intervals of $0.5L$ because integrating throughout the entire length of the patch relative to the center point entails integrating over half a patch length (i.e. expanding the radius of the patch relative ot the center). Also note the second integral is divided by $4v$ because there are always $4v$ sites of distance v from a central point under Manhattan distance. This formulation makes the assumption that integrating radially over discrete square grid-cells is an adequate approximation.

The seed rain density at location x of species i, D_{ix}, can be calculated by summing over the proportion of seeds dispersed by all adults of species i to location x. Let z_{ix} represent the distance

of the z_{th} closest patch to x occupied by species i. Then,

$$D_{ix} = \sum_{\text{all } z} d_i(z_{ix}) \tag{4.35}$$

This implementation is used in the simulations.

Derivation of Invasion Criteria

General Setup

As noted in the main text, I examine how demographic traits and CNDD impact species diversity using a simple competition model. I consider a community of X patches on which each patch contains an adult tree. Adult trees disperse a fixed proportion of their seeds, D, uniformly throughout the environment and locally disperse the remaining $1 - D$ seeds on the local patch (x). Therefore, x now indexes the identity of the tree occupying the patch. Then, let D_{ii} and D_{ik} represent the proportion of seeds of species i dispersed to patches occupied by species i and j, respectively ($i \neq j$). Then, $D_{ii} = 1 - D + p_i D$ and $D_{ik} = p_i D$ where p_i is the proportion of patches occupied by species i. Adults of each species die at rate δ. When an adult dies, it is replaced by a randomly selected individual in the plot weighted by a species-specific competitive ability parameter, C (a lottery model). Therefore, the probability species i replaces a patch occupied by species k is: $\mathrm{R}^*_{ik} C_i / \sum_{\text{all } j} R^*_{jk} C_j$.

The simplified form of dispersal limitation means that the model can be described spatially implicitly (patches need only be described by the occupant but not their absolute position). Therefore, adult dynamics can be described by the following system of Ordinary Differential Equations:

$$\frac{dp_i}{dt} = \delta \left[\frac{\mathrm{R}^*_{ii} C_i}{\sum_{\text{all } j} \mathrm{R}^*_{ji} C_j} p_i + \sum_{k \neq i} \frac{\mathrm{R}^*_{ik} C_i}{\sum_{\text{all } j} \mathrm{R}^*_{jk} C_j} p_k - p_i \right] \tag{4.36}$$

For numerical implementations, I use exact values for R^*_{ii} and R^*_{ji}. For the invasion criteria, I use the approximate values derived in the above section. The recruit equilibrium abundances are equal

to:

$$
\begin{aligned}
R^*_{ii} &= \underbrace{\big[(1-D)+p_iD\big]\frac{f_i}{g_{\mathrm{S}_i}+m_{\mathrm{S}_i}}\frac{g_{\mathrm{S}_i}g_{\mathrm{T}_i}}{g_{\mathrm{T}_i}+m_{\mathrm{T}_i}}}_{\text{Baseline Recruit density}}\underbrace{\frac{1}{1+\big[(1-D)+p_iD\big]\rho_i}}_{\text{CNDD strength}} \\
R^*_{ik} &= \underbrace{p_iD\frac{f_i}{g_{\mathrm{S}_i}+m_{\mathrm{S}_i}}\frac{g_{\mathrm{S}_i}g_{\mathrm{T}_i}}{g_{\mathrm{T}_i}+m_{\mathrm{T}_i}}}_{\text{Baseline Recruit density}}\underbrace{\frac{1}{1+p_iD\rho_i}}_{\text{CNDD strength}}
\end{aligned}
\tag{4.37}
$$

noting that, for future notation, let

$$
Y_i = C_i\frac{f_i}{g_{\mathrm{S}_i}+m_{\mathrm{S}_i}}\frac{g_{\mathrm{S}_i}g_{\mathrm{T}_i}}{g_{\mathrm{T}_i}+m_{\mathrm{T}_i}} \tag{4.38}
$$

and that the values of ρ are summarized in Table 4.1 of the main text.

In addition, I use the notation

$$
I_i = \sum_{\text{all } j}\mathrm{R}^*_{ji}C_j = \big[(1-D)+p_iD\big]Y_i\frac{1}{1+\big[(1-D)+p_iD\big]\rho_i} + D\sum_{j\neq i}p_jY_j\frac{1}{1+p_jD\rho_j} \tag{4.39}
$$

which will be convenient in the derivation.

Derivation

I follow provide a derivation of the invasion criteria similar to Stump and Comita (2018).

Basic Setup

Firstly, based on the ODE, species i can invade if its growth rate is greater than zero. That is, letting r_i represent the per capita growth rate of species i scaled by adult mortality rate, or

$$
\frac{1}{p_i}\frac{1}{\delta}\frac{dp_i}{dt} = r_i = \left((1-D)+p_iD\right)\frac{Y_i\frac{1}{1+(1-D+p_iD)\rho_i}}{I_i} + D\sum_{k\neq i}\frac{p_iY_i\frac{1}{1+p_iD\rho_i}}{I_k} - 1 \tag{4.40}
$$

Species i can invade if $r_i > 0$. The below analytical treatment is to obtain a relatively simple expressions for the right-hand-side terms in the above expression.

Firstly, note that if A/B does not differ very largely from one, the approximation $A/B \approx 1+\log A-\log B$ serves as a good approximation. In the context of the model, a useful approximation to make is

$$\begin{aligned}\frac{Y_i\frac{1}{1+(1-D+p_iD)\rho_i}}{I_i} &\approx 1+\log Y_i-\log\big(1+(1-D+p_iD)\rho_i\big)-\log I_i \\ &\approx 1+\log Y_i-\log\big(1+(1-D)\rho_i\big)-p_iD\rho_i-\log I_i\end{aligned} \tag{4.41}$$

noting that $\log(A+B)\approx\log(A)+B$ if B is fairly small, which is used for the approximation $\log\big(1+(1-D+p_iD)\rho_i\big)\approx\log\big(1+(1-D)\rho_i\big)+p_iD\rho_i$.

Using similar methods to above,

$$\frac{Y_i\frac{1}{1+p_iD\rho_i}}{I_k}\approx 1+\log Y_i-p_iD\rho_i-\log I_k \tag{4.42}$$

noting that these approximations assume "small effects" which implies fitness differences and the strength of CNDD are not *very* large.

Approximation of I_i term

In this section, I derive a simplification for I_i. I make several changes in notation for this section, as follows:

$$\begin{aligned}y_i &= \frac{Y_i}{\overline{Y}} \\ y_k &= \frac{Y_k}{\overline{Y}} \\ \rho_i' &= \big[(1-D)+p_iD\big]\rho_i \\ \rho_k' &= p_kD\rho_k\end{aligned} \tag{4.43}$$

where $\overline{Y}$ represents the mean intrinsic fitness of the community. These simplifications will help in simplifying the expression. Then, it follows that

$$\frac{I_i}{\overline{Y}} = y_j\big[(1-D)+p_iD\big]\frac{1}{1+\rho_i'}+D\sum_{k\neq i}y_kp_k\frac{1}{1+\rho_k'} \tag{4.44}$$

I then take the linearization of the right hand side of this expression around the points $y_i = y_k = 1$ and $\rho'_i = \rho'_k = 0$. That is, letting F represent a function depicts the right hand side of the above equation,

$$\begin{aligned}
\frac{I_i}{\overline{Y}} &= F(y_i, y_k, \rho'_i, \rho'_k) \\
&\approx F(1,1,0,0) + F'_{y_i}(1,1,0,0)(y_i - 1) + F'_{y_k}(1,1,0,0)(y_k - 1) \\
&\quad + F'_{\rho'_i}(1,1,0,0)\rho' + F'_{\rho'_i}(1,1,0,0)\rho'_i \\
&= 1 + (y_i - 1)\big[1 - D + p_i D\big] + D\sum_{k\neq i}(y_k - 1)p_k - \rho'_i\big[1 - D + p_i D\big] - D\sum_{k\neq i} p_k \rho'_k
\end{aligned} \tag{4.45}$$

noting that F'_x indicates the derivative of F with respect to x. Then, substituting back in

$$\begin{aligned}
\rho'_i &= \big[(1 - D) + p_i D\big]\rho_i \\
\rho'_k &= p_k D \rho_k
\end{aligned} \tag{4.46}$$

and doing some rearranging of the above expression yields

$$\frac{I_i}{\overline{Y}} \approx 1 + (y_i - 1)(1 - D) + D\sum_{\text{all } k}(y_k - 1)p_k - \rho_i\big[(1 - D)^2 + 2D(1 - D)p_i\big] - D^2\sum_{\text{all } k} p_k^2 \rho_k \tag{4.47}$$

then, assuming y is not very different from 1, one can make the approximation that $y_i = \frac{Y_i}{\overline{Y}} \approx 1 + \log Y_i - \log \overline{Y}$. Substituting this into the Equation 4.47 then yields

$$\frac{I_i}{\overline{Y}} \approx 1 + \log Y_i(1 - D) + \underbrace{D\sum_{\text{all } k}\log Y_k p_k}_{\gamma_Y} - \rho_i\big[(1 - D)^2 + 2D(1 - D)p_i\big] - \underbrace{D^2\sum_{\text{all } k} p_k^2 \rho_k}_{\gamma_\rho} \tag{4.48}$$

noting the terms in braces, which will be substituted into the following expressions.

Furthermore, if the fitness of a particular species on a patch, I_i, does not vary that much from the mean fitness ($\overline{Y}$), one can make the approximation that $\frac{I_i}{\overline{Y}} \approx 1 + \log I_i - \log \overline{Y}$. Then, substituting this into equation 4.48 and doing some rearring gives

$$\log I_i \approx (1 - D)\log Y_i + \gamma_Y - \rho_i\big[(1 - D)^2 + 2D(1 - D)p_i\big] - \gamma_\rho \tag{4.49}$$

Additionally, if ρ_i is relative small, $\rho(1-D) \approx \log\big(1+\rho(1-D)\big)$. Then, the above can be rearranged as

$$\log I_i \approx (1-D)\log Y_i + \gamma_Y - (1-D)\log\big(1+\rho_i(1-D)\big) + 2D(1-D)p_i - \gamma_\rho \tag{4.50}$$

which will be useful for combining and canceling several terms.

Simplification of growth rate

Returning to Equation 4.40 and substituting some of the above approximations, species i's growth rate is

$$\begin{aligned} r_i \approx \Big(1 - D + p_i D\Big)\Big(1 + \log Y_i - \log\big(1+\rho_i(1-D)\big) - Dp_i\rho_i - \log I_i\Big) \\ + D\sum_{k\neq i} p_k\big(1 + \log Y_i - p_i D\rho_i - I_k\big) - 1 \end{aligned} \tag{4.51}$$

From here, it is useful to make several simplifications. Firstly, note that the term $D\sum_{k\neq i} p_k(-p_i D\rho_i)$ can be taken out of the summation, which can be rearranged as $-D^2 p_i D\rho_i \sum_{k\neq i} p_k = D^2 p_i\rho_i(1-p_i)$ noting that $\sum_{k\neq i} p_k = 1-p_i$ on the basis that $\sum_{\text{all } k} p_k = 1$. Similarly, several terms can be moved in and outside of the summation. Doing this and canceling several terms yields the expression:

$$\begin{aligned} r_i \approx \log Y_i - (1-D)\log\big(1+\rho_i(1-D)\big) - p_i D\log\big(1+\rho_i(1-D)\big) \\ - (1-D)Dp_i\rho_i - D^2\rho_i p_i - (1-D)\log I_i - D\underbrace{\sum_{\text{all } k} p_k I_k}_{\gamma_\Sigma} \end{aligned} \tag{4.52}$$

From here, it is convenient to make an additional approximation by letting $p_i D\log\big(1+\rho_i(1-D)\big)$ $\approx p_i\rho_i(1-D)D$ (similar to the approximation from earlier). Then, the above expression becomes

$$r_i \approx \log Y_i - (1-D)\log\big(1+\rho_i(1-D)\big) - D(2-D)p_i\rho_i - (1-D)\log I_i - D\gamma_\Sigma \tag{4.53}$$

noting $\sum_{\text{all } k} p_k I_k = \gamma_\Sigma$. Then, substituting Equation 4.50 for $\log I_i$, this yields

$$\begin{aligned} r_i \approx\ & D(2-D)\log Y_i - D(1-D)\log\big(1+\rho_i(1-D)\big) \\ & - D^2(3-2D)p_i\rho_i - (1-D)\gamma_Y + (1-D)\gamma_\rho - D\gamma_\Sigma \end{aligned} \tag{4.54}$$

From here, it is useful to use a property first highlighted by Chesson (1994). If the resident species are at equilibrium, it follows that their growth rates are at zero. Therefore,

$$r_i = r_i - \frac{1}{N}\sum_{k\neq i} r_k \tag{4.55}$$

which is convenient for canceling several terms. Plugging the appropriate values of r_k from equation 4.53 into the summation yields

$$\begin{aligned} \frac{1}{N}\sum_{k\neq i} r_k = \frac{1}{N}\sum_{k\neq i}\Big[& D(2-D)\log Y_k - D(1-D)\log\big(1+\rho_k(1-D)\big) \\ & - D^2(3-2D)p_k\rho_k - (1-D)\gamma_Y + (1-D)\gamma_\rho - D\gamma_\Sigma\Big] \\ = D(2-D)\overline{\log Y} & - D(1-D)\overline{\log\big(1+\rho(1-D)\big)} \\ & - \frac{1}{N}D^2(3-2D)\sum_{k\neq i} p_k\rho_k - (1-D)\gamma_Y + (1-D)\gamma_\rho - D\gamma_\Sigma \end{aligned} \tag{4.56}$$

Then, by noting the property $\mathbb{E}[AB] = \overline{AB} + \text{Cov}(A,B)$ where $\overline{A}$ denotes the mean of A (i.e. $\mathbb{E}(A) = \overline{A}$), it follows that

$$\begin{aligned} \frac{1}{N}\sum_{k\neq i} p_k\rho_k &= \overline{p}\,\overline{\rho} + \text{Cov}(p,\rho) \\ &= \frac{\overline{\rho}}{N} + \text{Cov}(p,\rho) \end{aligned} \tag{4.57}$$

Then, to calculate the invader growth rate of species i, I substitute Equation 4.57 into Equation 4.56, which I then substitute with along with Equation 4.54 into Equation 4.55. Additionally, I take the limit of the resulting expression as $p_i \to 0$, which yields the growth rate of species i when it is rare in the community. Doing so, several terms will cancel and, ultimately, yield an expression

which is conveniently expressed as

$$r_i \approx \Delta Y_i + \Delta \rho_i + P_i \tag{4.58}$$

where

$$\begin{aligned}
\Delta Y_i &= D(2-D)\big(\log Y_i - \overline{\log Y}\big) \\
\Delta \rho_i &= D(1-D)\bigg(\log\big(1+(1-D)\rho_i\big) - \overline{\log\big(1+(1-D)\rho\big)}\bigg) \\
P_i &= D^2(3-2D)\bigg(\frac{\overline{\rho}}{N} + \mathrm{Cov}(p,\rho)\bigg)
\end{aligned} \tag{4.59}$$

where ΔY_i represents fitness differences induced by density-independent fitness, $\Delta \rho_i$ is the fitness difference related to CNDD (entirely dependent on ρ), and P_i is the stabilizing effect species i experiences due to CNDD (in essence, the advantage species i enjoys because it is rare).

Chapter 5

Masting, Janzen-Connell effects, and coexistence: a theoretical perspective

5.1 Abstract

Seed and seedling predation are potent forces of juvenile tree mortality and play an important role in determining recruitment. Many studies examine how Janzen-Connell effects – distance-dependent specialized seed and seedling predation – facilitate species coexistence by producing negative density dependence. At the same time, masting (synchronized inter-annual seed production) is frequently observed in perennial forest communities. Predator satiation generated by mast events are observed to saturate seed predator functional forms, leading to positively density-dependent seed survival. Current theory does not examine how negative density dependence generated by Janzen-Connell effects and positive density dependence created by masting interact to shape species coexistence in competitive communities. To fill this gap, I present a theoretical model that incorporates both processes. I show that masting can increase or decrease the ability of specialized predators to maintain species richness. First, I show that the ability of specialized predation to promote coexistence depends on the ratio of specialized predation to generalized predation that seeds experience. This result applies regardless as to whether masting occurs. Then, I show that the impact of masting on species richness depends on the relative non-linearity of the functional forms of specialists and generalists: masting promotes coexistence if specialists have less non-linear functional forms than

generalists and masting erodes coexistence if specialists have more non-linear functional forms that generalists. These results directly reflect how masting affects the relative importance of specialized predation relative to generalized predation.

5.2 Introduction

Seed and seedling predation are fundamental processes that shape plant communities (Crawley, 2000). Two forms of predation are frequently discussed in the literature: specialized predation and generalized predation. A large body of research investigates how seed predation impacts species coexistence (e.g. Janzen, 1970; Connell, 1971; Hubbell, 1980; Armstrong, 1989; Kuang and Chesson, 2009, 2010; Adler et al., 2013; Larios et al., 2017). Despite this, how interactions between generalist and specialist predators in temporally varying environments affect tree species diversity remains under-studied.

Masting, intra-specifically synchronized production of a large number of seeds over (most often) irregular periods of two or greater years, is an important source of temporal variation in forest communities. However, little theory examines how it affects tree coexistence. Masting is a common phenomenon for a large number of perennial trees worldwide (Janzen, 1971; Kelly and Sork, 2002; Koenig, 2021; Pesendorfer et al., 2021; Zwolak et al., 2022). A number of hypotheses have been suggested to explain the evolution of masting, including resource matching (seed production simply reflects yearly resource availability; Kelly, 1994), wind pollination (synchronous flowering increases pollination efficiency Janzen, 1978; Kelly and Sork, 2002), and predation satiation (Janzen, 1971). In this study, I will focus on predator satiation.

Predator satiation is based on a simple premise: trees produce a large numbers of seeds in synchrony (a mast event) such that they over-satiate the predators that consume them (Janzen, 1971; Silvertown, 1980). Due to this over-satiation, mast events increase the proportion of seeds that escape predation. More formally, if it is assumed that seed predators have non-linear (concave-down) type II functional responses (Holling, 1959), inter-annual variation in seed production will reduce the mean predation seeds experience (due to non-linear averaging; Jensen's inequality; Jensen, 1906)

decreasing seed predation and seed predator growth rate. Simultaneously, gaps between mast events may starve seed predators, further reducing seed predator abundance and predation during mast events (Salisbury et al., 1942; Kelly and Sullivan, 1997; Kelly and Sork, 2002). These processes are thought to jointly increase the proportion of seeds that escape predation on mast years. Notably, I do not claim that predator satiation is the ultimate evolutionary cause of masting; rather, I simply note that there is empirical evidence masting leads to predator satiation in a large number of communities worldwide (e.g. Zwolak et al., 2022). Therefore, it is important to elucidate its impact on species coexistence.

At the same time, Janzen Connell effects (JCEs) are widely thought to play an important role in maintaining species richness in a number of forest communities (Janzen, 1970; Connell, 1971; Wright, 2002; Terborgh, 2012). JCEs are a specialized-predation-based species coexistence mechanism: JCEs posit that distance-dependent specialized predators of seeds and seedlings are attracted to adults and locally reduce offspring survival. Empirical evidence strongly suggests that JCEs occur in a number of systems (e.g. Hyatt et al., 2003; Petermann et al., 2008; Mangan et al., 2010; Swamy and Terborgh, 2010; Johnson et al., 2012; Comita et al., 2014; Bever et al., 2015; Hazelwood et al., 2021). The logic behind how JCEs maintain diversity is relatively straightforward: as a species becomes more common, its specialized predators occupy an increasingly large proportion of the environment, generating stabilizing negative frequency dependence.

Both ideas (JCEs and predator satiation) were proposed (or, at least, popularized) by Daniel Janzen despite their potentially contradictory implications: predation satiation (i.e. the saturating of a functional response) yields *positive* density dependence while specialized predation (i.e. JCEs) depend on negative density dependence (Janzen, 1970, 1971; Connell, 1971). While past work has noted the potential tension between these processes (e.g. Janzen, 1978; Koenig et al., 2003), only relatively recent empirical work that examines their potentially antagonistic interactions (Xiao et al., 2017; Bogdziewicz et al., 2018; Cannon et al., 2020; Martini et al., 2022; O'Brien et al., 2022). Moreover, theoretical investigations of their interactions are virtually non-existent. As a recent analysis shows that generalist and specialist predators alike experience satiation induced by mast events (Zwolak et al., 2022), it is important to develop a theoretical understanding of how interactions

between generalist predation, specialist predation, and masting affect species coexistence. This is particularly pertinent given recent evidence that the impacts of masting on predator satiation are changing (Zwolak et al., 2022).

To this end, I analyze a model incorporating generalist predation, localized specialist predation (as described by JCEs) and seed masting. I report two key results. First, I show that the ability of specialized predation to maintain coexistence fundamentally depends on the ratio of specialized predation to generalized predation that species experience. Second, I find that the impact of masting on species diversity depends on the relative of non-linearity of the functional responses of generalist and specialist predators. Ultimately, masting is stabilizing (promotes coexistence) if predator satiation affects generalists more than specialists and destabilizing if predation satiation impacts specialists more than generalists. I then discuss how this process may impact empirical measurements of negative density dependence and discuss future avenues of theoretical research.

5.3 Methods

5.3.1 Model

I consider a patch occupancy model that incorporates specialist predation, generalist predation, and seed masting. The community consists of L patches and N tree species. Each patch is occupied by a single adult tree that disperses seeds throughout the community. Masting events are incorporated into the model by assuming temporal variation in seed production rate (see below). Each patch contains seeds and a specialist seed predator; a single generalist species persists in the community that attacks seeds on every patch.

First, I describe seed dynamics. Adult trees of species i uniformly disperse seeds throughout the community at rate $f_i\big(X_i(t)\big)$ (defined below) in which case $f_i\big(X_i(t)\big)p_i$ seeds are dispersed to each patch where p_i is the proportion of patches occupied by adults of species i in the population. Seeds of species i die at density-independent mortality rate m_i and experience generalized predation (see below) on all patches. Seeds of species i on patches occupied or previously occupied by species i additionally experience mortality due to specialized predation (see below). Overall, seed dynamics

are described by

$$\begin{aligned}\frac{d\mathrm{S}_{ii}}{dt} &= f_i\big(X_i(t)\big)p_i - m_i\mathrm{S}_{ii} - \mathrm{P}_i F^i_{\mathrm{P}}\big(\mathrm{S}_{ii}\big)\mathrm{S}_{ii} - \mathrm{P}_{\mathrm{G}} F_{\mathrm{G}}\big(\mathbf{S}\big)\mathrm{S}_{ii} \\ \frac{d\mathrm{S}_{ik}}{dt} &= f_i\big(X_i(t)\big)p_i - m_i\mathrm{S}_{ik} - \mathrm{P}_{\mathrm{G}} F_{\mathrm{G}}\big(\mathbf{S}\big)\mathrm{S}_{ik}\end{aligned} \tag{5.1}$$

where S_{ii} is the number of seeds of species i on patches occupied (or previously occupied) by species i and and S_{ik} is the number of seeds of species i on patches occupied (or previously occupied) by species k ($i = 1, 2, ..., N$, $k \neq i$). Note that the previous occupant of a patch is important because it determines which species specialized natural enemies are present and the seed composition therein. P_i and $F^i_{\mathrm{P}}\big(\mathrm{S}_{ii}\big)$ represent the abundance and functional form of specialized predators of species i, respectively (see below). P_{G} and $F_{\mathrm{G}}\big(\mathbf{S}\big)$ represent generalist predator abundance and the functional form of the generalist predator, respectively.

Masting is incorporated into the model with the function $f_i\big(X_i(t)\big)$:

$$f_i\big(X_i(t)\big) = \begin{cases} f_{0,i}, & \text{no mast event} \\ f_{M,i} & \text{mast event} \end{cases} \tag{5.2}$$

for which $f_{0,i}$ is species i's seed production rate on non-mast years and $f_{M,i}$ is species i's seed production rate on mast years. I assume that masting occurs on an annual schedule (i.e. a mast event increases seed production over the course of a year). Mast events of species i follow a random variable, $X_i(t)$. For simulations in this study, I assume mast years follow a Poisson process with variance σ^2.

Now, I describe the predators' population dynamics and functional forms. Given that there are N tree species, there are also N specialist seed predators. Specialized predators persist on patches occupied by adults of the patch of seeds they specialize on (in line with how JCEs are classically imagined). That is, I model an independent population of specialized predators on each patch occupied (or previously occupied) by species i and locally consume species i's seeds. I assume the generalist predators attack all seeds in the community at random (attacking all seeds on all patches at a constant rate, spending an equal amount of time on each of the L patches in the community).

The dynamics of all specialist predators and the generalist predator, respectively, are described by:

$$\begin{aligned}\frac{d\mathrm{P}_i}{dt} &= e_{\mathrm{P}}\mathrm{P}_i F_{\mathrm{P}}^{i}\big(\mathrm{S}_{ii}\big)\mathrm{S}_{ii} - m_{\mathrm{P}}\mathrm{P}_i \\ \frac{d\mathrm{P}_{\mathrm{G}}}{dt} &= e_{\mathrm{G}}\mathrm{P}_{\mathrm{G}} F_{G}^{\mathrm{all}}\big(\mathbf{S}\big) - m_{\mathrm{G}}\mathrm{P}_{\mathrm{G}}\end{aligned} \tag{5.3}$$

Importantly, the above equation for specialized predators (P_i, $i = 1, 2, ..., N$) describes their population dynamics on the local patch level (these dynamics occur separately on every patch occupied by species i). However, the equation for the generalist predator (P_{G}) describes its global population dynamics (the total number of generalists throughout the entire community). For both predators, I consider type II functional responses:

$$\begin{aligned}F_{\mathrm{P}}^{i}\big(\mathrm{S}_{ii}\big) &= \frac{a_{\mathrm{P}}}{1 + a_{\mathrm{P}}h_{\mathrm{P}}\mathrm{S}_{ii}} \\ F_{\mathrm{G}}\big(\mathbf{S}\big) &= \frac{1}{L}\frac{a_{\mathrm{G}}}{1 + a_{\mathrm{G}}h_{\mathrm{G}}\sum_{\mathrm{all}j}\sum_{\mathrm{all}k}\mathrm{S}_{kj}(p_j + E_j)} \\ F_{\mathrm{G}}^{\mathrm{all}}\big(\mathbf{S}\big) &= \frac{a_{\mathrm{G}}\sum_{\mathrm{all}j}\sum_{\mathrm{all}k}\mathrm{S}_{kj}(p_j + E_j)}{1 + a_{\mathrm{G}}h_{\mathrm{G}}\sum_{\mathrm{all}j}\sum_{\mathrm{all}k}\mathrm{S}_{kj}(p_j + E_j)}\end{aligned} \tag{5.4}$$

$F_{\mathrm{P}}^{i}\big(\mathrm{S}_{ii}\big)$ is the functional response of specialist predators of species i (which quantifies the effect of specialized natural enemies on individual patches). $F_{\mathrm{G}}\big(\mathbf{S}\big)$ is the functional response of the generalist predator on individual patches (i.e. it quantifies how generalists attack seeds of each species on individual patches). $F_{\mathrm{G}}^{\mathrm{all}}$ describes the overall (population-level) rate at which seeds are consumed by generalists (i.e. it quantifies generalist predation over all patches). a_{G} is the generalist predator attack rate, a_{P} is the specialist predator attack rate, h_{G} is the generalist predator handling time, h_{P} is the specialist predator handling time, L is the number of patches in the community, and E_j is the proportion of patches in the community that were previously occupied by species j but are now unoccupied (see below for details). $F_{\mathrm{G}}\big(\mathbf{S}\big)$ contains a $1/L$ term because it is used to calculate seed *per patch* seed consumption rate. Notably, as long as it is assumed that there are enough patches that no species stochastically goes extinct, the value of L does not affect community dynamics. Larger L increases the number of patches in the community and decreases the amount of time each generalist spends on each patch (in which case, larger L increases *total* generalist

abundance, but does not affect its impact on any individual patch). Simulations confirm that the value of L does not affect seed and tree dynamics.

Now, I describe adult dynamics. Adults occupying patches die at rate δ. Upon the death of the adult, the patch enters an "empty" state, E (e.g. $p_i \rightarrow E_i$). After a patch is emptied, I assume the specialist predator previously occupying the patch stays the same until the patch is colonized by another species (noting that the specialist predator's population is maintained by seeds currently located on and dispersed to the patch). The tree that colonizes a patch is determined by a lottery model (i.e. the probability a species colonizes a patch is proportional to the number of its seeds on it Chesson and Warner, 1981). The rate at which empty patches are colonized depends on the number of seeds on the patch (described by ϕ, see below). With this, adult tree dynamics and empty patch dynamics are described by

$$\begin{aligned} \frac{dp_i}{dt} &= \sum_{\text{all } k} \frac{\mathrm{S}_{ik} C_i}{\sum_{\text{all } j} \mathrm{S}_{jk} C_j} E_k \phi_k - \delta p_i \\ \frac{dE_i}{dt} &= \delta p_i - E_i \phi_i \end{aligned} \tag{5.5}$$

where C_i represents the relative competitive ability of species i and E_i is the proportion of patches previously occupied by species i that are vacated. ϕ_k is the rate at which a vacated patch previously occupied by k gets occupied. I assume

$$\phi_k = c\left[1 - \exp\left(- g \sum_{\text{all } j} S_{jk} \right)\right] \tag{5.6}$$

where c is the maximum possible colonization rate and g is a constant that defines the rate at which seed density affects colonization rate. In other words, the rate at which vacated patches are colonized increases monotonically toward c as a function of the number of seeds therein scaled by a constant, g. Notably, $E_i \phi_i$ defines the overall colonization (or recruitment) rate of patches previously occupied by species i.

5.3.2 Presentation of results

I present analyses of the above model using a combination of analytical results and simulations. First, I derive a simple metric ($\overline{\alpha_t}$) which quantifies the strength of JCEs (i.e. the strength of specialist predation relative to generalist predation). Then, I present simulations of the model (i.e. equation 5.5) under various scenarios (masting and non-masting cases). For the non-masting case, I examined how the strength of specialist predation relative to generalist predation affects species coexistence. I ran simulations of equation 5.5 with 50 initial species while assuming species vary in fitness (specifically, varying in relative competitive ability, C). To assess the impact of specialized predation rate on species richness, I varied the strength of specialized predation attack rate (a_{P}) between simulations. Simulations were run for 10^6 generations, more than sufficient for the system to reach equilibrium.

For cases incorporating masting, I performed three analyses. First, I examined how variation in seed availability affects $\overline{\alpha_t}$ under different parameterizations of seed predator traits (namely h_{P} and h_{G}) to examine how the relative non-linearity of functional responses affects JCE strength (as defined by $\overline{\alpha_t}$). Second, I ran simulations of equation 5.5 in a community in which all species mast on the same year (no inter-annual masting variation) which allows analysis of masting and predation in isolation (without the influence of the temporal storage effect). Specifically, I examined how the relative non-linearity of generalist and specialist functional responses (h_{P} compared to h_{G}) interacted with masting to shape species richness. Third, I performed simulations similar to those described above, but allowing inter-specific variation in mast years. All simulations were performed in [R] (R Core Team, 2021) using the deSolve package (Soetaert et al., 2010).

5.4 Results

5.4.1 Analytical results

Assuming a separation of timescales such that seed dynamics are faster than predator dynamics, the abundance of seeds on conspecific occupied and heterospecific occupied patches are given by

$$\begin{aligned} S_{ii}(t) &= p_i \underbrace{\frac{f_i\big(X_i(t)\big)}{F_{\mathrm{G}}(\mathbf{S}) + m_i}}_{\text{abundance}} \underbrace{\frac{1}{1 + \frac{\mathrm{P}_i F^i_{\mathrm{P}}(\mathrm{S}_{ii})}{\mathrm{P}_{\mathrm{G}} F_{\mathrm{G}}(\mathbf{S}) + m_i}}}_{\alpha_i} \\ S_{ik}(t) &= p_i \underbrace{\frac{f_i\big(X_i(t)\big)}{F_{\mathrm{G}}(\mathbf{S}) + m_i}}_{\text{abundance}} \end{aligned} \tag{5.7}$$

respectively. The above expressions are broken into two terms: the "abundance" term and α_i. The abundance term describes the number of seeds of species i that would persist on a patch in the absence of any specialized predation. α_i describes the proportion of seeds that survive in the presence of specialists (noting that $\alpha_i = 1$ if $F^i_{\mathrm{P}}(\mathrm{S}_{ii}) = 0$). Notably,

$$\frac{S_{ii}(t)}{S_{ik}(t)} = \alpha_i = \frac{1}{1 + \frac{\mathrm{P}_i F^i_{\mathrm{P}}(\mathrm{S}_{ii})}{\mathrm{P}_{\mathrm{G}} F_{\mathrm{G}}(\mathbf{S}) + m_i}} \tag{5.8}$$

in which case, α_i is a metric of the decrease in survival of species i's seeds due to localized specialized predation. α_i depends on the rate at which specialists kill species i's seeds ($\mathrm{P}_i F^i_{\mathrm{P}}(\mathrm{S}_{ii})$) relative to the rate at which species i's seeds die due to non-specialized mechanisms ($P_G F_G(\mathrm{S}) + m_i$, the sum of total generalized predation seeds of species i experience and density-independent mortality). In other words, α_i is a metric of the portion of seeds that survive in the presence of specialized predators. On the community level, the smaller $\overline{\alpha}$ is (i.e. the smaller the mean proportion of seeds surviving specialized predation, defined below) the stronger negative frequency dependence within the community is, and the more effectively specialized predation promotes coexistence (Stump and Chesson, 2015; Stump and Comita, 2018, also see Fig. 5.1). I refer to α as "JCE strength", with smaller α indicating stronger JCEs.

To examine how masting impacts α and the importance of JCEs, I introduce a simple metric of

the impact of specialized predation over time:

$$\overline{\alpha_t} = \mathbb{E}_t \left[\frac{1}{\overline{E(t)\,\phi(t)}} \frac{1}{N} \sum_{i=1}^{N} \alpha_i(t) E_i(t) \phi_i(t) \right] \tag{5.9}$$

$\overline{\alpha_t}$ provides a metric of the strength of JCEs. Firstly, $0 \leq \overline{\alpha_t} \leq 1$. This is easy to show by noting $0 \leq \alpha_i \leq 1$. If one sets $\alpha_i = 1$ for all i, equation 5.9 reduces to 1; if one sets $\alpha = 0$ for all i, equation 5.9 goes to 0. $\overline{\alpha_t}$ quantifies how specialized predation affects seed survival scaled by recruitment rate. First, consider the terms inside the expectation. $E_i(t)\phi_i(t)$ is the rate at patches previous occupied by species i are colonized (i.e. recruitment rate; see equation 5.5). Therefore, the terms inside the expectation can be interpreted as the proportion of seeds that survive specialized predation throughout recruitment events at time t.

Equation 5.9 takes the expectation with respect to time ($\mathbb{E}_t$). Importantly, both JCE strength ($\alpha_i(t)$) and recruitment rate ($E_i(t)\phi_i(t)$) potentially vary over time due to masting because both are explicit functions of seed abundance. How $\alpha(t)$ and $E_i(t)\phi_i(t)$ vary over time affects $\overline{\alpha_t}$. For example, if $\alpha(t)$ is negatively correlated with $E(t)\phi(t)$ (meaning JCEs tend to be strongest when recruitment is highest), $\overline{\alpha_t}$ will be smaller and, consequently, JCEs will be stronger than in the absence of temporal fluctuations. Conversely, a positive correlation between $\alpha(t)$ and $E(t)\phi(t)$ will increase $\overline{\alpha_t}$ (decreasing the strength of JCEs relative to when there are no fluctuations). I use this metric in the following analyses.

5.4.2 Non-variable environment

When there is no temporal variation in seed production (i.e. no masting) species richness depends on $\overline{\alpha_t}$ (noting that the expectation with respect to time is unneeded; Fig. 5.1). Species richness increases with smaller $\overline{\alpha_t}$. This reflects the relative impacts of specialized and non-specialized mortality – a greater ratio of specialized mortality to non-specialized mortality generates negative frequency dependence, which stabilizes fitness differences and promotes species richness (Chesson, 2000b).

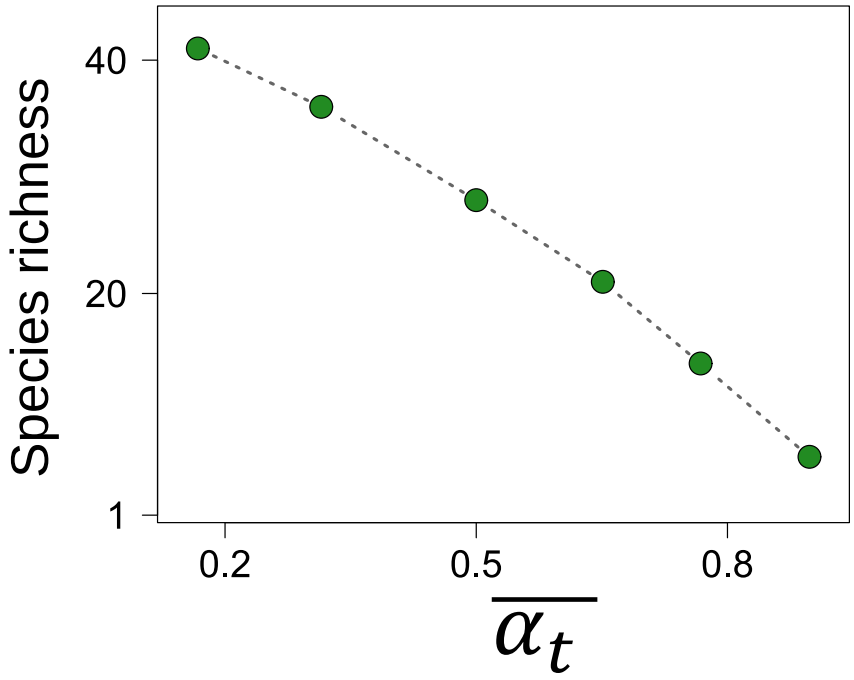

Figure 5.1: How the strength of specialized predation (quantified by $\overline{\alpha_t}$, JCE strength) impacts species richness in a non-variable environment (no masting). The y-axis show species richness; the x-axis shows $\overline{\alpha_t}$ (noting the expectation with respect to time is unnecessary in the non-masting case). Each point shows a simulation beginning with 50 species at equal abundance that ran for 10^6 generations. In each simulation, species were assumed to vary in intrinsic fitness in the exact same way. Each simulation differs in their parameterization of a_{P}, specialist predator attack rate. Larger a_{P} leads to stronger JCEs, smaller $\overline{\alpha_t}$, and greater species richness. Parameters are as follows: $a_{\mathrm{G}} = 0.5$, $h_{\mathrm{G}} = 0.05$, $h_{\mathrm{P}} = 0.05$, $e_{\mathrm{G}} = .05$, $e_{\mathrm{P}} = 0.05$, $m_{\mathrm{G}} = 0.025$, $m_{\mathrm{P}} = 0.025$ $m_i = 0.1$, $f = 10$ (where f fecundity), and $C \sim U[1, 1.1]$ (recalling C is the relative competitive ability of species; variation in C generates fitness differences). Simulations vary a_{P} between 0.1 and 1.0.

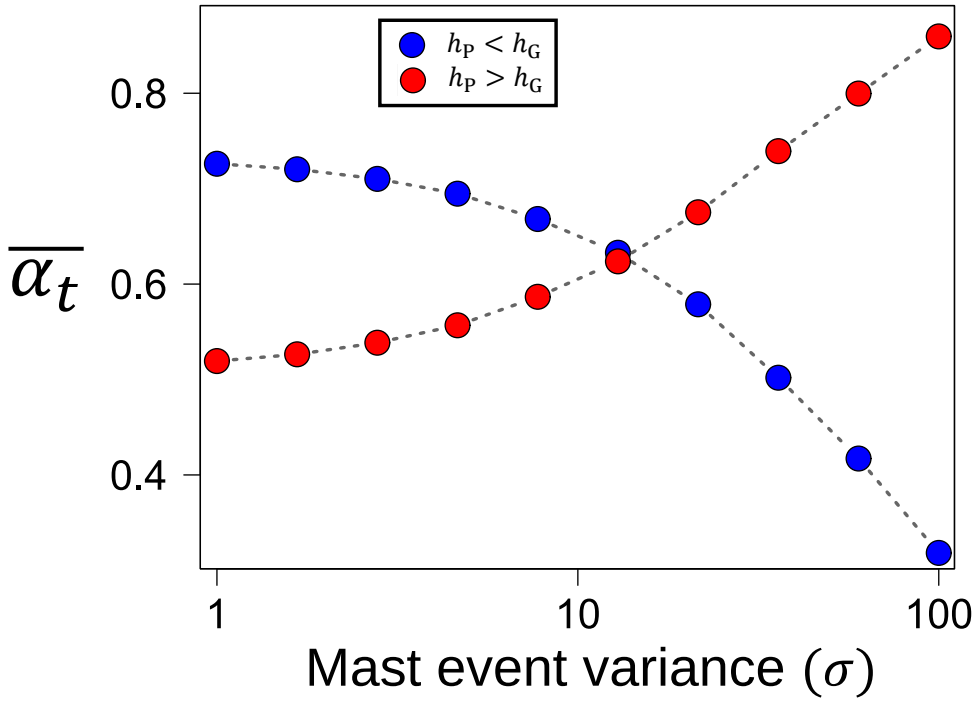

Figure 5.2: The effect of inter-annual fluctuations in seed production (masting) on $\overline{\alpha_t}$ as mediated by each predators' functional response. The x-axis shows mast event variance (σ, the variance of the Poisson process, $X(t)$, that defines mast events). The y-axis shows $\overline{\alpha_t}$, JCE strength. Each point shows the result of a simulation of $\overline{\alpha_t}$ under different σ. For simplicity, these plots were generated under the assumption that generalist and specialist predator abundance were equal and fixed. The color of points indicates the relative non-linearity of each predator's functional response. When the specialist had a more non-linear functional response than the generalist ($h_P > h_G$, red points), greater mast event variance (larger fluctuations in seed abundance) increased $\overline{\alpha_t}$ (decreasing JCE strength). When the specialist had a less non-linear functional response than the generalist ($h_P < h_G$, blue points), greater mast event variance increased $\overline{\alpha_t}$ (decreasing JCE strength). Parameters are as follows. $m_i = 0.1$ and $\overline{f(t)} = 10$ (where $f(t)$ is fecundity) for all simulations. For the red points: $h_G = 0.01$, $h_P = 0.075$, $a_G = 0.05$, and $a_P = 0.1$. For the blue points: $h_G = 0.075$ and $h_P = 0.01$, $a_G = 0.1$, and $a_P = 0.05$.

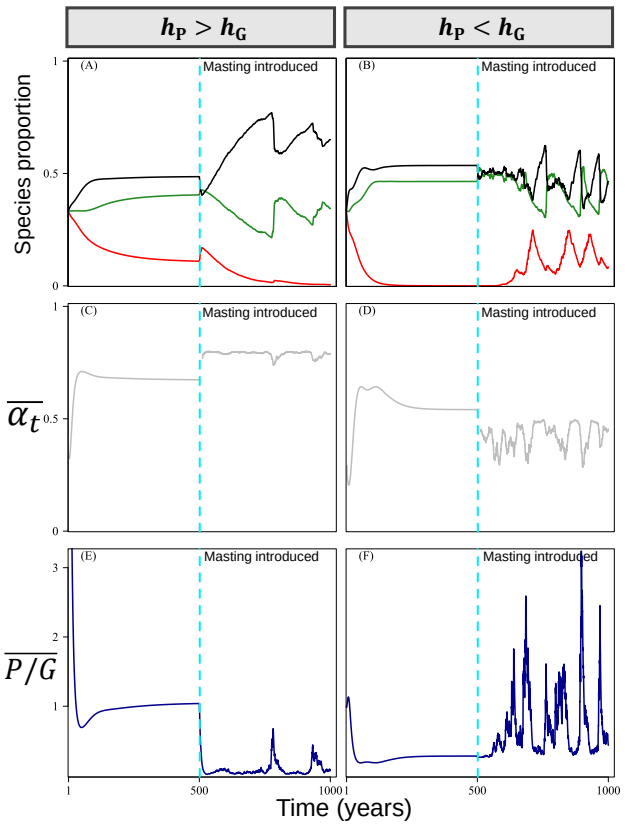

Figure 5.3: How masting interacts with the relative non-linearity of functional responses to shape species richness. The x-axis of each plot shows time in years. Panels A and B show relative species proportion. Panels C and D show $\overline{\alpha_t}$ (JCE strength). Panels E and F show the mean ratio of specialized predators to generalist predators per patch. In each panel, simulations begin with three species at equal proportion that vary in fitness. Initially, trees do not mast. Halfway through the simulation, trees begin to mast; the dashed turquoise line delineates the introduction of masting. When the functional response of specialists are more non-linear that of the generalist ($h_P > h_G$, column 1), the introduction of masting causes the weakest competitor (red) to go extinct (panel A). This is driven by an increase in $\overline{\alpha_t}$ (decreasing JCE strength; panel C). The introduction of masting increases the ratio generalists to specialists (panel E). When $h_P < h_G$ (column 2), the introduction of masting allows the weakest competitor (red) to invade when it would otherwise go extinct (panel B). This is driven by a decrease in $\overline{\alpha_t}$ (increasing JCE strength; panel C). In this case, the introduction of masting increases the ratio specialists to generalists (panel F). Note that panels C and D show a 10 year moving average of $\overline{\alpha_t}$ (i.e. the expectation in equation 5.9 is taken over 10 year periods). Parameters are as follows. Column 1: $a_P = 0.5$, $a_G = 0.5$, $h_G = 0.01$, $h_P = 0.1$, $e_G = .05$, $e_P = 0.05$, $m_G = 0.025$, $m_P = 0.025$ $m_i = 0.1$, and $C \sim U[1, 1.1]$. Column 2: $a_P = 0.5$, $a_G = 0.5$, $h_G = 0.1$, $h_P = 0.01$, $e_G = .05$, $e_P = 0.05$, $m_G = 0.025$, $m_P = 0.025$ $m_i = 0.1$, and $C \sim U[1, 1.25]$. When there is no masting, all trees constantly produce seeds at rate $f = 25$. Mast events occur according to a Poisson process with $\sigma = 5$. $f_{0,i} = 5$ and $f_{M,i} = 105$ for all species. All species follow the same Poisson process for mast events ($X_1(t) = X_2(t) = X_3(t)$).

5.4.3 Variable environment

Variation in seed availability affects the ratio of specialized mortality to non-specialized mortality, potentially increasing or decreasing JCE strength and, correspondingly, potentially increasing or decreasing species richness.

Simulating variable seed availability (i.e. masting) shows that $\overline{\alpha_t}$ depends on the relative non-linearity of the specialists' and generalists' functional responses (Fig. 5.2). When the specialists have a more linear functional response than the generalist ($h_P < h_G$), more intense masting (greater inter-annual seed variability; greater σ) leads to smaller $\overline{\alpha_t}$ (generating stronger JCE strength; Fig. 5.2, blue points). Conversely, when the specialists have more non-linear functional responses than the generalist ($h_P > h_G$) the opposite occurs: more intense masting leads to greater $\overline{\alpha_t}$ (causing weaker JCE strength; Fig. 5.2, red points). This simply reflects how satiation affects the functional response of each class of predator (generalist or specialists) – the species with the less non-linear functional response benefits more from higher seed abundance (which modifies $\overline{\alpha_t}$ accordingly).

This result mirrors how masting affects species coexistence in simulations. When $h_P > h_G$, the introduction of masting can erode coexistence in a community that coexists in a non-variable seed environment (Fig. 5.3A). The introduction of masting in this instance immediately increases $\overline{\alpha_t}$, destabilizing coexistence (Fig. 5.3C). Conversely, when $h_P < h_G$, masting can allow for coexistence when a non-variable seed environment does not (Fig. 5.3B). Upon the introduction of masting, $\overline{\alpha_t}$ decreases, stabilizing coexistence (Fig. 5.3D). These results are robust to whether all species mast on the same year (i.e. masting is both intra- and inter-specifically synchronized; Fig. 5.3) or when the probability that each species masts on a given year is independent of (Fig. 5.4).

These results reflect several factors: the relative non-linearity of functional responses of the generalist and specialists, their numerical responses, and competition between generalists and predators. As shown in Fig. 5.2, masting affects $\overline{\alpha_t}$ via how satiation affects each type of predator. However, $\overline{\alpha_t}$ also depends on the abundances of specialists and generalist. Importantly, the introduction of masting modifies the relative abundance of specialists and generalists (Fig. 5.3E, 5.3F). This, in part, reflects how the numerical response of each predator is affected by satiation (the more non-linear the functional response, the less efficiently the predator can convert high seed biomass into new off-

spring). Secondly, the class of predator (generalist or specialist) with the more non-linear functional response is at a competitive disadvantage relative to the predator with a less non-linear functional response when resource availability exhibits temporal fluctuations. In extreme cases, this can likely result in the extinction of either generalists or specialists (though I do not explicitly examine this situation). The combination of these factors causes the ratio of specialist to generalist abundance to decrease or increase when masting is introduced when $h_{\mathrm{P}} > h_{\mathrm{G}}$ or $h_{\mathrm{P}} < h_{\mathrm{G}}$, respectively.

5.5 Discussion

Generalist and specialist seed predators are ubiquitous in nature and are thought to play important roles in tree species coexistence. Using a theoretical model, I show that the ability of predation to maintain tree specices coexistence fundamentally depends on the ratio of specialized predation to generalized predation (Fig. 1). I extend this framework to incorporate masting (a wide-spread phenomenon associated with seed predation). I demonstrate that masting interacts with both generalized and specialized predation and is capable of either either stabilizing or destabilizing coexistence.

For masting to be stabilizing, it must increase the proportion of seeds consumed by specialists relative to generalists. This requires that the handling time of generalists exceeds that of specialists ($h_{\mathrm{P}} < h_{\mathrm{G}}$). This is relevant in the context of interpreting how masting and high seed densities impact the proportion of seeds that escape predation. Importantly, empirical evidence that suggests masting increases the *total* proportion of surviving seeds (see Seget et al., 2022) is not inconsistent with the possibility that masting stabilizes coexistence via strengthing JCEs. Classic theory assumes predators can cause negative density dependence if predators increase the relative proportion of a prey item they consume when said prey is at high abundance (which can occur via prey switching as described by a type III functional response; e.g. Real, 1977). However, in this study, I show masting can promote coexistence when it satiates generalists more than it satiates specialists (Figs. 5.2 and 5.3). In such cases, masting increases the proportion of seed mortality attributable to specialists relative to generalists, which increases the strength of frequency dependence species

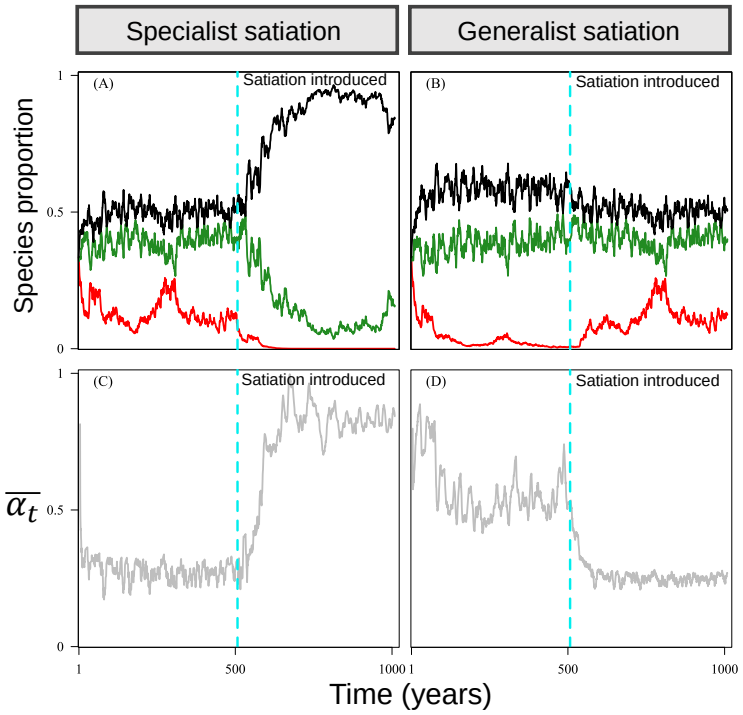

Figure 5.4: How generalist vs. specialist satiation influences coexistence when the temporal storage effect operates. For all panels, the x-axis shows time in years. Panels A and B show relative species proportion. Panels C and D show $\overline{\alpha_t}$ (JCE strength). Mast events for each species occur according to independent Poisson process. At the start of each simulation, it is assumed generalists and specialists have linear functional responses ($h_{\mathrm{P}} = h_{\mathrm{G}} = 0$). Upon the turquoise dashed lines, satiation in introduced by increasing the handling time of either the specialist predator (column 1) or the generalist predator (column 2). Similar to Fig. 5.3, specialist satiation decreases JCE strength (increasing $\overline{\alpha_t}$, panel C) and erodes diversity (panel A). Conversely, generalist satiation increases JCE strength (smaller $\overline{\alpha_t}$, panel D) and promotes coexistence (panel B). Notably, the introduction of satiation also affects the mean rate at which species consume seeds irrespective of fluctuations and satiation. To control for this, the introduction of satiation is coupled with a modification to seed attack rate such that mean seed consumption is unchanged. For example, let $\overline{S_{ii}}$ be the mean abundance of seeds of species i on conspecific occupied patches throughout the first half of the simulation. Let $P1$ and $P2$ index the specialist predators traits before and after the introduction of satiation, respectively. Satiation is introduced in panel A by changing $h_{\mathrm{P1}} \rightarrow h_{\mathrm{P2}}$ and $a_{\mathrm{P1}} \rightarrow a_{\mathrm{P2}}$ such that $F^i_{\mathrm{P1}}(\overline{S_{ii}}) = F^i_{\mathrm{P2}}(\overline{S_{ii}})$. A similar operation is performed in panels B and D. This guarantees that the introduction of satiation affects dynamics due to its interaction with variation in seed availability due to non-linear averaging. Other parameters are as follows. Column 1: $a_{\mathrm{G}} = 0.5$, $e_{\mathrm{G}} = .05$, $e_{\mathrm{P}} = 0.05$, $m_{\mathrm{G}} = 0.025$, $m_{\mathrm{P}} = 0.025$ $m_i = 0.1$, and $C \sim U[1, 1.5]$. Column 2: $a_{\mathrm{G}} = 0.5$, $e_{\mathrm{G}} = .05$, $e_{\mathrm{P}} = 0.05$, $m_{\mathrm{G}} = 0.025$, $m_{\mathrm{P}} = 0.025$ $m_i = 0.1$, $C \sim U[1, 2]$. $\sigma = 5$ $f_{0,i} = 5$ and $f_{M,i} = 105$ for all species.

experience. However, this need not decrease the *total* proportion of seeds that survive. For example, if masting halves the rate at which generalist consume seeds but does not affect the proportion specialists consume, this will generate a stabilizing effect (increasing $\overline{\alpha_t}$) despite increasing the proportion of seeds that escape predation. Therefore, to examine how masting and the associated predator satiation affects species coexistence, it is necessary to examine how masting affects the *relative* proportion of seeds predated by generalists and specialists, not just the total proportion of seeds that survive. For example, evidence that localized density-dependent mortality (in line with JCEs) is more important at the local level while satiation (and, therefore, positive density-dependence) are more important on the population level hints that satiation might be stabilizing rather than destabilizing (Xiao et al., 2017). More broadly, compelling evidence that seed predation pressure increases on latitudinal gradients from the arctic to the tropics (Hargreaves et al., 2019) does not necessarily constitute evidence that seed predators play an elevated role in maintaining species diversity in tropical communities – rather, it is necessary to evaluate how the proportion of specialized to generalized seed predation varies with latitude.

In this study, I emphasize how masting modifies the relative impacts of generalist and specialist predation to shape coexistence. However, a large body of literature examines how species-specific responses to the environment can maintain species coexistence (the temporal storage effect; Chesson and Warner, 1981; Chesson, 1994). Masting may contribute to coexistence via the temporal storage effect if species mast in different years (which occurs in Figs. 5.4A and 5.4B). Previous work shows that generalized predation pressure weakens the temporal storage effect by generating apparent competition and reducing the covariance between environment and competition (Kuang and Chesson, 2009). By extension, adding generalist predator satiation to generalized predation may increase the strength of the storage effect. This is reflected in Fig. 5.4. While the coexisting species in Fig. 5.4B are clearly stabilized at least in part through how satiation concentrates specialized predation relative to generalist predation (increasing $\overline{\alpha_t}$; Fig. 5.4D), it is also possible that adding generalist satiation increases the covariance between environment and competition (thereby increasing the strength of the storage effect). Conversely, predator satiation can be destabilizing in a variable environment if generalized predators are assumed to be optimally foraging (MacArthur

and Pianka, 1966; Charnov, 1976) such that common species can satiate the generalist predator while rare species cannot (Stump and Chesson, 2017). Future analytical investigations of these dynamics should examine a larger variety of predator behavior in order to tease apart the extent to which specialized predation and storage effects contribute to coexistence.

This model makes several simplifying assumptions that future work should address. Future models should examine how ecological drift interacts with masting. The analysis in this paper is deterministic insomuch that I assume species cannot stochastically go extinct. However, masting may generate fluctuations in tree abundance which may make rarer species more susceptible to demographic stochasticity. In particular, the probability of extinction likely depends on the parameters c and g (maximum colonization rate and the sensitivity of colonization rate to local seed density, respectively). Sensitivity analyses of these parameters using a stochastic model may allow for more nuanced analyses of how masting affects long-term species richness.

Another assumption is that all species either mast or do not mast. When species do mast, they all do so with the same variance. Neither of these assumption are reflected in nature – masting intervals (if a species masts at all) vary inter-specifically. Such variation likely has implications regarding how masting affects species coexistence. Similarly, I assume masting is Poisson distributed – modeling masting with using alternative renewal processes may provide additional insights. Furthermore, this study considers masting in a purely ecological context, but fundamental questions about its evolution remain unanswered. Results broadly indicate that masting affects inter-specific competition – how inter-specific competition mediates the evolution of masting is an unexplored area of research.

Future models should also consider a broader range of ecology scenarios than those presented here. In particular, the biological agents of JCEs may demand slightly more nuanced modeling efforts. JCEs and conspecific negative density dependence are more often observed to affect seedlings rather than seeds (Comita et al., 2014) and are often caused by pathogens (Bagchi et al., 2014; Chen et al., 2019; Hazelwood et al., 2021). This may affect how masting and predator satiation interact with JCE strength. For example, satiation of generalist predators (resulting in positive density dependence) may allow seedlings to build to a sufficiently high density such that specialist pathogen outbreaks become more likely. Alternatively, previous theoretical work shows that gener-

alist pathogens can increase the strength of the storage effect if they affect germinating seedlings (Mordecai, 2015). How this dynamic interacts with masting and predation satiation is an intriguing avenue for future research.

5.5.1 Conclusion

This study demonstrates that fairly complicated non-linear processes involving both positive and negative density dependence modulate how masting qualitatively affects species richness. These sorts of seemingly antagonistic interactions may be common in nature. For example, mutualistic and pathogenic fungi are both important agents of plant-soil feedbacks (Bever et al., 2015). While this is often modeled as a fixed effect that conceptually represents the cumulative sum of mutualistic and pathogenic effects (i.e. feedbacks are positive if mutualists are more important than pathogens and feedbacks are negative if pathogens are more important than mutualists; e.g. Ke and Wan, 2020; Miller and Allesina, 2021), this may ignore complicated interactions between the positive and negative feedbacks therein. For example, mutualists may initially increase seedling abundance, but high seedling densities may ultimately lead to a pathogen outbreak (similar to the above discussion). More generally, future theoretical studies should explore how positive and negative density-dependence generated by natural enemies and mutualists affecting different life history stages interact to shape the overall type of density-dependence species' offspring experience and its subsequent effect on species richness.

Chapter 6

Synopsis: toward a synthesis of distance and density dependent effects in sessile organisms

6.1 Introduction

Much work in community ecology has historically focused on species interactions that take place within a defined environment that exists independent of them – that species are figuratively like actors upon an environmental stage that preexists them. This view is no longer substantiated: recent decades have seen an explosion of research in how organisms shape their environments (Jones et al., 1994). While I have mainly discussed forest communities in this thesis, biotically-driven modifications to the environment occur in a wide variety of ecology scenarios ranging from the pathogens and host trees associated with Janzen-Connell effects (JCEs), to microbial nutrient exchange (Seth and Taga, 2014), and filter feeders altering the light environment of benthic communities (Abrahams and Kattenfeld, 1997). In short, it is clear that the historical view that species and their interactions cannot be imagined as occurring on an independent environmental stage. Rather, ecological communities and the diversity therein are the products of feedbacks between species and the localities they occupy – these feedbacks likely strongly influence natural environments and shape species composition.

These processes are not just relevant in the context of diversity in natural ecosystems – crop rotations are often implemented as a means of controlling specialized pathogens and pests that are

attracted to areas of high host density (Paulitz et al., 2010; Bolluyt et al., 2011). In essence, local feedbacks are highly relevant in fundamental human practices such as agriculture. This points to a broader fact: while I have restricted my discussion to how local feedbacks impact forest communities (and I will continue to do so within this text) it is important to note that the dynamics described throughout this thesis are conceptually applicable to many systems. Returning our focus to forested ecological communities – while specialized pests and pathogens are often a nuisance and threat in the anthropocentric world of agriculture, they may have profound and fascinating implications for species interactions in the natural world.

The regenerative pathway of trees in highly diverse forest communities is complex, depending on a combination of interacting biotic and abiotic factors that both affect and are generated by individuals at multiple life history stages (Schupp and Fuentes, 1995). An important question relevant to this thesis is: "to what extent can we capture the key components of this complexity with tractable models?". A subset of theoretical work stresses the importance of highly simplified models because they are relatively easy to work with. To this effect, such models have been useful tools to develop baseline predictions related to how plant-soil feedbacks, JCEs, and similar processes that may impact coexistence in natural communities (e.g. Bever et al., 1997). However, as I have highlighted in this thesis, model predictions for how local feedbacks such as JCEs impact species composition and richness are highly contingent on many fairly complex factors. Such factors include: the functional form of distance-dependent processes (e.g. how JCE strength decays with distance; Chapter 2, density-dependent processes (e.g. how JCE strength is modified by conspecific density and which life history stage induces negative density dependence; Chapters 2 and 4), the explicit spatial structure of the environment (i.e. the level of spatial autocorrelation, which interacts with local feedbacks; Chapter 3), and spatial-temporal variation (e.g. how tree masting modifies the relative strengths of generalist and specialist predation; Chapter 5). All of these factors combine to shape how processes such as JCEs can concentrate intra-specific competition relative to inter-specific competition (the key feature necessary for species coexistence). In this sense, minimal models likely present a projection of these complicated processes in the same way that Lotka-Volterra models may be seen as phenomenological representations or approximations of greater

underlying complexity. Ultimately (as is often the case) forward progress requires a careful balance of tractability and biological realism. This thesis highlights the importance of several features that impact the strength of local feedbacks and regulate their impact on species coexistence. It is my hope this work will provide guidance on which features of natural systems are of highest importance to model and measure.

Despite the advances presented here, empirical and theoretical work on these topics are in their infancy: many gaps (both theoretically and empirically) remain. To help illuminate the many unanswered open questions, I present a brief review and synopsis of theoretical and empirical literature related to distance and density dependent effects in communities of sessile organisms. I discuss several theoretical assumptions common in the literature, highlight areas of recent progress in relation to the work presented in this thesis, and discuss several avenues on which a better integration of empirical and theoretical ideas will provide a fruitful synthesis.

6.2 Theoretical advances in spatially structured density-dependent processes

6.2.1 Janzen-Connell effects, conspecific limitation, and heterospecific limitation

Theoretical investigations of JCEs seek to understand if they are "strong" enough to maintain species diversity. The key (and empirically motivated) assumption is that species are susceptible to specialized natural enemies such that a species' offspring are less likely to survive in areas of high conspecific density or nearby conspecific adults (for simplicity, I will discuss the latter case). Many models only directly incorporate conspecific effects (i.e. species i's natural enemies are perfectly specialized and do not affect heterospecifics; e.g. Adler and Muller-Landau, 2005; Muller-Landau and Adler, 2007; Levi et al., 2019; Chisholm and Fung, 2020) or that a species' natural enemies affect all heterospecifics equally (e.g. Chisholm and Muller-Landau, 2011; Stump and Chesson, 2015). For example (considering the latter case), it might be assumed that species i's offspring

die with probability $\alpha_{i,i}$ underneath conspecifics and probability $\alpha_{i,\neq i}$ beneath heterospecifics such that $\alpha_{i,i} > \alpha_{i,\neq i}$. Therefore, as a species becomes more common, its offspring experience decreased survivorship on a increasingly large proportion of the environment. As a consequence, a species' per capita growth rate inevitably declines with its frequency in the population – JCEs therefore guarantee species experience negative frequency dependence. In the more familiar terms of a Lotka-Volterra competition model, consider the two species case for which $\alpha_{ii} > \alpha_{ij}$ and $\alpha_{jj} > \alpha_{ji}$ (substituting $\neq i \rightarrow j$). Some rearranging yields $\frac{\alpha_{ii}\alpha_{jj}}{\alpha_{ji}\alpha_{ij}} > 1$ which constitutes the classic necessary condition for coexistence (Chesson, 2000b). In short, JCE-related theory work often assumes a *stable* equilibrium and examines the conditions under which it is *feasible*.

While in practice, implementations of the above-describe feature (i.e. $\alpha_{i,i} > \alpha_{i,\neq i}$) in spatially explicit JCE-inspired models do not track one-to-one with a Lotka-Volterra model, the key point is that JCEs are by definition stabilizing (Chesson, 2000b). Therefore, theoretical JCE-related studies examine whether specialized predation in spatially structured communities is *sufficiently* stabilizing to prevent the erosion of species diversity via ecological drift (when it is assumed the community is otherwise neutral; e.g. Hubbell, 1980; Adler and Muller-Landau, 2005; Levi et al., 2019) or prevent competitive exclusion (when it is assumed there are inter-specific fitness differences; e.g. Stump and Chesson, 2015; Chisholm and Fung, 2020; Smith, 2022a,b). Notably, the assumption that $\alpha_{i,i} > \alpha_{i,\neq i}$ is not arbitrarily – the entire theoretical literature built around JCEs and plant-soil feedbacks is motivated by empirical observations that natural enemies are indeed specialized enough such that this inequality naturally emerges.

6.2.2 How the structure of predation affects diversity

The above discussion (as well as most of this thesis) ignores the structure of natural enemy overlap. While empirical measurements indicate natural enemies are often specialized (e.g. Comita et al., 2014; Sarmiento et al., 2017; Gripenberg et al., 2019), they also exhibit taxonomic spillover: species more phylogenetically similar are often more likely to share natural enemies than more distantly related species (Ødegaard et al., 2005; Gilbert and Webb, 2007; Novotny et al., 2010, see Fig. 6.1). I will refer to this as "natural enemy spillover". A key question is: how important is its structure

and how does it affect coexistence? Empirically, this is still a fairly open question. However, synthesizing and building on previous work allows several baseline theoretical predictions that may serve as guidance for future efforts.

Several previous models examine JCEs and plant-soil feedbacks in this capacity. Sedio and Ostling (2013), analyzing a model loosely parameterized with several of the above-mentioned studies, find that specialization in tropical forests (at least, in Panama) can maintain considerably higher diversity than a neutral model. However, Sedio and Ostling (2013), in the same spirit as other highly similar models (Adler and Muller-Landau, 2005; Muller-Landau and Adler, 2007; Levi et al., 2019), assume that species have identical fitness. However, as outlined by Stump (2017), the structure of niche overlap (such as which species share predators) affects fitness difference, stabilizing effects, and species coexistence.

Here, I examine a relatively simple "natural enemy spillover" model inspired by Sedio and Ostling (2013), Stump (2017), and Smith (2022a) that helps clarify how the structure of natural enemy spillover may affect species richness in forest communities; see Box 1 for model details. In the model, I assume species vary in intrinsic fitness. How shared predators affects species richness is contingent on how predator overlap correlates with fitness. If species with similar fitness tend to share predators, some degree of shared predation pressure can dramatically increase species richness (Fig. 6.2, blue points). This might occur if phylogenetic similarity causes species to have similar traits and, therefore, are similarly fit *and* chemically similar such that they are susceptible to an overlapping sweep of natural enemies. Alternatively, this may occur if character displacement is more common in closely related species. Conversely, if predator overlap is random with respect to fitness, greater predator overlap decreases species richness relative to when predators are not shared (Fig. 6.2, green points).

Box 1: JCE model with natural enemy spillover

I extend the model presented in Chapter 2, Appendix D to species exhibiting natural enemy overlap. I consider a tree community of N species that contains M patches in which the center of every patch contains a single adult tree. Each tree produces a set number of seeds each time-step. For simplicity, I assume seeds are uniformly and globally distributed across patches in the community. The number of offspring species i disperses to each patch is proportional to Y_i, henceforth intrinsic fitness (a composite parameter of fecundity and density-independent offspring survival). On each patch, specialized predators kill offspring. Let $J_i(x)$ define the probability an offspring of species i survives predation pressure induced by natural enemies on a patch at location x. Then, letting $S_i(x)$ represent the number of offspring of species i on a patch at a location x:

$$S_i(x) = Y_i J_i(x), \qquad S_{all}(x) = \sum_{k=1}^{N} S_k(x) \tag{6.1}$$

where p_i is the proportion of species i in the population, $i = 1, 2, ..., N$. If the adult on the patch at location x dies during the time-step, a lottery determines which species replaces the adult. As noted above, I assume that predation pressure increases linearly with adult density and decays exponentially with distance. Thus:

$$J_i(x) = \exp\Bigg[- a_i \sum_{k=1}^{N} \sum_{m=1}^{p_k M} \rho_{ik}\, e^{-x_{k,m}/v} \Bigg] \tag{6.2}$$

This summation describes the effect of all adults on offspring of species i at location x. The first summation sums over all species; the second summation sums over all adults of species k in the population ($p_k M$). $x_{k,m}$ represents the distance (in meters) of the m_{th} closest individual of species k to location x. a_i is the baseline susceptibility of natural enemies of species i, v is the rate at which predation pressure declines with distance and ρ_{ik} is the proportion of natural enemies affecting species k that also affect species i. $\rho_{ii} = 1$ and $\rho_{ik} \leq 1$.

Using methods similar to Chapter 2, a spatially implicit approximation of the spatially explicit model is derived by taking the expectation of offspring mortality with respect to space. This yields:

$$\mathbb{E}[S_i(x)] = Y_i \exp\Bigg[- a_i g \sum_{k=1}^{N} \rho_{ik} p_k E_D H(a_i\, \rho_{ik}) \Bigg] \tag{6.3}$$

where $H(a_i\, \rho_{ik}) = {}_3F_3(1, 1, 1; 2, 2, 2; -a_i\, \rho_{ik})$, a Generalized Hypergeometric Function and g is tree density (tree per square meter). Population dynamics are described with a system of ODEs:

$$\frac{dp_i}{dt} = \delta \Bigg[\sum_{\text{all } k} \frac{\mathbb{E}[S_i(x)]}{\mathbb{E}[S_k(x)]} p_k - p_i \Bigg] \tag{6.4}$$

where $k = 1, 2, ..., N$ and δ represents the mortality rate of all adults. I assume symmetric effects ($\rho_{ik} = \rho_{ki}$) and that ρ takes the functional form: $\rho_{ik} = \max\left[1 - |\tau_i - \tau_k|^r / c, 0\right]$ for which τ_i and τ_k represent the location of species i and k in trait space related to natural enemy susceptibility, respectively. $0 \leq \tau \leq 1$. $|\tau_i - \tau_k|$ represents the distance between species i and k in trait space. r determines the functional form of overlap as a function of trait difference and c quantities the proportion of species with non-zero natural enemy overlap.

This can be understood as follows. First consider perfect specialization (i.e., JCEs as they are classically imagined; Fig. 6.2, dashed lines). Recent work demonstrates that the ability of JCEs to maintain species richness is highly contingent on the number of species in the community (N) relative to the spatial scale over which JCEs occur (Levi et al., 2019; Chisholm and Fung, 2020; Smith, 2022a,b). If said spatial scale is too small relative to the number of species in the community, even relatively common species escape predation on most patches and, consequently, frequency dependence is too weak to maintain very high species richness. Now, consider when species have overlapping predators. Species with higher fitness tend to have relatively equilibrium abundances. A species that shares natural enemies with a common (i.e. highly fit) experiences predation on a larger proportion of the spatial environment, decreasing its fitness. This constitutes an example of the "common competitor effect" (Stump, 2017). Conversely, a species that shares predators with rare species is weakly impacted by the additional predation pressure it experiences (as it encounters overlapping predators correspondingly rarely). When fitness is highly correlated with predator overlap (Fig. 6.2, blue points), relatively fit (and, therefore, common) species tend

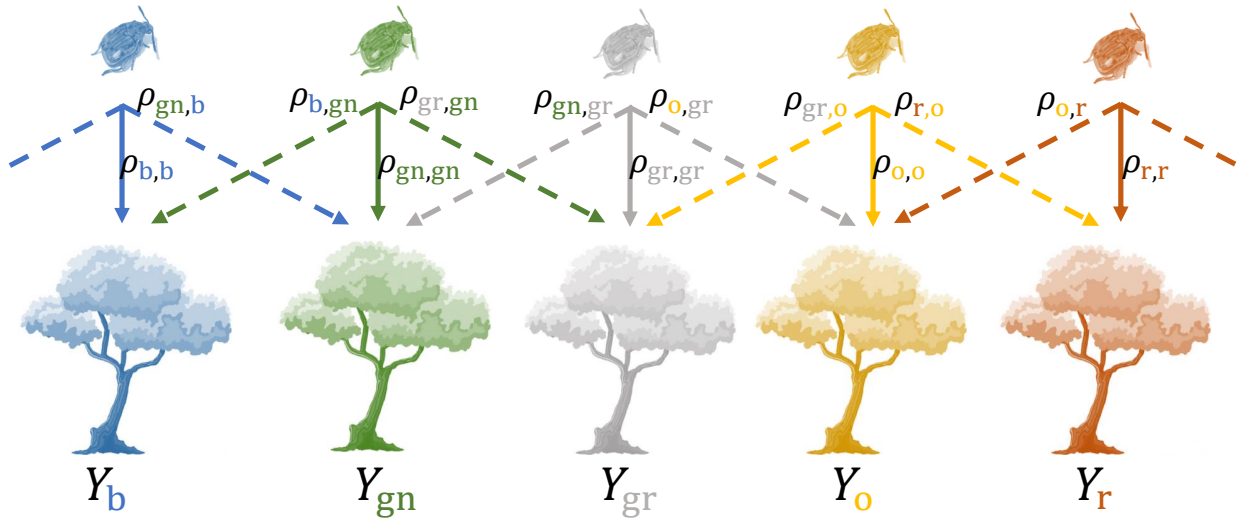

Figure 6.1: Visual representation of natural enemy spillover. $\rho_{x,y}$ is the overlap of natural enemies shared by species x and y, indexed by color. Classic JCEs are equivalent to assuming $\rho_{x,x} = 1$, $\rho_{x,y} = 0$ for $x \neq y$ (ignoring all the dashed lines). Y_x indicates the intrinsic fitness of species x, also indexed by color. How predator overlap affects species richness depends strongly on the relationship between species' intrinsic fitness and the probability they share natural enemies (see Fig. 6.2).

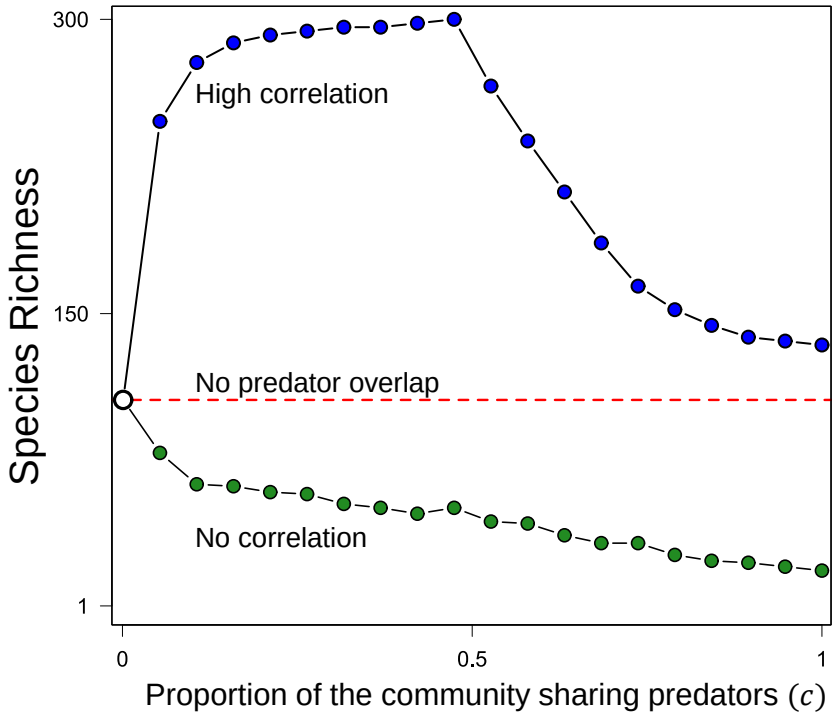

Figure 6.2: How natural enemy spillover affects species richness. The x-axis depicts the average portion of natural enemies that tree species share (i.e. the probability that $\rho_{xy} > 0$ for two randomly sampled tree species; this is equal to c, see Box 1). The y-axis depicts the equilibrium species richness out of a pool of 300 initial species from simulations of equation 6.4 in a community that varies in intrinsic fitness (Y). Blue points show when there is a high correlation between the probability species share predators and their intrinsic fitness (generated by assuming $|\tau_i - \tau_k|$ and $|Y_i - Y_k|$ exhibit a correlation coefficient of 0.85). Green points show when predator overlap is random with respect to intrinsic fitness. The white point and red dashed line show species richness under classic JCEs (when there is no natural enemy spillover). Species richness can increase with c when there is a positive correlation between fitness and natural enemy overlap, but declines rapidly if there is no correlation. Parameters are as follows: $a = 1.0$, $Y \sim U[1, 20]$, $g = 0.1$, $\delta = 0.1$, $r = 0.5$.

to be mutually limiting. While rare (low fitness) species are also technically mutually limiting in this scenario, the impact is negligible. Thus, common (fit) species experience a fitness loss, but rare (low fitness) species do not – this equalizes fitness difference, allowing for higher equilibrium species richness. However, when predator overlap and fitness are uncorrelated (Fig. 6.2, green points), many rare species share natural enemies with common species. This undermines rare species advantage and, as a result, greater natural enemy spillover erodes species richness.

Overall, the key point is that a modest amount of natural enemy spillover has the potential to erode or strongly allow for species richness depending on how natural enemy spillover is structured with respect to fitness differences. Quantifying this structure, possibly with existing food web data (e.g. Gripenberg et al., 2019) and census data (e.g. Wright et al., 2005) may provide a means of probing this question.

Demystifying the complicated interactions between natural enemies and their hosts

These results (along with nearly every model presented in this thesis and cited above) represent a highly phenomenological approach. The next (and perhaps most important) challenge in JCE-related research is to develop mechanistic models of the interactions between host species (i.e. trees), natural enemies, and mutualists. Very little theory investigates this problem (but see Schroeder et al., 2020). This is understandable: while modeling a single spatially structured tropic level is difficult, incorporating an additional trophic level dramatically increases the dimensionality of the problem (particularly if both mutualists and pathogens are considered). However, the Janzen-Connell Hypothesis, plant-soil feedbacks, and (more generally) natural enemy and mutualist-mediated species coexistence in spatially structured communities will not constitute complete theories until both trophic levels are explicitly modeled. For example, the model used in the above analysis (see Box 1) assumes all effects of all adults occur additively (i.e. the survival of a species' offspring is determined by the sum of all adult trees with which they share natural enemies). However, inter-specific interactions between natural enemies may alter how the presence of adult trees impacts the success of their offspring.

However, the limitations of current work go far beyond questions regarding how natural enemies

maintain tree diversity. One can reasonably argue that less than half of the question is being asked: while the theoretical literature emphasizes how a large number of natural enemies maintain tree diversity in spatially structured communities, far fewer models investigate how coexistence between these natural enemies is affected by the spatial structure and relative abundance of plants and trees. Even in Chapter 5, in which I explicitly model specialized and generalist predators, analyses are framed to examine the effects of natural enemies on host species diversity and not the other way around. This omission from the literature is non-trivial: if a single species experiences no negative-density dependence (i.e. a single species' natural enemies go extinct, releasing it from negative density dependence), it is likely to competitively exclude all its competitors. Evolutionary dynamics offer a promising lens to address this issue. Microbes (e.g. fungal pathogens causing JCEs) and canopy trees differ in size and generation time by many orders of magnitude. This massive time-scale separation implies that evolutionary change of the natural enemies between tree recruitment events is very likely the norm – this may play a key role in the evolution of specialization and prevent any particular species from escaping natural enemies (Lloyd-Smith, 2013, i.e. a species that is released from natural enemies may generate strong selection for specialization in pathogens, akin to a vacated niche). Conversely, the evolution of specialization in natural enemies may shape both species-specific life history strategies (involving trade-offs between defense against pathogens and growth rate; e.g. McCarthy-Neumann and Kobe, 2008; Lebrija-Trejos et al., 2016; Zhu et al., 2018; Zang et al., 2021; Song et al., 2021b) and the relative abundance of host species (Comita et al., 2010). Overall, the next frontier of theoretical analysis requires careful consideration of the eco-evolutionary dynamics governing tree-pathogen interactions.

6.2.3 Toward a theoretical synthesis of distance and density-dependent effects in sessile organisms

Throughout this thesis, I have highlighted how different aspects of the functional form of negative density dependence, the specific life history stage or stages in which density-dependent interactions occur, spatial aggregation, and dispersal interact to shape species richness. These results are

part of a growing theoretical literature seeking to understand how complicated interactions between distance-dependent effects, density-dependent effects, and dispersal structure competitive communities composed of sessile organisms. However, it is often confusing to make sense of the myriad of different scenarios presented in the literature. A handful of theoretical studies over the last twenty years examine subtly different models that make small yet important distinctive assumptions regarding how density and distance impact competitive interactions in spatially structured communities. While many distinctions between these models can be discussed, I focus on three different features of recent models, how the interactions between these modeling assumptions likely impact their qualitative outputs, and then discuss future directions of empirical and theoretical research.

Different assumptions in the theoretical literature

First, different models make different assumptions regarding which life history stage induces and experiences density dependence. While this is examined in Chapter 4, the topic is broader than the situations discussed therin. Previous work, broadly, examine three possibilities (see Fig. 6.3A for visualizations). (1) Adults may impact juveniles (A→J; e.g. Adler and Muller-Landau, 2005). This constitutes the classical conceptualization of JCEs and, in principle, how patch dynamic plant-soil feedback models incorporate soil legacy effects (e.g. Bever et al., 1997; Ke and Wan, 2020). In each case, the presence of an adult tree (current or past) modifies conspecific offspring survival or patch colonization success. (2) Juveniles may impact other juveniles (J↔J). CNDD is often attributed to pathogens that outbreak at high densities – thus, several papers consider when it is the density of juveniles *per se* that leads to negative density-dependent effects. This is the assumption in Chapter 4. When species experience dispersal limitation, parsing out the signal of distance-dependent adult effects vs. density-dependent effects driven by local juvenile density presents a difficult challenge (Terborgh, 2012). (3) Density-dependence may occur via adult-adult interactions (e.g. Detto and Muller-Landau, 2016). This represents a considerably different biological motivation and mechanism than the previous cases. Factors such as resource competition or apparent competition generated by high adult density could mediate this dynamic. Parsing out how each different type of density-

dependent interaction uniquely shapes species richness may lead to deep insights.

Second, models differ in the functional form of density-dependent effects (discussed in Chapter 2 and Smith, 2021). Broadly speaking, previous models tend to present either linearly additive distance/density-dependent effects or non-additive effects (see Fig. 6.3B for visualizations). Non-additive models often conceptualize JCEs as occurring within a fixed distance of a conspecific adult in a "presence-absence" capacity (i.e. juveniles experience a fixed increase in mortality; Hubbell, 1980; Levi et al., 2019; Chisholm and Fung, 2020). Spatially implicit models (e.g. Chisholm and Muller-Landau, 2011; Stump and Chesson, 2015; Stump and Comita, 2018) and plant-soil feedback patch dynamic models (e.g. Miller and Allesina, 2021) in which juveniles experience increased mortality or lower colonization probability when they are on patches occupied (or previously occupied) by conspecifics are also implicitly non-additive in this respect. Conversely, other models assume density effects are linearly additive (i.e. conspecific effects are proportional to conspecific density; e.g. Adler and Muller-Landau, 2005; Muller-Landau and Adler, 2007; Sedio and Ostling, 2013; Wiegand et al., 2021). However, this binary is a false dichotomy. More broadly, the extent to which density affects survival can be described on a spectrum of sub-linear to linear to super-linear. For example, let $Z_i(x)$ represent the distance weighted neighborhood density of species i at location x. The effect of conspecific density on seedling survival probability, $p(S)$, might be calculated with the expression $p(S) = e^{-aZ^b}$ where a represents the baseline strength of CNDD and b defines the functional form of density effects; $b \approx 0$ represents non-additive effects, $0 \leq b \leq 1$ represents sub-additive effects, $b = 1$ represents linearly additive effects, and $b > 1$ represents super-additive effects (Fig. 6.3B). This sort of weighting (b) has been directly implemented in recent empirical measurements of CNDD in forest communities with the purpose of calculating unbiased neighborhood density effects (Detto et al., 2019; LaManna et al., 2022; Xu et al., 2022).

Third, theoretical studies integrate various distinctive forms of dispersal into models (see Fig. 6.3C for visualizations). Some papers consider "global dispersal", in which seeds are evenly distributed throughout the environment (although some studies implement Poisson distributed seed dispersal on each patch to incorporate seed limitation; e.g. Muller-Landau, 2010). A second (and frequent) form of dispersal limitation assumes "local dispersal". Local dispersal is often implemented

spatially explicitly through the use of a dispersal kernel (e.g. Adler and Muller-Landau, 2005) in which juveniles are aggregated in space nearby conspecific adults. This impacts the spatial composition of trees and can generate species aggregation. Alternatively, several models implement local dispersal limitation implicitly, where adults disperse a local proportion of seeds locally (directly on the patch on which the adult occupies) and uniformly distribute the remaining seeds throughout the community (Chesson, 2000a; Stump and Chesson, 2015; Stump and Comita, 2018; Smith, 2022a). Finally, a recent theoretical study considers "clustered dispersal" (Wiegand et al., 2021) in which recruits of each species are dispersed in space to one of several predefined locations as might occur through animal seed dispersal. This decouples adult density from recruit location and potentially influences patterns of aggregation.

Interactions between assumptions

These various assumptions regarding density-dependnet interactions, functional form, and dispersal have intriguing population-level implications that are reflected in the theoretical literature. Examining how dispersal limitation impacts species richness within these previous models yields some insights (Table 6.1).

Many theoretical papers examining Adult-Juvenile and Juvenile-Juvenile interactions find local dispersal (both explicit and implicit) decreases species richness (Stump and Chesson, 2015; Stump and Comita, 2020; Chisholm and Fung, 2020; Krishnadas and Stump, 2021). Interestingly, these apparently consistent outcomes may reflect distinctive mechanisms. Papers that use non-additive models (Stump and Chesson, 2015; Chisholm and Fung, 2020) or sub-additive models (Krishnadas and Stump, 2021) likely measure a direct decrease in stabilizing effects. As noted in Chapter 2 (see Appendix F), spatially implicit local dispersal decreases species richness when density-dependent effects are non-additive but when they are additive (or, at least, the negative effect of dispersal is weak; see fig. 2.2). This is because if rare species' locally dispersed offspring experience mortality at a rate equal to resident species' locally dispersed offspring (which occurs when density-dependent effects are non-additive, but not when it is additive) rare species advantage is diminished relative to when dispersal is global. However, the model used in Chapter 2 examines local dispersal limitation

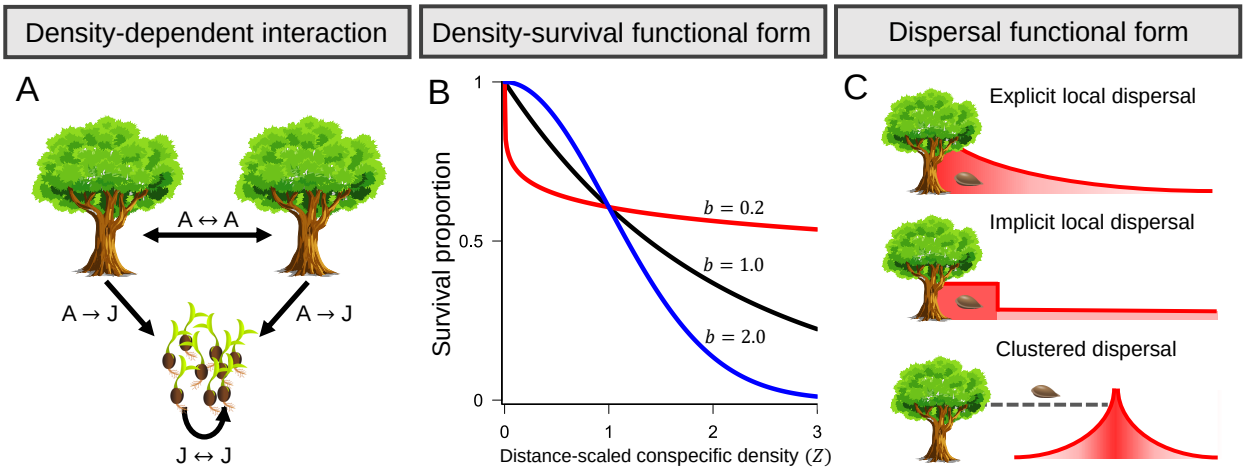

Figure 6.3: Visualizations of the various assumptions in theoretical studies examining distance and density-dependent processes. Panel A depicts the life history stage(s) inducing and experiencing density-dependent effects. Panel B shows how the functional form of density-dependence, b, may affect an individual's probability of survival as a function of conspecific density (Z). $b < 1$ indicates sub-additive effects – if $b \approx 0$, conspecific density exhibit a "presence-absence"-like effect. $b = 1$ indicates linearly additive effects. $b > 1$ indicates super-additive effects. Panel C illustrates different forms of dispersal used in models. "Explicit local dispersal" is used in spatially explicit models and assumes the number of seeds a tree disperses to a location declines monotonically with distance. "Implicit local dispersal" is used in spatially implicit models. Trees disperse a portion of their seeds on the local patch they occupy and uniformly disperse the remaining portion of seeds throughout the environment. "Clustered dispersal", examined in Wiegand et al. (2021), is intended to represent processes such as animal dispersal. Seeds of each tree are dispersed in clusters to locations decoupled from the parent tree.

in a spatially implicit manner. This ignores how dispersal limitation may modify species aggregation. Several papers find using spatially explicit local dispersal combined with additive effects can decrease species richness (Muller-Landau and Adler, 2007; Stump and Comita, 2020), at least in part attributable to rare species aggregation. Consistent with this, recent work demonstrates that clumping generally reduces rare species advantage (Ellner et al., 2022). Interestingly, Muller-Landau and Adler (2007) find spatially explicit local dispersal limitation increases species richness when natural enemies disperse over a wide range yet decreases species richness when natural enemies disperse over a short range. This is likely related to how each dispersal kernel impacts rare species aggregation. While Adler and Muller-Landau (2005) find a combination of local spatially explicit dispersal limitation in combination with highly localized natural enemies strongly increases species richness, later work shows this is likely due to a combination of immigration and transient effects (Stump and Chesson, 2015).

Paper	Density interaction	Functional form	Type of dispersal	Effect of dispersal limitation on diversity
Adler and Muller-Landau (2005)	A→J	Additive	Explicit, local	Positive
Muller-Landau and Adler (2007)	A→J	Additive	Explicit, local	Mixed
Stump and Chesson (2015)	A→J	Non-additive	Implicit, local	Negative
Detto and Muller-Landau (2016)	A↔A	Additive	Explicit, local	Positive
Chisholm and Fung (2020)	A→J	Non-additive	Explicit, local	Negative
Stump and Comita (2020)	A→J, J↔J	Additive	Explicit, local	Negative
Krishnadas and Stump (2021)	J↔J	Sub-additive	Explicit, local	Negative
Wiegand et al. (2021)	A↔A	Additive	Explicit, local	Positive
Wiegand et al. (2021)	A↔A	Additive	Explicit, clustered	Positive
Smith (2022)	A→J	Non-additive	Implicit, local	Negative
Smith (2022)	A→J	Additive	Implicit, local	No effect

Table 6.1: A non-comprehensive summary of theoretical papers that examine how distance/density-dependent processes and dispersal limitation interact to shape species richness. "Density interaction" describes which life history stage induces and experiences negative density dependence (depicted with arrows) where A represents adults and J represents juveniles (see Fig. 6.3A). "Functional form" depicts how offspring survival scales with density; see 6.3B. "Dispersal limitation" describes how adults disperse seeds in space; see Fig. 6.3C. The final column describes the effect of increasing dispersal limitation on species richness (for example, "negative" implies greater dispersal limitation decreases species richness)

Detto and Muller-Landau (2016) and Wiegand et al. (2021) unambiguously demonstrate that dispersal limitation can interact with density-dependent effects to increase species richness. Importantly, these models are unique among those examined thus far because they consider linearly

additive adult-adult density-dependent effects. Detto and Muller-Landau (2016) examine a model in which all species are equal (neutrality). Adult mortality rate (the probability of mortality) increases with the neighborhood density of adults. Overall, they find this leads to species segregation; thus, when a particular species falls to low abundance, it tends to occupy areas of relatively low density (previously occupied by conspecifics, but currently at relatively low density) – thus, the adults of rare species experience lower mortality, generating a stabilizing effect. Wiegand et al. (2021) explore a similar model incorporating clustered dispersal (Fig. 6.3C) in which each species' seeds are dispersed to each of a set number of sites located independently of adult locations. Through this, rare species often recruit in areas of relatively low density and, ultimately, rare species tend to have fewer neighbors that common species; because adult mortality is density-dependent, this generates a stabilizing fitness-density covariance (Chesson, 2012).

Putting the pieces together

Unsurprisingly, assumptions vary between theoretical models examining how distance and density dependent processes shape species richness. Such assumptions are necessary to reduce model complexity – the key is to tease apart how each individual assumption affects results and produce robust predictions. The work in this thesis and previous theoretical studies have made advances (see Table 6.1). For example, dispersal limitation tends to decrease the propensity for distance/density dependent effects to maintain species richness under non-additive (or sub-additive) functional forms. However, generally, we still lack a general theory of density-dependent feedbacks in spatially structured environments and many potential scenarios remain unexamined.

For example, Wiegand et al. (2021) examine the interaction between clustered dispersal and adult-adult density-dependent effects. However, given the robust evidence that density-dependence occurs at the seedling level (Comita et al., 2014), it is necessary to examine this novel means of modeling dispersal for all potential density-dependent interactions. Similarly, studies modeling adult density-dependent interactions (Detto and Muller-Landau, 2016; Wiegand et al., 2021) assume a linearly additive functional form; how breaking this assumption would qualitatively affect results is unknown. Within this, it is important to understand what *generates* said functional form in the first

place. Some work in this thesis provides insights: in Chapter 4, I demonstrate that the life stage that induces negative density dependence and the vital rate it affects interact to regulate the functional form of density-dependent survival when seedlings experience CNDD (see Fig. 4.1). It would be useful and informative to extend this lens of analyses to all the potential types of density-dependent interactions highlighted above.

Furthermore, as highlighted in Chapter 3, density-dependent interactions do not occur in a vacuum. Rather, they occur on top of existing abiotic heterogeneity. Analyzing the interaction between JCEs and habitat partitioning (Chapter 3) represents a step forward in terms of integrating the spatial variables that mediate density-dependent interactions. However, the model therein leaves some unanswered questions. For example, dispersal is assume to be global – how might dispersal limitation affect the results? Does the density-dependent interaction (Fig. 6.3A) or the type dispersal (Fig. 6.3C) affect these results? For the latter question, existing literature surrounding habitat partitioning stresses how abiotic heterogeneity and dispersal limitation affect the spatial composition of sessile organisms (Snyder and Chesson, 2003; Hart et al., 2017) which indicates the answer is likely *yes*. However, broadly, the complicated interactions between abiotic spatial heterogeneity, local density-dependent feedbacks, and dispersal limitation remain under-explored.

6.3 Integrating theoretical and empirical efforts

This thesis predominantly focuses on gaps in the theoretical Janzen-Connell effect and CNDD-related literature while noting qualitative connections to empirical patterns (e.g. see Chapter 4, Fig. 4.6). However, it is equally important to better integrate the above-discussed theoretical advances with measurements performed in natural systems. The golden standard of synthesizing theoretical and empirical results is, of course, to parameterize sufficiently mechanistic models with measurements of nature in order to evaluate if community dynamics can be described by the processes of interest (i.e, if the parameterized models predict coexistence and accurately describe relative species abundance). However, doing so is often extremely difficult – especially in the very forest communities that JCEs are thought to structure.

6.3.1 Measuring CNDD

Some recent work casts doubt on the ability of CNDD and JCEs to maintain diversity – not from a theoretical perspective, but because reliable and unbiased measurements are difficult to perform (Freckleton, 2011; Broekman et al., 2019; Detto et al., 2019; Hülsmann et al., 2021). In forest communities, this is in part because the long lifespan of adult trees (long, at least, relative to time over which most studies can feasibly be conducted) makes direct measurements of the probability of species recruitment (from seed to adult) as a function of conspecific density highly impractical. Therefore, measurements often examine CNDD effects over relatively small time-scales, focus on individual life history stages, and use a number of (possibly error-prone) proxies of factors representing natural enemy density to quantify negative density-dependence. While the statistical issues involved in detecting CNDD are deserving of careful discussion (see Chisholm and Fung, 2018; Hülsmann and Hartig, 2018; Detto et al., 2019) I will focus on the difficult task of accurately evaluating how CNDD affects species coexistence under the assumption that measurements are unbiased.

In tree communities, most analyses examine how conspecific (and, often, heterospecific) densities affect the survival probability of species' offspring. Several strategies are used in different studies, but I focus on two very common methods. As examined in Chapter 4, many studies examine the number of seedling recruits that emerge at multiple locations of different initial seed densities (e.g. Bagchi et al., 2014; Krishnadas and Stump, 2021). Such studies fit the equation $\text{Seedlings} = \alpha \times \text{seeds}^{\beta}$ for which α is the baseline proportion of seeds that survive (density-independent survival) and β quantifies the strength of CNDD. If $\beta < 1$, the proportion of seedlings that recruit from an initial cohort of seeds decreases as a function of initial seed density; this indicates the presence of CNDD. Alternately, many studies examine censuses that track the survival of seedling or sapling survival over multiple years (e.g. Comita et al., 2010). Using spatial data, GLMMs are fit using a logic link function such that $p(S) = \left(1 + \exp(-B_0 - B_1 Z_1 - B_2 Z_2)\right)^{-1}$ for which $p(S)$ is the probability a seedling or sapling of a focal species survives over the course of the observations, B_0 reflects density-independent survival, B_1 and B_2 are conspecific and heterospecific effects on seedling/sapling survival, and Z_1 and Z_2 are distance-weighted conspecific and heterospecific densities, respectively (Fig. 6.3B). In principle, if $-B_1 > -B_2$, conspecific effects are stronger

than heterospecific effects.

It is genuinely difficult to use these measurements to parameterize ecological models that incorporate inter-specific competition. Firstly, each statistical fit assumes a particular functional form that may not reflect nature. Therefore, while the above-models may yield accurate fits for the densities and time periods over which they measure seedling or sapling survival, it is unclear how well these fits will reflect reality when subjected to the range of conditions that are necessary to model (e.g. when seeds become highly abundant or scarce; when a particular species becomes very common or rare). Secondly, quantifying the ability of CNDD to stabilize coexistence requires how conspecific density affects the probability of an individual's recruitment over the entire seed-to-adult transition. Therefore, unless these measurements take place at a key (or, perhaps *the* key) bottle neck in the regenerative pathway, measurements may be uninformative. Thus, while several recent studies directly implement these measurements into models (Stump and Comita, 2018; Krishnadas and Stump, 2021) it is unclear if the parameterizations are informative or not.

Therefore, it is important to elucidate precisely how informative the above measurements are. One solution is to perform extensive fits of simulated communities. This would require the development of a spatially explicit actor based model of a multi-species tree community that models seeds, juveniles, adults, realistic levels of stochasticity, and a realistic implementation of negative density-dependence. Various scenarios could be simulated and each simulation treated as if it were a field study in which the most common methods of measuring CNDD are implemented (such as those detailed above). Simulated measurements could then be analyzed using analytical tools from theoretical ecology (e.g. modern coexistence theory; Barabás et al., 2018; Chesson, 2018; Ellner et al., 2019) to asses their accuracy in predicting stabilizing effects and species coexistence.

6.3.2 CNDD and fitness differences

Even if the above difficulties are overcome, the detection of CNDD is insufficient to guarantee it is important for species coexistence. Rather, the strength of CNDD must be sufficiently strong relative to heterospecific effects to compensate for inter-specific fitness differences. Therefore, fitness differences must be precisely quantified to understand the importance of CNDD in natural

communities. To this effect, much of this thesis (Chapters 2-4) is motivated by the observation that available evidence indicates annual plant communities and tropical forests exhibit large inter-specific fitness variation (Levine and HilleRisLambers, 2009; Kraft et al., 2015; Chisholm and Fung, 2020). However, some ambiguity remains. Whether inter-specific variation in traits like seed production rate or low density seedling recruitment (as examined in Chisholm and Fung, 2020) are good proxies for tree fitness is unclear. Assuming these estimates do accurately represent inter-specific fitness differences, stabilizing mechanisms (JCEs or otherwise) must be correspondingly strong to maintain coexistence. Additionally, fitness differences can be driven by inter-specific variation in CNDD and plant-soil feedback strength (Stump and Comita, 2018; Kandlikar et al., 2021; Yan et al., 2022). This adds an additional axis of parameter space and further complicates how CNDD may affect coexistence.

A path toward reducing this complexity is to better integrate CNDD into life history theory (as argued in Chapter 4). Trade-offs between life history traits such as fecundity and seed size may offset inter-specific fitness differences. However, it is extremely unlikely trade-offs *entirely* equalize fitness (at least, for known trade-offs such as the trade-off between fecundity and seed survival as mediated by seed size; Fenner et al., 2000; Muller-Landau, 2010). How species-specific CNDD strength correlates with traits such as fecundity represents an additional important piece of the puzzle – unstructured inter-specific variation on both axes of fitness (CNDD and density-independent traits like fecundity) is highly likely to undermine coexistence (Cannon et al., 2021). Consequently, the there is a desperate need for more empirical papers analyzing trait associations with CNDD (following in the footsteps of Zhu et al., 2018; Brown et al., 2020; Song et al., 2021b; Zang et al., 2021; Qin et al., 2022). From a theoretical perspective, Stump and Comita (2020) represents an important conceptual advancement for thinking about CNDD through the lens of life history; Chapter 4 of this thesis constitutes a step toward developing a demographic theory of CNDD from which trade-offs naturally emerge and allow for null hypotheses for how negative density-dependent effects and demographic traits combine to shape the probability of recruitment.

6.4 Conclusion

The Janzen-Connell hypothesis was first proposed more than 50 years ago. Despite its age, debate on its relevance in the maintenance of species richness has only intensified in recent years (Terborgh, 2020). In this thesis, I have filled several theoretical gaps. In Chapter 2, I highlight the need to precisely quantify how density-dependent conspecific interactions in spatially structured environments affect recruitment. In Chapter 3, I elucidate how these processes interact with spatially varying abiotic heterogeneity. Chapter 4 emphasizes how we must develop better demographic models of Janzen-Connell effects to understand both what underlies patterns of its empirical measurement and its impact on species richness. Finally, in Chapter 5, I hint at how specialized and generalized predation may interact with spatial-temporal variation in offspring production.

While I view these results as important steps forward, they are precisely that – *steps*. Scientists have been arguing about Janzen-Connell effects for decades and I have no delusion that the conclusions of this thesis will amount to anything approaching an end to the discussion. Rather, I hope my work will further fan the flames such that debate over local feedback mechanisms such as Janzen-Connell effects spreads far and wide throughout the entire field of ecology.

References

Mark V Abrahams and Michael G Kattenfeld. The role of turbidity as a constraint on predator-prey interactions in aquatic environments. *Behavioral Ecology and Sociobiology*, 40(3):169–174, 1997.

Frederick R Adler and Helene C Muller-Landau. When do localized natural enemies increase species richness? *Ecology Letters*, 8(4):438–447, 2005.

Peter B Adler, Alex Fajardo, Andrew R Kleinhesselink, and Nathan JB Kraft. Trait-based tests of coexistence mechanisms. *Ecology letters*, 16(10):1294–1306, 2013.

Patricia Alvarez-Loayza and John Terborgh. Fates of seedling carpets in an amazonian floodplain forest: intra-cohort competition or attack by enemies? *Journal of Ecology*, 99(4):1045–1054, 2011.

Priyanga Amarasekare. Competitive coexistence in spatially structured environments: a synthesis. *Ecology letters*, 6(12):1109–1122, 2003.

Priyanga Amarasekare, Martha F Hoopes, Nicolas Mouquet, and Marcel Holyoak. Mechanisms of coexistence in competitive metacommunities. *The American Naturalist*, 164(3):310–326, 2004.

Robert A Armstrong. Competition, seed predation, and species coexistence. *Journal of Theoretical Biology*, 141(2):191–195, 1989.

Robert A Armstrong and Richard McGehee. Competitive exclusion. *The American Naturalist*, 115 (2):151–170, 1980.

Víctor Arroyo-Rodríguez, Romeo A Saldana-Vazquez, Lenore Fahrig, and Braulio A Santos. Does forest fragmentation cause an increase in forest temperature? *Ecological research*, 32(1):81–88, 2017.

Heidi Asbjornsen, Mark S Ashton, Daniel J Vogt, and Sergio Palacios. Effects of habitat fragmentation on the buffering capacity of edge environments in a seasonally dry tropical oak forest ecosystem in oaxaca, mexico. *Agriculture, Ecosystems & Environment*, 103(3):481–495, 2004.

Bénédicte Bachelot, Richard K Kobe, and Corine Vriesendorp. Negative density-dependent mortality varies over time in a wet tropical forest, advantaging rare species, common species, or no species. *Oecologia*, 179(3):853–861, 2015.

Robert Bagchi, Tom Swinfield, Rachel E Gallery, Owen T Lewis, Sofia Gripenberg, Lakshmi Narayan, and Robert P Freckleton. Testing the janzen-connell mechanism: Pathogens cause overcompensating density dependence in a tropical tree. *Ecology letters*, 13(10):1262–1269, 2010.

Robert Bagchi, Peter A Henrys, Patrick E Brown, David FR P Burslem, Peter J Diggle, CV Savitri Gunatilleke, IAU Nimal Gunatilleke, Abdul Rahman Kassim, Richard Law, Supardi Noor, et al. Spatial patterns reveal negative density dependence and habitat associations in tropical trees. *Ecology*, 92(9):1723–1729, 2011.

Robert Bagchi, Rachel E Gallery, Sofia Gripenberg, Sarah J Gurr, Lakshmi Narayan, Claire E Addis, Robert P Freckleton, and Owen T Lewis. Pathogens and insect herbivores drive rainforest plant diversity and composition. *Nature*, 506(7486):85–88, 2014.

Xuejiao Bai, Simon A Queenborough, Xugao Wang, Jian Zhang, Buhang Li, Zuoqiang Yuan, Dingliang Xing, Fei Lin, Ji Ye, and Zhanqing Hao. Effects of local biotic neighbors and habitat heterogeneity on tree and shrub seedling survival in an old-growth temperate forest. *Oecologia*, 170(3):755–765, 2012.

György Barabás, Rafael D'Andrea, and Simon Maccracken Stump. Chesson's coexistence theory. *Ecological monographs*, 88(3):277–303, 2018.

Eyal Ben-Hur and Ronen Kadmon. Heterogeneity–diversity relationships in sessile organisms: a unified framework. *Ecology letters*, 23(1):193–207, 2020.

Jonathan A Bennett, Hafiz Maherali, Kurt O Reinhart, Ylva Lekberg, Miranda M Hart, and John Klironomos. Plant-soil feedbacks and mycorrhizal type influence temperate forest population dynamics. *Science*, 355(6321):181–184, 2017.

James D Bever, Kristi M Westover, and Janis Antonovics. Incorporating the soil community into plant population dynamics: the utility of the feedback approach. *Journal of Ecology*, pages 561–573, 1997.

James D Bever, Scott A Mangan, and Helen M Alexander. Maintenance of plant species diversity by pathogens. *Annual review of ecology, evolution, and systematics*, 46:305–325, 2015.

Michał Bogdziewicz, Josep M Espelta, Alberto Muñoz, Jose M Aparicio, and Raul Bonal. Effectiveness of predator satiation in masting oaks is negatively affected by conspecific density. *Oecologia*, 186(4):983–993, 2018.

Jody Bolluyt, Sue Ellen Johnson, Peter Lowy, Margaret Tuttle McGrath, Charles L Mohler, Anusuya Rangarajan, Kimberly A Stoner, Eric Toensmeier, and Harold van Es. Crop rotation on organic farms: A planning manual (nraes-177), 2011.

Maarten JE Broekman, Helene C Muller-Landau, Marco D Visser, Eelke Jongejans, SJ Wright, and Hans de Kroon. Signs of stabilisation and stable coexistence. *Ecology letters*, 22(11):1957–1975, 2019.

Alissa J Brown, Christopher J Payne, Peter S White, and Robert K Peet. Shade tolerance and mycorrhizal type may influence sapling susceptibility to conspecific negative density dependence. *Journal of Ecology*, 108(1):325–336, 2020.

Alissa J Brown, Peter S White, and Robert K Peet. Environmental context alters the magnitude of conspecific negative density dependence in a temperate forest. *Ecosphere*, 12(3):e03406, 2021.

Patrick G Cannon, Michael J O'Brien, Kalsum M Yusah, David P Edwards, and Robert P Freckleton. Limited contributions of plant pathogens to density-dependent seedling mortality of mast fruiting bornean trees. *Ecology and evolution*, 10(23):13154–13164, 2020.

Patrick G Cannon, David P Edwards, and Robert P Freckleton. Asking the wrong question in explaining tropical diversity. *Trends in Ecology & Evolution*, 2021.

Eric L Charnov. Optimal foraging, the marginal value theorem. *Theoretical population biology*, 9 (2):129–136, 1976.

Jonathan M Chase, Peter A Abrams, James P Grover, Sebastian Diehl, Peter Chesson, Robert D Holt, Shane A Richards, Roger M Nisbet, and Ted J Case. The interaction between predation and competition: a review and synthesis. *Ecology letters*, 5(2):302–315, 2002.

Lei Chen, Xiangcheng Mi, Liza S Comita, Liwen Zhang, Haibao Ren, and Keping Ma. Community-level consequences of density dependence and habitat association in a subtropical broad-leaved forest. *Ecology letters*, 13(6):695–704, 2010.

Lei Chen, Nathan G Swenson, Niuniu Ji, Xiangcheng Mi, Haibao Ren, Liangdong Guo, and Keping Ma. Differential soil fungus accumulation and density dependence of trees in a subtropical forest. *Science*, 366(6461):124–128, 2019.

Si-Chong Chen and Angela T Moles. Factors shaping large-scale gradients in seed physical defence: Seeds are not better defended towards the tropics. *Global ecology and biogeography*, 27(4):417–428, 2018.

Peter Chesson. Multispecies competition in variable environments. *Theoretical population biology*, 45(3):227–276, 1994.

Peter Chesson. General theory of competitive coexistence in spatially-varying environments. *Theoretical population biology*, 58(3):211–237, 2000a.

Peter Chesson. Mechanisms of maintenance of species diversity. *Annual review of Ecology and Systematics*, 31(1):343–366, 2000b.

Peter Chesson. Scale transition theory: its aims, motivations and predictions. *Ecological Complexity*, 10:52–68, 2012.

Peter Chesson. Updates on mechanisms of maintenance of species diversity. *Journal of ecology*, 106 (5):1773–1794, 2018.

Peter Chesson and Jessica J Kuang. The interaction between predation and competition. *Nature*, 456(7219):235, 2008.

Peter L Chesson. Coexistence of competitors in spatially and temporally varying environments: a look at the combined effects of different sorts of variability. *Theoretical Population Biology*, 28 (3):263–287, 1985.

Peter L Chesson and Robert R Warner. Environmental variability promotes coexistence in lottery competitive systems. *The American Naturalist*, 117(6):923–943, 1981.

Ryan A Chisholm and Tak Fung. Comment on "plant diversity increases with the strength of negative density dependence at the global scale". *Science*, 360(6391):eaar4685, 2018.

Ryan A Chisholm and Tak Fung. Janzen-connell effects are a weak impediment to competitive exclusion. *The American Naturalist*, 196(5):649–661, 2020.

Ryan A Chisholm and Helene C Muller-Landau. A theoretical model linking interspecific variation in density dependence to species abundances. *Theoretical Ecology*, 4(2):241–253, 2011.

Philip J Clark and Francis C Evans. Distance to nearest neighbor as a measure of spatial relationships in populations. *Ecology*, 35(4):445–453, 1954.

Phyllis D Coley. Effects of leaf age and plant life history patterns on herbivory. *Nature*, 284(5756): 545–546, 1980.

Liza S Comita. How latitude affects biotic interactions. *Science*, 356(6345):1328–1329, 2017.

Liza S Comita and Simon M Stump. Natural enemies and the maintenance of tropical tree diversity: Recent insights and implications for the future of biodiversity in a changing world1. *Annals of the Missouri Botanical Garden*, 105(3):377–392, 2020.

Liza S Comita, Salomón Aguilar, Rolando Pérez, Suzanne Lao, and Stephen P Hubbell. Patterns of woody plant species abundance and diversity in the seedling layer of a tropical forest. *J. Veg. Sci.*, 18(2):163–174, 2007.

Liza S Comita, Maria Uriarte, Jill Thompson, Inge Jonckheere, Charles D Canham, and Jess K Zimmerman. Abiotic and biotic drivers of seedling survival in a hurricane-impacted tropical forest. *Journal of Ecology*, 97(6):1346–1359, 2009.

Liza S Comita, Helene C Muller-Landau, Salomón Aguilar, and Stephen P Hubbell. Asymmetric density dependence shapes species abundances in a tropical tree community. *Science*, 329(5989): 330–332, 2010.

Liza S Comita, Simon A Queenborough, Stephen J Murphy, Jenalle L Eck, Kaiyang Xu, Meghna Krishnadas, Noelle Beckman, and Yan Zhu. Testing predictions of the janzen–connell hypothesis: a meta-analysis of experimental evidence for distance-and density-dependent seed and seedling survival. *Journal of Ecology*, 102(4):845–856, 2014.

R Condit, R Pérez, S Aguilar, S Lao, R Foster, and S Hubbell. Complete data from the barro colorado 50-ha plot: 423617 trees, 35 years, 2019 version, 2019.

Richard Condit, Bettina MJ Engelbrecht, Delicia Pino, Rolando Pérez, and Benjamin L Turner. Species distributions in response to individual soil nutrients and seasonal drought across a community of tropical trees. *Proceedings of the National Academy of Sciences*, 110(13):5064–5068, 2013.

Joseph H Connell. On the role of natural enemies in preventing competitive exclusion in some marine animals and in rain forest trees. *Dynamics of populations*, 298:312, 1971.

Mick J Crawley. Seed predators and plant population dynamics. *Seeds: the ecology of regeneration in plant communities*, pages 167–182, 2000.

Matteo Detto and Helene C Muller-Landau. Stabilization of species coexistence in spatial models through the aggregation–segregation effect generated by local dispersal and nonspecific local interactions. *Theoretical Population Biology*, 112:97–108, 2016.

Matteo Detto, Marco D Visser, S Joseph Wright, and Stephen W Pacala. Bias in the detection of negative density dependence in plant communities. *Ecology Letters*, 22(11):1923–1939, 2019.

Rafael D'andrea, John Guittar, James P O'dwyer, Hector Figueroa, SJ Wright, Richard Condit, and Annette Ostling. Counting niches: Abundance-by-trait patterns reveal niche partitioning in a neotropical forest. *Ecology*, 101(6):e03019, 2020.

Stephen P Ellner, Robin E Snyder, Peter B Adler, and Giles Hooker. An expanded modern coexistence theory for empirical applications. *Ecology letters*, 22(1):3–18, 2019.

Stephen P Ellner, Robin E Snyder, Peter B Adler, and Giles Hooker. Toward a "modern coexistence theory" for the discrete and spatial. *Ecological Monographs*, page e1548, 2022.

Michael Fenner et al. *Seeds: the ecology of regeneration in plant communities.* Number Ed. 2. CABI publishing, 2000.

Pavel Fibich, Masae I Ishihara, Satoshi N Suzuki, Jiří Doležal, and Jan Altman. Contribution of conspecific negative density dependence to species diversity is increasing towards low environmental limitation in japanese forests. *Scientific reports*, 11(1):1–11, 2021.

Robert J Fletcher Jr, Raphael K Didham, Cristina Banks-Leite, Jos Barlow, Robert M Ewers, James Rosindell, Robert D Holt, Andrew Gonzalez, Renata Pardini, Ellen I Damschen, et al. Is habitat fragmentation good for biodiversity? *Biological conservation*, 226:9–15, 2018.

Robert P Freckleton. Dealing with collinearity in behavioural and ecological data: model averaging and the problems of measurement error. *Behavioral Ecology and Sociobiology*, 65(1):91–101, 2011.

Robert P Freckleton and Owen T Lewis. Pathogens, density dependence and the coexistence of tropical trees. *Proceedings of the Royal Society B: Biological Sciences*, 273(1604):2909–2916, 2006.

Evan C Fricke and S Joseph Wright. Measuring the demographic impact of conspecific negative density dependence. *Oecologia*, 184(1):259–266, 2017.

Georgii Frantsevich Gause. Experimental studies on the struggle for existence: I. mixed population of two species of yeast. *Journal of experimental biology*, 9(4):389–402, 1932.

Gregory S Gilbert and Campbell O Webb. Phylogenetic signal in plant pathogen–host range. *Proceedings of the National Academy of Sciences*, 104(12):4979–4983, 2007.

Peter T Green, Kyle E Harms, and Joseph H Connell. Nonrandom, diversifying processes are disproportionately strong in the smallest size classes of a tropical forest. *Proceedings of the National Academy of Sciences*, 111(52):18649–18654, 2014.

Jacopo Grilli, György Barabás, Matthew J Michalska-Smith, and Stefano Allesina. Higher-order interactions stabilize dynamics in competitive network models. *Nature*, 548(7666):210–213, 2017.

Sofia Gripenberg, Yves Basset, Owen T Lewis, J Christopher D Terry, S Joseph Wright, Indira Simón, D Catalina Fernández, Marjorie Cedeño-Sanchez, Marleny Rivera, Héctor Barrios, et al. A highly resolved food web for insect seed predators in a species-rich tropical forest. *Ecology Letters*, 22(10):1638–1649, 2019.

Ilkka Hanski. Habitat fragmentation and species richness. *Journal of Biogeography*, 42(5):989–993, 2015.

Garrett Hardin. The competitive exclusion principle: An idea that took a century to be born has implications in ecology, economics, and genetics. *science*, 131(3409):1292–1297, 1960.

Anna L Hargreaves, Esteban Suárez, Klaus Mehltreter, Isla Myers-Smith, Sula E Vanderplank, Heather L Slinn, Yalma L Vargas-Rodriguez, Sybille Haeussler, Santiago David, Jenny Muñoz, et al. Seed predation increases from the arctic to the equator and from high to low elevations. *Science Advances*, 5(2):eaau4403, 2019.

Kyle E Harms, S Joseph Wright, Osvaldo Calderón, Andres Hernandez, and Edward Allen Herre. Pervasive density-dependent recruitment enhances seedling diversity in a tropical forest. *Nature*, 404(6777):493–495, 2000.

Simon P Hart, Jacob Usinowicz, and Jonathan M Levine. The spatial scales of species coexistence. *Nature Ecology & Evolution*, 1(8):1066–1073, 2017.

Kirstie Hazelwood, Harald Beck, and CE Timothy Paine. Negative density dependence in the mortality and growth of tropical tree seedlings is strong, and primarily caused by fungal pathogens. *Journal of Ecology*, 109(4):1909–1918, 2021.

Jan Holík, David Janík, and Dušan Adam. Light can modify density-dependent seedling mortality in a temperate forest. *Journal of Vegetation Science*, 32(1):e12992, 2021.

Crawford S Holling. Some characteristics of simple types of predation and parasitism1. *The canadian entomologist*, 91(7):385–398, 1959.

Robert D Holt. Predation, apparent competition, and the structure of prey communities. *Theoretical population biology*, 12(2):197–229, 1977.

Joaquin Hortal, Kostas A Triantis, Shai Meiri, Elisa Thébault, and Spyros Sfenthourakis. Island species richness increases with habitat diversity. *The American Naturalist*, 174(6):E205–E217, 2009.

Teng-He Huang, Chun-Lin Huang, Yi-Ching Lin, and I-Fang Sun. Seedling survival simultaneously determined by conspecific, heterospecific, and phylogenetically related neighbors and habitat heterogeneity in a subtropical forest in taiwan. *Ecology and Evolution*, 12(1):e8525, 2022.

Stephen P Hubbell. Seed predation and the coexistence of tree species in tropical forests. *Oikos*, pages 214–229, 1980.

Stephen P Hubbell, Jorge A Ahumada, Richard Condit, and Robin B Foster. Local neighborhood effects on long-term survival of individual trees in a neotropical forest. *Ecological Research*, 16 (5):859–875, 2001.

Jef Huisman and Franz J Weissing. Biodiversity of plankton by species oscillations and chaos. *Nature*, 402(6760):407–410, 1999.

Lisa Hülsmann and Florian Hartig. Comment on "plant diversity increases with the strength of negative density dependence at the global scale". *Science*, 360(6391):eaar2435, 2018.

Lisa Hülsmann, Ryan A Chisholm, and Florian Hartig. Is variation in conspecific negative density dependence driving tree diversity patterns at large scales? *Trends in Ecology & Evolution*, 36(2): 151–163, 2021.

George C Hurtt and Stephen W Pacala. The consequences of recruitment limitation: reconciling chance, history and competitive differences between plants. *Journal of theoretical biology*, 176(1): 1–12, 1995.

G Evelyn Hutchinson. The paradox of the plankton. *The American Naturalist*, 95(882):137–145, 1961.

Laura A Hyatt, Michael S Rosenberg, Timothy G Howard, Gregory Bole, Wei Fang, Jean Anastasia, Kerry Brown, Rebecca Grella, Katharine Hinman, Josepha P Kurdziel, et al. The distance dependence prediction of the janzen-connell hypothesis: a meta-analysis. *Oikos*, 103(3):590–602, 2003.

Wolfram Research Inc. Mathematica, Version 13.0.0, 2021. URL `https://www.wolfram.com/mathematica`. Champaign, IL, 2021.

Faith Inman-Narahari, Rebecca Ostertag, Stephen P Hubbell, Christian P Giardina, Susan Cordell, and Lawren Sack. Density-dependent seedling mortality varies with light availability and species abundance in wet and dry hawaiian forests. *Journal of Ecology*, 104(3):773–780, 2016.

Daniel H Janzen. Herbivores and the number of tree species in tropical forests. *The American Naturalist*, 104(940):501–528, 1970.

Daniel H Janzen. Seed predation by animals. *Annual review of ecology and systematics*, pages 465–492, 1971.

Daniel H Janzen. Seeding patterns of tropical trees. *Tropical trees as living systems*, pages 83–128, 1978.

Johan Ludwig William Valdemar Jensen. Sur les fonctions convexes et les inégalités entre les valeurs moyennes. *Acta mathematica*, 30(1):175–193, 1906.

Shihong Jia, Xugao Wang, Zuoqiang Yuan, Fei Lin, Ji Ye, Guigang Lin, Zhanqing Hao, and Robert Bagchi. Tree species traits affect which natural enemies drive the janzen-connell effect in a temperate forest. *Nature Communications*, 11(1):1–9, 2020.

Daniel J Johnson, Wesley T Beaulieu, James D Bever, and Keith Clay. Conspecific negative density dependence and forest diversity. *Science*, 336(6083):904–907, 2012.

Daniel J Johnson, Norman A Bourg, Robert Howe, William J McShea, Amy Wolf, and Keith Clay. Conspecific negative density-dependent mortality and the structure of temperate forests. *Ecology*, 95(9):2493–2503, 2014.

Daniel J Johnson, Richard Condit, Stephen P Hubbell, and Liza S Comita. Abiotic niche partitioning and negative density dependence drive tree seedling survival in a tropical forest. *Proceedings of the Royal Society B: Biological Sciences*, 284(1869):20172210, 2017.

Clive G Jones, John H Lawton, and Moshe Shachak. Organisms as ecosystem engineers. In *Ecosystem management*, pages 130–147. Springer, 1994.

Valentin Journé, Robert Andrus, Marie-Claire Aravena, Davide Ascoli, Roberta Berretti, Daniel Berveiller, Michal Bogdziewicz, Thomas Boivin, Raul Bonal, Thomas Caignard, et al. Globally, tree fecundity exceeds productivity gradients. *Ecology letters*, 25(6):1471–1482, 2022.

Gaurav S Kandlikar, Xinyi Yan, Jonathan M Levine, and Nathan JB Kraft. Soil microbes generate stronger fitness differences than stabilization among california annual plants. *The American Naturalist*, 197(1):E30–E39, 2021.

Po-Ju Ke and Joe Wan. Effects of soil microbes on plant competition: a perspective from modern coexistence theory. *Ecological Monographs*, 90(1):e01391, 2020.

Dave Kelly. The evolutionary ecology of mast seeding. *Trends in ecology & evolution*, 9(12):465–470, 1994.

Dave Kelly and Victoria L Sork. Mast seeding in perennial plants: why, how, where? *Annual review of ecology and systematics*, pages 427–447, 2002.

Dave Kelly and Jon J Sullivan. Quantifying the benefits of mast seeding on predator satiation and wind pollination in chionochloa pallens (poaceae). *Oikos*, pages 143–150, 1997.

John N Klironomos. Feedback with soil biota contributes to plant rarity and invasiveness in communities. *Nature*, 417(6884):67, 2002.

Richard K Kobe, Stephen W Pacala, John A Silander Jr, and Charles D Canham. Juvenile tree survivorship as a component of shade tolerance. *Ecological applications*, 5(2):517–532, 1995.

Walter D Koenig. A brief history of masting research. *Philosophical Transactions of the Royal Society B*, 376(1839):20200423, 2021.

Walter D Koenig, Dave Kelly, Victoria L Sork, Richard P Duncan, Joseph S Elkinton, Mikko S Peltonen, and Robert D Westfall. Dissecting components of population-level variation in seed production and the evolution of masting behavior. *Oikos*, 102(3):581–591, 2003.

Nathan JB Kraft, Oscar Godoy, and Jonathan M Levine. Plant functional traits and the multidimensional nature of species coexistence. *Proceedings of the National Academy of Sciences*, 112 (3):797–802, 2015.

Meghna Krishnadas and Simon Maccracken Stump. Dispersal limitation and weaker stabilizing mechanisms mediate loss of diversity with edge effects in forest fragments. *Journal of Ecology*, 109(5):2137–2151, 2021.

Meghna Krishnadas, Robert Bagchi, Sachin Sridhara, and Liza S Comita. Weaker plant-enemy interactions decrease tree seedling diversity with edge-effects in a fragmented tropical forest. *Nature Communications*, 9(1):1–7, 2018.

Jessica J Kuang and Peter Chesson. Coexistence of annual plants: generalist seed predation weakens the storage effect. *Ecology*, 90(1):170–182, 2009.

Jessica J Kuang and Peter Chesson. Interacting coexistence mechanisms in annual plant communities: frequency-dependent predation and the storage effect. *Theoretical population biology*, 77(1): 56–70, 2010.

Andrew Kulmatiski, Karen H Beard, John R Stevens, and Stephanie M Cobbold. Plant–soil feedbacks: a meta-analytical review. *Ecology letters*, 11(9):980–992, 2008.

Joseph A LaManna, Maranda L Walton, Benjamin L Turner, and Jonathan A Myers. Negative density dependence is stronger in resource-rich environments and diversifies communities when stronger for common but not rare species. *Ecology Letters*, 19(6):657–667, 2016.

Joseph A LaManna, R Travis Belote, Laura A Burkle, Christopher P Catano, and Jonathan A Myers. Negative density dependence mediates biodiversity–productivity relationships across scales. *Nature ecology & evolution*, 1(8):1107–1115, 2017a.

Joseph A LaManna, Scott A Mangan, Alfonso Alonso, Norman A Bourg, Warren Y Brockelman, Sarayudh Bunyavejchewin, Li-Wan Chang, Jyh-Min Chiang, George B Chuyong, Keith Clay, et al. Plant diversity increases with the strength of negative density dependence at the global scale. *Science*, 356(6345):1389–1392, 2017b.

Joseph A LaManna, F Andrew Jones, David M Bell, Robert J Pabst, and David C Shaw. Tree species diversity increases with conspecific negative density dependence across an elevation gradient. *Ecology Letters*, 25(5):1237–1249, 2022.

Loralee Larios, Dean E Pearson, and John L Maron. Incorporating the effects of generalist seed predators into plant community theory. *Functional Ecology*, 31(10):1856–1867, 2017.

Edwin Lebrija-Trejos, Peter B Reich, Andres Hernández, and S Joseph Wright. Species with greater seed mass are more tolerant of conspecific neighbours: a key driver of early survival and future abundances in a tropical forest. *Ecology letters*, 19(9):1071–1080, 2016.

Mathew A Leibold and Jonathan M Chase. *Metacommunity ecology*, volume 59. Princeton University Press, 2017.

Mathew A Leibold, Marcel Holyoak, Nicolas Mouquet, Priyanga Amarasekare, Jonathan M Chase, Martha F Hoopes, Robert D Holt, Jonathan B Shurin, Richard Law, David Tilman, et al. The metacommunity concept: a framework for multi-scale community ecology. *Ecology letters*, 7(7): 601–613, 2004.

Taal Levi, Michael Barfield, Shane Barrantes, Christopher Sullivan, Robert D Holt, and John Terborgh. Tropical forests can maintain hyperdiversity because of enemies. *Proceedings of the National Academy of Sciences*, 116(2):581–586, 2019.

Simon A Levin. Community equilibria and stability, and an extension of the competitive exclusion principle. *The American Naturalist*, 104(939):413–423, 1970.

Jonathan M Levine and Janneke HilleRisLambers. The importance of niches for the maintenance of species diversity. *Nature*, 461(7261):254–257, 2009.

Haikun Liu, Fenglin Xie, Hang Shi, Xiao Shu, Kerong Zhang, Quanfa Zhang, and Haishan Dang. Disentangling the effects of biotic neighbors and habitat heterogeneity on seedling survival in a deciduous broad-leaved forest. *Forest Ecology and Management*, 519:120339, 2022.

Xubing Liu, Minxia Liang, Rampal S Etienne, Yongfan Wang, Christian Staehelin, and Shixiao Yu. Experimental evidence for a phylogenetic janzen–connell effect in a subtropical forest. *Ecology letters*, 15(2):111–118, 2012.

Yu Liu, Suqin Fang, Peter Chesson, and Fangliang He. The effect of soil-borne pathogens depends on the abundance of host tree species. *Nature Communications*, 6(1):1–7, 2015.

James O Lloyd-Smith. Vacated niches, competitive release and the community ecology of pathogen eradication. *Philosophical Transactions of the Royal Society B: Biological Sciences*, 368(1623): 20120150, 2013.

Junmeng Lu, Daniel J Johnson, Xiujuan Qiao, Zhijun Lu, Qinggang Wang, and Mingxi Jiang. Density dependence and habitat preference shape seedling survival in a subtropical forest in central china. *Journal of Plant Ecology*, 8(6):568–577, 2015.

Robert MacArthur. Species packing and competitive equilibrium for many species. *Theoretical population biology*, 1(1):1–11, 1970.

Robert H MacArthur and Eric R Pianka. On optimal use of a patchy environment. *The American Naturalist*, 100(916):603–609, 1966.

Keenan ML Mack, Maarten B Eppinga, and James D Bever. Plant-soil feedbacks promote coexistence and resilience in multi-species communities. *PloS one*, 14(2):e0211572, 2019.

Lukas Magee, Amy Wolf, Robert Howe, Jonathan Schubbe, Kari Hagenow, and Benjamin Turner. Density dependence and habitat heterogeneity regulate seedling survival in a north american temperate forest. *Forest Ecology and Management*, 480:118722, 2021.

Scott A Mangan, Stefan A Schnitzer, Edward A Herre, Keenan ML Mack, Mariana C Valencia, Evelyn I Sanchez, and James D Bever. Negative plant–soil feedback predicts tree-species relative abundance in a tropical forest. *Nature*, 466(7307):752, 2010.

Francesco Martini, Chia-Hao Chang-Yang, and I-Fang Sun. Variation in biotic interactions mediates the effects of masting and rainfall fluctuations on seedling demography in a subtropical rainforest. *Journal of Ecology*, 110(4):762–771, 2022.

Felix May, Thorsten Wiegand, Andreas Huth, and Jonathan M Chase. Scale-dependent effects of conspecific negative density dependence and immigration on biodiversity maintenance. *Oikos*, 2020.

Sarah McCarthy-Neumann and Inés Ibáñez. Plant–soil feedback links negative distance dependence and light gradient partitioning during seedling establishment. *Ecology*, 94(4):780–786, 2013.

Sarah McCarthy-Neumann and Richard K Kobe. Tolerance of soil pathogens co-varies with shade tolerance across species of tropical tree seedlings. *Ecology*, 89(7):1883–1892, 2008.

Sarah McCarthy-Neumann and Richard K Kobe. Site soil-fertility and light availability influence plant-soil feedback. *Frontiers in Ecology and Evolution*, 7:383, 2019.

Krista L McGuire. The contribution of ectomycorrhizal fungal feedbacks to the maintenance of tropical monodominant rain forests. *Ectomycorrhizal symbioses in tropical and neotropical forest*, pages 185–199, 2014.

Valerie R Milici, Dipanjana Dalui, James G Mickley, and Robert Bagchi. Responses of plant–pathogen interactions to precipitation: Implications for tropical tree richness in a changing world. *Journal of Ecology*, 108(5):1800–1809, 2020.

Zachary R Miller and Stefano Allesina. Metapopulations with habitat modification. *Proceedings of the National Academy of Sciences*, 118(49):e2109896118, 2021.

António Miranda, Luís M Carvalho, and Francisco Dionisio. Lower within-community variance of negative density dependence increases forest diversity. *PloS one*, 10(5):e0127260, 2015.

Angela T Moles and Mark Westoby. Seedling survival and seed size: a synthesis of the literature. *Journal of Ecology*, 92(3):372–383, 2004.

Angela T Moles, David I Warton, and Mark Westoby. Do small-seeded species have higher survival through seed predation than large-seeded species? *Ecology*, 84(12):3148–3161, 2003.

Angela T Moles, Stephen P Bonser, Alistair GB Poore, Ian R Wallis, and William J Foley. Assessing the evidence for latitudinal gradients in plant defence and herbivory. *Functional Ecology*, 25(2): 380–388, 2011.

Erin A Mordecai. Pathogen impacts on plant diversity in variable environments. *Oikos*, 124(4): 414–420, 2015.

Nicolas Mouquet and Michel Loreau. Community patterns in source-sink metacommunities. *The american naturalist*, 162(5):544–557, 2003.

HC Muller-Landau and FR Adler. How seed dispersal affects interactions with specialized natural enemies and their contribution to the maintenance of diversity. *Seed dispersal: Theory and its application in a changing world*, pages 407–446, 2007.

Helene Muller-Landau. The tolerance–fecundity trade-off and the maintenance of diversity in seed size. *Proceedings of the National Academy of Sciences*, 107(9):4242–4247, 2010.

Tamara Münkemüller, Harald Bugmann, and Karin Johst. Hutchinson revisited: patterns of density regulation and the coexistence of strong competitors. *Journal of Theoretical Biology*, 259(1):109–117, 2009.

Stephen J Murphy, Thorsten Wiegand, and Liza S Comita. Distance-dependent seedling mortality and long-term spacing dynamics in a neotropical forest community. *Ecology letters*, 20(11):1469–1478, 2017.

RAN Nathan and Renato Casagrandi. A simple mechanistic model of seed dispersal, predation and plant establishment: Janzen-connell and beyond. *Journal of Ecology*, 92(5):733–746, 2004.

Roger M Nisbet and William Gurney. *Modelling fluctuating populations*. The Blackburn Press, Caldwell, NJ, 1982.

Vojtech Novotny and Yves Basset. Host specificity of insect herbivores in tropical forests. *Proceedings of the Royal Society B: Biological Sciences*, 272(1568):1083–1090, 2005.

Vojtech Novotny, Yves Basset, Scott E Miller, George D Weiblen, Birgitta Bremer, Lukas Cizek, and Pavel Drozd. Low host specificity of herbivorous insects in a tropical forest. *Nature*, 416 (6883):841, 2002.

Vojtech Novotny, Scott E Miller, Leontine Baje, Solomon Balagawi, Yves Basset, Lukas Cizek, Kathleen J Craft, Francesca Dem, Richard AI Drew, Jiri Hulcr, et al. Guild-specific patterns of species richness and host specialization in plant–herbivore food webs from a tropical forest. *Journal of Animal Ecology*, 79(6):1193–1203, 2010.

Michael J O'Brien, Andy Hector, Roman T Kellenberger, Colin R Maycock, Robert Ong, Christopher D Philipson, Jennifer S Powers, Glen Reynolds, and David FRP Burslem. Demographic consequences of heterogeneity in conspecific density dependence among mast-fruiting tropical trees. *Proceedings of the Royal Society B*, 289(1977):20220739, 2022.

Frode Ødegaard, Ola H Diserud, and Kjartan Østbye. The importance of plant relatedness for host utilization among phytophagous insects. *Ecology Letters*, 8(6):612–617, 2005.

TC Paulitz, KL Schroeder, and WF Schillinger. Soilborne pathogens of cereals in an irrigated cropping system: Effects of tillage, residue management, and crop rotation. *Plant disease*, 94(1): 61–68, 2010.

Mario B Pesendorfer, Davide Ascoli, Michał Bogdziewicz, Andrew Hacket-Pain, Ian S Pearse, and Giorgio Vacchiano. The ecology and evolution of synchronized reproduction in long-lived plants, 2021.

Jana S Petermann, Alexander JF Fergus, Lindsay A Turnbull, and Bernhard Schmid. Janzen-connell effects are widespread and strong enough to maintain diversity in grasslands. *Ecology*, 89 (9):2399–2406, 2008.

Tiefeng Piao, Liza S Comita, Guangze Jin, and Ji Hong Kim. Density dependence across multiple life stages in a temperate old-growth forest of northeast china. *Oecologia*, 172(1):207–217, 2013.

Lourens Poorter. Are species adapted to their regeneration niche, adult niche, or both? *The American Naturalist*, 169(4):433–442, 2007.

Xucai Pu, Yu Zhu, and Guangze Jin. Effects of local biotic neighbors and habitat heterogeneity on seedling survival in a spruce-fir valley forest, northeastern china. *Ecology and evolution*, 7(13): 4582–4591, 2017.

Xucai Pu, Monique Weemstra, Guangze Jin, and María Natalia Umaña. Tree mycorrhizal type mediates conspecific negative density dependence effects on seedling herbivory, growth, and survival. *Oecologia*, pages 1–12, 2022.

Jianghuan Qin, Chunyu Fan, Yan Geng, Chunyu Zhang, Xiuhai Zhao, and Lushuang Gao. Drivers of tree demographic trade-offs in a temperate forest. *Forest Ecosystems*, page 100044, 2022.

Simon A Queenborough, David FRP Burslem, Nancy C Garwood, and Renato Valencia. Taxonomic scale-dependence of habitat niche partitioning and biotic neighbourhood on survival of tropical tree seedlings. *Proceedings of the Royal Society B: Biological Sciences*, 276(1676):4197–4205, 2009.

R Core Team. *R: A Language and Environment for Statistical Computing*. R Foundation for Statistical Computing, Vienna, Austria, 2021. URL `https://www.R-project.org/`.

R Core Team. *R: A Language and Environment for Statistical Computing*. R Foundation for Statistical Computing, Vienna, Austria, 2022. URL `https://www.R-project.org/`.

Benjamin S Ramage, Daniel J Johnson, Erika Gonzalez-Akre, William J McShea, Kristina J Anderson-Teixeira, Norman A Bourg, and Keith Clay. Sapling growth rates reveal conspecific negative density dependence in a temperate forest. *Ecology and evolution*, 7(19):7661–7671, 2017.

Leslie A Real. The kinetics of functional response. *The American Naturalist*, 111(978):289–300, 1977.

Heather L Reynolds, Alissa Packer, James D Bever, and Keith Clay. Grassroots ecology: plant–microbe–soil interactions as drivers of plant community structure and dynamics. *Ecology*, 84(9): 2281–2291, 2003.

Brian D Ripley. The second-order analysis of stationary point processes. *Journal of applied probability*, 13(2):255–266, 1976.

Nadja Rüger, Andreas Huth, Stephen P Hubbell, and Richard Condit. Response of recruitment to light availability across a tropical lowland rain forest community. *Journal of Ecology*, 97(6): 1360–1368, 2009.

Edward James Salisbury et al. The reproductive capacity of plants. studies in quantitative biology. *The reproductive capacity of plants. Studies in quantitative biology.*, 1942.

Carolina Sarmiento, Paul-Camilo Zalamea, James W Dalling, Adam S Davis, Simon M Stump, Jana M U'Ren, and A Elizabeth Arnold. Soilborne fungi have host affinity and host-specific effects on seed germination and survival in a lowland tropical forest. *Proceedings of the National Academy of Sciences*, 114(43):11458–11463, 2017.

Dietmar Saupe. Algorithms for random fractals. In *The science of fractal images*, pages 71–136. Springer, 1988.

John W Schroeder, Andrew Dobson, Scott A Mangan, Daniel F Petticord, and Edward Allen Herre. Mutualist and pathogen traits interact to affect plant community structure in a spatially explicit model. *Nature communications*, 11(1):1–10, 2020.

Eugene W Schupp and Marcelino Fuentes. Spatial patterns of seed dispersal and the unification of plant population ecology. *Ecoscience*, 2(3):267–275, 1995.

Marco Sciaini, Matthias Fritsch, Cédric Scherer, and Craig Eric Simpkins. Nlmr and landscapetools: An integrated environment for simulating and modifying neutral landscape models in r. *Methods in ecology and evolution*, 9(11):2240–2248, 2018.

Brian E Sedio and Annette M Ostling. How specialised must natural enemies be to facilitate coexistence among plants? *Ecology letters*, 16(8):995–1003, 2013.

Barbara Seget, Michał Bogdziewicz, Jan Holeksa, Mateusz Ledwoń, Fiona Milne-Rostkowska, Łukasz Piechnik, Alicja Rzepczak, and Magdalena Żywiec. Costs and benefits of masting: economies of scale are not reduced by negative density-dependence in seedling survival in sorbus aucuparia. *New Phytologist*, 233(4):1931–1938, 2022.

Erica C Seth and Michiko E Taga. Nutrient cross-feeding in the microbial world. *Frontiers in microbiology*, 5:350, 2014.

Lauren G Shoemaker and Brett A Melbourne. Linking metacommunity paradigms to spatial coexistence mechanisms. *Ecology*, 97(9):2436–2446, 2016.

Jonathan W Silvertown. The evolutionary ecology of mast seeding in trees. *Biological journal of the Linnean Society*, 14(2):235–250, 1980.

Daniel JB Smith. The functional form of specialized predation dramatically affects whether janzen-connell effects can prevent competitive exclusion. *bioRxiv*, 2021.

Daniel JB Smith. The functional form of specialised predation affects whether janzen–connell effects can prevent competitive exclusion. *Ecology Letters*, 2022a.

Daniel JB Smith. On the interaction between janzen-connell effects and habitat partitioning in spatially structured environments. *bioRxiv*, 2022b.

Robin E Snyder and Peter Chesson. Local dispersal can facilitate coexistence in the presence of permanent spatial heterogeneity. *Ecology letters*, 6(4):301–309, 2003.

Karline Soetaert, Thomas Petzoldt, and R. Woodrow Setzer. Solving differential equations in R: Package deSolve. *Journal of Statistical Software*, 33(9):1–25, 2010. doi:10.18637/jss.v033.i09.

Xiaoyang Song, Daniel J Johnson, Min Cao, Maria Natalia Umaña, Xiaobao Deng, Xiaofei Yang, Wenfu Zhang, and Jie Yang. The strength of density-dependent mortality is contingent on climate and seedling size. *Journal of Vegetation Science*, 29(4):662–670, 2018.

Xiaoyang Song, Jun Ying Lim, Jie Yang, and Matthew Scott Luskin. When do janzen–connell effects matter? a phylogenetic meta-analysis of conspecific negative distance and density dependence experiments. *Ecology Letters*, 24(3):608–620, 2021a.

Xiaoyang Song, Jie Yang, Min Cao, Luxiang Lin, Zhenhua Sun, Handong Wen, and Nathan G Swenson. Traits mediate a trade-off in seedling growth response to light and conspecific density in a diverse subtropical forest. *Journal of Ecology*, 109(2):703–713, 2021b.

Anke Stein, Katharina Gerstner, and Holger Kreft. Environmental heterogeneity as a universal driver of species richness across taxa, biomes and spatial scales. *Ecology letters*, 17(7):866–880, 2014.

Simon Maccracken Stump. Multispecies coexistence without diffuse competition; or, why phylogenetic signal and trait clustering weaken coexistence. *The American Naturalist*, 190(2):213–228, 2017.

Simon Maccracken Stump and Peter Chesson. Distance-responsive predation is not necessary for the janzen–connell hypothesis. *Theoretical population biology*, 106:60–70, 2015.

Simon Maccracken Stump and Peter Chesson. How optimally foraging predators promote prey coexistence in a variable environment. *Theoretical Population Biology*, 114:40–58, 2017.

Simon Maccracken Stump and Liza S Comita. Interspecific variation in conspecific negative density dependence can make species less likely to coexist. *Ecology letters*, 21(10):1541–1551, 2018.

Simon Maccracken Stump and Liza S Comita. Differences among species in seed dispersal and conspecific neighbor effects can interact to influence coexistence. *Theoretical Ecology*, pages 1–31, 2020.

Varun Swamy and John W Terborgh. Distance-responsive natural enemies strongly influence seedling establishment patterns of multiple species in an amazonian rain forest. *Journal of Ecology*, 98(5):1096–1107, 2010.

Tom Swinfield, Owen T Lewis, Robert Bagchi, and Robert P Freckleton. Consequences of changing rainfall for fungal pathogen-induced mortality in tropical tree seedlings. *Ecology and evolution*, 2(7):1408–1413, 2012.

John Terborgh. Enemies maintain hyperdiverse tropical forests. *The American Naturalist*, 179(3): 303–314, 2012.

John Terborgh. At 50, janzen–connell has come of age. *BioScience*, 70(12):1082–1092, 2020.

François P Teste, Paul Kardol, Benjamin L Turner, David A Wardle, Graham Zemunik, Michael Renton, and Etienne Laliberté. Plant-soil feedback and the maintenance of diversity in mediterranean-climate shrublands. *Science*, 355(6321):173–176, 2017.

David Tilman. Resource competition and community structure.(mpb-17), volume 17. In *Resource Competition and Community Structure.(MPB-17), Volume 17*. Princeton university press, 1982.

María Uriarte, Richard Condit, Charles D Canham, and Stephen P Hubbell. A spatially explicit model of sapling growth in a tropical forest: does the identity of neighbours matter? *Journal of Ecology*, 92(2):348–360, 2004.

María Uriarte, Robert Muscarella, and Jess K Zimmerman. Environmental heterogeneity and biotic interactions mediate climate impacts on tropical forest regeneration. *Global change biology*, 24 (2):e692–e704, 2018.

Boliang Wei, Lei Zhong, Jinliang Liu, Fangdong Zheng, Yi Jin, Yuchu Xie, Zupei Lei, Guochun Shen, and Mingjian Yu. Differences in density dependence among tree mycorrhizal types affect tree species diversity and relative growth rates. *Plants*, 11(18):2340, 2022.

Thorsten Wiegand and Kirk A Moloney. *Handbook of spatial point-pattern analysis in ecology*. CRC press, 2013.

Thorsten Wiegand, Xugao Wang, Kristina J Anderson-Teixeira, Norman A Bourg, Min Cao, Xiuqin Ci, Stuart J Davies, Zhanqing Hao, Robert W Howe, W John Kress, et al. Consequences of spatial patterns for coexistence in species-rich plant communities. *Nature Ecology & Evolution*, pages 1–9, 2021.

S Joseph Wright. Plant diversity in tropical forests: a review of mechanisms of species coexistence. *Oecologia*, 130(1):1–14, 2002.

S Joseph Wright, Helene C Muller-Landau, Richard Condit, and Stephen P Hubbell. Gap-dependent recruitment, realized vital rates, and size distributions of tropical trees. *Ecology*, 84(12):3174–3185, 2003.

S Joseph Wright, Helene C Muller-Landau, Osvaldo Calderón, and Andrés Hernandéz. Annual and spatial variation in seedfall and seedling recruitment in a neotropical forest. *Ecology*, 86(4): 848–860, 2005.

S Joseph Wright, Kaoru Kitajima, Nathan JB Kraft, Peter B Reich, Ian J Wright, Daniel E Bunker, Richard Condit, James W Dalling, Stuart J Davies, Sandra Díaz, et al. Functional traits and the growth–mortality trade-off in tropical trees. *Ecology*, 91(12):3664–3674, 2010.

Junjie Wu, Nathan G Swenson, Calum Brown, Caicai Zhang, Jie Yang, Xiuqin Ci, Jie Li, Liqing Sha, Min Cao, and Luxiang Lin. How does habitat filtering affect the detection of conspecific and phylogenetic density dependence? *Ecology*, 97(5):1182–1193, 2016.

Zhishu Xiao, Xiangcheng Mi, Marcel Holyoak, Wenhua Xie, Ke Cao, Xifu Yang, Xiaoqun Huang, and Charles J Krebs. Seed–predator satiation and janzen–connell effects vary with spatial scales for seed-feeding insects. *Annals of botany*, 119(1):109–116, 2017.

Zhichao Xu, Daniel J Johnson, Kai Zhu, Fei Lin, Ji Ye, Zuoqiang Yuan, Zikun Mao, Shuai Fang, Zhanqing Hao, and Xugao Wang. Interannual climate variability has predominant effects on seedling survival in a temperate forest. *Ecology*, 103(4):e3643, 2022.

Xinyi Yan, Jonathan M Levine, and Gaurav S Kandlikar. A quantitative synthesis of soil microbial effects on plant species coexistence. *Proceedings of the National Academy of Sciences*, 119(22): e2122088119, 2022.

Jie Yao, Benedicte Bachelot, Lingjun Meng, Jianghuan Qin, Xiuhai Zhao, and Chunyu Zhang. Abiotic niche partitioning and negative density dependence across multiple life stages in a temperate forest in northeastern china. *Journal of Ecology*, 108(4):1299–1310, 2020.

Shafia Zahra, Vojtech Novotny, and Tom M Fayle. Do reverse janzen-connell effects reduce species diversity? *Trends in Ecology & Evolution*, 36(5):387–390, 2021.

Lipeng Zang, Han Xu, Yide Li, and Runguo Zang. Conspecific negative density dependence of trees varies with plant functional traits and environmental conditions across scales in a 60-ha tropical rainforest dynamics plot. *Biotropica*, 53(2):693–702, 2021.

Yan Zhu, Xiangcheng Mi, Haibao Ren, and Keping Ma. Density dependence is prevalent in a heterogeneous subtropical forest. *Oikos*, 119(1):109–119, 2010.

Yan Zhu, Liza S Comita, Stephen P Hubbell, and Keping Ma. Conspecific and phylogenetic density-dependent survival differs across life stages in a tropical forest. *Journal of Ecology*, 103(4):957–966, 2015.

Yan Zhu, Simon A Queenborough, Richard Condit, Stephen Hubbell, Keping Ma, and Liza S Comita. Density-dependent survival varies with species life-history strategy in a tropical forest. *Ecology letters*, 21(4):506–515, 2018.

Rafał Zwolak, Paulina Celebias, and Michał Bogdziewicz. Global patterns in the predator satiation effect of masting: A meta-analysis. *Proceedings of the National Academy of Sciences*, 119(11): e2105655119, 2022.